



# 4D Printing of Shape-Changing Thermo-Responsive Textiles

A Thesis Submitted for the Degree of Doctor of Philosophy

By

Hsiang Hsiang Loh

Department of Design

College of Engineering, Design and Physical Sciences

Brunel University London

August 2021

## **Abstract**

This research reviews the state-of-the-art literature on the two-emerging material-driven Additive Manufacturing (AM) strategies, Functionally Graded Additive Manufacturing (FGAM) and 4D Printing (4DP) to recognise, select and implement the appropriate materials, design and fabrication methods to produce shape-changing thermo-responsive textiles. Shape-memory polymers (SMPs) are required to provide the active properties required to sense and self-actuate when subjected to an appropriate stimulus over time. The current availability of SMPs for AM in the commercial market is limited and expensive. To ensure a wider uptake of 4DP, the aim of this research is to develop a material selection framework to discover, define and select commercially available thermoplastics as potential SMPs for use in material extrusion (ME) 4DP. The theoretical and practical knowledge to create a thermally actuated dual-state mechanism (DSM) active structure is described at a feasible level for users with different backgrounds and knowledge levels in 4DP. The experiments showed that commercial AM filaments could be used for 4DP, but not all materials exhibit shape memory properties despite belonging to the same material type. The shape recovery performance and repeatability of an SMP would also vary according to the programming condition. The next stage of this research details the development and testing of polymer-textile composites using direct ME of PLA filaments on synthetic mesh fabrics. T-peel test results revealed that the compatibility between the printing material and the textile substrate fibre type has a dominant effect on the peel resistance of ME polymer-textile composite. The research demonstrated the use of 4DP as an alternative and novel technique for the 3D manipulation of textile fabrics. The shape transformation studies presented a proof-of-concept that the accuracy of deformation and the shape-shifting patterns of the thermo-responsive textiles can be controlled by the geometrical dimensions and structural arrangement of the printed SMP structure on the textile substrate. The findings will enable researchers and designers to take advantage of the optimum parameters to discover new shape transformations and to create potential applications in the AM fashion and textile industry.

## **Keywords**

Additive Manufacturing; Functionally Graded Additive Manufacturing; 4D Printing; Polymer-Textile Composite; Stimulus-responsive Textiles; Shape Transformation.

## **Declaration**

I hereby declare that I am the sole author of this thesis. This work in this thesis was carried out following the requirements of the University's Regulations for PhD and is the result of my own investigations and evaluations except where otherwise indicated by specific reference in the text. I can confirm that this work has not previously been accepted for any degree nor is it currently submitted and under consideration for any other academic award.

Hsiang Hsiang Loh

August 2021

## **Acknowledgement**

This research has been a long and challenging yet undoubtedly rewarding journey. It would be impossible without the contribution and support of many valuable people in my life. First and foremost, my sincere thanks to my family, especially my parents and grandparents for their continued encouragement, care and support in making this PhD journey possible.

A heartfelt gratitude to my principal supervisor, Dr. Eujin Pei for his guidance and invaluable advice at all stages of this PhD research. You have always been a great inspiration and encouraging advisor who have provided me with many great opportunities to develop new skills and explore new ideas to shape this research. Appreciation is also extended to my second supervisor, Professor David Harrison for his guidance, support and assistance throughout my research.

My sincere thanks to my fellow research colleagues for their moral support and for providing the office a sociable working environment. I would like to particularly acknowledge the support of Dr. Adeayo Sotayo for his expertise for the testing of Material Extrusion (ME) polymer-textile composites. My appreciation is also extended to senior technicians, Mr Neil Mcfayden and Mr Ali Ahmadnia for their assistance and provision of mechanical testing facilities and equipment for this research. I am also grateful to the professionals and doctoral researchers for their valuable participation and feedback to validate the material selection framework for 4D Printing.

Finally, million thanks to my spouse, Edmond Yuen for his constant encouragement, care and support throughout my PhD journey.

## **Used Acronyms/ Abbreviations**

3MF – 3D Manufacturing Format

4DP – Four-Dimensional Printing (4D Printing)

AM – Additive Manufacturing

AMF – Additive Manufacturing Format

BJ – Binder Jetting

BRC – Bend Recovery Chart

BS – British Standards

CAD – Computer Aided Design

CAE – Computer Aided Engineering

CAL – Computer Axial Lithography

CFD – Computational Fluid Dynamics

CTE – Coefficient of Thermal Expansion

CVD – Chemical Vapour Deposition

CVI – Chemical Vapour Infiltration

DED – Directed Energy Deposition

DLP – Digital Light Processing

DMLS – Direct Metal Laser Sintering

DOE – Design of Experiments

DSM – Dual State Mechanism

EBM – Electron Beam Melting

EDS – Energy-Dispersive Spectroscopy

FAV – Fabricatable Voxel

FDM – Fused Deposition Modelling

FEF – Freeze-form Extrusion Fabrication

FEM – Finite Elements Method

FFF – Fused Filament Fabrication

FGAM – Functionally Graded Additive Manufacturing

FRC – Fold Recovery Chart

IBAD – Ion Beam Assisted Deposition

LMD – Laser Metal Deposition

LOM – Laminated Object Material

ME – Material Extrusion

ME – Material Extrusion

MIP-SL – Mask-Image-Projection based Stereolithography

MJF – Multi Jet Fusion

NC – Numerical Control

PBF – Powder Bed Fusion

PEI – Polyetherimide

PJT – PolyJet Technology

PLA – Polylactic Acid

PPE – Personal Protective Equipment

PVD – Physical Vapour Deposition

$R_r$  – Shape Recovery

SCE – Shape Change Effect

SFC – Shape Fixity Chart

SHS – Self-propagating High Temperature Synthesis

SLM – Selective Laser Melting

SLS – Selective Laser Sintering

SMA – Shape Memory Alloy

SME – Shape Memory Effect

SMP – Shape Memory Polymer

SMS – Selective Mask Sintering

SPI – Stitches Per Inch

SPS – Spark Plasma Sintering

SRMs – Stimuli-Responsive Materials

SVX – Simple Voxels

T – Temperature

Ta – Rate of Shape Morphing Activation

Td – Shape Deforming Temperature

TEM – Transmission Electron Microscopy

Tg – Glass Transition Temperature

Tm – Melt Temperature

Tr – Shape Recovery Temperature

UC – Ultrasonic Consolidation

VP – Vat Photopolymerization

WAAM – Wire Arc Additive Manufacturing

## **List of Terms**

### **4D Printing (4DP)**

The use of AM to produce a freeform stimulus-responsive component that can sense and actuate in response to an appropriate stimulus over time, without the reliance on power-source, robotics or electro-mechanical devices.

### **Active Materials**

Materials that can change their properties or perform actions using energy or nutrients from the environment.

### **Active Origami**

A design to create an origami object that has the ability to self-fold or self-unfold.

### **Additive Manufacturing (AM)**

The process of joining materials to make parts from 3D model data, usually layer upon layer, as opposed to subtractive manufacturing and formative manufacturing methodologies.

### **Adaptive Materials**

Materials that can sense changes in the environment, respond and adjust to new properties or behaviour that adapt to those conditions.

### **Dual-State Mechanism (DSM)**

A basic working mechanism for the heating-responsive shape memory effect in polymeric materials.

### **Fixing Temperature**

It is the working temperature at which the temporary shape of a deformed SMP is fixed.

### **Functionally Graded Additive Manufacturing (FGAM)**

A layer-by-layer fabrication process that involves gradationally varying the material organisation within a component to achieve an intended function.

**Glass Transition Temperature ( $T_g$ )**

The glass transition temperature is the temperature range where the polymer substrate changes from a rigid glassy material to soft rubbery material.

**Material Extrusion (ME)**

An AM process in which material is selectively dispensed through a nozzle or orifice.

**Multi-material Additive Manufacturing (MMAM)**

A technology that enhances the performance of AM parts by adding more complexity and functionality. MMAM technologies improve part performance by varying compositions or type with the layers.

**Pleat**

A type of fold formed by doubling fabric back upon itself and securing it in place.

**Projecting Pleat**

Folds are lifted from the surface of the fabric and structured into roll arrangements that stand out from the fabric itself.

**Rate of Shape Morphing Activation ( $T_a$ )**

The time taken to trigger the shape-morphing of a stimuli-responsive component.

**Response Rate**

The time taken for an SMP to self-actuate and transforms into a predetermined shape when subjected to a defined stimulus.

**Self-adaptability**

The ability to respond and adjust to new conditions through properties or behaviour changes that are adapted to those conditions.

**Self-assembly**

A process by which disordered parts build an ordered structure through only local interaction.

**Self-repair**

A process of self-healing materials to automatically repair damages to themselves without any external diagnosis of the problem or human intervention.

**Self-shape Change Actuation**

An automatic shape changing without a shape programming step.

**Shape Change Cycle Life**

Cycle life represents the number of consecutive shape change cycles that Shape Change Material (SCM) can achieve without a noticeable decrease in shape change effect (SCE).

**Shape Change Effect (SCE)**

An effect in which a material returns to its original shape either instantly or gradually when the applied stimulus is removed.

**Shape Deforming Temperature (Td)**

It is the temperature at which the SMP is deformed to a certain strain to get the temporary shape.

**Shape Fixity**

The extent of a temporary shape being fixed. Shape fixity characterises the ability of an SMP to fix the strain imparted in the sample during the deformation step after subsequent cooling and unloading.

**Shape Memory Actuation**

A shape transformation process involves a shape programming-recovery step by submitting the structure to a thermo-mechanical cycle.

**Shape Memory Alloy (SMA)**

A class of alloys that can remember their shape and can return to their pre-deformed shape when heated.

**Shape Memory Cycle Life**

The number of consecutive shape memory cycles that SMP can achieve without a noticeable decrease in shape recovery and shape fixity.

**Shape Memory Effect (SME)**

The ability of an SMP to recover to its original shape from a temporary configuration.

**Shape Memory Polymer (SMP)**

Polymeric smart materials that can return from a deformed state to their original shape induced by an external stimulus, such as temperature change.

**Shape Recovery**

Shape recovery characterises the ability of an SMP to recover the accumulated strain during the deformation step after subsequent cooling and unloading upon reheating to the rubbery state.

**Shape Recovery Temperature ( $T_r$ )**

It is the temperature at which the permanent shape of the SMP is recovered.

**Smart Textiles**

A class of fabrics that possess aesthetic and feature augmentations when exposed to external stimuli.

**Stimuli-Responsive Actuator Materials**

Materials that produce strain in response to the applied stimuli.

**Stimuli-Responsive Energy Conversion Materials**

Materials that exhibit an electric current, electrical resistance, magnetic field or temperature change as a primary response to the applied stimuli.

**Stimuli-Responsive Materials (SRMs)**

Materials that have the particularity to change one or more of their properties under a defined stimulus.

**Stimuli-Responsive Optical Materials**

Materials that exhibit an optical response, such as light emission or a change in optical properties as a response to the applied stimuli.

**Stimuli-Responsive State-Changing Materials**

Materials that alter their physical properties, such as viscosity, in response to the applied stimuli.

**Thermo-responsive Textiles**

A class of fabrics that possess aesthetic and feature augmentations such as switchable volume, wettability, and appearance when exposed to heat.

**Voxel**

A unit of graphic information that defines a point in three-dimensional space.

# Table of Contents

<b>Abstract</b> .....	<b>I</b>
<b>Keywords</b> .....	<b>I</b>
<b>Declaration</b> .....	<b>II</b>
<b>Acknowledgement</b> .....	<b>III</b>
<b>Used Acronyms/ Abbreviations</b> .....	<b>IV</b>
<b>List of Terms</b> .....	<b>VII</b>
<b>Table of Contents</b> .....	<b>XII</b>
<b>List of Figures</b> .....	<b>XVI</b>
<b>List of Tables</b> .....	<b>XXI</b>
<b>Citation for this Thesis</b> .....	<b>XXIV</b>
<b>Chapter 1 Introduction</b> .....	<b>1</b>
1.1. Research Background.....	1
1.2. Research Aim, Objectives and Research Questions .....	3
1.3. Research Scope.....	4
1.4. Organisation of the Thesis .....	6
1.5. Research Methodology .....	9
1.6. Chapter Summary .....	13
<b>Chapter 2 Functionally Graded Additive Manufacturing (FGAM)</b> .....	<b>14</b>
2.1. Introduction .....	14
2.2. The Concept of FGAM .....	18
2.2.1. Homogeneous Composition – Single material FGAM.....	20
2.2.2. Heterogeneous Composition – Multi-material FGAM.....	22
2.2.3. Combined Composition.....	24
2.2.4. Types of Gradients.....	24
2.3. Process Flow of FGAM .....	26
2.4. AM Technologies for FGAM.....	30
2.4.1. Material Extrusion .....	31
2.4.2. Vat Photopolymerization .....	33
2.4.3. Powder Bed Fusion .....	35
2.4.4. Material Jetting.....	36
2.4.5. Sheet Lamination .....	38
2.4.6. Directed Energy Deposition .....	38

2.5.	The Advancement of FGAM.....	40
2.5.1.	FGAM Applications .....	41
2.6.	Challenges, Research Gaps and Future Work .....	42
2.6.1.	Materials.....	42
2.6.2.	Design, Modelling and Simulation .....	44
2.6.3.	AM Processes .....	46
2.7.	Chapter Summary .....	48
	<b>Chapter 3 4D Printing (4DP).....</b>	<b>49</b>
3.1.	Introduction .....	49
3.2.	The Concept of 4DP .....	50
3.2.1.	AM Technologies for 4DP .....	52
3.2.2.	Stimuli-Responsive Materials (SRMs) and Stimuli .....	53
3.2.2.1.	Shape-Change Materials (SCMs) .....	55
3.2.2.2.	Shape-Memory Materials (SMMs).....	58
3.2.2.3.	Shape-Change Effect (SCE) versus Shape-Memory Effect (SME).....	60
3.2.2.4.	Shape Memory Polymers (SMPs).....	61
3.2.2.5.	Thermo-Responsive SMPs .....	63
3.2.3.	Design of Actuation Mechanism, Geometric and Material Distribution .....	71
3.2.4.	Modelling and Simulation .....	73
3.3.	Process Flow of 4DP.....	75
3.4.	The Advancement of 4DP .....	77
3.4.1.	4D Printing Applications .....	78
3.4.1.1.	Self-assembly.....	78
3.4.1.2.	Self-adaptability.....	79
3.4.1.3.	Self-repair.....	80
3.5.	Types of Shape-Shifting Behaviours and Shape Transformation Actuation .....	80
3.6.	Challenges, Research Gaps and Future Work .....	97
3.6.1.	Materials.....	97
3.6.2.	Design, Modelling and Simulation.....	99
3.6.3.	AM Processes .....	100
3.7.	Comparison of FGAM and 4DP .....	101
3.8.	Chapter Summary .....	103
	<b>Chapter 4 A Framework for Selecting Thermo-Responsive Shape Memory Polymers for 4D Printing (4DP).....</b>	<b>104</b>
4.1.	Introduction .....	104
4.2.	Material Selection Process Framework.....	105
4.3.	Methods .....	109

4.3.1.	Materials and Fabrication of Test Specimens .....	109
4.3.2.	Tools and Equipment .....	112
4.3.3.	Experimental Procedures for Thermo-rheological Characterisation .....	114
4.3.3.1	Process 1: Thermomechanical Programming Process .....	115
4.3.3.2	Process 2: Shape Recovery Process .....	116
4.3.4.	Measuring and Recording of Results .....	116
4.4.	Results and Discussions .....	121
4.4.1.	Phase 1 Filament .....	121
4.4.2.	Phase 2 ME Printed Structure .....	137
4.5.	Framework Validation .....	150
4.5.1.	Workshops .....	150
4.5.2.	Semi-structured Interviews .....	154
4.5.3.	Framework Validation Findings .....	155
4.5.4.	Design Refinements to The Framework .....	163
4.5.5.	User Guide .....	164
4.5.6.	Limitations of the Validation Study and the Framework .....	177
4.6.	Chapter Summary .....	178
	<b>Chapter 5 Development and Testing of Material Extrusion Additive Manufactured Polymer-Textile Composites .....</b>	<b>180</b>
5.1.	Introduction .....	180
5.2.	Factors affecting ME Printed Polymer-Textile Composites .....	184
5.2.1.	Printing Material .....	185
5.2.2.	Textile Substrate .....	187
5.2.3.	Printer Settings .....	190
5.3.	Methods .....	193
5.3.1.	Materials and AM Process .....	193
5.3.2.	Test Procedures .....	197
5.4.	Results and Discussion .....	198
5.5.	Chapter Summary .....	209
	<b>Chapter 6 4D Printed Shape-Changing Thermo-responsive Textiles .....</b>	<b>211</b>
6.1.	Introduction .....	211
6.2.	Shape Transformation Studies .....	213
6.3.	Methods .....	228
6.3.1.	Materials and AM Processes .....	228
6.3.2.	Experimental Procedures .....	231

6.4.	Results and Discussion.....	236
6.4.1.	Geometrical Dimensions .....	236
6.4.1.1.	Experiment 1: Effect of Tr and Structural Thickness .....	236
6.4.1.2.	Experiment 2: Effect of Structural Width and Length .....	240
6.4.2.	Structural Arrangements .....	246
6.4.2.1.	Experiment 3: Single Column and Multiple Rows .....	246
6.4.2.2.	Experiment 4: Multiple Columns and Single Row .....	250
6.4.2.3.	Experiment 5: Multiple Columns and Rows.....	255
6.4.2.4.	Experiment 6: Varied Row arrangements .....	257
6.4.2.5.	Experiment 7: Print Configuration .....	262
6.4.2.6.	Experiment 8: Print Configuration with Varied Row arrangements .....	264
6.4.3.	Potential Applications.....	267
6.4.4.	Limitations of the Study and Future Work .....	268
6.5.	Chapter Summary .....	269
	<b>Chapter 7 Conclusions and Suggestions for Future Work.....</b>	<b>272</b>
7.1.	Summary of Work to Answer the Research Questions.....	272
7.2.	Summary of Contribution to New Knowledge .....	274
7.2.1.	Theoretical Knowledge on FGAM and 4DP .....	274
7.2.2.	Material Selection Framework for 4DP .....	276
7.2.3.	Development and Testing of ME Polymer-Textile Composite.....	277
7.2.4.	Development of 4D Printed Shape-Changing Thermo-Responsive Textiles ..	278
7.3.	Suggestions for Future Work .....	279
7.3.1.	Study on 4DP .....	279
7.3.2.	Material Selection Framework for 4DP .....	280
7.3.3.	Development and Testing of ME Polymer-Textile Composite.....	280
7.3.4.	Development of 4D Printed Shape-Changing Thermo-Responsive Textiles ..	281
	<b>List of Publications .....</b>	<b>282</b>
	<b>References.....</b>	<b>284</b>
	Appendix I. ME Troubleshooting.....	311
	Appendix II. Semi-structured Expert Interview Questions.....	312
	Appendix III. Summary of FGAM Findings.....	314
	Appendix IV. BREO Acceptance Letter .....	319
	Appendix V. Participation Information Sheet .....	320
	Appendix VI. Material Framework Selection User Guide.....	322
	Appendix VII. Expert Interview Questions.....	326

# List of Figures

## Chapter 1 Introduction

Figure 1.1. Scope of research.....	5
------------------------------------	---

## Chapter 2 Functionally Graded Additive Manufacturing (FGAM)

Figure 2.1. Metal-ceramic reinforced-based FGM adapted by Gupta and Talha (2015). ....	16
Figure 2.2. Fabrication methods for thin and bulk FGMs.....	17
Figure 2.3. Differences between conventional MMAM and multi-material FGAM, with reference to Takahashi <i>et al.</i> (2016).....	19
Figure 2.4. Conceptual diagram showing voxels arranged in 3D form, produced for ISO/ASTM TR52912 (2020), with reference to Takahashi <i>et al.</i> (2016). ....	19
Figure 2.5. Types of FGM compositions. ....	20
Figure 2.6. Varied densification of FGAM.....	21
Figure 2.7. FGM in nature. Cross section of (A) palm trees and (B) bone. ....	21
Figure 2.8. Functionally graded concrete by Keating (2012). ....	22
Figure 2.9. Weight reduction using radially graded density by Keating (2012).....	22
Figure 2.10. Two materials FGAM.....	23
Figure 2.11. Types of composition gradient. (A) three materials and (B) switched composition.....	23
Figure 2.12. Combined composition. ....	24
Figure 2.13. Forms of gradient. (A) discrete or discontinuous and (B) continuous.....	25
Figure 2.14. Types of compositional gradient. (A) radial and (B) longitudinal. ....	25
Figure 2.15. Representation of classifying FGAM gradients adapted by Muller, Mognol and Hascoet (2012). ....	26
Figure 2.16. FGAM process flow. ....	27
Figure 2.17. Printing directions for each section represented from the top view. (A) Unidirectional deposition and (B) multi-directional deposition. ....	32
Figure 2.18. Schematic diagram of static mixer and triple extruder, produced for ISO/ASTM TR52912 (2020).....	33
Figure 2.19. CAL system for volumetric AM adapted by Kelly <i>et al.</i> (2019). ....	34
Figure 2.20. Compliant gripper with discrete gradient of composition change at 7.62mm each layer, adapted by Chung and Das (2008). ....	35
Figure 2.21. Sub-materials continuously fused together in a gradient manner. ....	36
Figure 2.22. Multi-material mullion interface by Grigoriadis (2018) using material jetting. (A) Exploded view of multi-material mesh and (B) fabricated specimen. ....	37
Figure 2.23. Microstructural analysis of a specimen built from UC. (A) FGM specimen and (B) metallography.....	38
Figure 2.24. Discrete gradient composition change between 304L SS and Inconel 625 using a 910W YAG laser with hatch angle of 60° by Carroll <i>et al.</i> (2016). (A) schematic diagram and (B) photograph of specimen after sectioning. ....	39

## Chapter 3 4D Printing (4DP)

Figure 3.1 The behaviour of <i>Mimosa Pudica</i> as a direct manifestation of the 4DP concept (Alamy, 2021).....	50
--	----

Figure 3.2. The key bases of 4DP. ....	52
Figure 3.3. Projection Microstereolitho-graphy (PμSL) machine by Ge et al. (2016). ....	53
Figure 3.4. SRMs and their transition phenomena that link between their associated input (stimulus) and output (response). ....	55
Figure 3.5. Various shape-shifting configurations achieved through inhomogeneous SCE demonstrated by Thérien-Aubin <i>et al.</i> (2013). ....	56
Figure 3.6. A larger shape change structure constructed using the ring stretching primitives capable of two dimensional (2D) folding and stretching into a double curvature (Raviv <i>et al.</i> , 2014). ....	58
Figure 3.7. Letter formation (S-A-L) constructed using joints of folding primitives (Raviv <i>et al.</i> , 2014). ....	58
Figure 3.8. The magnitude of the barrier of SCE and SME. (A) printed shape and (B) actuated shape (X. Wu <i>et al.</i> , 2013).. ....	60
Figure 3.9. Molecular mechanism of thermally induced SME with dual-shape capability. ...	62
Figure 3.10. One-way SME.....	65
Figure 3.11. Two-way SME.....	66
Figure 3.12. Multi-way SME.....	67
Figure 3.13. Different thermally induced shape-shifting behaviours are achieved by modifying the orientation and position of the deposited materials within a bilayer multi-material structure, demonstrated by Wu et al. (2016) through heating in water. ....	73
Figure 3.14. Software architecture and types of solutions for 4DP.....	74
Figure 3.15. 4DP process flow showing the four major phases.....	76
Figure 3.16. Magnetic stent adapted by Wei <i>et al.</i> , (2017). (A) the temporary shape for deployment and (B) the permanent shape for performance. ....	80
Figure 3.17. Introducing varied recovery speed and asymmetrical shape change within a printed structure using different print patterns and infill density (A and B) by Nam and Pei (2020). ....	83
Figure 3.18. Helical line with graded hinge sections to perform sequential folding recovery adapted by Yu <i>et al.</i> (2015). ....	83
Figure 3.19. Grayscale 4DP method for DLP to introduce different degree of cure and crosslinking densities within a photopolymerized sample proposed by J. Wu et al. (2018). ....	84
Figure 3.20. The relationship of FGAM and 4DP in AM.....	102

#### **Chapter 4 A Framework for Selecting Thermo-Responsive Shape Memory Polymers for 4D Printing (4DP)**

Figure 4.1. The material selection process workflow.....	106
Figure 4.2. The forming jig to program the material specimen into a 25mm diameter circular bend.....	112
Figure 4.3. The forming jig to program the material specimen into a 90° fold. ....	113
Figure 4.4. Objects that can be used as alternative forming jigs. (A) plastic bottle (B) right-angle cube. ....	113
Figure 4.5. Experiment set up.....	114
Figure 4.6. The three stages of DSM heat induced SMP. (A) printed shape, (B) programmed (temporary) shape and (C) recovered shape.....	115
Figure 4.7. The shape fixity chart (not in actual size). ....	118
Figure 4.8. The bend recovery chart (not in actual size). ....	119
Figure 4.9. The fold recovery chart (not in actual size).....	120

Figure 4.10. The shape fixity of materials specimens of different polymer types. ....	123
Figure 4.11. The ranking of materials based on their shape recovery ratings, ranging from the highest to the lowest, from left to right, for both programming conditions (bending and folding). ....	127
Figure 4.12. The ranking of materials based on their shape recovery ratings, ranging from the highest to the lowest, from left to right, for both programming conditions (P1 S3 bending and folding). ....	129
Figure 4.13. The shape memory properties of materials in five repetitive thermo-mechanical cycle. ....	137
Figure 4.14. The shape memory properties of materials in filament form (P1 S2) versus ME printed structure (P2 S2). ....	139
Figure 4.15. An inverse curvature shape recovery from fold deformation. ....	139
Figure 4.16. Comparison of the shape recovery percentages of the filaments (P1 S3) with the ME printed structures (P2 S3) for both programming conditions (bending and folding). ....	142
Figure 4.17. Comparison of the shape recovery ratings of Material No. 11 filaments (P1 S4) with the ME printed structures (P2 S4) after five repetitive thermo-mechanical cycles. ....	147
Figure 4.18. The experiment setup and prepared material specimens by a participant. ....	151
Figure 4.19. Participant conducting the practical task. ....	152
Figure 4.20. The disciplines of the participants. ....	155
Figure 4.21. The average rating for the material selection process. ....	158
Figure 4.22. The corrected method to measure an inverse curvature using the fold recovery chart. (A) previous version and (B) updated version. ....	162
Figure 4.23. The average rating for the measuring charts. ....	162
Figure 4.24. The correct placement and alignment of the material specimen on the shape fixity and shape recovery charts. ....	163
Figure 4.25. The design refinements to the fold recovery chart. (A) previous version, the initial label “-0” was modified into the rating system and (B) highlighted area was added to initiate the placement and alignment of the specimen. ....	164
Figure 4.26. Introduction to the material selection framework. ....	166
Figure 4.27. Fabrication of material specimens, tools and equipment. ....	167
Figure 4.28. Thermo-rheological characterisation: Process 1. ....	168
Figure 4.29. Thermo-rheological characterisation: Process 2. ....	169
Figure 4.30. The material selection process workflow. ....	170
Figure 4.31. The material selection process flowchart. ....	171
Figure 4.32. Experimental procedures and evaluation criteria (Stage 1 and 2). ....	172
Figure 4.33. Experimental procedures and evaluation criteria (Stage 3 and 4). ....	173
Figure 4.34. Measuring and recording of results. ....	174
Figure 4.35. Technical drawing of the circular bend forming jig (not in actual size). ....	175
Figure 4.36. Technical drawing of the 90° fold forming jig (not in actual size). ....	176

## **Chapter 5 Development and Testing of Material Extrusion (ME) Additive Manufactured Polymer-Textile Composite**

Figure 5.1. Fully AM fabricated structure. ....	181
Figure 5.2. AM polymer-textile composite snap fastener demonstration. (A) secured and (B) open. ....	182

Figure 5.3. Desktop ME printer (Original Prusa i3 MK3S 3D Printer) setup for ME onto the textile substrate.....	184
Figure 5.4. Print layout B. (A) PLA printed on net textile substrate and (B) PLA printed on voile textile substrate. ....	190
Figure 5.5. Illustration of the ME polymer-textile composite for the T-Peel test panel.....	194
Figure 5.6. T-Peel test specimen (not drawn to scale). ....	195
Figure 5.7. Technical drawing of the T-Peel test specimen in line with BS EN ISO 11339 (2010).....	197
Figure 5.8. (A) Test setup, (B) failure mode for the PLA – Nylon (net structure) – PLA orientation and (C) failure of an adherend (cohesive substrate failure). (F1-1 to F1-6= sample label).....	199
Figure 5.9. (A) Test setup, (B) failure mode for the PLA – Polyester (voile structure) – PLA orientation and (C) adhesion failure (delamination). (F2-1 to F2-6= sample label). ....	200
Figure 5.10. (A) Test setup, (B) failure mode for the PLA – Nylon (voile structure) – PLA orientation and (C) failure of an adherend (cohesive substrate failure). (F3-1 to F3-6= sample label).....	201
Figure 5.11. Force versus extension plots for six specimens with the PLA – Nylon (net structure) – PLA orientation. ....	202
Figure 5.12. Force versus extension plots for six specimens with the PLA – Polyester (voile structure) – PLA orientation. ....	204
Figure 5.13. Force versus extension plots for six specimens with the PLA – Nylon (voile structure) – PLA orientation. ....	205
Figure 5.14. Comparison of the force versus extension plots for the three bonded ME printed polymer-textile composites. ....	207

## **Chapter 6 4D Printed Shape-Changing Thermo-Responsive Textiles**

Figure 6.1. The differences in thermally induced shape changing behaviour. (A) SMP printed on its own and (B) SMP printed onto a textile substrate.....	212
Figure 6.2. Experiment 1 Structural thickness manipulation.....	217
Figure 6.3. Experiment 2 Structural width and length manipulation. ....	217
Figure 6.4. Experiment 4 Multiple columns and single row with structural width and length manipulation.....	221
Figure 6.5. Experiment 5 Multiple columns and rows manipulation.....	221
Figure 6.6. Direct ME of polymers onto textile fabrics using print layout A.....	228
Figure 6.7. Lifting and curling of the printed structure when did not bond properly with the previous layer.....	230
Figure 6.8. Printed single-line border to prevent frayed edges when the fabric was cut and to enable the specimens to be cut into the same size. ....	231
Figure 6.9. The specimen immersed in the heated water undergoing shape transformation into a circular bend.....	232
Figure 6.10. The impact of the water circulation generated by the thermal immersion circulator on shape transformation.....	233
Figure 6.11. Deformation classifications and their assigned colour codes. ....	234
Figure 6.12. The bend recovery chart (15mm - 45mm). ....	235
Figure 6.13. Bend occurred in an opposite direction to the first print layer. (A) schematic diagram and (B) photograph of specimen. ....	236
Figure 6.14. Effect of $T_r$ and structural thickness on the response time.....	238

Figure 6.15. The controllability and accuracy of deformation can be improved by increasing the number of printed rows instead of modifying the structural width. ....	247
Figure 6.16. Continuous cartridge pleats with double pinch pleats on the other side.....	250
Figure 6.17. Increase the precision of the projecting pleats by introducing multiple printed rows. ....	251
Figure 6.18. Pipe organ pleats.....	255
Figure 6.19. The shape-shifting behaviour when printed in multiple columns and rows with column spacing of 35mm.....	255
Figure 6.20. Sinusoidal strip by Tibbits et al. (2014) operates under the principle of a bilayer actuator made up of expanding material (water-responsive hydrogel) and passive rigid material. ....	262
Figure 6.21. Cartridge pleats with waving effect.....	262
Figure 6.22. 4DP as a novel technique for 3D manipulation of textile fabrics. (Top with 3D printed shoulder piece by Labeledby (2021)). ....	267

## **Chapter 7 Conclusions and Suggestions for Future Work**

Figure 7.1. Brainstorming session with AM experts to specify and analyse the limitations and research gaps of FGAM.....	276
---	-----

## List of Tables

### Chapter 1 Introduction

Table 1.1. Key topics within each research scope.....	5
Table 1.2. Research methods for collecting and analysing data. ....	10
Table 1.3. Justification of methodological choices, with reference to Hu (2019). ....	13

### Chapter 2 Functionally Graded Additive Manufacturing (FGAM)

Table 2.1. Material structure and properties of a (A) traditional composite, (B) coated or laminated composite and (C) FGM composite.....	15
Table 2.2. Manufacturing methodology of FGAM. ....	28
Table 2.3. AM technologies for FGAM.....	30
Table 2.4. Locally controlled properties by changing the build parameters investigated by Li et al. (2002).....	32
Table 2.5. FGAM applications (Gilbert et al., 2011; Mahamood and Akinlabi, 2017a; Loh et al., 2018; Parihar, Setti and Sahu, 2018; Sarathchandra, Subbu and Venkaiah, 2018; Saleh et al., 2020; Pei et al., 2021).....	41

### Chapter 3 4D Printing (4DP)

Table 3.1 The classifications of different types of SRMs (Laitinen et al., 2020). ....	54
Table 3.2. Examples of linear volume expansion, contraction and folding shape change through water activation by Raviv et al. (2014). (A) printed shape and (B) actuated shape. ....	57
Table 3.3. The comparison between SMP and SMA (Liu, Qin and Mather, 2007; Yüce, 2017).....	59
Table 3.4. Comparisons between SCM and SMM.....	61
Table 3.5. The classification of SMPs based on their structure (Kolesov, Dolynchuk and Radusch, 2015; Jose et al., 2020; Strzelec, Sienkiewicz and Szmechtyk, 2020).....	62
Table 3.6. The shape memory thermomechanical characterisation of DSM thermo-responsive SMP.....	69
Table 3.7. Characterisation techniques for SMPs (Wagermaier et al., 2009; Basit, 2016; Jose et al., 2020; Parameswaranpillai et al., 2020). ....	70
Table 3.8. 4DP software solutions and function. ....	74
Table 3.9. Manufacturing methodology of 4DP. ....	76
Table 3.10. Basic shape-shifting behaviours. ....	81
Table 3.11. Examples of combined shape-shifting behaviours. ....	82
Table 3.12. Types of shape transformation actuation.....	86
Table 3.13. Examples of self-actuated shape change (Multi-material mechanism: SCM and passive material).....	88
Table 3.14. Examples of self-actuated shape change (Multi-material mechanism: SCM and active material).....	89
Table 3.15. Examples of self-actuated shape change (Multi-material mechanism: SMP and passive material).....	91
Table 3.16. Examples of self-actuated shape change (Multi-material mechanism: SMP and active material).....	92
Table 3.17. Examples of one-way shape-memory transformation. ....	93

Table 3.18. Examples of multi-material one-way shape-memory transformation.....	95
Table 3.19. Examples of two-way shape-memory transformation.....	96
Table 3.20. FGAM versus 4DP.....	101

#### **Chapter 4 A Framework for Selecting Thermo-Responsive Shape Memory Polymers for 4D Printing (4DP)**

Table 4.1. The material selection process.....	107
Table 4.2. The material list with their tradenames and printing temperatures.....	109
Table 4.3. The dimensions for the filament and ME printed structure test specimen.....	111
Table 4.4. The fabrication settings for ME printed specimen.....	111
Table 4.5. Types of measuring charts.....	116
Table 4.6. P1 S1 Shape fixity.....	122
Table 4.7. P1 S2 Bending.....	125
Table 4.8. P1 S2 Folding.....	126
Table 4.9. P1 S3 Bending.....	127
Table 4.10. P1 S3 Folding.....	130
Table 4.11. P1 S4 Bending.....	133
Table 4.12. P1 S4 Folding.....	135
Table 4.13. P2 S1 Shape Fixity.....	138
Table 4.14. P2 S2 Bending.....	138
Table 4.15. P2 S2 Folding.....	141
Table 4.16. P2 S3 Bending.....	143
Table 4.17. P2 S3 Folding.....	145
Table 4.18. P2 S4 Bending.....	148
Table 4.19. P2 S4 Folding.....	149
Table 4.20. Likert Scale 1 for the material selection process.....	153
Table 4.21. Likert Scale 2 for the measuring charts.....	154
Table 4.22. The general background of participants and the validation phase involved....	156
Table 4.23. Quantitative feedback collected from the participants to evaluate the completeness, effectiveness and usability of the material selection process.....	157
Table 4.24. Quantitative feedback collected from the participants to evaluate the effectiveness and usability of the shape fixity chart.....	159
Table 4.25. Quantitative feedback collected from the participants to evaluate the effectiveness and usability of the bend recovery chart.....	160
Table 4.26. Quantitative feedback collected from the participants to evaluate the effectiveness and usability of the fold recovery chart.....	161
Table 4.27. User guide contents.....	164

#### **Chapter 5 Development and Testing of Material Extrusion (ME) Additive Manufactured Polymer-Textile Composite**

Table 5.1. Examples of applications and future research direction for ME polymer-textile composite.....	183
Table 5.2. Common thermoplastics used in ME and their properties.....	186
Table 5.3. Different variables of textile substrates that can affect the polymer-textile adhesion.....	187

Table 5.4. Types of print layout. (A) polymer – textile substrate – polymer and (B) polymer – textile substrate.....	189
Table 5.5. The list of ME printer settings taken into consideration during the fabrication of the polymer-textile composites. ....	191
Table 5.6. Scenarios that indicate the Z–distance was set too high.....	192
Table 5.7. Properties of the three textile substrates (mesh fabrics) used for the ME polymer-textile composites. ....	193
Table 5.8. The printing procedure involved in manufacturing ME polymer-textile composite (print layout A) to create T-Peel test panel. ....	196
Table 5.9. The peel forces and strength, standard deviation and coefficient of variation for the six specimens with the PLA – Nylon (net structure) – PLA orientation.....	203
Table 5.10. The peel forces and strength, standard deviation and coefficient of variation for the six specimens with the PLA –Polyester (voile structure) – PLA orientation.....	204
Table 5.11. The peel forces and strength, standard deviation and coefficient of variation for the six specimens with the PLA – Nylon (voile structure) – PLA orientation. ....	205
Table 5.12. Average peel forces and strengths and coefficients of variation for the three bonded ME printed polymer-textile composites.....	207

## **Chapter 6 4D Printed Shape-Changing Thermo-Responsive Textiles**

Table 6.1. List of experiments to study the shape transformation of 4D printed shape-changing thermo-responsive textiles. ....	214
Table 6.2. Experiment 3 Structural width and number of rows manipulation.....	218
Table 6.3. Experiment 6 Varied row arrangements. ....	222
Table 6.4. Experiment 7 Print configuration.....	224
Table 6.5. Experiment 8 Print configuration with varied row arrangements. ....	226
Table 6.6. The printing procedure for Experiments 8 and 9 specimens. ....	229
Table 6.7. Effect of Tr and structural thickness on the response rate and SCE. ....	237
Table 6.8. Effect of structural thickness on the shape deformation. ....	239
Table 6.9. Effect of structural width and length on the response rate and SCE. ....	242
Table 6.10. Effect of structural width on the shape deformation.....	243
Table 6.11. Effect of structural width and number of rows on the response rate and SCE. ....	247
Table 6.12. Single column and multiple rows. ....	248
Table 6.13. The influence of structural width and length on the response rate and SCE of multiple columns and single row. ....	253
Table 6.14. The influence of column spacing on the bending diameter and shape-shifting pattern.....	256
Table 6.15. The influence of structural width on the response rate and SCE of multiple columns and rows. ....	257
Table 6.16. The influence of row arrangements on the response rate and SCE.....	259
Table 6.17. The influence of structural width on the response rate and shape-shifting behaviour. ....	263
Table 6.18. The influence of row arrangements on the response rate and SCE.....	265
Table 6.19. Summary of key findings.....	270

## **Chapter 7 Conclusions and Suggestions for Future Work**

Table 7.1. Research questions and objectives defined for this research. ....	272
--	-----

## **Citation for this Thesis**

Loh, H.H. (2021) "4D Printing of Shape-Changing Thermo-Responsive Textiles". (PhD Thesis). College of Engineering, Design and Physical Sciences. Department of Design. Brunel University London, United Kingdom.

## Chapter 1

### Introduction

This chapter introduces the topic of this research, presents the research aim, questions and objectives, and discusses the research methods used to collect and analyse data. Finally, this chapter provides an outline of the thesis.

#### 1.1. Research Background

Additive Manufacturing (AM), commonly known as 3D Printing (3DP) enables the fabrication of geometrically complex components by precisely placing material(s) one layer at a time in position within a design domain from digital information. It is defined as the process of joining materials to make parts from 3D model data, usually layer upon layer, as opposed to subtractive manufacturing and formative manufacturing methodologies (ISO/ASTM 52900, 2017). AM benefits from entirely customised objects with a high level of geometrical complexity, reduced manufacturing costs and lead times, shorter product development cycles, and increase research and development efficiency (Redwood, Schöffner and Garret, 2017; Pérez *et al.*, 2020). The AM industry has been growing rapidly throughout the last 10 years expanding from making one-off prototypes to the creation of full-scale end-use products across different industrial sectors, pioneering aerospace, automotive and biomedical sectors, followed by consumer products (Wohlers Associates, 2021). The awareness and adoption of AM in the fashion and textile industry rose in 2010 when an influential designer, Iris Van Herpen showcased her first 3D printed dress (Van Herpen, 2010). Since then, AM technologies are being adopted by more fashion designers to conceive new polymer-textile functionalisation and innovative aesthetic print techniques that cannot be achieved by the conventional textile fabric itself or using traditional manufacturing processes. This led to new growth of wearables AM parts, promotion of sustainability, and localised production of on-demand and personalised garments. Recently, AM was instrumental in the fight against COVID-19, through the development of personal protective equipment (PPE) and other medical equipment such as test swabs and ventilators (Singh, Prakash and Ramakrishna, 2020).

New printing methods, machinery, software and materials are actively being researched and advanced to open new AM markets and applications. The advancement of today's AM systems has introduced two emerging material-driven AM strategies for fabricating functionally graded materials (FGMs) and stimuli-responsive materials (SRMs), termed as

Functionally Graded Additive Manufacturing (FGAM) and 4D Printing (4DP), respectively. This research defined FGAM as a layer-by-layer fabrication process that involves gradationally varying the material organisation within a component to achieve an intended function. Whilst 4DP is defined as the use of AM to produce a freeform stimuli-responsive component that can sense and actuate in response to an appropriate stimulus over time, without the reliance on power-source, robotics or electro-mechanical devices (Tibbits, 2013). This research aims to take a new perspective and extend the forefront of the discipline of FGAM and 4DP to facilitate new interpretation of functional AM textiles that possess aesthetic and functional features when exposed to external stimuli.

Although both fields have attracted substantial interests from academia and industry of different disciplines ever since being introduced, the theoretical knowledge about FGAM and 4DP is fragmented. Very little information was found in the literature of FGAM compared to 4DP. The types of AM technologies that can support FGAM and 4DP and their process chain from design to manufacturing are underexplored. The interpretations of their concepts, current state-of-the-art and capabilities require greater clarifications in order to identify the appropriate AM strategy, materials, design and fabrication methods to create thermo-responsive textiles. In addition, a common conceptual understanding and standardised use of terms in FGAM and 4DP need to be defined and established to encourage researchers to adopt a more consistent approach and standardised set of vocabulary associated with these emerging fields.

To enable thermo-responsive textiles to self-actuate and reconfigure when subjected to heat, thermo-responsive shape-memory polymers (SMPs) need to be integrated into textile structures. Review findings have shown that the current availability of SMPs for AM in the commercial market is very limited and expensive. Most SMPs found in the literature mostly centre around laboratories-based developed materials that cannot be easily purchased or obtained, or their product names and sources are kept confidential. Furthermore, the characterisation methods of SMPs presented in most academic and research publications are usually advanced with the use of complex algorithms and expensive specialist equipment accessible only by specialist users. This is a significant drawback as some researchers and most non-technical users such as designers, practitioners, academics and students who are interested in the area do not have the same knowledge and background to fully understand the advanced scientific theories and practices. To address the fundamental issues of material availability and affordability, a material selection framework for experimenting with material shape memory properties and functional behaviours, as well as discovering commercially available thermoplastics as potential SMPs for use in ME 4DP

had to be developed. Such framework would be purposeful for the exploration of 4DP or can be added into the wider context of 4DP product design development. The theoretical knowledge and practical process workflow tailored for non-technical audiences for developing self-transforming structures should be made available to increase wider adoption and accelerate new applications and research outputs, such as thermo-responsive textiles.

## 1.2. Research Aim, Objectives and Research Questions

This research aims to propose a material selection framework for commercially available thermoplastics as SMPs to create shape-changing thermo-responsive textiles. Four research questions and objectives were defined to fulfil the aim of this research.

### **Research question (1)**

What are the key differences between 4D Printing (4DP) and Functionally Graded Additive Manufacturing (FGAM)?

### **Research objective (1)**

To examine the state of the art of 4D Printing (4DP) and Functionally Graded Additive Manufacturing (FGAM) through literature review and expert interviews.

### **Research question (2)**

How do we select suitable shape memory polymers (SMPs) for material extrusion to produce 4D printed parts?

### **Research objective (2)**

To develop a material selection process to confirm the material characteristics that are suitable for 4D Printing (4DP).

**Research question (3)**

Which material extrusion build parameters and textile properties influence the adhesion of a polymer-textile composite?

**Research objective (3)**

To undertake literature reviews and experimental work to examine the build parameters and textile properties that influence the polymer and textile adhesion.

**Research question (4)**

How do the geometrical dimensions and structural arrangement influence the shape transformation of the thermo-responsive textile?

**Research objective (4)**

To undertake experimental work and analyse the results to highlight the factors that influence the shape transformation of thermo-responsive textiles.

### 1.3. Research Scope

The scope of this research can be categorised into four subjects as shown in Figure 1.1. The topics defined in Table 1.1 were progressively investigated to determine the AM strategy, materials, design and fabrication process for shape-changing thermo-responsive textiles.

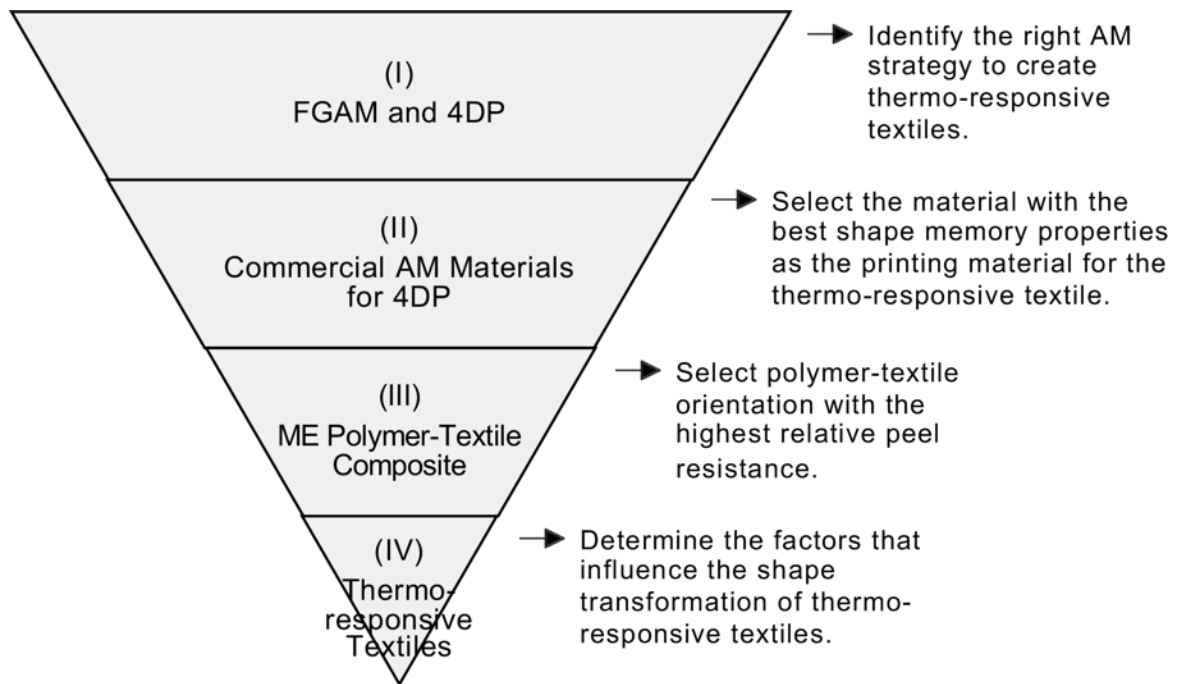


Figure 1.1. Scope of research.

Table 1.1. Key topics within each research scope.

Research Scope	Key Topics
(I) FGAM and 4DP	Concept and background Key terms and definitions Process flow Materials, design and fabrication methods Advancements and potential applications Challenges, research gaps and limitations
(II) Commercial AM Materials for 4DP	Development of material selection framework Thermo-rheological characterisation Methods and tools Shape memory properties results and discussions Framework validation
(III) ME Polymer-Textile Composite	Factors affecting ME printed polymer-textile composite Methods and tools T-Peel test Adhesion strength results and discussions
(IV) Thermo-Responsive Textile	Factors influencing the shape transformation of thermo-responsive textile

	Methods and Tools Shape transformation results and discussions Potential applications
--	---

## 1.4. Organisation of the Thesis

This thesis is formatted in a manuscript-based consist of seven chapters, structured into three research phases: (1) research exploration and review, (2) development, experimental work, evaluation, revision and discussion, followed by (3) conclusion.

### 1) Research exploration and review:

The research started with the collection of theoretical knowledge for FGAM and 4DP by literature reviewing scientific papers, following discussions with respected academia and industry experts from the two fields to confirm the findings.

#### **Chapter 1. Introduction**

Chapter one gives the introduction, background, aim, questions and objectives of this research, presents the organisation of this thesis, and discusses the research approach and methods adopted to answer the research questions.

#### **Chapter 2. FGAM**

Chapter two reviews the state-of-art literature to define and establish the terminologies and fundamental concepts of FGAM. This chapter also provides an overview of the FGAM process chain from design to manufacturing and its advancement enabled by present AM technologies. Furthermore, this chapter identifies the current challenges and research gaps concerning "materials-product-manufacturing" that need to be addressed to exploit the true potential of FGAM practices on a commercial or economic scale. The possible strategies in overcoming barriers and recommendations for future directions for FGAM to take off are discussed. These findings help to identify the applicability of FGAM for the creation of shape-changing thermo-responsive textiles.

### **Chapter 3. 4DP**

Chapter three gives an overview of the concept, process flow, advancement and potential applications of 4DP. This chapter extensively reviews the key bases in 4DP and their current research development, focusing on ME technology, stimuli-responsive actuator materials, predominantly thermo-responsive SMPs. The concept and underlying mechanisms of shape change effect (SCE) in shape change materials (SCMs) and the shape memory effect (SME) in SMPs are studied and compared. This chapter also analyses the different types of shape-shifting behaviours and shape transformation actuation. Different use of SRMs, structure design, modelling and fabrication methods of 4DP structure to perform certain controlled shape-shifting behaviours when subjected to appropriate stimuli are exemplified. To conclude, this chapter outlines the current barriers and limitations of this emerging AM strategy for SMPs-based fabrication. Finally, this chapter analyses the key aspects that separate and bridges FGAM and 4DP, and addresses selection of the best AM strategy to answer the research aim and objectives.

2) Development, experimental work, revision and evaluation:

Chapters four to six are structured to discuss the findings gained from the state-of-the-art review of each literature, followed by the methods, results and discussion, and conclusion.

### **Chapter 4. Material Selection Framework for 4DP**

Chapter four proposes a material selection framework to discover, define and select commercially available thermoplastics as potential SMPs for use in material extrusion 4DP. A systematic material selection process is designed to test, qualitatively and quantitatively measure the shape fixity, response rate and SME of an SMP through thermo-rheological characterisation, without complex algorithms. This chapter also describes the basic theoretical and practical knowledge to create a single-material thermo-responsive dual-state mechanism (DSM) active structure, including design, fabrication, and experimental procedure for programming-recovery characterisation. The shape memory properties of the materials in filament-form and post printed form when activated by different shape recovery temperatures ( $T_r$ ) are investigated and analysed in this chapter.

## **Chapter 5. Development and Testing of ME Additive Manufactured Polymer-Textile Composite**

Chapter five presents the development and testing of polymer-textile composites using PLA filaments on synthetic mesh fabrics using direct ME. This chapter highlights the appropriate combination of printing material, textile substrate, and printer settings to achieve excellent polymer-textile adhesion. Details of the printing process to create polymer-textile composites are described, as are the interfacial strength results of the T-peel tests, and the observed failure modes post-testing. The peel strengths for different ME bonded polymer-textile composites are examined and used to identify the compatibility of materials. The polymer-textile orientation with the highest relative peel resistance is then applied for the creation of 4D printed shape-changing thermo-responsive textiles in Chapter 6.

## **Chapter 6. 4D Printed Shape-Changing Thermo-Responsive Textiles**

The top-performing material and the polymer-textile orientation with the highest relative peel resistance discovered in chapters four and five, respectively, were applied for 4DP of thermo-responsive textiles. Chapter six discusses the design, fabrication, actuation and characterisation methods for the 4D printed shape-changing thermo-responsive textile. This chapter also investigates the opportunity to control the shape deformation and produce different types of shape-shifting behaviours using the geometrical dimensions and structural arrangements of the printed SMP structure on the textile substrate. The optimum geometric parameters to achieve the most predictable and accurate deformation are analysed, and the structural arrangements to achieve particular shape-shifting behaviours are reported. The findings present a design parameter selection guide for designers and researchers to design or produce relevant shape transformations, develop new applications or facilitate future research development. This chapter concludes by providing insight into the potential applications and the limitations in creating 4D printed shape-changing thermo-responsive textiles.

3) Conclusion:

## **Chapter 7. Conclusion**

Chapter seven concludes the thesis by presenting the summary of the work and how the research objectives were met. This chapter also highlights the contribution to knowledge for each chapter, describes the research limitations and suggestions for future work.

## **1.5. Research Methodology**

This section discusses the research approach and methods adopted to answer the research questions (Table 1.2). A mixed-methods approach was taken to collect and analyse both qualitative and quantitative data. The qualitative methods allow in-depth exploration and understanding of the research topics, identify relevant theories, methods, generate descriptive statements and discover ideas. On the other hand, quantitative methods through the use of statistical data in the form of numerical measurements allow the validation of the research findings (Robson and McCartan, 2015; McCombes, 2019). This thesis combines the use of inductive and deductive research approaches. Inductive research was first conducted to observe a pattern, develop a theory and as a starting point for the deductive study. Deductive research is later conducted to test and confirm or invalidate the theory (Streefkerk, 2019).

For this research, the qualitative data was collected using literature review, semi-structured interviews and workshops. The quantitative data was collected using literature review, experiments and questionnaires. Table 1.2 specifies the objectives, while Table 1.3 justifies the methodological choices to answering the research questions. The Design of Experiments (DOE) for material selection for 4DP, development and testing of ME polymer-textile composite and 4D printed shape-changing thermo-responsive textiles are discussed in chapters four, five and six, respectively. Details on the questions used, the sampling method, when and where the activity took place, the response rate for the workshop and semi-structured interview are identified in Chapters 4.5.1 and 4.5.2.

The approaches used to analyse qualitative data include content analysis and thematic analysis. The content analysis quantifies and analyses the meaning, themes and concepts from the collected literature review data (Luo, 2021), while thematic analysis examines the data collected from semi-structured interviews, workshops and questionnaires. Comparative analysis was used to compare and contrast the patterns and trends in the quantitative data.

Table 1.2. Research methods for collecting and analysing data.

Phases	Chapter		Research Questions	Data Collection Methods	Primary or Secondary	Qualitative or Quantitative	Objectives	Data Analysis Methods
Research exploration and review	2	FGAM	What are the key differences between 4DP and FGAM?	Literature review	Secondary	Both	<ol style="list-style-type: none"> <li>1. To obtain an in-depth understanding and evaluation of the state of the art of 4DP and FGAM.</li> <li>2. To identify themes and research gaps that require more investigation.</li> <li>3. To identify the right AM strategy for the creation of thermo-responsive textiles.</li> </ol>	Content analysis
	3	4DP		Semi-structured interviews	Primary	Qualitative	<ol style="list-style-type: none"> <li>1. To validate the literature review findings and confirm the key terms and definitions regarding FGAM.</li> </ol>	Thematic analysis
Development, experimental work, revision and evaluation	4	Material Selection Framework for 4DP	How do we select suitable shape memory polymers (SMPs) for material extrusion to produce 4D printed parts?	Literature review	Secondary	Both	<ol style="list-style-type: none"> <li>1. To develop a material selection process to confirm the material characteristics that are suitable for 4DP.</li> <li>2. To search, evaluate and select the methods and approaches to create a DSM active structure.</li> </ol>	Content analysis

			Experiment	Primary	Quantitative	1. To characterise the shape memory properties of the selected materials.	Comparative analysis
			Workshop	Primary	Qualitative	1. To test the framework with the target users. 2. To gain a deeper understanding of the participants' perceptions. 3. To evaluate and validate the completeness, effectiveness, and usability of the framework. 4. To refine the material selection framework based on the feedback received from the participants.	Thematic analysis
			Semi-structured interviews	Primary	Qualitative		
			Questionnaires	Primary	Quantitative		
5	Development and Testing of ME Additive Manufactured Polymer-Textile Composite	Which material extrusion build parameters and textile properties influence the adhesion of a polymer-textile composite?	Literature review	Secondary	Both	1. To examine the potential correlation between the build parameters and textile properties on the polymer and textile adhesion.	Content analysis
			Experiment	Primary	Quantitative		Comparative analysis
6	4D Printed Shape-Changing Thermo-	How do the geometrical dimensions and structural arrangement influence the	Experiment	Primary	Quantitative	1.1. To investigate the cause-and-effect relationship on the factors that influence the shape	Comparative analysis

		Responsive Textiles	shape transformation of the thermo- responsive textile?				transformation of thermo- responsive textiles.	
--	--	------------------------	---	--	--	--	---	--

Table 1.3. Justification of methodological choices, with reference to Hu (2019).

<b>Research Methods</b>	<b>Reason of Selection/ Strengths</b>	<b>Weaknesses</b>
Semi-structured interview	Informal, flexible and open for discussion, easy to administer, provide in-depth findings and allow follow up or variation.	The pattern might change according to the participant's response. The interviewer must be focused to ensure that the discussion is within scope.
Workshop	Allow direct participant observations, can gain a holistic perspective by seeing full context, allow direct study of participant's reaction, behaviour and attitude, receive instant feedback and opinions, can reveal any challenges, limitations or unexpected outcomes from the study.	Time-consuming, low response rate as suitable only for a specific group of people, might be instructive and affect the behaviour of participants.
Experiments	Discerns cause-and-effect relationships between variables	Cannot accurately or fully simulate real-life situations.
Questionnaire	Quick turnaround, time-effective in gathering information from multiple people at once, standardised responses easy to analyse and less ongoing labour.	Low response rate and wording can bias responses.

## 1.6. Chapter Summary

This chapter has discussed the introduction, background, aim, questions and objectives of this research. The organisation of this thesis and the research approach and methods adopted to answer the research questions were discussed. The next chapter will provide an overview of FGAM in order to identify its applicability for the development of shape-changing thermo-responsive textiles.

## Chapter 2

### **Functionally Graded Additive Manufacturing (FGAM)**

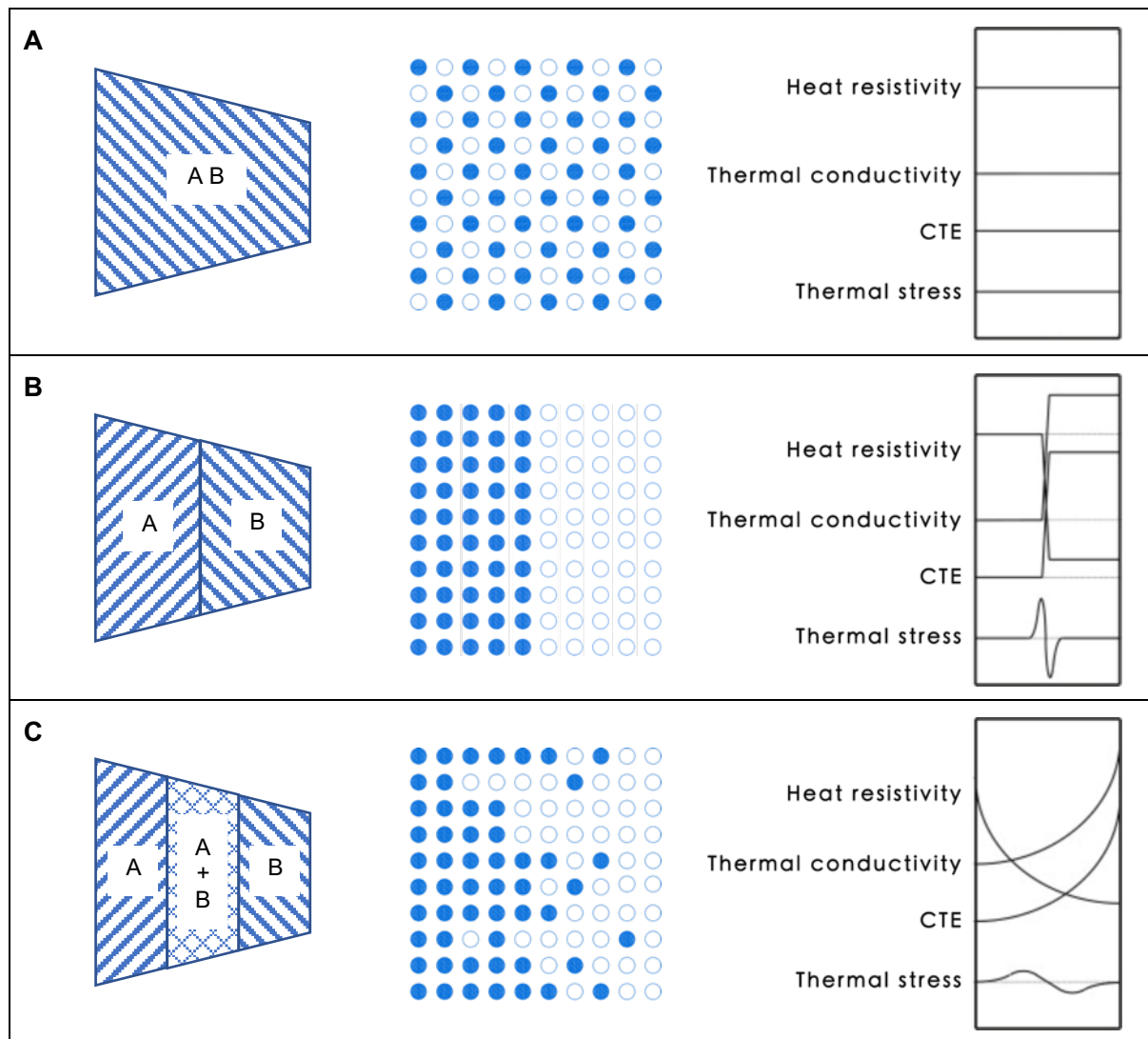
Chapter two reviews the state-of-art literature to define and establish the terminologies and fundamental concepts of FGAM. This chapter also provides an overview of the FGAM process chain from design to manufacturing and its advancement enabled by present AM technologies. Furthermore, this chapter identifies the current challenges and research gaps concerning “materials-product-manufacturing” that need to be addressed to exploit the true potential of FGAM practices on a commercial or economic scale. The possible strategies in overcoming barriers and recommendations for future directions for FGAM to take off are discussed. Based on the findings, it was decided that FGAM was not the appropriate AM strategy to create shape-changing thermo-responsive textiles as it involves a process of modifying material organisation within a component to achieve graded functionalities, on-demand or site-specific properties. This research requires AM strategy that principally integrates stimuli-responsive materials (SRMs) to fabricate products with smart and dynamic features that can self-sense and self-actuate after printing. Although, it can be foreseen that FGAM can be incorporated to create variable-property stimuli-responsive structures with strategically tailored compositions or microstructure as the technology matures.

#### **2.1. Introduction**

Functionally Graded Materials (FGMs) are a class of advanced materials characterised by spatial variation in composition or microstructure across the volume, leading to corresponding changes in the material properties in line with the functional requirements (Oxman, Keating and Tsai, 2012). FGMs attain its multi-functional status by mapping the intended performance requirements to the strategies of material structuring and allocation. They were first developed in 1984 as ultrahigh temperature resistant materials for propulsion system and airframe of space planes to sustain high thermal barriers to overcome the shortcomings of traditional composite materials to withstand harsh working conditions. Traditional composites are homogeneous mixtures which usually require a compromise between the constituent materials to meet the desirable properties (Table 2.1A). The mixing of different materials is often limited by the thermodynamic behaviour of the constituent materials and the limitation imposed by the degree of materials can be mixed with other materials. FGMs can minimise the interfacial stresses between different materials and avoid problems associated with the presence of sharp interface in a coated or laminated composite, such as delamination, cracks caused by the surface tension due to discrete change of

materials properties (Table 2.1B). FGMs overcome this issue by replacing the sharp interface with a gradual transition or systematic transition between two or more material mixtures (Table 2.1C). The magnitude of thermal stress at critical locations can also be controlled. FGMs distribute the material functions using a continuous or quasi-continuous change of material constituents to obtain the best combined properties of both materials and retaining structural stability of the whole part. The differences in micro-structural phases contribute to properties and functions deviations, such as heat resistivity, thermal conductivity, coefficient of thermal expansion (CTE) and thermal stress throughout a one-body material (Shinohara, 2013).

Table 2.1. Material structure and properties of a (A) traditional composite, (B) coated or laminated composite and (C) FGM composite.



● : Ceramic ○ : Metal

Figure 2.1 presents a metal-ceramic reinforced-based FGM which is a classic example of a FGM. The common material combinations of metal–ceramic FGM are Aluminium–Silicon Carbide (Al–SiC), Al–Aluminium Oxide (Al–Al<sub>2</sub>O<sub>3</sub>) and Nickel–Zirconium Dioxide (Ni–ZrO<sub>2</sub>) (El-Galy, Saleh and Ahmed, 2019). The ceramic face enables the FGM to withstand extreme temperatures and harsh chemical environments while the metal reinforcement provides the overall strength and resistance to brittle fracture. Other possible types of material combinations include metal–metal, ceramic–ceramic and ceramic–polymer (El-Galy, Saleh and Ahmed, 2019). Examples of metal–metal FGMs include Al–Copper (Al–Cu), Al–Ni, Ni–Titanium (Ni–Ti), ceramic–ceramic FGMs include SiC–Carbon, SiC–SiC and Carbon–Carbon, and ceramic–polymer FGMs include Glass–Epoxy and Carbon–Epoxy.

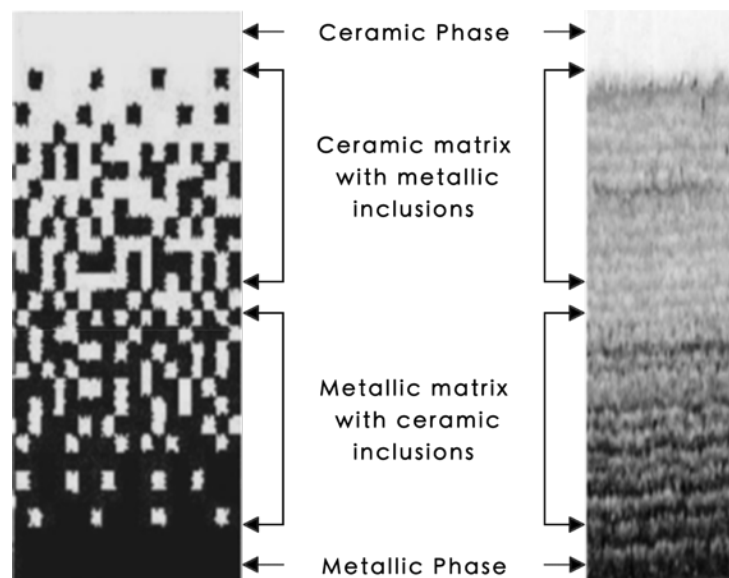


Figure 2.1. Metal-ceramic reinforced-based FGM adapted by Gupta and Talha (2015).

FGMs can be further classified into thin and bulk FGMs. Thin FGMs are processed in the form of thin sections or as surface coating ranges from 5nm to 120µm to have properties of another material that are different from the main material. Thick FGMs are bulk material developed along one, two or three directions, usually ranges 5mm and above (El-Galy, Saleh and Ahmed, 2019).

The conventional fabrication processes of FGM can be divided into gaseous, liquid and solid phase processes based on the state of the starting material. Examples of gaseous fabrication processes include chemical vapour deposition (CVD) or infiltration (CVI), physical vapour deposition (PVD), thermal spraying, plasma spraying and surface reaction. Liquid

processes include doctor blade process, tape casting, slip casting, gel casting, electrophoretic deposition, chemical solution deposition, directed solidification, sedimentation, electrochemical gradation and centrifugal casting. Whilst solid processes include self-propagating high temperature synthesis (SHS), powder metallurgy and spark plasma sintering (SPS) (Mahamood *et al.*, 2012; Shinohara, 2013; Naebe and Shirvanimoghaddam, 2016; Mahamood and Akinlabi, 2017b; El-Galy, Saleh and Ahmed, 2019). Figure 2.2 categorises the process of manufacturing for thin and bulk FGMs. Thermal spraying, electrophoretic deposition and laser cladding can produce both thin and bulk FGMs.

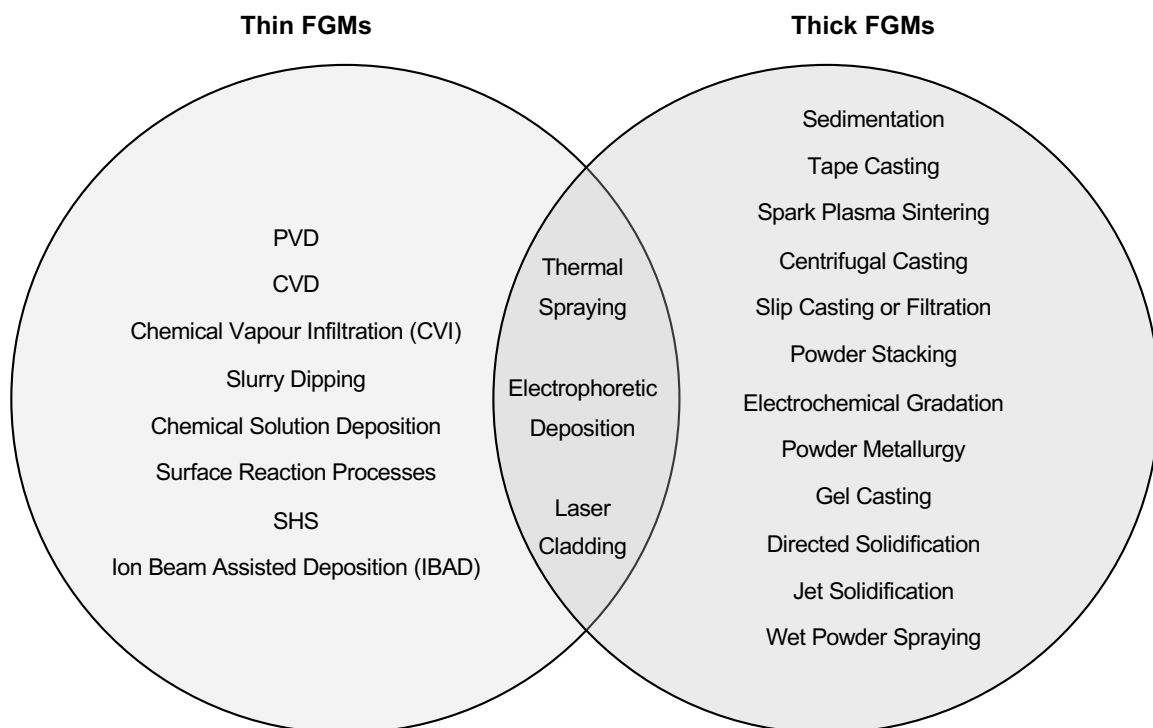


Figure 2.2. Fabrication methods for thin and bulk FGMs.

The use of AM has given a novel technique to produce bulk and thin FGMs with high complexity and a high degree of property gradient control of more than 90% (El-Galy, Saleh and Ahmed, 2019). The advancement of AM technologies makes it possible to strategically control the density and directionality of material deposition within a complex three-dimensional (3D) distribution or to combine various materials to produce a seamless monolithic structure using the same machine (Oxman, 2011; Loh *et al.*, 2018). This process is termed Functionally Graded Additive Manufacturing (FGAM). In 2017, this area of work

was relatively new, driven mainly by academic research. There is very limited information about its concept, current state-of-art and capabilities. Due to the lack of available standardisation, there is no general definition of FGAM and clarification of key terms. There have been multiple different names proposed by different researchers in different publications as terms for FGAM, for example, functionally graded prototyping (Oxman, Keating and Tsai, 2012), varied property rapid prototyping (Oxman, 2011), and site-specific properties additive manufacturing (Hascoet, Muller and Mognol, 2011). This chapter aims to define and establish standardised terminologies and fundamental concepts of FGAM. The investigation started by breaking down the area into particular keywords relevant to FGAM.

## **2.2. The Concept of FGAM**

Drawing from the available research, the author defines FGAM as a layer-by-layer fabrication technique that intentionally modifies process parameters and gradationally varies the spatial distribution of the material(s) organisation within one component to meet the intended function. This definition has been validated through semi-structured expert interviews in consensus-based meetings. This has been published as ISO/ASTM TR52912 (2020). The interview script and summary of findings can be found in Appendix II and Appendix III, respectively.

In contrast to conventional single material AM and multi-material AM (MMAM) which concentrate on shape-centric prototyping, FGAM is a material-centric fabrication process that establishes a radical shift from contour modelling to performance modelling (Figure 2.3). It is a method to produce efficiently engineered freeform structures driven by their graduated or site-specific material(s) behaviours and properties. The amount, volume, shape, material characteristics and properties can be tailored for a specific application by altering the material composition, phase or microstructure at pre-determined positions through voxel-level design (Figure 2.4) (Dalal, 2016; Aremu et al., 2017). Voxel is identified as “3D Pixels”, a unit of graphic information that defines a point in three-dimensional space (Tech Target, 2007).

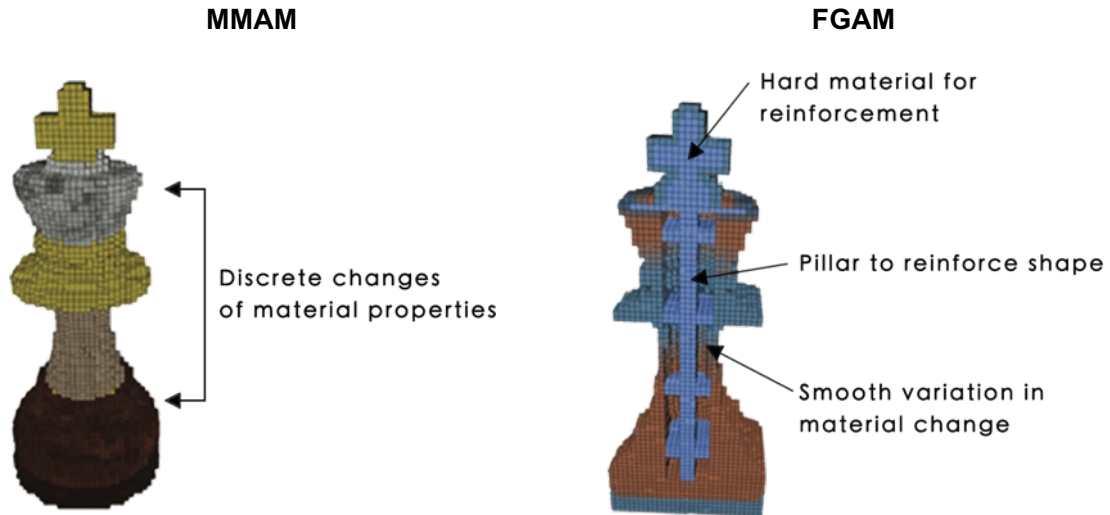


Figure 2.3. Differences between conventional MMAM and multi-material FGAM, with reference to Takahashi *et al.* (2016).

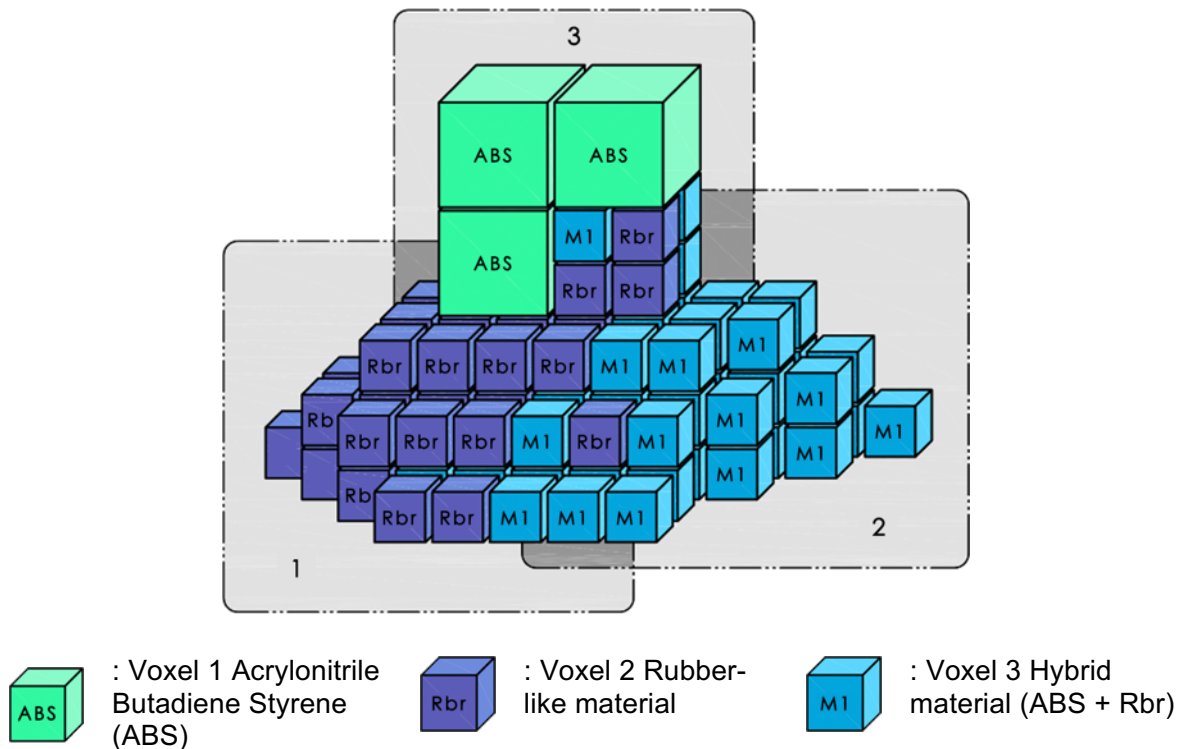


Figure 2.4. Conceptual diagram showing voxels arranged in 3D form, produced for ISO/ASTM TR52912 (2020), with reference to Takahashi *et al.* (2016).

The key parameters that control the properties of a FGAM component are the (I) material composition, (II) gradient distribution, (III) mathematical modelling, (IV) AM process and (V) build strategies. The material composition can be single material or multi-material, distinguished as homogeneous composition or heterogeneous composition respectively. Based on Figure 2.5, the types of FGM composition can be further characterised into (I)

variable densification within a homogeneous composition (varied densification FGAM), (II) heterogeneous composition through simultaneously combining two or more materials through gradient transition (multi-material FGAM), and (III) a combined composition.

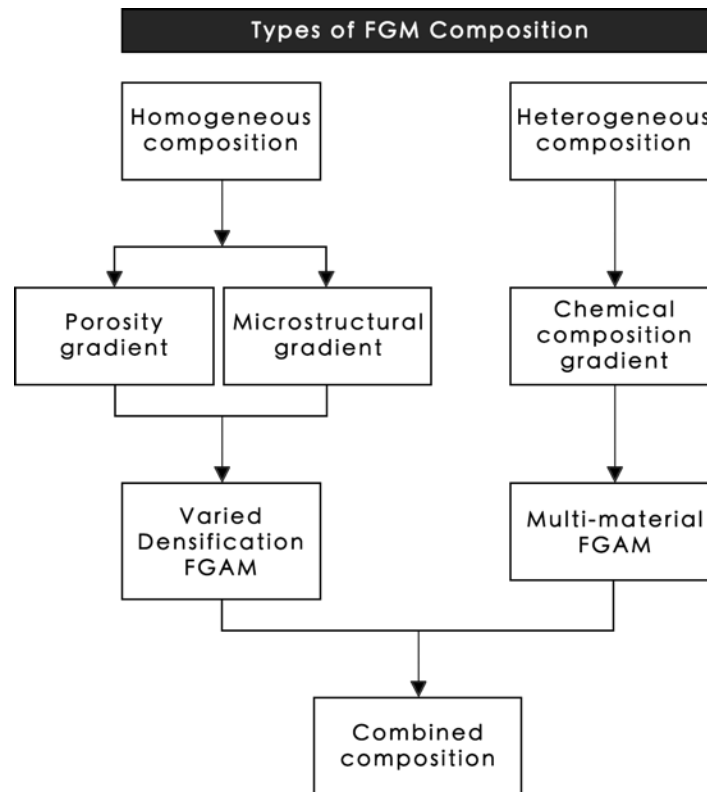


Figure 2.5. Types of FGM compositions.

### 2.2.1. Homogeneous Composition – Single material FGAM

Homogeneous FGAM composition attributes with porosity or microstructural gradients across the volume of bulk material, usually achieved by strategically modulating the microstructure using different sizes, shapes or fractions of pores (Figure 2.6). This method can be termed as varied densification FGAM or porosity graded FGAM. Varied densification FGAM enables the production of light-weight structures with functional deviations (i.e., stiffness and elasticity) by adjusting the lattice arrangement or the directional, magnitude and density concentration of the material substance within the monolithic structure. AM structures with a single type of material would no longer have uniform and homogeneous properties. Oxman, Keating and Tsai (2012) described this as a biological-inspired AM as it can mimic the natural structural density gradient in palm trees (Figure 2.7A) and spongy trabecular structure of bone (Figure 2.7B).

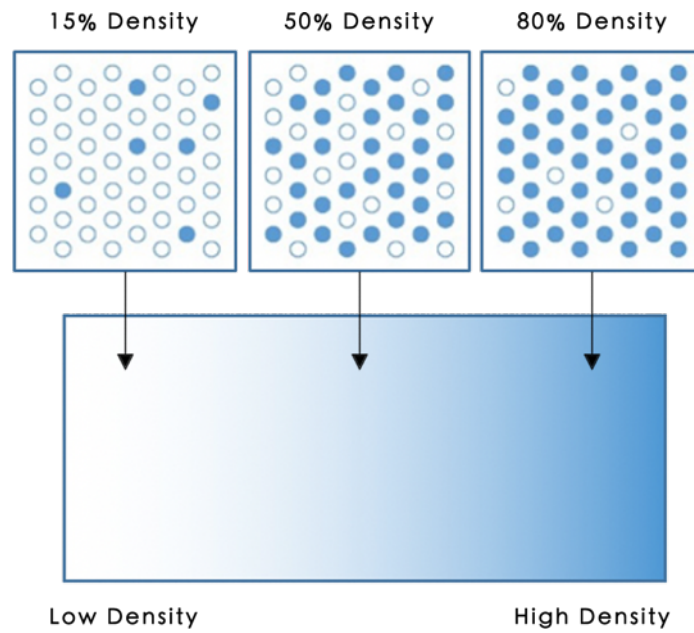


Figure 2.6. Varied densification of FGAM.

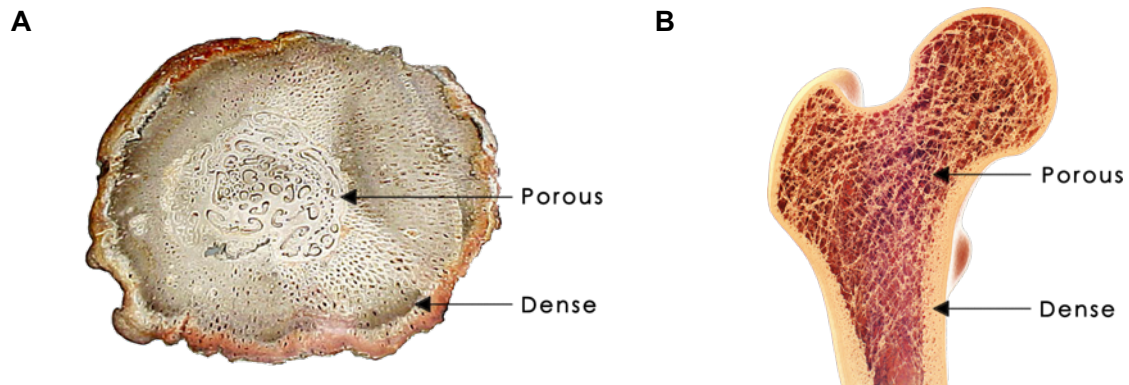


Figure 2.7. FGM in nature. Cross section of (A) palm trees and (B) bone.

This concept is demonstrated by Keating (2012) in creating a functionally graded concrete piece using a MakerBot machine with a modified material extruder (Figure 2.8). The spatial pore size distribution from a solid exterior to a porous core was achieved by varying the powder particle sizes assigned in different locations during the gradation process and through varying the production process parameters. Radially graded density led to an excellent strength-to-weight ratio, reducing the overall weight and yet maintaining the structural strength (Figure 2.9).



Figure 2.8. Functionally graded concrete by Keating (2012).



Figure 2.9. Weight reduction using radially graded density by Keating (2012).

### **2.2.2. Heterogeneous Composition – Multi-material FGAM**

FGAM addresses the aspect of multi-materiality using dynamically composed gradient or morphology. By continuously fusing one material to another material three-dimensionally in one volume without the use of mechanical connections, the printed component can have the optimum properties of both materials. Multi-material FGAM seeks to improve the interfacial bond by removing the distinct boundaries between dissimilar or incompatible materials through a heterogeneous compositional transition from a dispersed to an interconnected second phase structure, layered graded with discrete compositional parameters or smooth concentration gradients. In-plane and transverse stresses by different expansion coefficients at critical locations can be largely reduced (Tammas-Williams and Todd, 2017). Whilst the residual stress distribution material properties can be improved and enhanced (Kumar, 2016). The material arrangement and orientation gradient control the overall functions and properties change of the component. It can be transitional in physical, chemical or biochemical or mechanical properties (Hascoet, Muller and Mognol, 2011).

The design of heterogeneous compositional gradient can be a smooth and seamless transition between two materials from 0% at one end to 100% to at the other end (Figure 2.10), three materials or above (Figure 2.11A) or switched composition (Figure 2.11B). Multi-material FGAM can also be site-specific, tailored at small sections or strategic locations around a component.

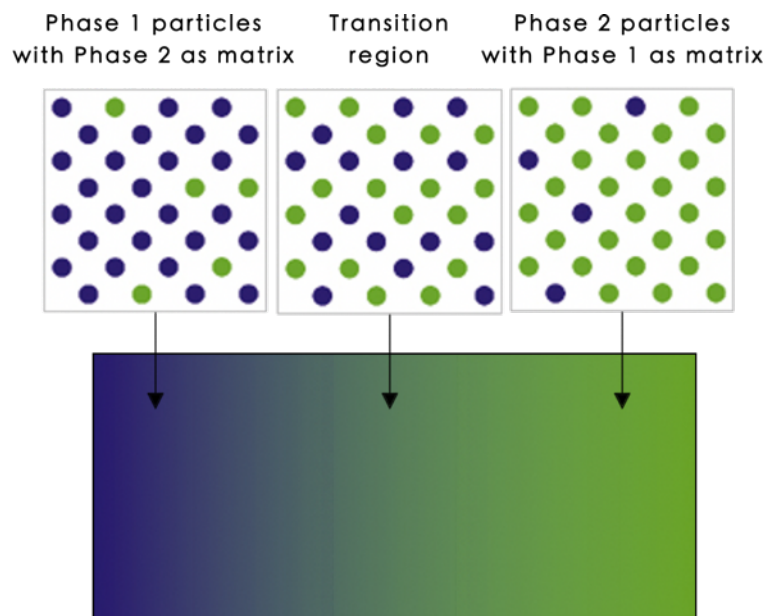


Figure 2.10. Two materials FGAM.

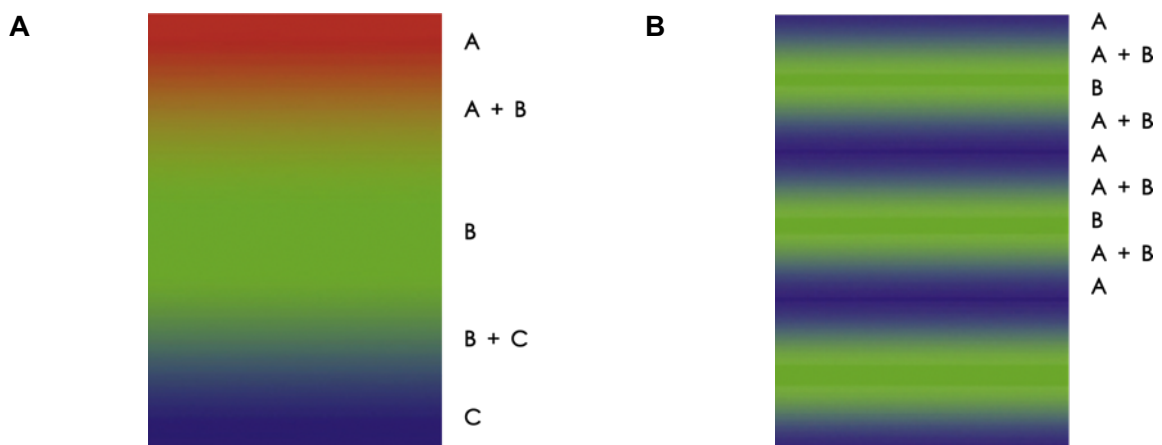


Figure 2.11. Types of composition gradient. (A) three materials and (B) switched composition.

According to Vaezi *et al.* (2013), the compositional variation of a structure has to be controlled by computer program in order to be considered as FGAM. Raw materials that are

pre-mixed or composed prior to deposition or solidification are not considered to be FGAM. On the other hand, Mahamood *et al.* (2012) explained that the continuous variation within the three-dimensional space can be produced by controlling the ratios in which two or more materials that are mixed prior to the deposition and curing of the substances.

### 2.2.3. Combined Composition

Combined composition is a combination of graded density and chemical compositional change within a single print as shown in Figure 2.12. The features and functionality of a FGAM component are further characterised by the form, direction and design of volumetric gradient within the composition which will be discussed in chapter 2.2.4.

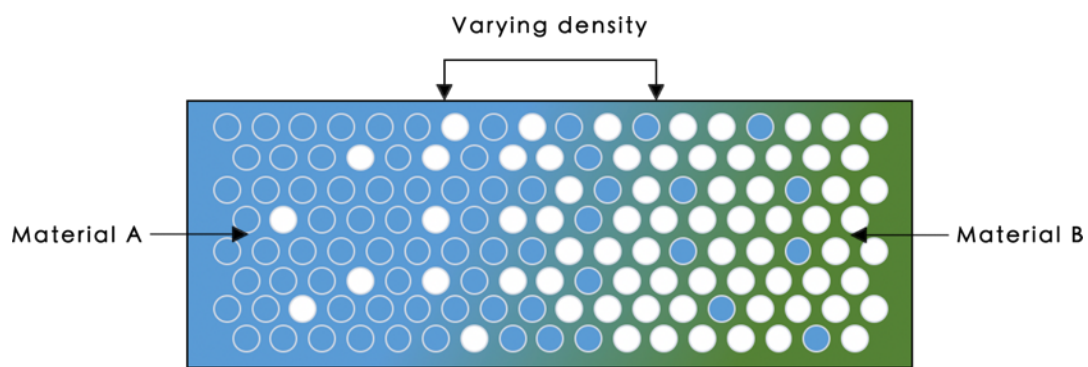


Figure 2.12. Combined composition.

### 2.2.4. Types of Gradients

The forms of gradient can be categorised as discrete or discontinuous gradient with interface (Figure 2.13A) or continuous gradient with flowing and seamless transition between different materials (Figure 2.13B). The types of compositional gradient can be arranged as radial or longitudinal gradient (Shinohara, 2013; El-Galy, Saleh and Ahmed, 2019).

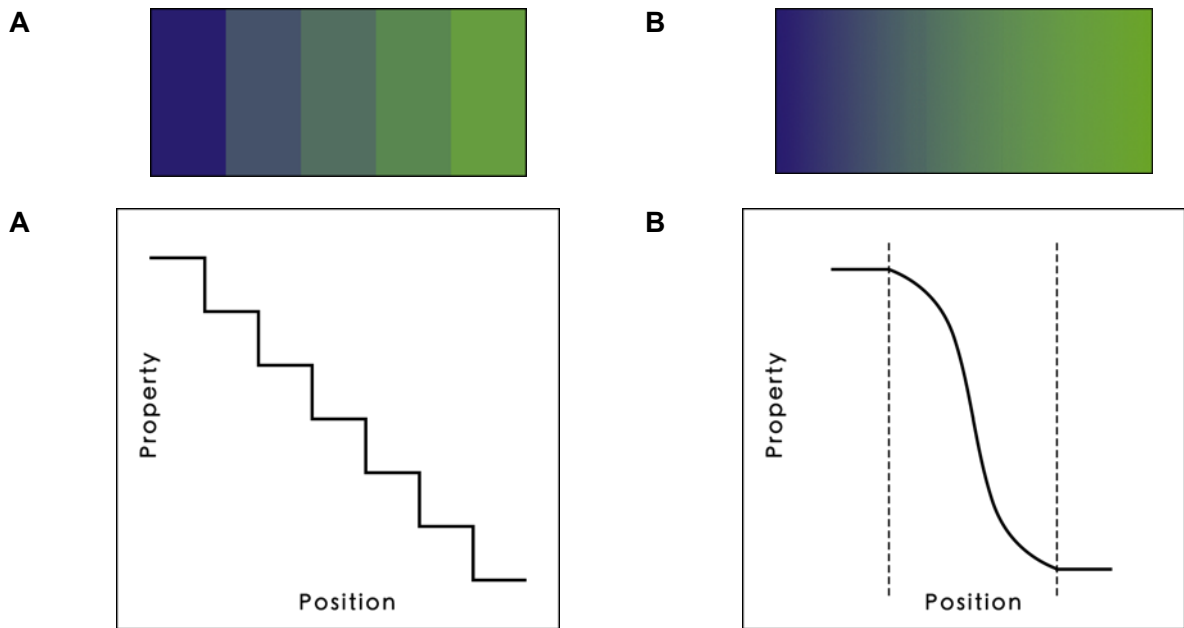


Figure 2.13. Forms of gradient. (A) discrete or discontinuous and (B) continuous.

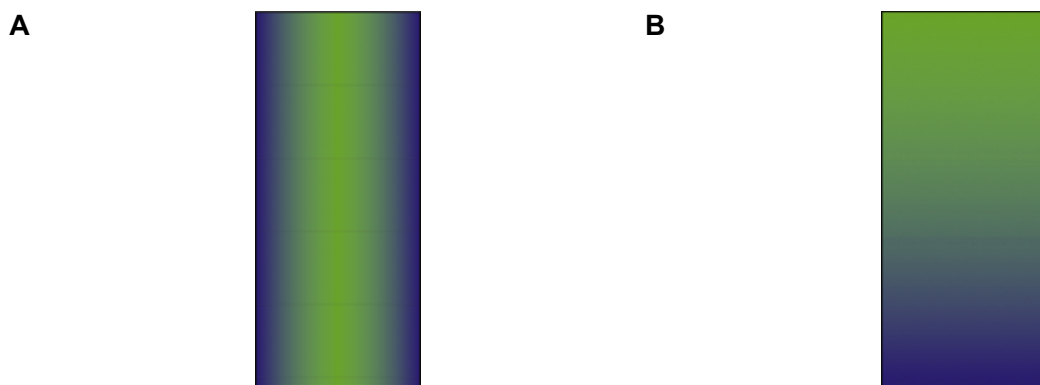


Figure 2.14. Types of compositional gradient. (A) radial and (B) longitudinal.

Muller, Mognol and Hascoet (2012) further assigned the composition or microstructure gradation into one-dimensional (1D), two-dimensional (2D) and 3D gradient as visualised in Figure 2.15.

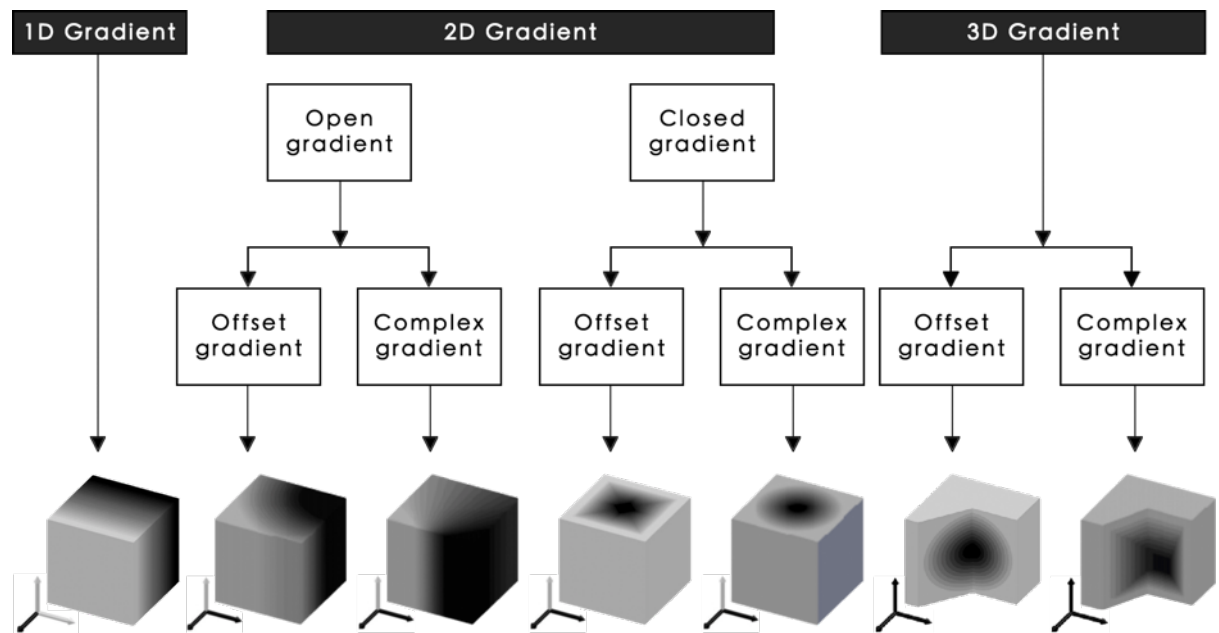


Figure 2.15. Representation of classifying FGAM gradients adapted by Muller, Mognol and Hascoet (2012).

### 2.3. Process Flow of FGAM

FGAM shares the main process flow of AM, from model generation using CAD, file preparation, the conversion of CAD files into an appropriate data exchange file format, verification of the data, determination of optimal orientation, support generation, and layer-by-layer fabrication to post-processing. Figure 2.16 presents the summary of FGAM workflow from design to manufacturing. Table 2.2 elaborates the process involved and manufacturing methodology for each stage (Wu, Liu and Wang, 2008; Muller, Mognol and Hascoet, 2012; Muller, Hascoet and Mognol, 2014; Loh *et al.*, 2018). The methodology of FGAM introduces the importance of the descriptions and assignment of material properties to every voxel within the voxel model (Stevenson, 2018) and toolpath definition based on a triptych “material-product-manufacturing” approach (Muller, Mognol and Hascoet, 2012). Path planning is the key influence on the material distribution of the manufactured parts.

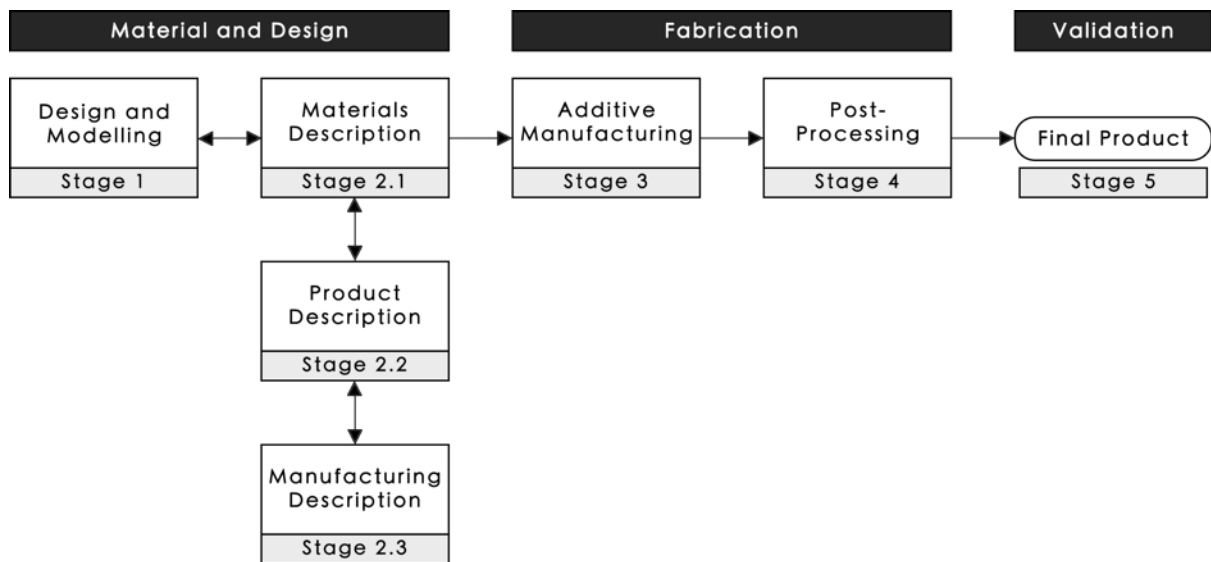


Figure 2.16. FGAM process flow.

Table 2.2. Manufacturing methodology of FGAM.

Phases	Stage		Process	Description	Ref
Material and Design	1	Design and modelling	Product concept generation Definition of the main part Modelling and simulation Topology and infill optimisation	The mechanical function of the part is defined by describing the fundamental attributes including the geometry and material composition. Some parts can be optimised by the lattice or cellular structure. Other attributes include topology optimization, gradient dimension or vector, the geometric of equi-composition or equi-property surfaces, the material characteristics, and mechanical parameters before developing a modelling scheme.	(Zhang <i>et al.</i> , 2016)
	2.1	Materials description	Material selection Defining optimum material properties orientation, allocation and distribution Gradient classification Analysis of area void density	The material data that concerns the chemical composition and characteristics of the material(s) used is gathered and modelled. Digital simulation is used to represent the materials, formulate a matching epistemology for the material selection, gradient discretisation, volume of support, residual stresses, etc. The void density needs to be taken into account in the theoretical calculation.	(Grigoriadis, 2019)
	2.2	Product description	Classification of the part (geometry and material repartition) with mathematical data	Mathematical data is used to identify an appropriate manufacturing strategy and process control.	(Muller, Mognol and Hascoet, 2012; Muller, Hascoet and Mognol, 2014)
	2.3	Manufacturing description	Classifying information from stage 2.2 into part slices	The mathematical data from product and material description are used to define the slicing orientation, categorised as planar or complex slices.	
Fabrication	3	AM	Manufacturing strategy and process plan determination Paths classification	The type of path strategy is defined and evaluated according to the geometry and material repartition. NC programming involves the generation of paths and modification of process parameters using, but not limited	

			Numerical control (NC) Programming Process control and monitoring	to G-code programming language. The file is sent to the AM machine for fabrication.	
	4	Post-processing	Part removal End part surface finishing	Post-processing techniques are used to improve the surface quality and dimensional accuracy of the printed part. The methods include, but not limited to, hand-finishing, machining operation (i.e., turning, milling, CNC machining), abrasive machining, chemical machining, laser surface finishing operations and abrasive flow machining.	(Redwood, Schöffner and Garret, 2017; Kumbhar and Mulay, 2018)
Validation	5	Final product	Quality assurance	Experimental analysis such as non-destructive testing, stress analysis or microscopic imaging is carried out to validate the final product and resultant part properties.	(Leu <i>et al.</i> , 2012)

## 2.4. AM Technologies for FGAM

AM technologies can be classified into seven classes, which are ME, vat photopolymerization (VP), powder bed fusion (PBF), material jetting, sheet lamination, directed energy deposition (DED) and binder jetting. In principle, all of them can be potentially used for the fabrication of FGMs, but not all can support FGAM in full capability at this current time. Table 2.3 presents a list of supporting AM processes for FGAM and its classifications with reference to ISO/ASTM 52900 (2017). The FGAM methods for the AM technologies are further discussed in the subsequent sections.

Table 2.3. AM technologies for FGAM.

AM Technology	Power source	Description	Supporting Processes for FGAM	Materials
ME	Thermal Energy	Material selectively is dispensed through a nozzle or extruder.	Fused deposition modelling (FDM), Freeze-form Extrusion Fabrication (FEF)	Thermoplastics, composite, ceramic pastes or slurries, biocompatible cellular gel, bio-ink.
VP	Ultraviolet laser	Liquid photopolymer in a vat is selectively cured by light-activated polymerization.	Mask-Image-Projection based Stereolithography (MIP-SL), Digital Light Processing (DLP), Computed Axial Lithography (CAL)	Photo-curable polymer resin
PBF	High-powdered laser beam Electron beam	Feedstock is deposited and selectively fused by means of a heat source or bonded by means of an adhesive to build up parts.	Selective Laser Sintering (SLS), Multi Jet Fusion (MJF)	Polyamides or polymer powder, ceramic powder
			Direct Metal Laser Sintering (DMLS), Selective Laser Melting (SLM), Electron Beam Melting (EBM)	Atomized metal powder
Material jetting	Photo curing	Droplets of build material are selectively	PolyJet Technology (PJT)	Photopolymers, Waxes

		deposited layer by layer.		
Sheet lamination	Laser Beam	Sheets of material are bonded together and selectively cut in each layer to create a desired 3D object.	Laminated Object Material (LOM),	Polymer sheet, ceramic tape
			Ultrasonic Consolidation (UC)	Metal sheet
DED	Laser beam or electron beam	Thermal energy is used to fuse materials by melting as they are being deposited.	Laser Metal Deposition (LMD), Wire Arc Additive Manufacturing (WAAM)	Metal powder or wire
Binder jetting	Thermal energy	Liquid bonding agent is selectively spread to join the powder material.	Drop on Powder (DOP), Powder Bed Printing	Polymer powder, ceramic powder, metal powder, Gypsum powder, Sand

### 2.4.1. Material Extrusion

ME is an AM process in which material is selectively dispensed through a nozzle or orifice (Loughborough University, 2021b). ME can fabricate FGAM parts with locally-controlled properties by regulating the deposition density and orientation of filament material (Huang *et al.*, 2009). Li *et al.* (2002) prototyped a functionally graded ABS composite part by changing the raster angle between the laminates. The study revealed that altering the printing directions (Figure 2.17) and the build parameters (including the raster width, raster angle, contour width and air gap) between deposition within layers can control the elastic stiffness and density of a component (Table 2.4).

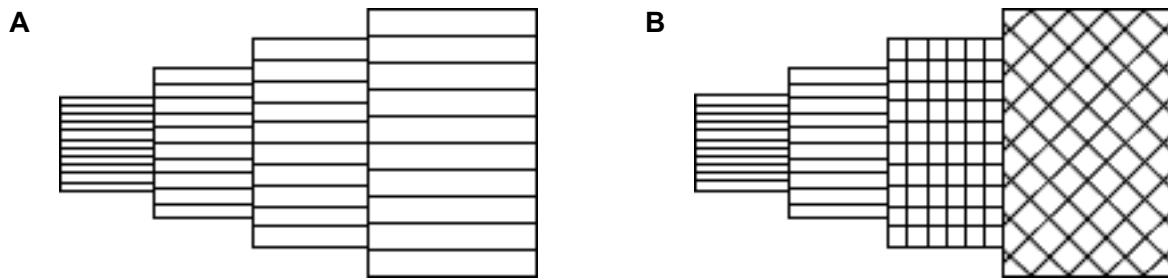


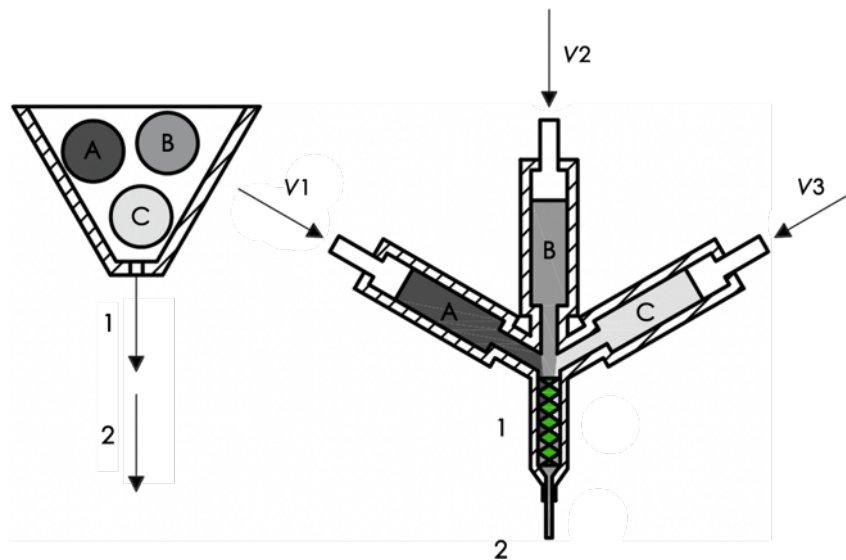
Figure 2.17. Printing directions for each section represented from the top view. (A) Unidirectional deposition and (B) multi-directional deposition.

Table 2.4. Locally controlled properties by changing the build parameters investigated by Li *et al.* (2002).

	Void density in unidirectional fibre packing	Positive gap in unidirectional deposition	Geometry of negative gap
Theoretical model			
Cross-sectional photo under microscopy			

Freeze-form extrusion fabrication (FEF) is another ME process of building parts layer-by-layer through computer-based controlled extrusion and deposition. FEF uses a triple-extruder mechanism, each carrying a paste of the material (Huang *et al.*, 2009). The different material pastes from the three cylinders are subsequently sent to a static mixer to be mixed into a homogeneous paste known as the green part, as shown in Figure 2.18. The plunger velocities ( $V$ ), the flow rates and ratio of materials have to be effectively controlled to create the desired paste mixture and to ensure correct material gradation. In Leu *et al.* (2012) investigation, a green part made up of alumina ( $Al_2O_3$ ) and zirconia ( $ZrO_3$ ) is freeze-dried at  $-25^\circ C$  and with a pressure of 3000Pa for 24 hours. Consequently, sintered at a high temperature of  $1^\circ C/min$  up to  $600^\circ C$  at the first heating to burn out the organic binder. The second heating was at  $10^\circ C/min$  up to  $1550^\circ C$  for another 90 minutes, then brought to cool

back to room temperature at 25°C/min. The heating temperature usually does not exceed the melting temperature of the constituent material. Energy-dispersive spectroscopy (EDS) was used to analyse the material composition of the sintered FGM parts.



1: Static mixer

2: FGM green part

Figure 2.18. Schematic diagram of static mixer and triple extruder, produced for ISO/ASTM TR52912 (2020).

## 2.4.2. Vat Photopolymerization

VP fabricates part through solidifications of photo-curable resins layer by layer using a UV light (SLA) from a laser or visible light from a digital projector (DLP) (Loughborough University, 2021f). Zhou *et al.* (2013) presented a mask-image projection-based stereolithography (MIP-SL) system with dual switchable resin vats and micro-mirror devices (DMD) to fabricate multi-material components systematically through a single build process. This technique allows two different concentration base materials to be combined and selectively solidified to produce FGM. On the other hand, Kelly *et al.* (2019) developed a Computer Axial Lithography (CAL) system that uses a video projector with a consistent rotation rate to output 2D patterned illumination from many directions to fabricate arbitrary geometries volumetrically through photopolymerization (Figure 2.19). CAL permits different polymerisation rate using dissimilar exposure dose, solidification at various locations and angles and multiple components integration, which may widen the material landscape to enhance graded functionality.

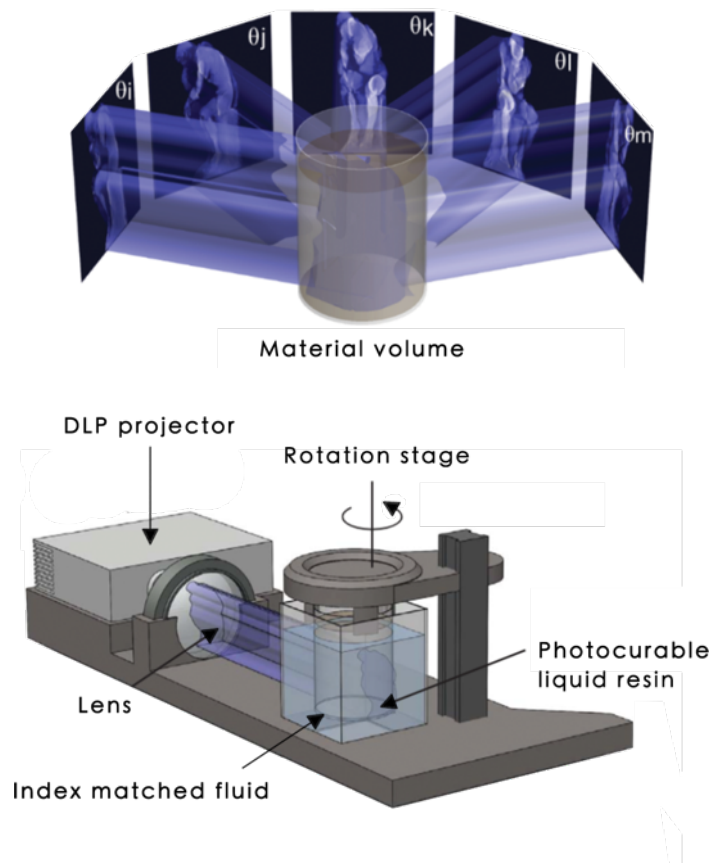


Figure 2.19. CAL system for volumetric AM adapted by Kelly et al. (2019).

Gonzalez *et al.* (2019) used a specifically developed DLP printer that fabricates ceramic–polymer FGMs to create a varied densification implant made up of aluminium oxide polymeric mixtures. The suspensions or slurries are made up of different fraction amount of polymeric resin and ceramic powder to have varied refractive index to the light. The differences in the refractive index values lead to differentiation in the dimensional accuracy of the layers and the total light dose to trigger the polymerization rate and reaction. Kuang *et al.* (2019) introduced a single-vat grayscale DLP (g-DLP) printer that uses grayscale light patterns and a two-stage curing ink to fabricate FGAM components with stiffness variations. The effect of voxel discrete grayscale pattern on the photopolymerization of the hybrid ink and print resolution were studied.

### 2.4.3. Powder Bed Fusion

PBF comprised SLS and MJF to process polymeric and ceramic materials, and DMLS, SLM and EBM to process metallic materials. The processes involve spreading and sintering of 0.1 mm thick powder material layer-by-layer with a roller in between fusion of layers, selectively melt and fused by a heat source (Loughborough University, 2021d). SLS and SLM use single or multiple focused high-power laser beams as heating media while EBM uses electron beam to fuse the powder materials. Unlike SLM and EBM, SLS consolidates the powder materials through selective sintering instead of melting, resulting in less dense printed components. Chung and Das (2008) utilised SLS to create functionally graded Nylon-11 nanocomposites structure with tailored mechanical properties by adjusting the volume fractions of 15nm fumed silica nanoparticles (Figure 2.20). In Chung and Das (2008) investigation, the SLS processing parameters for the different compositions were developed by Design of Experiments (DOE). The densities and microstructures of the nanocomposites were examined using optical microscopy and transmission electron microscopy (TEM). The tensile and compressive properties for each composition were then tested. These properties exhibit a nonlinear variation as a function of filler volume fraction.

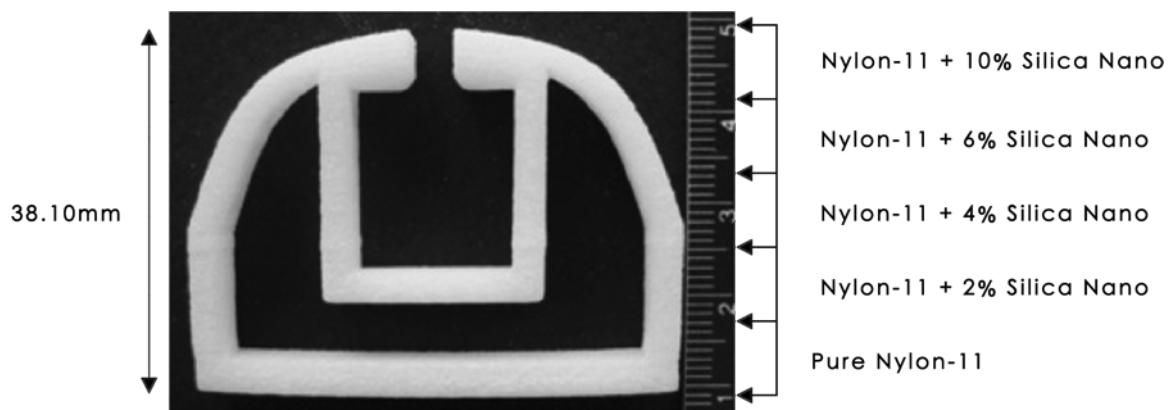


Figure 2.20. Compliant gripper with discrete gradient of composition change at 7.62mm each layer, adapted by Chung and Das (2008).

SLM is predominantly employed to fabricate metallic FGAM components. Heterogeneous composition can be achieved if multiple powder delivery systems are used. The research by Anstaett, Seidel and Reinhart (2017) investigated successive allocation and solidification of two materials spots (Copper-Chrome-Zirconia and Tool Steel 1.2709) without mixing the materials before the process in-situ. Niendorf *et al.* (2014) used two laser SLM systems to create 316 L stainless steel (SS) FGM. Their study revealed that the microstructure can be

manipulated directly by changing the processing parameters, which lead to distinct local mechanical properties. Maskery *et al.* (2016) use SLM to create a uniform and graded density Al-Si10-Mg periodic lattice structures. A microstructure-altering heat treatment framework was presented to improve the mechanical behaviour and energy absorption capability of the lightweight graded-lattice structure.

#### 2.4.4. Material Jetting

Material jetting works like a two-dimensional inkjet printer in which droplets of photosensitive polymer or waxes material are jetted onto the build platform continuously or through a drop on demand (DOD) approach, then cured and smooth using a UV light (Loughborough University, 2021c). PolyJet technology is currently the most successful and widely applied FGAM process. It has high dimensional accuracy and can achieve better control in material gradation. There are a variety of materials used for material jetting of distinctive properties such as shore hardness, transparency, colour and biocompatibility available in the material library for different applications (Stratasys, 2021a). Material jetting incorporates multiple inject heads to deposit and blend multiple base materials to create hybrid composite materials. Figure 2.21 shows a heterogeneous composite with graded chemical composition and properties made up of transparent rubber-like material, Tango Plus and two opaque materials, Vero Magenta and Vero Yellow. The resultant blend in mechanical and physical properties can be pre-set and configured using the Objet Studio and PolyJet Studio software.

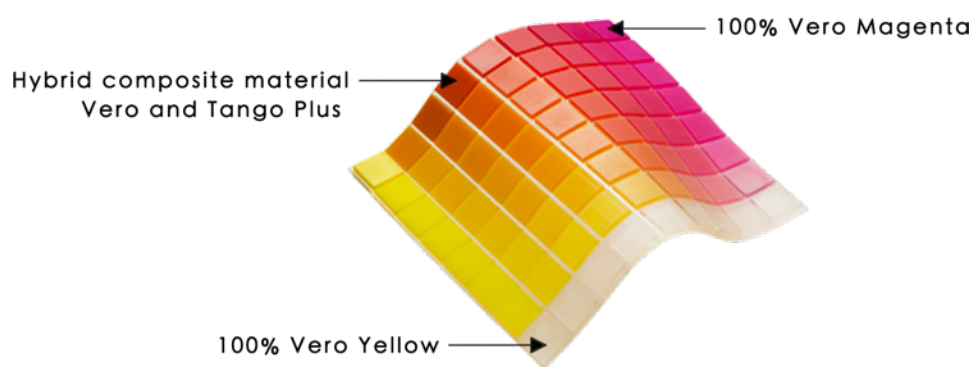


Figure 2.21. Sub-materials continuously fused together in a gradient manner.

This is exemplified in the work undertaken by Salcedo *et al.* (2018) with graded fusion models made up of elastic rubber-based materials Tango Black Plus, DM95 and DM60 and rigid material Vero White Plus and the multi-material mullion interface by Grigoriadis (2018)

using Vero Magenta, Vero Clear and RGD-CMT-001 (Figure 2.22). Computational fluid dynamics (CFD) simulations are used to emulate the fusion of materials based on their physical properties (Grigoriadis, 2019).

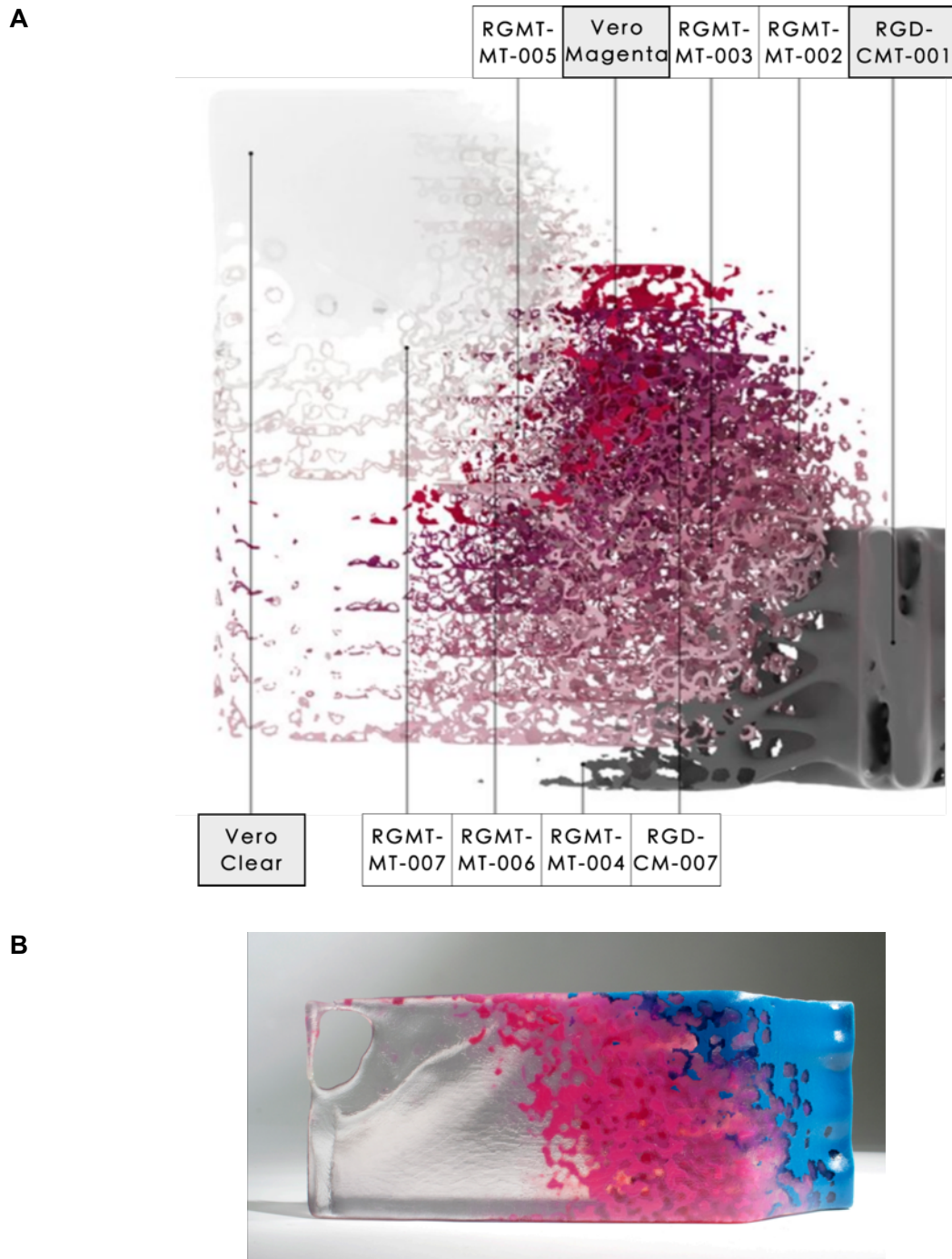


Figure 2.22. Multi-material mullion interface by Grigoriadis (2018) using material jetting. (A) Exploded view of multi-material mesh and (B) fabricated specimen.

### 2.4.5. Sheet Lamination

Sheet lamination processes consist of UC and LOM. UC uses metal sheets or ribbons such as aluminium, copper, SS and titanium joined together using ultrasonic welding, whereas LOM uses paper, polymer film or ceramic tape joined using adhesive (Loughborough University, 2021e). Figure 2.23 presents a graded metallic FGM produced by Kumar (2010) using UC. Three different metallic foils, CU, SS and Aluminium (Al 1100 and 3003) were joined by ultrasonic welding at 20 kHz. The work aimed to fabricate samples with best graded strength and thermal conductivity in the deposition direction of foils through the optimisation of process parameters used to combine the materials such as the weld force, speed, amplitude and substrate temperature.

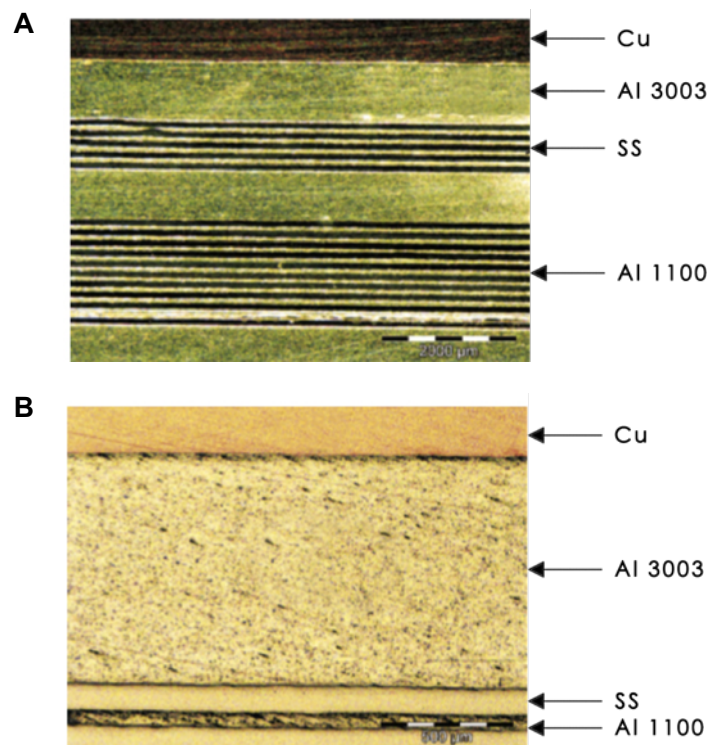


Figure 2.23. Microstructural analysis of a specimen built from UC. (A) FGM specimen and (B) metallography.

### 2.4.6. Directed Energy Deposition

DED is a process where thermal energy, either laser, electron beam or kinetic energy is used to fuse the materials while being deposited layer-by-layer on a substrate. The raw materials are fed by blowing powder through multiple nozzles or in a wire form or as gas

mixtures in the build chamber (Loughborough University, 2021a). DED technologies can modify, repair, reinforce components or add materials to existing base structures from a 3D CAD model in one single process, which is not achievable with other AM technologies (Gibson, Rosen and Stucker, 2010). LMD and WAAM are two DED processes that can fabricate metallic parts with a graded chemical composition, achieved by controlling the individual wire feeding speed or adjusting the volume of metallic powders delivered to the melt pool as a “function of position” (Carroll *et al.*, 2016; Li *et al.*, 2020). The examples of changing compositions and material combination produced include, but not limited to, pure Titanium and 1080 pure Aluminium (J. Wang *et al.*, 2018), 304L SS and Inconel 625 (Carroll *et al.*, 2016) (Figure 2.24), Nickel alloy (Ni- Cr-B-Si) and 316L SS (Banait *et al.*, 2020), and pure iron and Nickel alloy (Liu *et al.*, 2020).

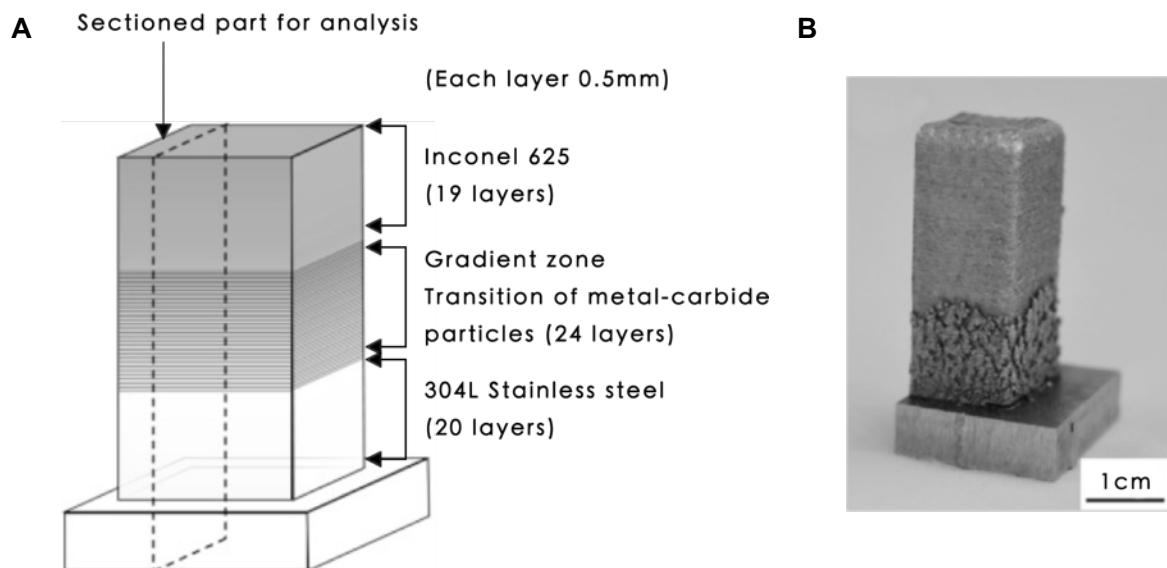


Figure 2.24. Discrete gradient composition change between 304L SS and Inconel 625 using a 910W YAG laser with hatch angle of 60° by Carroll *et al.* (2016). (A) schematic diagram and (B) photograph of specimen after sectioning.

Thermodynamic computational modelling of the DED process is often used for optimising the process parameters and to reduce undesirable properties during solidifications especially at the intermetallic phases in the gradient zone. Carroll *et al.* (2016) adjusted the distribution of the composition of the metallic powder mixtures through a simulation technique to improve the interface properties. Qian *et al.* (2014) utilised a similar method to manufacture a varied mass aircraft beam using high strength TA15 (Ti-6.5Al- 2Zr-1Mo-1 V) and high ductility TA2 (Grade 3 CP-Ti).

## 2.5. The Advancement of FGAM

FGAM offers the general AM advancement such as personalisation, part consolidation, enhanced weight-to-cost ratio, zero stock and choice of shape complexity using a single-step manufacturing process with no extra tooling costs (Pei *et al.*, 2017). Having the performance-driven functionality built directly into the material is a fundamental advancement to AM technologies. It creates the next generation of advanced and multifunctional materials tailored to adapt to changes in the environment and to meet multiple demands. FGAM establishes a radical shift from monolithic materials to combined hybrid composite materials using AM. FGAM simplified the assembly of complex components using dynamic gradients, enables customisable internal features with integrated functionalities, on-demand and site-specific properties.

The emergence of FGAM optimises the exploitation of materials and expands the design toolbox available in AM processes leading to a vast range of innovative opportunities for design, performance, cost and lifecycle management (AM Platform, 2014; Richards and Amos, 2014). It can solve a number of problems in engineering applications in which reliable mechanical, thermal or chemical properties are required, especially in extreme wear resistance and corrosion resistance applications (Mahamood *et al.*, 2012). FGAM parts can be made aesthetically pleasing through the incorporation of multiple digital materials to create customisable colour, rigidity and opacity gradient (Hadid, 2015; Oxman, 2021)

The potential to achieve more environmentally sustainable and efficient engineered structures increases as the material processability advances (Oxman, 2011). Global problems related to energy and environment can be resolved due to more efficient material use and energy consumption. Graduated building components envisioned in the construction industry can be manufactured for materials, energy and CO<sub>2</sub> savings (Federal Institute for Research on Building, 2018). Although part forming via AM consumes a longer time than conventional manufacturing, having the capability to consolidate several machining processes into a single manufacturing sequence can vastly reduce the overall manufacturing time-to-market. FGAM will become a powerful technique for future AM system, assembly processes, supply chains and a source of economic growth (Shinohara, 2013).

### 2.5.1. FGAM Applications

FGAM adoption targets markets that demand customized geometry with multifunctional and enhanced mechanical properties within a single product. Table 2.5 lists some potential applications anticipated using FGAM in different sectors, alongside the primarily applied types of FGM composition to achieve the targeted advanced properties.

Table 2.5. FGAM applications (Gilbert et al., 2011; Mahamood and Akinlabi, 2017a; Loh et al., 2018; Parihar, Setti and Sahu, 2018; Sarathchandra, Subbu and Venkaiah, 2018; Saleh et al., 2020; Pei et al., 2021).

Sector	Potential applications	Composition Types	Advanced Properties
Aerospace	Rocket engine components, spacecraft truss structure, heat exchange panels, reflectors, solar panels, turbine wheels and turbine blades.	Chemical composition gradient	Minimise thermal and mechanical stress concentration, increase loadbearing capacity by preventing interfacial crack or delamination, provide thermal barriers, improve fatigue properties and surface finishing.
Automotive	Engine cylinder liners, leaf springs, spark plugs, combustion chambers, driveshafts, shock absorbers and racing vehicle frame.	Chemical composition gradient	Improve thermal management by gradual change in thermal diffusivity and insulation, reduce thermal stress concentration to improve product life.
Biomedical and tissue engineering	Dental implants, skeletal replacement implants, tissue scaffolds, assistive, surgical and prosthetic devices.	Porosity gradient, microstructural gradient	Biocompatibility, biological gradient and mechanical function with improved strength-to-weight ratio. The graded porosity and microstructural encourage cells and tissues growth and regulate biofluid transmission.
Energy, optoelectronic and thermoelectric	The inner wall of nuclear reactors, piezoelectric ultrasonic transducers, fuel cell unit, solar panels, and photodetector.	Chemical composition gradient, porosity gradient	Gradient porosity distribution with variable electronic permeability and optical refractive index considering structural integrity.
Construction and architecture	Graduated building components, sidewalls and bridges.	Porosity gradient	Deliver structural support distribution and acoustic absorption property. Enhance structural stability and thermal insulation.

Defence	Bullet-proof vests and armoured components.	Chemical composition gradient, porosity gradient	Improve strength and hardness with enhanced shock resistance in lightweight components.
Commercial and Industrial	Cutting tools, mould lining, drilling tubes, drilling motor shaft, graded arm for soft robotics, helmet, protective gloves, wrist splint, fashion pieces and furniture.	Chemical composition gradient, porosity gradient	Improve surface wear and hardness resistance, increase product life, allow customisable product features with site-specific properties and functionalities.

## 2.6. Challenges, Research Gaps and Future Work

FGAM requires a comprehensive knowledge of the “design-material-manufacturing” relationship. As the field of FGAM is still developing, existing information about the material, design, modelling, simulation and AM processing methods are limited and inadequate to support variable property printing. This section identifies some of the interlinked limitations that need to overcome to make FGAM competent for practical applications on an industrial scale.

### 2.6.1. Materials

FGMs have a variable composition or structure to achieve properties such as stiffness, density, mechanical properties, etc. The key challenges in the material aspect lie in the material selection, understanding the composition, defining the optimum material property distribution and defining tolerances to ensure the material properties of the manufactured component (Tammam-Williams and Todd, 2017; Loh *et al.*, 2018; Pei and Loh, 2018a). Currently, it is difficult for designers or engineers without a background in material science to fully utilise the potential of FGAM as the characterisation of FGAM parts requires extensive knowledge of material data, chemical composition, characteristics, properties and manufacturing constraints (Muller, Mognol and Hascoet, 2012; Zhang *et al.*, 2016).

The current material selection support for FGAM is relatively limited. For multi-material FGAM, the situation becomes much more complex as it involves mixing materials with variable and non-uniform properties. Not all materials are compatible or can be smoothly altered to be transitioned between with ease. For instance, Shinohara (2013) explained that

glass is generally difficult to join with metal due to significant differences in their thermal expansion coefficients values. In such a case, a third material, Kovar metal, has to be used as an intermediate layer between glass and metal to form a successful graded structure. While choosing the compatible neighbouring materials for material combination, the selected materials have to satisfy the processing criteria of the same AM process. Agreeing with Grigoriadis (2019), there is a need for dedicated topics on identifying the list of appropriate materials that can be mixed, specifying their mixing range and transition efficiency to form an FGAM structure.

Apart from describing materials, specifying the gradient transition on top of the geometric information is significant for both single and multi-material FGAM to achieve the expected performance of the FGAM part. The modifications of porosity, microstructure or chemical compositions have to be carefully measured and quantified. Besides, it is also crucial to identify the fixed regions that cannot be altered without compromising the part integrity. The available information on defining the optimum material property distribution such as choice of spatial, gradient distribution, the arrangement and orientation of transition phases are lacking and remain unclear. Tamas-Williams and Todd (2017) argued that most works have little consideration to the effects of a steeper or shallower gradient, how rapidly the step-change in properties can be varied to the overall mechanical, thermal and other properties result of the FGAM part. The level of complications increases when multiple transitions are introduced. Saleh *et al.* (2020) highlighted the need to study the influence of mixing sizes to produce multiple gradients zone within a single print.

Furthermore, the distribution of chemical compositions and material properties of the manufactured parts may deviate from the actual production material due to the variability in the interaction of the different materials at different operating conditions (Zhang *et al.*, 2016). For example, in LMD, Li, Zhang and Liou, (2018) noted a substantial deviation and inconsistency in compositions between the pre-mixed powder fed to a printer versus the final deposited material. A contributing factor would be the differences in densities and sizes of dissimilar particles in the powder mixture, causing them to accelerate and interact differently under the same argon gas flow. Pei and Loh (2018) highlighted the importance to establish test methods to validate the quality of raw feedstock materials before manufacturing. Physical and technical factors such as macro segregation of the solutes during solidification and poor process control can lead to variable tolerances and inferior parts being produced. Property tolerances may need to be redefined, comprising the overall variation in components and local variation to ensure correct properties at specific locations. In-situ or in-process monitoring of the phases and chemistry during the build process may offer a

solution or provide more information about the result. Techniques such as full-field infrared thermography (Bartlett *et al.*, 2018) and Acoustic Emission monitoring (Shevchik *et al.*, 2018) can help to monitor in situ product quality, detect localising defects and concentration during the build sequence. Consequently, help operators minimise downstream defects and increase reproducibility and process reliability.

To aid the process of describing the “processing-structure-property” of FGAM components, there are needs for a shared database or online portal that covers a large portfolio of materials and multi-material combination specifically designed for FGAM. It should also provide detailed guidelines and information on the design of material systems (including geometry characterisation, assign coordinate systems, part orientation, support materials), parameters, material preparation, performance evaluation and long-term reliability for specific applications. Together with a systematic methodology to identify a specific AM process, required equipment and discuss the technique that would work best for the production of envisioned FGAM component. Like the Senvol Database by Granta Design (2021), the database would allow users to search and compare materials, identify and compare machines based on supported processes, manufacturer, required part size, cost, compatible materials types and properties, and decide the most likely method to fabricate an achievable FGAM part.

### **2.6.2. Design, Modelling and Simulation**

Most CAD software for AM focuses on traditional boundary representation, BREP oriented design workflow. They are not built for hierarchical volumetric modelling and designing with graded information (Oxman, 2011; Michalatos and Payne, 2016). FGAM requires new modelling approaches for multi-physics, multiscale modelling to predict the graded microstructures to measure and account for strength, fatigue and service life of FGAM parts (Pei and Loh, 2018a). A new approach of CAD and Computer-Aided-Engineering (CAE) analysis that can specify, model and manage the material information for Local Composition Control (LCC) is essential. There are limited commercial voxel-based modelling and analysing software available, such as Stratasys GrabCAD Voxel Print, Autodesk Monolith (Michalatos and Payne, 2016) and VoxCad (VoxCad, 2021). Custom computational approaches are actively developed by researchers but a majority of them are not available for commercial use. Richards and Amos (2014) utilised CPPN (Compositional Pattern Producing Network) encodings and a scalable algorithm using NEAT (Neuroevolution of Augmented Topologies) to embed functional morphologies and macro-properties of physical

features using multi-material FGAM through voxel-by-voxel descriptions by a function of its Cartesian (X, Y, Z) coordinates. Such an approach is challenging and less accessible for designers, engineers and manufacturers without appropriate background knowledge in mathematical modelling.

Topology optimization methodologies should be included during the design phase to move from feature-based design to performance-based design. Another limitation is the shortfall of material simulation for FGAM design for reality outcomes (Grigoriadis, 2019). Although various simulation tools are available, they are incompetent to predict the material properties and behaviour of FGAM components. In addition, it is difficult to measure the material properties at all locations within sites. Tammas-Williams and Todd (2017) have suggested two methods to represent the property variation, based on measured values using the exponential law idealisation or through materials elements "Maxels". It has to be assumed that the material contains no weak interface, then such elements arrangement could be analysed using the Finite Elements Method (FEM). Any extra phases generated by the interface between different sites is identified as they could result in a step-change in properties. Some CAE software provides tools for assessing the material properties as a function of field variables (i.e., ABAQUS). The predictions based on individual phase properties may be inadequate if there is any weak bond between phases. Sarathchandra, Subbu and Venkaiah (2018) also criticised that limited works have been carried out on the real-time application of these predictive models for a specific manufacturing process.

Another challenge is the huge consumption of computational power needed for calculations and the long processing time to generate voxels for every layer. The conversion of volumetric data sets is extremely computationally demanding especially using a large volume of voxels used to describe highly refined details, curves and undulation. This further leads to large file size (Aremu *et al.*, 2017). Editing is also difficult due to the lack of a robust method to relate and integrate the data with modelling and analysis. In such a case, Tammas-Williams and Todd (2017) described that it has to be assumed that the properties of the FGAM model are predictable. Otherwise, each voxel needs to be edited individually if the design requires re-modification. In line with Li *et al.* (2020) and Saleh *et al.* (2020), taking full advantage of FGAM will require theoretical models and numerical simulation capable of simulating physical FGAM processes, predicting geometries, properties and functional requirement and generate hybrid methods for compositional gradient, together with reliable guidelines to provide methods of creating gradient layers and interacting with the matrix.

Moreover, the standard data format recognised by most AM technologies is STL. which only describes raw, unstructured, triangular facet model represented by polygonal meshes. The

level of detail is limited. STL file format does not describe the micro-scale physical properties of materials and restricted path planning steps to define material properties in a continuous or non-discrete manner within the internal composition or for the solid (Tammam-Williams and Todd, 2017; Xometry Europe, 2020). Alternative data exchange format that can store and support file specification including the colour, material, gradients, lattices and constellations beyond a fixed geometric description (i.e., geometry, scale, duplicates and orientation) is required for successful printing (Loh *et al.*, 2018). The potential data exchange formats that can support FGAM include AMF (Additive Manufacturing Format) (ISO/ASTM52915, 2020), FAV (Fabricatable Voxel) (Takahashi *et al.*, 2016), SVX (Simple Voxels) (AbFab3D, 2014) and 3MF (3D Manufacturing Format) (Kočí, 2019). The potential and capability of each file formats are discussed in detail in the ISO/ASTM TR52912 (2020) technical report. Among the lists, Xometry Europe (2020) recommended the AMF and 3MF file formats as they are the most technically superior among the list, with the ability to store every information on a model, ease of file sharing and more likely to be compatible with supporting software and the “slicing” program. Novel approaches to slice, analyse and prepare related commands for a FGAM component to the AM system for fabrication is also needed. Steuben, Iliopoulos and Michopoulos (2016) presented a slicing algorithm based on the generation of toolpaths derived from arbitrary heuristics-based or physics-based fields. Hascoet, Muller and Mognol (2011) established a set of mathematical formulations for the slicing of four possible typologies of a bi-material gradient. Each class of topology has an associated part orientation strategy that can be implemented for FGAM.

### **2.6.3. AM Processes**

In general, every AM process has its advantages and limitations, alongside the equipment and manufacturing cost, material processability, availability and compatibility of the feedstock materials to the chosen process for the required application (Sarathchandra, Subbu and Venkaiah, 2018). FGAM parts require an efficient AM system that can perform efficient mixing, highly accurately place and switch materials within and between each print layers across a printed volume (Vaezi *et al.*, 2013). Present demonstrations in published studies only dealt with fabricating small functional parts with simple morphology of variable property gradient. Muller, Hascoet and Mognol (2014) explained by the mixing strategies, toolpaths planning, management of the entire AM process and parameters for FGAM would be too difficult to control if produce at a relatively large volume or with complex morphology.

Although researchers have exploited various FGAM methods for different classes of AM technologies, the vast majority of the machines are specially developed or involve upgrades and modifications to perform a particular FGAM strategy. The basic strategy of commercial machines operates predominantly on isotropic materials. Most AM processes have demonstrated the feasibility of multi-material printing but limited to delivering single form feedstock materials or supply phase, unable to support non-discrete material definitions and in-situ mixing to form a monolithic gradient structure. Unlike material jetting, most materials cannot be mixed at a different ratio within a voxel fill to form hybrid composite materials. Li *et al.* (2020) underlined that sheet lamination is incompetent AM technology in realising material gradients.

Another challenge is to ensure that the materials can be deposited in a precise position to achieve an accurate multi-material gradient and precise internal structure, especially at nanoscale and microscale. Although the printing materials, process parameters and machining strategy can be effectively varied, most printers are still highly prone to printer-associated, deposition-associated error and print quality problems which affects the voxel resolution, finished product composition, accuracy and quality (Loh *et al.*, 2020). Appendix I presents the most common problems of ME processes and their causes. New material delivery systems for FGAM that can print multi-material and graded materials at higher accuracy and faster speed should be developed. New metrology equipment, inspection and quality control system needs to be established to ensure the quality of printed parts, improve product reproducibility, reduce cost and loss of production (Li *et al.*, 2020; Pei *et al.*, 2021).

An optimal manufacturing strategy is vital. For example, the curing condition for VP has a large effect on the molecular structure and mechanical properties of the cured polymer samples (Kuang *et al.*, 2019). There are limited design guidelines to support designers, engineers and manufacturers in understanding each AM process capabilities, requirements, regulations and operational variables for FGAM (Pei and Loh, 2018a). There remains a need to investigate the procedures and protocols that can guarantee a reliable and predictable outcome when dealing with the distribution of materials with constituent phases and transitioned properties throughout the structure, alongside considerations on the material usage, platform structure, deposition rate and fabrication speed.

As FGAM parts are produced in a non-conventional way, post-processing methods should be considered in which they will not alter the microstructures of FGAM parts. Conventional approaches of using heat treatment or the use of chemicals may not be suitable as may affect the integrity of the FGAM parts. Established methods to certify FGAM parts should be developed to encourage mainstream adoption (Pei and Loh, 2018a).

## 2.7. Chapter Summary

A detailed review and semi-structured expert interviews were carried out to define the fundamental concepts and terminologies of FGAM. This chapter provides an insight into the relationship among FGM properties, discusses the technology development, advanced trend and future perspectives of FGAM. The content of this chapter provides new researchers in this field, interested researchers and manufacturers with a straightforward resource to understand FGAM from design to manufacturing. Based on today's state of FGAM, extensive research and actions are necessary to accelerate the design, application and implementation, namely developing comprehensive "material-product-manufacturing" guidelines and standards, appropriate computational tools, process workflow, verification and validation.

With the findings from chapter two, it has been clear that FGAM is not deemed as the appropriate AM strategy and design concept to produce thermo-responsive textiles. FGAM is a fabrication technique that intentionally modifies process parameters and gradationally varies the spatial of the material(s) organisation within one component to meet the intended function. The product state is static. FGAM does not fabricate product with smart and dynamic features that can self-sense and self-actuate after printing. Based on today's state of FGAM, there are many technological constraints and unknown limitations that require extensive research and investments to accelerate the design, application and implementation, namely the development of comprehensive "material-product-manufacturing" guidelines and standards, appropriate computational tools, advanced printing method, process workflow, verification and validation. This contributes to another reason that FGAM is determined not to be carried forward due to limited resources and knowledge which were beyond the focus of this research. The following chapter investigates the state-of-art of 4DP and comparative analysis between the FGAM and 4DP.

## Chapter 3

### 4D Printing (4DP)

Chapter three gives an overview of the concept, process flow, advancement and potential applications of 4DP. This chapter extensively reviews the key bases in 4DP and their current research development, focusing on ME technology, stimuli-responsive actuator materials, predominantly thermo-responsive SMPs. The concept and underlying mechanisms of shape change effect (SCE) in shape change materials (SCMs) and the shape memory effect (SME) in SMPs are studied and compared. This chapter also analyses the different types of shape-shifting behaviours and shape transformation actuation. Different use of SRMs, structure design, modelling and fabrication methods of 4DP structure to perform certain controlled shape-shifting behaviours when subjected to appropriate stimuli are exemplified. To conclude, this chapter outlines the current barriers and limitations of this emerging AM strategy for SMPs-based fabrication. Finally, this chapter analyses the key aspects that separate and bridges FGAM and 4DP, and addresses selection of the best AM strategy to answer the research aim and objectives.

#### 3.1. Introduction

4D Printing is an emerging material-driven AM strategy that uses AM technologies with stimuli-responsive materials (SRMs) to fabricate dynamic smart structures that can sense fluctuations in the external environment and generate a response by either changing their material properties or performing actions. The Mimosa Pudica, often identified as the shameplant, which would fold its compound leaves inward when responding to human touch or shaken, is a direct analogy of the 4DP concept (Figure 3.1). 4D printed structure is time-dependent (Momeni *et al.*, 2017). Hence, introducing time as the fourth dimension to 3D Printing (3DP). The concept of 4DP was proposed and the first additive manufactured one-way SMP was presented by Tibbits (2013) at a TED conference in 2013. The first heterogeneous 4DP composite using multiple SMPs was developed by Wu *et al.* (2016) in 2016, in line with the first two-way reversible 4DP structure by (Wang, Liu and Leng, 2016). 4DP has attracted intense interest owing to its various and versatile applications. It has been profoundly explored alongside the development of SRMs and effective computational design and digital fabrication software solutions. The number of research publications on 4DP has continuously increased over the past few years with over 9220 publications in 2020 and

2210 new publications up to the second quarter of 2021 on Google Scholar, which are based on research contributions from both academia and industry.



Figure 3.1 The behaviour of Mimosa Pudica as a direct manifestation of the 4DP concept (Alamy, 2021).

### **3.2. The Concept of 4DP**

4DP is defined as the use of AM to produce a freeform stimulus-responsive structure that can sense and actuate in response to an appropriate fluctuation of stimulus over a particular domain of time, without the reliance on power-source, robotics or electro-mechanical devices (Tibbits, 2013). It is known as the programmable AM which dependent on the “material-stimuli-structure-function” relationship (Khare et al., 2017). The main capabilities of 4DP structures are self-adaptability, self-assembly and self-repair when activated by stimuli, such as temperature and moisture (Momeni et al., 2017). Self-adaptability is defined as the ability to sense changes in the environment, response and adjust to new conditions through properties or behaviour change. Self-assembly is defined as “a process by which disordered parts build an ordered structure through only local interaction” by Tibbits (2013). Whilst, self-repair is defined as a process of self-healing materials to automatically repair damages to themselves without any external diagnosis of the problem or human intervention (Ghosh, 2009). A 4DP structure would acquire a minimum of two configurations, a printed

shape before the stimulus is applied and an actuated shape when or after the stimulus is applied.

4DP relies predominantly and holistically on the (I) AM process, (II) stimuli-responsive materials (SRMs), (III) stimuli, (IV) smart structure design, and (V) mathematical modelling (Momeni *et al.*, 2017; Jian *et al.*, 2018; Pei and Loh, 2018b; Scalet, 2020) to achieve an ascribed function upon activation. Figure 3.2 presents the key bases and variables to consider and select in the 4DP workflow (categorised into material, design and fabrication). For material, the consideration includes the types of SRMs, their transition phenomena that link between their associated input (stimulus) and output (response) (Chapter 3.2.2). The design of the 4DP smart structure includes, but is not limited to, the design of actuation mechanism, geometric and material distribution. The processes involved in modelling and simulation include model construction, design simulation, testing and optimisation (Jian *et al.*, 2018) (Chapters 3.2.3 and 3.2.4). Regarding the fabrication, it includes, but is not limited to, the AM process selection (Chapter 3.2.1), identifying the manufacturing strategy, followed by post-processing.



Figure 3.2. The key bases of 4DP.

### 3.2.1. AM Technologies for 4DP

The AM technologies facilitate the direct fabrication of a 4DP component through the successive layering of SRM at set positions within a design domain. Most AM processes can support 4DP considering the specified input material (SRMs) and the AM technology are compatible. The most viably applied AM processes for 4DP are material extrusion (ME), material jetting (PolyJet technology) and vat photopolymerization (VP) (Stereolithography

(SLA), Digital Light Processing (DLP)), followed by powder bed fusion (Selective Laser Sintering (SLS)) (Kuang, Roach, *et al.*, 2018; Zafar and Zhao, 2019; Ma *et al.*, 2020). For multi-material 4DP structure, AM technologies capable of multiple-material printing are required in order to combine two or more materials to produce a heterogeneous composition in a single print. Material jetting is one of the widely used processes to create multi-material 4DP structure with mixed and varied material distributions. Stratasys Connex printer is usually used with PolyJet photopolymers Vero (Stratasys, 2021c) and Tango (Stratasys, 2021b) which can be seen in the work undertaken by, but not limited to, Mao *et al.* (2015) and Raviv *et al.*, (2014). ME processes with multiple nozzle extrusion system are also commonly used. There are currently many reliable multi-material ME printers commercially available which include the Original Prusa multi-material upgrade (Prusa Research, 2021), Geeetech A10M/ A20M, Monoprice dual extruder printer and many more, as reviewed by 3D Sourced (2021). Some researchers design their bespoke multi-material AM system. For example, Ge *et al.* (2016) developed a high-resolution Projection Microstereolithography (P $\mu$ SL) machine with an automated material exchange system that enables the fabrication of multiple photo-curable materials (Figure 3.3).

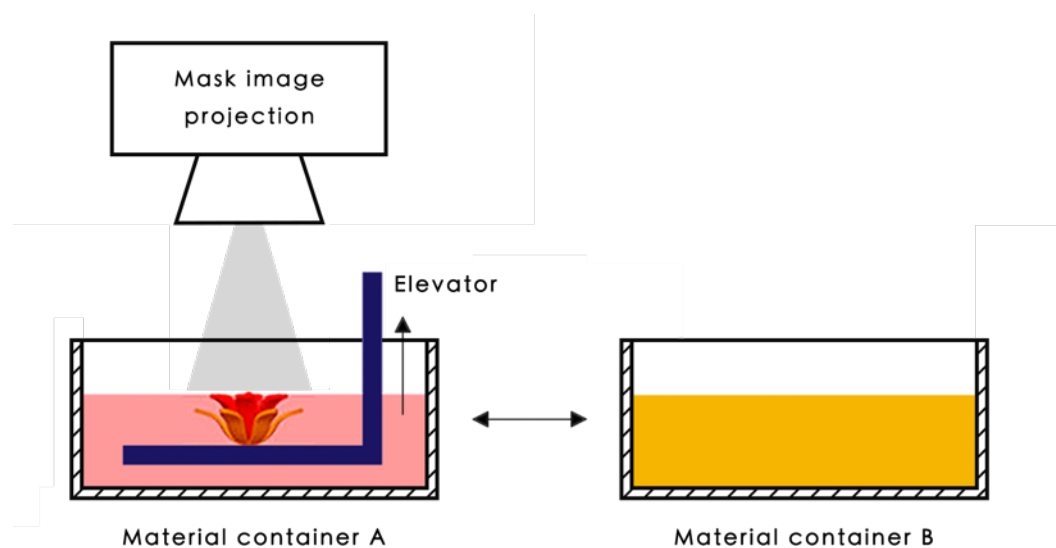


Figure 3.3. Projection Microstereolithography (P $\mu$ SL) machine by Ge *et al.* (2016).

### 3.2.2. Stimuli-Responsive Materials (SRMs) and Stimuli

SRMs, often known as smart materials, are adaptive and multifunctional materials engineered to respond in a controllable and usually reversible way. SRMs are highly dynamic in form and functions (Tibbitts, 2017). They are capable of self-sensing and actuation by coupling or converting energy between physical domains as a result of external

stimuli (Pei and Loh, 2018b). The coupling of energy can be direct or indirect. Direct energy coupling refers to mechanical response due to field-induced eigenstrain in the SRMs, whereas indirect energy coupling refers to mechanical response due to field-induced change in the stiffness and other properties.

According to Piselli *et al.* (2018, 2019), the selection of the most suitable SRM is a fundamental decision-making process as it is the core element that determines the type of stimulus required to trigger a response such as property change or behaviour change, such as shape-changing, self-assembly, self-diagnosing and self-repair. The SRM also directly influences the printability, aesthetic, mechanical properties and smartness of the 4D printed structure. The considerations for the smartness in SRM include single or dual responsiveness, its self-sensing and self-actuating capabilities, transformation efficiency and decision speed (Momeni *et al.*, 2017). The types of SRMs can be categorised into four distinct classifications, which are explained in Table 3.1.

Table 3.1 The classifications of different types of SRMs (Laitinen *et al.*, 2020).

<b>Class</b>	<b>Definition</b>
Stimuli-responsive actuator materials	Materials that produce strain in response to the applied stimuli.
Stimuli-responsive energy conversion materials	Materials that exhibit an electric current, electrical resistance, magnetic field or temperature change as a primary response to the applied stimuli.
Stimuli-responsive optical materials	Materials that exhibit an optical response, such as light emission or a change in optical properties as a response to the applied stimuli.
Stimuli-responsive state-changing materials	Materials that alter their physical properties, such as viscosity, in response to the applied stimuli.

Figure 3.4 presents the common groups of SRMs and their transition phenomena that link between their associated input (stimulus) and output (response) with reference to Lefebvre *et al.* (2015). The sources of input (stimulus) can be grouped into physical, chemical and biological categories. Physical stimuli include light, temperature change, movement, deformation, pressure, magnetic field and electric field. Chemical stimuli include chemical concentration, oxidants, reductants, ionic strength and pH levels. Biological stimuli include glucose, enzymes and antigens. The types of output (response) include changes in colour,

light, temperature, deformation, stress, stiffness viscosity, absorption and release, electric field, magnetic field, and resistance (Lefebvre et al., 2014; Momeni et al., 2017). Stimuli-responsive actuator materials are the predominant SRM investigated for 4DP. They are materials that produce strain in response to applied stimuli (Laitinen et al., 2020). This type of SRMs can be classified into shape-change materials (SCMs) and shape-memory materials (SMMs).

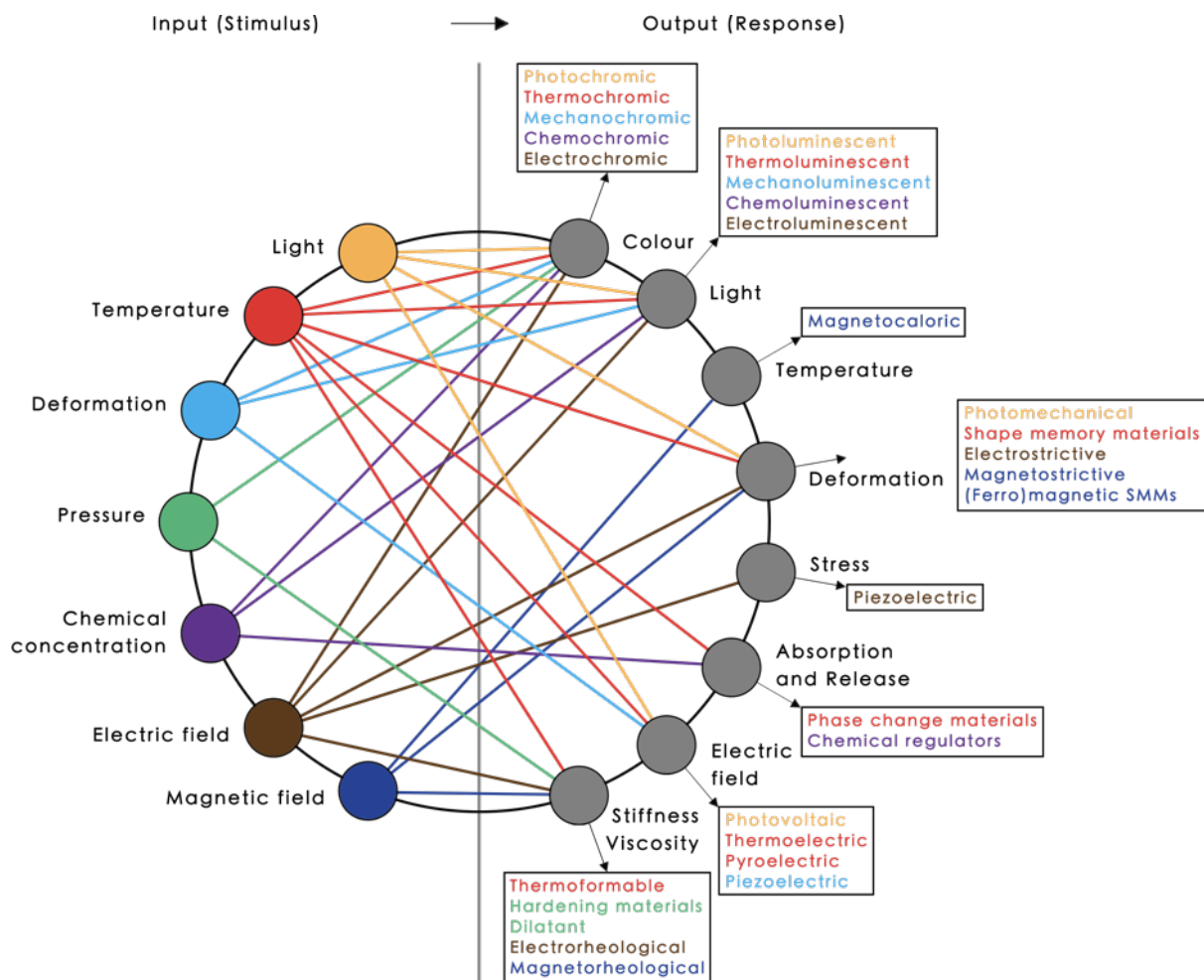


Figure 3.4. SRMs and their transition phenomena that link between their associated input (stimulus) and output (response).

### 3.2.2.1. Shape-Change Materials (SCMs)

SCMs are materials with stimulus-induced behaviour known as the shape-change effect (SCE). SCM transforms instantly and spontaneously under the presence of its defined stimulus and returns to its original shape either instantly or gradually when the stimulus is removed (X. Wu *et al.*, 2013). Its dual shape capability is reversible and repeatable. SCM

can undergo multiple times of deformations by switching between two configurations, but not programmable. Hydrophilic-based polymer (Hydrogel) is the most common SCM. Water-responsive hydrogels share the same swelling and shrinkage properties as a plant cell. They are highly flexible and can undergo large volume of homogeneous swelling up to two times their original sizes when placed underwater (Ionov, 2013; J. J. Wu *et al.*, 2018). Ionov (2013) described homogeneous swelling as an expansion in size at the same magnitude in all directions. Homogeneous macroscopic actuation does not induce any geometric shape-shifting configurations.

Shape-shifting configurations can be achieved through inhomogeneous SCE of a multi-material structure made up of either SCM and passive material or multiple SCMs (Figure 3.5). Inhomogeneous macroscopic actuation can be adjusted using different swelling magnitudes, volume, varying the arrangement and orientation of SCM to the secondary material (Kim *et al.*, 2012; Wu *et al.*, 2013; Thérien-Aubin *et al.*, 2015).

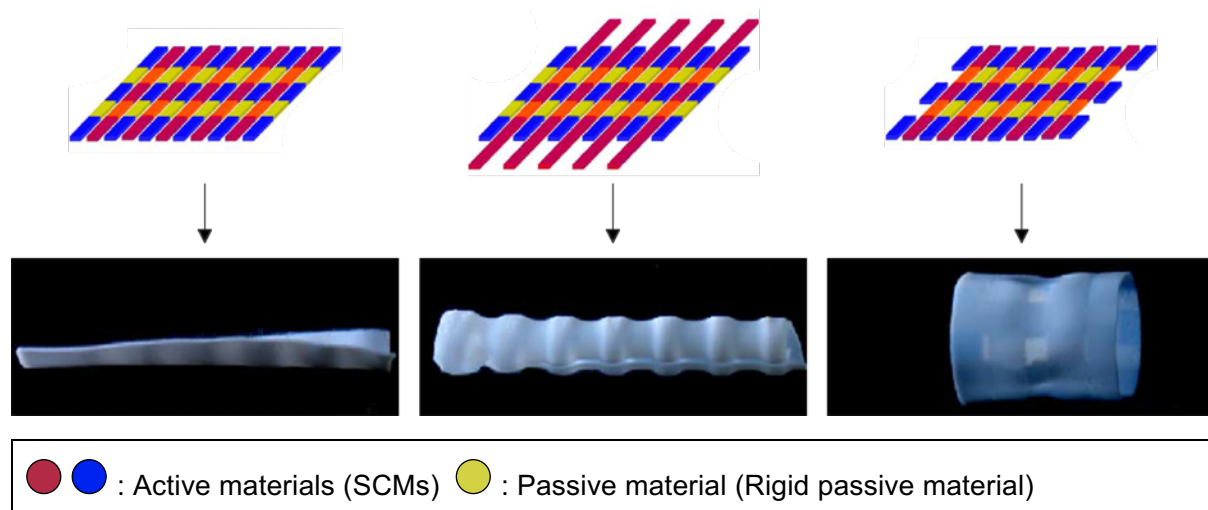
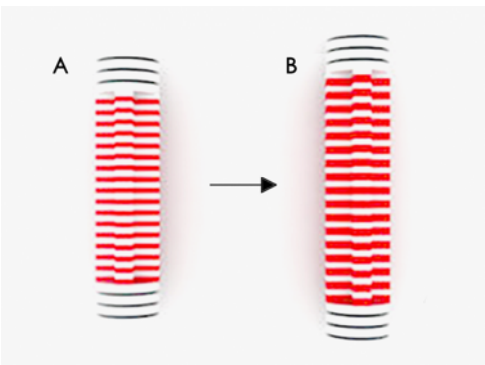
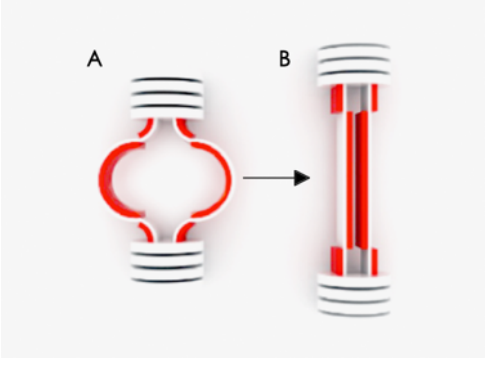
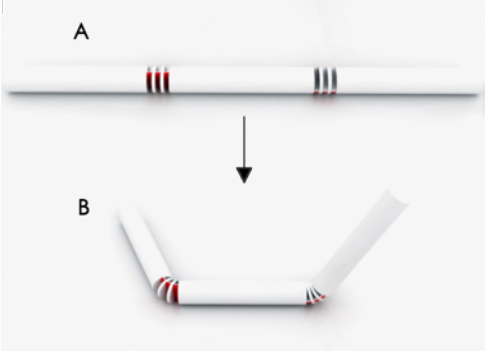


Figure 3.5. Various shape-shifting configurations achieved through inhomogeneous SCE demonstrated by Thérien-Aubin *et al.* (2013).

However, Raviv *et al.* (2014) and Zhou *et al.* (2015) claimed that inhomogeneous SCEs are usually limited to basic and affine alterations such as linear volume expansion (stretching), contraction (shrinking) and folding as shown in Table 3.2. Though, larger and more complex shape change structures can be designed by combining different basic primitives (Figure 3.6 and Figure 3.7). The magnitude of shape changes such as the length of expansion and the angle of fold can be controlled by the ratio of expansion volume, the SCM placement

within the heterogeneous structure, and the proportion of the applied stimulus (Sun et al., 2012; Raviv et al., 2014).

Table 3.2. Examples of linear volume expansion, contraction and folding shape change through water activation by Raviv *et al.* (2014). (A) printed shape and (B) actuated shape.

<p>Linear stretching primitive</p>		<p>Each SCM layer assembled between the rigid circular disks expands when submerged in water, leading to an overall increment in the component length over time. The ratio of active and passive materials controls the overall stretching length.</p>
<p>Ring stretching primitive</p>		<p>The passive material on the outer layer limits the deformation to one side. The SCM expands and forces the ring to shape into a bar. As a consequence, the component stretched and elongated. The radius or diameter of the ring controls the overall stretching length.</p>
<p>Folding primitive</p>		<p>The fold occurs in an opposed direction to the placement of the SCM strip. The rigid disks between the bars act as stoppers. The fold angle stops at the point where the corners of two passive disks hit. The diameters and distances between the passive disks control the folding angle, while the folding plane is adjusted by rotating the placement of active and passive strips.</p>
<p>● : Active material (SCM) ○ : Passive material (Rigid passive material)</p>		

The primitives in Figure 3.2 demonstrated by Raviv et al. (2014) were simulated using Autodesk Project Cyborg and fabricated through material jetting using the Stratasys Objet500 Connex3.



lower density, lower phase transformation temperature, higher deformation rate with lower required stress for deformation and easier to manufacture with more accessible AM technologies (Liu, Qin and Mather, 2007; Kong and Xiao, 2016; Strzelec, Sienkiewicz and Szmechtyk, 2020). Some SMPs are biocompatible, biodegradable and potentially recyclable, making them more suitable and cost-effective for commercial applications (i.e., consumer products and programmable textiles). The study by Strzelec, Sienkiewicz and Szmechtyk (2020) asserted that the shape memory cycle of SMPs can be repeated numerous times in much shorter intervals in comparison to SMAs. However, applications of SMPs may suffer from low tensile strength, low stiffness, low thermal conductivity, slower response rate and inertness to electromagnetic stimuli (Table 3.3). The material and functional elements selection depends upon the end application and usage. Although SMAs were less considered due to complex and expensive manufacturing technique, high material costs, toxic and their limited recovery. SMAs are still ideally suited for use over a range of robust engineering applications, for instance, in the offshore oil and gas industry (Patil and Song, 2017). More details about the classification criteria, properties and working mechanisms of SMPs will be discussed in chapter 3.2.2.4.

Table 3.3. The comparison between SMP and SMA (Liu, Qin and Mather, 2007; Yüce, 2017).

<b>Properties</b>	<b>SMP</b>	<b>SMA</b>
Density (g/cm <sup>3</sup> )	0.9 – 1.2	6 – 8
Extent of deformation (%)	50 – 600	< 8
Required stress for deformation (MPa)	1 – 3	200 – 400
Stress generated upon recovery (MPa)	1 – 3	150 – 300
Phase transformation	Glass transition	Martensite, R-phase
Transition temperature (°C)	35 – 65	50 – 110
Plasticity	Easy	Difficult
Recovery speed	> 1s	< 1s
Processing condition	< 200°C; low pressure	> 1000°C; high pressure
Thermal conductivity	Low	High
Cost	Low; < £16.5/kg	High; < £416.7/kg

### 3.2.2.3. Shape-Change Effect (SCE) versus Shape-Memory Effect (SME)

The fundamental programmability of the shape-shifting pathways differentiates SMMs from SCMs (J. J. Wu *et al.*, 2018). As shown in Figure 3.8, SME has a high magnitude of energy barrier ( $H$ ) between two states (A: printed shape; B: actuated shape), which require additional driving force for shape recovery ( $H$ ). By contrast, SCE has a low magnitude of energy barrier ( $H'$ ), hence the shape recovery can be released instantly or gradually (X. Wu *et al.*, 2013).

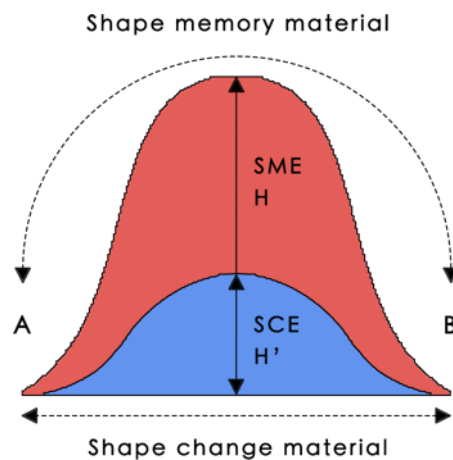


Figure 3.8. The magnitude of the barrier of SCE and SME. (A) printed shape and (B) actuated shape (X. Wu *et al.*, 2013)..

Table 3.4 compares and differentiates the key principles of SCMs and SMMs. Wu *et al.* (2013) and Zhou *et al.* (2015) described that SCE and SME may coexist in one material (i.e., PLA). A material may behave as an SCM or SMM depending on the working condition or environment. When the material is loaded within its elastic range at low temperatures, it is a SCM. However, when the material is loaded to beyond its elastic range, it is an SMM. The quasi-plastic deformation may be recovered upon heating.

Table 3.4. Comparisons between SCM and SMM.

Principles	SCM	SMM
Function	SCE	SME
Dual-shape capability	Yes	Yes
Shape-change	Yes	Yes
Shape-memory	No	Yes
Shape programming	Not required	Required
Mechanical loading for shape fixation	Not required	Required
Shape recovery	Automatically when the stimulus is removed	When the stimulus is applied
Reversibility	Yes	Shape reprogramming is required

#### 3.2.2.4. Shape Memory Polymers (SMPs)

SMPs are an emerging class of smart polymeric materials with the ability to memorise a permanent shape, be quasi-plastically deformed into a temporary secondary shape (programmed shape) and recover to its printed shape when induced by its driving stimuli (Figure 3.9). The shape-memory functionalisation with anticipated morphology of an SMP can be realised by a specific shape-memory creation procedure (Wagermaier *et al.*, 2009). SMPs can be dual-shape or triple-shape. They possess at least two phases, (1) a stable phase, which stabilises the polymer and also used to recover the part back to its original printed shape, and (2) a temporary secondary phase (Huang *et al.*, 2010; Pei *et al.*, 2020). The network elasticity of SMP determines the memory of one or more shapes. SMP is composed of hard segments and soft segments. It is the hard segments that remember the permanent shape of the SMP. Behl and Lendlein (2007) further described that the switching phase and the cross-linking phase within the polymer network determine the shape morphing capability. The switching phase is used to programme a metastable shape. The secondary shape is fixed by either reversible crystallisation, vitrification or supramolecular interactions until the stimulus is applied for recovery to the original printed shape (Table 3.8).

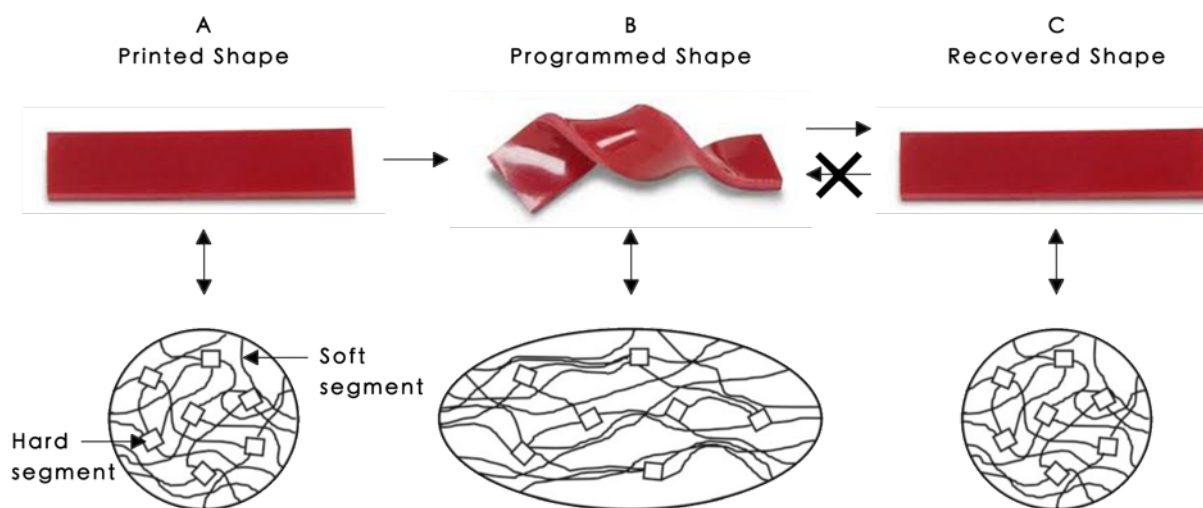


Figure 3.9. Molecular mechanism of thermally induced SME with dual-shape capability.

SMPs can be further categorised according to their structure and composition, types of stimulus-activated strategy and the characteristics of the shape-memory function. Table 5 describes the types of SMPs structure, their features and compositions. The stimulus-activated strategies for SMPs include temperature change, light, electric current, chemical reactions (i.e., water, ethanol, pH change), magnetic field and mechanical force (i.e., impact and pressure) (X. Wu *et al.*, 2013; Laitinen *et al.*, 2020; Strzelec, Sienkiewicz and Szmechtyk, 2020). The characteristics of shape-memory function can be categorised into one-way SME, two-way SME, triple-shape SME and multi-way SME, which will be discussed in the following section concentrating on thermo-responsive SMPs.

Table 3.5. The classification of SMPs based on their structure (Kolesov, Dolynchuk and Radusch, 2015; Jose *et al.*, 2020; Strzelec, Sienkiewicz and Szmechtyk, 2020).

Class	Types of Structure	Shape Transition Temperature	Permanent Shape Fixed By	Secondary Shape Fixed by	Examples
<b>Class I</b>	Chemically cross-linked amorphous SMPs	Glass transition temperature (T <sub>g</sub> )	Chemical cross-linking	Vitrification	Polynorbornene, Thermoset Polyurethane, Epoxy, Styrene copolymers, Polyethylene terephthalate – Polyethylene glycol (PET–PEG) copolymers, Poly (n-butyl methacrylate) – Poly (methyl

					methacrylate) PMMA–PBMA copolymers, Methacrylate.
<b>Class II</b>	Chemically cross-linked semi-crystalline SMPs	Melting temperature (T <sub>m</sub> )	Chemical cross-linking	Crystallisation	PCL–BA copolymer, Poly (cyclooctene), PE, PE/PP blends, Poly (ε-caprolactone) based systems, Acrylates, Poly (propylene sebacate).
<b>Class III</b>	Physically cross-linked amorphous SMPs	T <sub>g</sub> or T <sub>m</sub>	Physical cross-links (i.e., rigid amorphous domains, crystals, hydrogen bonding or ionic clusters)	Soft segments with lower T <sub>g</sub> or T <sub>m</sub>	POSS-PN block, Copolymer, Styrene block copolymer, PET-co-PEO, PE-co-nylon6, PE-co-PMCP, PCL-b-ODX, POSS telechelic, PVDF/PMMA blend, Polylactide-based systems oligo(ε-caprolactone).
<b>Class IV</b>	Physically cross-linked semi-crystalline SMPs	T <sub>g</sub> or T <sub>m</sub>	Physical cross-links (i.e., polar interaction, hydrogen bonding or crystallisation)	Crystallisation of soft segments	Styrene-trans-butadiene-styrene TBSP, Polyurethane copolymers with different soft segments, PCL-based systems, Copolyesters.

### 3.2.2.5. Thermo-Responsive SMPs

Temperature-based actuation, also known as heat-induced actuation, is one of the most exploited stimulus-activated strategies for 4DP (Q. Wang *et al.*, 2018; Rosales *et al.*, 2019; Shen *et al.*, 2019; Laitinen *et al.*, 2020). The common thermally induced methods include inductive heating, Joule heating directly from a medium (i.e., hot water, heated gas), mechanical heating and light heating.

The basic working mechanisms to achieve the SME for thermo-responsive SMPs can be classified into dual-state mechanism (DSM), dual-component mechanism (DCM) or partial-transition mechanism (PTM) (X. Wu *et al.*, 2013; Yang *et al.*, 2014). DSM and DCM thermo-responsive SMPs use its  $T_g$  as the threshold temperature to evoke shape transformation. It has an ability to produce strain, be fixed at a temporary programmed shape and recover to its original shape when heated above  $T_g$  for amorphous polymer or above  $T_m$  for crystalline polymer (Thakur and Hu, 2017; Laitinen *et al.*, 2020; Strzelec, Sienkiewicz and Szmechtyk, 2020). In contrast, PTM involve heating the polymer to a temperature within its transition range. As a result, the unsoftened part serves as the elastic component to store elastic energy while the softened part behaves as the transition component (Huang *et al.*, 2012). DSM and DCM are the two widely applied working mechanisms. Yang *et al.* (2014) explained that PTM is less explored and applied as it requires distinctive care in implementation.

The characteristics of shape-memory function can be categorised into one-way, two-way, and multi-way SME. One-way and two-way SME are DSM. The majority of SMPs have a one-way SME, characterised by their  $T_g$ . Two processes are required to form a complete shape memory cycle, which involve four successive steps from deformation, fixing, cooling to recovery (Figure 3.10). One-way SME is irreversible. The programming step has to be repeated to programme the material back to its secondary shape.

The first stage is the programming process, which involves shape deformation and fixation procedures to set the material into a desired secondary shape. The polymer is heated at its shape deforming temperature ( $T_d$ ) (may be equal, above or below its  $T_g$ ) to change from a glass state to a rubbery state. It would become soft and can be easily deformed by inducing stress through an external force or constraint (externally applied loading). The polymer is cooled under fixed strain at fixing temperature (usually 20°C below its  $T_g$ ) to return hard at its glass state before the removal of constraint. The secondary shape is maintained. SME enables the material to remain constant in its interim shape until the right optimum stimulus is applied to trigger shape recovery. The second stage is the shape recovery process by heating the polymer at its shape recovery temperature ( $T_r$ ) (equal or below  $T_d$ ). The relieving of stored elastic strain when cooling starts below  $T_g$  creates the driving force for shape recovery to its original shape (Jose *et al.*, 2020).

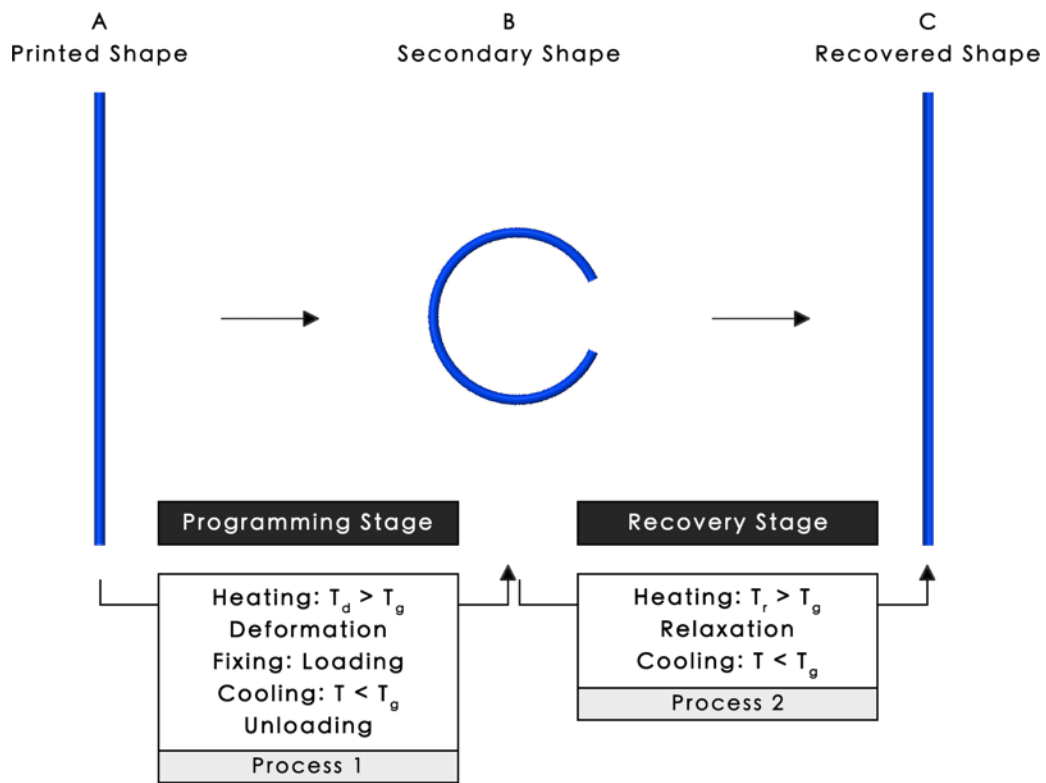


Figure 3.10. One-way SME.

Two-way SME is the ability of the polymer to remember two different shapes, one on heating equal or above its  $T_g$  ( $T$  high) and return to the alternative configuration on cooling at below  $T_g$  ( $T$  low). Two-way SMPs undergo a cyclic or reversible SME based on temperature change between  $T$  low and at  $T$  high (Zare *et al.*, 2019). The programming and recovery stages are performed in a like manner as one-way SME, commencing with heating the SMP above the  $T_g$ . However, two deformations are maintained at two fixing temperatures (Figure 3.11).

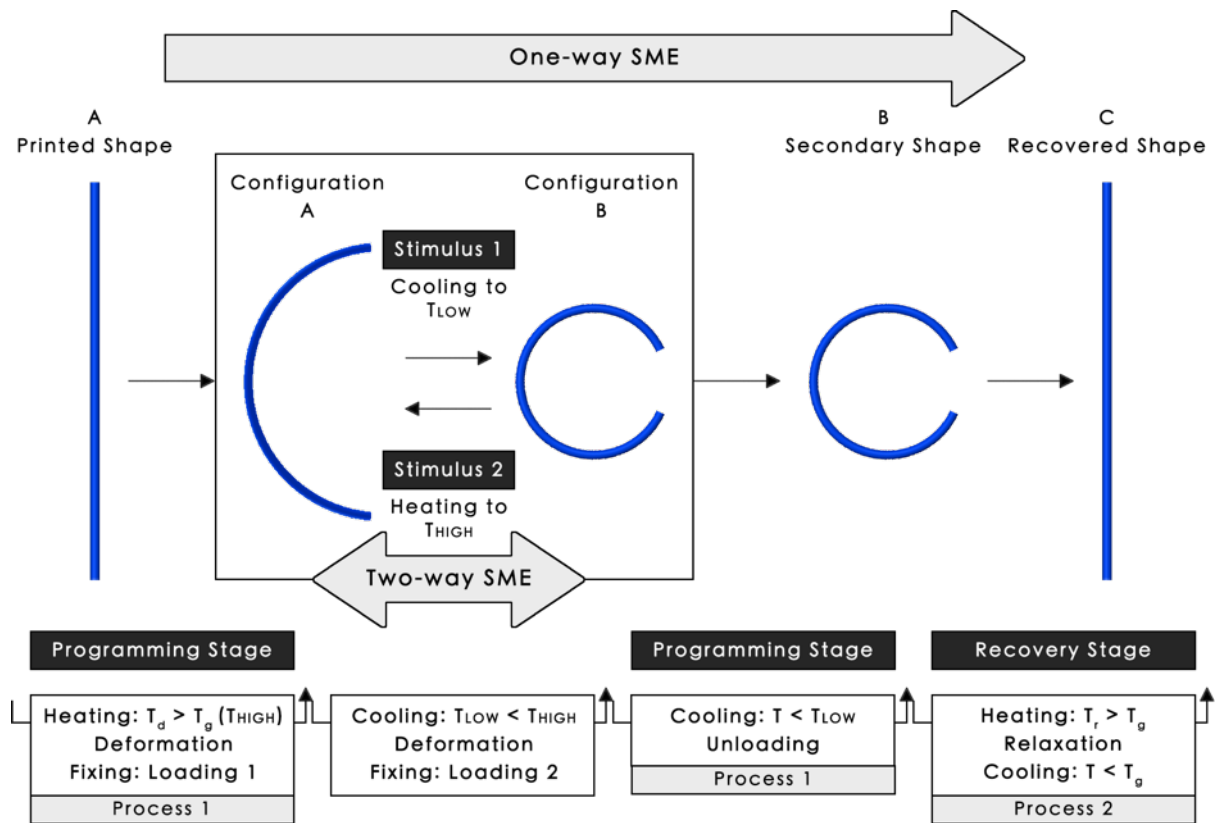


Figure 3.11. Two-way SME.

On the other hand, triple-shape SMPs have multi-way SME with a permanent original shape and two metastable shapes. They consist of two independent switching phases related to two different transitions which contain multi-step programming and recovery cycles (Figure 3.12) (Teoh, 2018; Strzelec, Sienkiewicz and Szmechtyk, 2020).

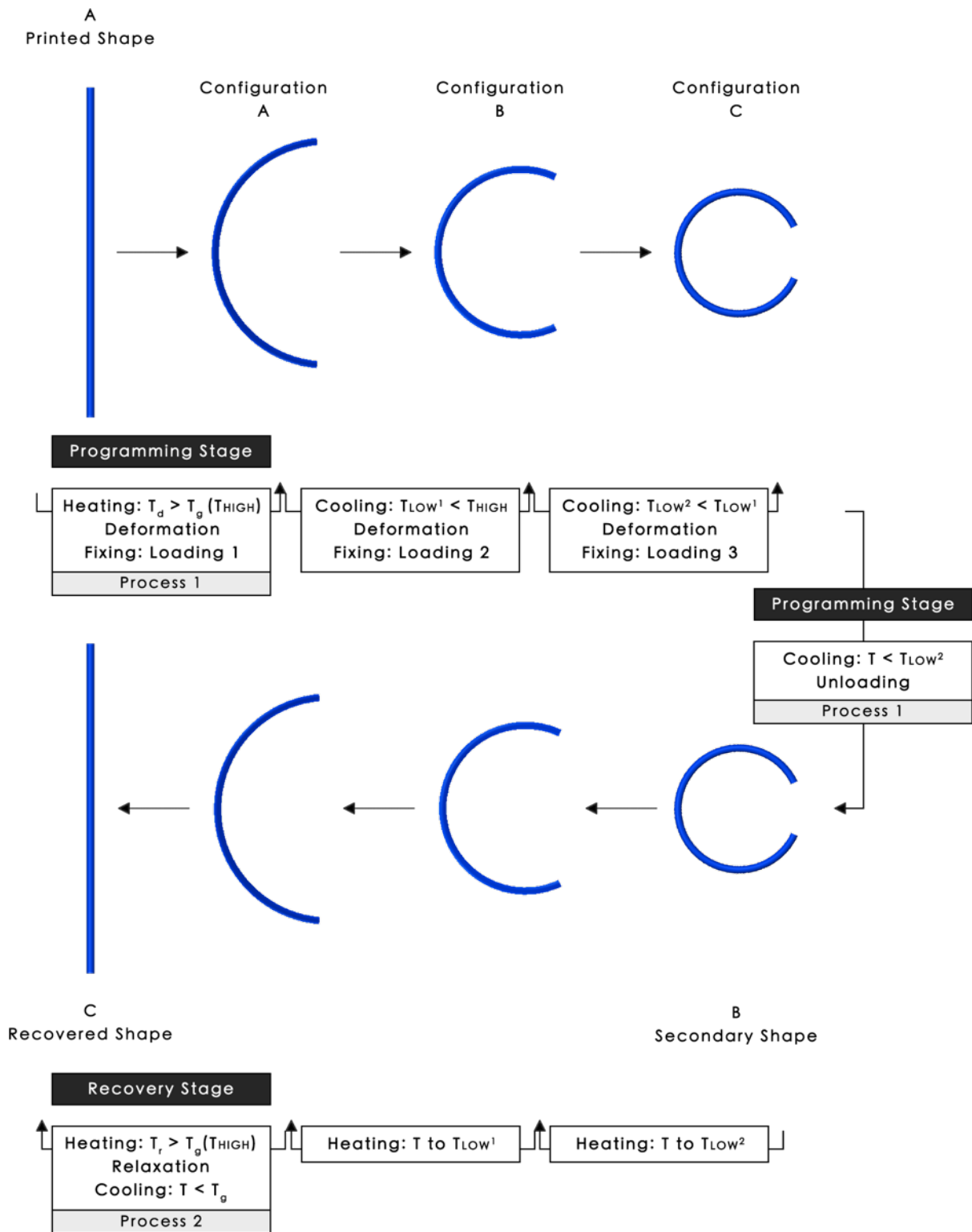


Figure 3.12. Multi-way SME.

Table 3.6 summarises the process flow, phenomena, activity involved, temperature and experimental measurement for the thermo-rheological characterisation of DSM thermo-responsive SMP with one-way SME for 4DP. The programming stage examine the shape

fixity of the SMP, which characterises its ability to fix the strain imparted in the sample during the deformation step after subsequent cooling and unloading (Basit, 2016).

The shape recovery stage investigates the shape recovery of the material, alongside the rate of shape morphing activation ( $T_a$ ) and the time taken for complete shape recovery. Shape recovery characterises the ability of the SMP to recover the accumulated strain during the deformation step after subsequent cooling and unloading upon reheating to the rubbery state (Basit, 2016).  $T_a$  is defined as the time taken to trigger the shape-morphing. The time taken for complete shape recovery, also known as the recovery speed, can be defined as the percentage of recovery per unit of time, which is manipulated by the recovery heating rate. The recovery speed increases, as the  $T_r$  increases.

Table 3.6. The shape memory thermomechanical characterisation of DSM thermo-responsive SMP.

Stage	Start	Programming Stage		Secondary Shape	Shape Recovery Stage		End
<b>Process Flow</b>	Printed shape	Subject to stimulus (Heating: $T_d > T_g$ )	Removal from stimulus (Cooling: $T < T_g$ )	Deformed shape	Subject to stimulus (Heating: $T_r > T_g$ )	Removal from stimulus (Cooling: $T < T_g$ )	Recovered shape
<b>Phenomena</b>	-	SCE		-	SME		-
<b>Activity</b>	Fabrication of the SMP into an original shape.	Shape deformation	Shape fixation (Loading)	Removal of constraint (Unloading)	Shape recovery		-
<b>Temperature</b>	-	$T_d$	Fixing temperature	-	$T_r$		-
<b>Experimental Measurement</b>	-	-		Shape fixity	Ta and the time taken for complete shape recovery		Shape recovery

Table 3.7 specifies the relevant characterisation techniques to study the structure-function relations, SME and morphological features of SMPs ranging from macroscopic level to the molecular level.

Table 3.7. Characterisation techniques for SMPs (Wagermaier *et al.*, 2009; Basit, 2016; Jose *et al.*, 2020; Parameswaranpillai *et al.*, 2020).

<b>Test Methods</b>	<b>Types of Characterisation</b>
Nuclear magnetic spectroscopy	Characterisation of molecular level hierarchal organization of polymer structure.
	Chemical net points (i.e., cross-link density and functionality).
Dynamic Mechanical Thermal Analysis (DMTA), Differential Scanning Calorimetry (DSC)	Thermal characterisation of SMPs (i.e., the crystallinity, phase transition and Tg behaviour).
Differential scanning calorimetry	To investigate the types of shape memory properties exhibited by the SMPs.
Conventional mechanical testing	The static mechanical properties of SMPs.
Dynamic mechanical testing	The shape-memory parameters (i.e., shape fixity and shape recovery).
High temperature nanoindentation technique	The shape memory process at a nanoscale dimension.
Scanning electron microscopy (SEM)	Micro-scale surface pattern, micro and nano-level structural features, evolution and population of nano-wrinkles and dispersion of nanomaterials in the SMP matrix.
Transmission electron microscopy (TEM)	Nano-level structural features.
Optical and polarized optical microscopy (OM and POM)	The structural organization and morphology evolutions of SMPs.
Atomic force microscopy (AFM)	Surface topography and the shape memory process.
Laser scanning confocal microscopy (LSCM)	3D visualisation of structural features of biological samples.
X-ray scattering	The shape memory behaviour of SMP through analysing the micro-state and nano-state structural features.

### 3.2.3. Design of Actuation Mechanism, Geometric and Material Distribution

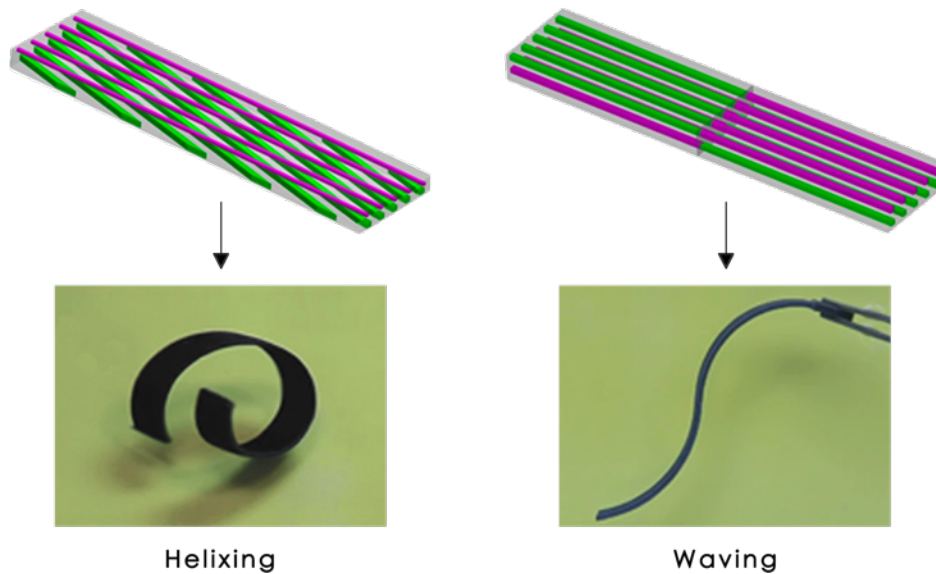
The printed design is the permanent shape and initial state of a 4DP structure. An encoded 4DP static structure will not perform its intended behaviour change in a timed approach upon activation by stimulus unless complemented with the right actuation mechanism design, geometric design, material structure, and material distribution. Pei *et al.* (2020) defined a timed approach as the exact moment that triggers the shape change reaction and the total duration for complete shape-change.

The actuation mechanism design involves analysing the objective property and the design of the actuation characteristic (Jian *et al.*, 2018). The shape transformation actuation of 4DP structures can either be self-actuated shape change or shape-memory actuation. Geometric design defines the design of the smart structure. The geometric design for both before and after activation needs to be well-thought-out. According to Jian *et al.* (2018), the first step is designing the geometry of the entire mechanism, followed by patterning and optimising the material distribution at different arrangements to reproduce the desired function. The key parameters to consider in geometric design include, the thickness, length, width, mass and the position or area of deformation of the printed structure. Other structural design parameters include the printing pattern, types of joint and hinges, and active origami (Peraza-Hernandez *et al.*, 2014).

The material structures can be described as being homogeneous or heterogeneous. A homogeneous structure is made up of a single SRM while a heterogeneous structure is made up of multiple materials, which can be (1) a combination of SRM and passive material, or (2) a mixture of two or more SRMs. A multi-material 4DP structure made of SRM and passive material is usually used to perform sequential control self-assembly. Self-assembly is induced by the difference in physical properties, such as the mismatching strain, CTE or different swelling ratio between the two (or more) materials (Zhou *et al.*, 2015). Jian *et al.* (2018) explained that passive materials act as functional elements to overcome the drawbacks of SRM (i.e., low strength, large deformation). The materials can take advantage of each other's properties to add more transformable characteristics and functionality for multi-functional 4DP structure. On the other hand, structure fabricated with multiple SRMs displays distinct actuation characteristics to perform switchable or reversible configurations when activated by different predefined stimuli (Kuksenok and Balazs, 2016; Mao *et al.*, 2016; Jian *et al.*, 2018).

The shape-shifting behaviours of homogeneous structures are usually shape-memory actuated, based on a designed interaction mechanism. Momeni *et al* (2017) described the interaction mechanism as the programming and recovery sequence of a 4DP structure. It involves a set of deformation mechanism to plan out the sequence of shape-shifting behaviours when triggered by the stimulus under an appropriate amount of time. Constrained-thermo-mechanics is one of the widely explored interaction mechanisms, in which the structure undergoes a thermo-rheological characterisation by submitting it to a thermo-mechanical cycle that includes programming and recovery processes. The programming process involves the phase fixation of material into a temporary shape either through mechanical loading using Universal Testing Machine (Chávez *et al.*, 2019; Rosales *et al.*, 2019) or physical deformation using specifically designed forming jig.

For heterogeneous structures, the design and the placement of geometric programme embed the capability for shape-shifting directly into the materials themselves (Ge, Qi and Dunn, 2013; Tibbits, 2014). The orientations, allocation and distributions of the active material and the passive material (strain limiting layer) within the matrix of a multi-material structure determine that the shape transformation occurs in a controlled approach and coordinated way as intended to meet the desired functional properties (Figure 3.13) (Kuksenok and Balazs, 2016; Mao *et al.*, 2016; Jian *et al.*, 2018). A controlled approach enables a pre-programmed shape transformation process to take place across a specified amount of time. In line with Pei *et al.* (2020), a coordinated way refers to synchronizing and unifying the behaviour of the parts to perform the shape-changing process. The materials can be arranged in a uniform and discrete pattern with different concentrations, using gradient distribution (FGAM) or special patterns (Momeni *et al.*, 2017; Loh *et al.*, 2018; Pei and Loh, 2018b).



● ● : Active materials (VeroWhite DM8530 and DM9895) ● : Passive material (Tango Black plus)

Figure 3.13. Different thermally induced shape-shifting behaviours are achieved by modifying the orientation and position of the deposited materials within a bilayer multi-material structure, demonstrated by Wu et al. (2016) through being heated in water.

### 3.2.4. Modelling and Simulation

Modelling and simulation, termed as mathematical modelling by Momeni *et al.* (2017), is the combined use of ‘CAD–CAE–CAM’ to develop theoretical and numerical models to build a target 4DP product, taking account of the material properties and characterisation, the material structure design, the corresponding working mechanism, constitutive behaviour modelling and the stimulus properties. On the whole, mathematical modelling provides both backward and forward predictions (Zhang, Demir and Gu, 2019). Backward prediction specifies the printing profile of a target shape and function while forward prediction simulates the transformation process based on the developed profile.

CAD software such as SolidWorks can design the geometry, hinges and patterns of the printed structure. However, the time characteristics of 4DP require specialised software solution to support the simulation, modelling, slicing, host or firmware, monitoring and printing management software (Table 3.8). Figure 3.14 presents the software architecture and types of solutions for 4DP as proposed by Chung, Song and Cho (2017). The printing management software connects, control and communicate with all the software in the five-stage process, from simulation to monitoring. For multi-materials 4DP, the software needs

to plan out additional variables, such as the materials distribution and orientation, calculate the different coefficient of thermal expansion (CTE) rates, strain or degree of swelling between materials, material optimisation, simulate the sequence of shape transformation and estimate the required amount of time for the stimulus to act on to create an effective stimulus-responsive output (Raviv *et al.*, 2014; Momeni and Ni, 2020).

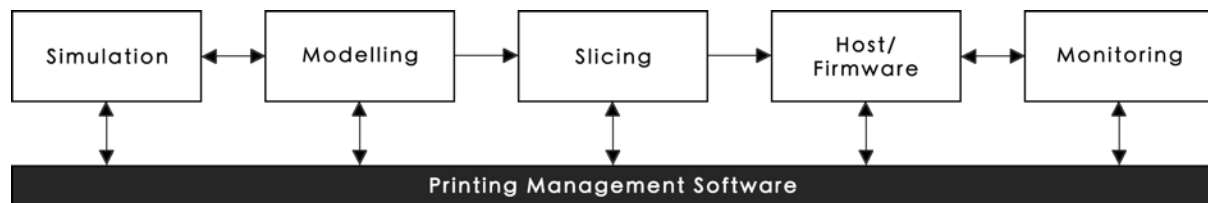


Figure 3.14. Software architecture and types of solutions for 4DP.

Table 3.8. 4DP software solutions and function.

Processes	Function	Types	Examples
Simulation	To imitate the behaviour of the structure to reduce failure risk before the actual product development.	Finite element analysis (FEA)	ABAQUS (Mao <i>et al.</i> , 2015, 2016; Wu <i>et al.</i> , 2016), COMSOL Multiphysics (Fairclough, 2018)
		Simulation by programming	Project Cyborg, 4D modeler (Ham and Lee, 2016)
Modelling	Generate 3D object modelling data.	Modelling software	AutoCAD, SolidWorks, Blender, CATIA
Slicing	Dividing the 3D object into a stack of 2D flat layers. The conversion of STL. (or 3MF/AMF) format into printer commands in G-code format.	Slicing software	Slic3r, Simplify3D, Cura, KISSlicer, Craftware
Host/ Firmware	Laminate the actual object according to the design instructed by the slicer software.	Printer own host software	-
		Open-source software	
Monitoring	The monitoring software is linked to the host/firmware to observe the self-transformation process and carries our appropriate actions if required.	3D printer monitoring software	Manufacturer provided software

Other proposed and development simulation software include VoxSmart (Sossou *et al.*, 2019) and Thermorph (An *et al.*, 2018). Unfortunately, there was no further update on the Project Cyborg since the year 2014 by Autodesk with the Self-Assembly Lab at MIT, which was initially introduced as potential cloud-based CAD software for modelling, simulation of self-assemblies and programmable materials, and multi-objective design optimisation for 4DP.

Fold pattern design software are available to generate the base of self-assembly active origami structure, although they are not targeted specifically for 4D printing. For instance, E-origami system (Eos) are developed for symbolic and numeric constraints solving, automated theorem proving, visualisation of an origami construction and interactions with a web browser (Eos Project, 2020). Origamizer is another specialised fold pattern design software that creates complex origami shapes by assigning nodes, edges, paths, polygons, vertices and creases. The software is capable of generating crease patterns that can fold solid geometries into a complex polyhedral model with a designated number of seams (Peraza-Hernandez *et al.*, 2014). TreeMaker is another lightweight program created by Lang (2015) that generates the triangular algorithm base from stick figure drawing to design the origami bases. Inversely, Peraza-Hernandez *et al.* (2013) established a simulation software to unfold a given convex polygonal mesh into either multiple or one-piece planar sheets.

### **3.3. Process Flow of 4DP**

Currently, there is no standardised design process flow and manufacturing methodology established for designing for 4DP. 4DP shares some identical stages involved in the process chain of 3DP, such as file preparation (CAD-based 3D model), the conversion of CAD file into an STL (or AMF) file, slicing the 3D model into 2D layers, layer-by-layer fabrication to post-processing. However, the dynamic properties and multi-functionality of SRMs make the design process of a 4DP product more complex compared to a 3DP product. The design strategy for 4DP is not as consistent as 3DP as it changes according to the desired functionality of a 4DP product. The 4DP process flow and manufacturing methodology presented in Figure 3.15 and Table 3.9 respectively are interpreted and established based on extensive research and findings from various works of literature, such as Jian *et al.* (2018) Sossou *et al.* (2018). The 4DP process flow can be classified into four phases, (1) material, (2) design, (3) fabrication and (4) actuation.

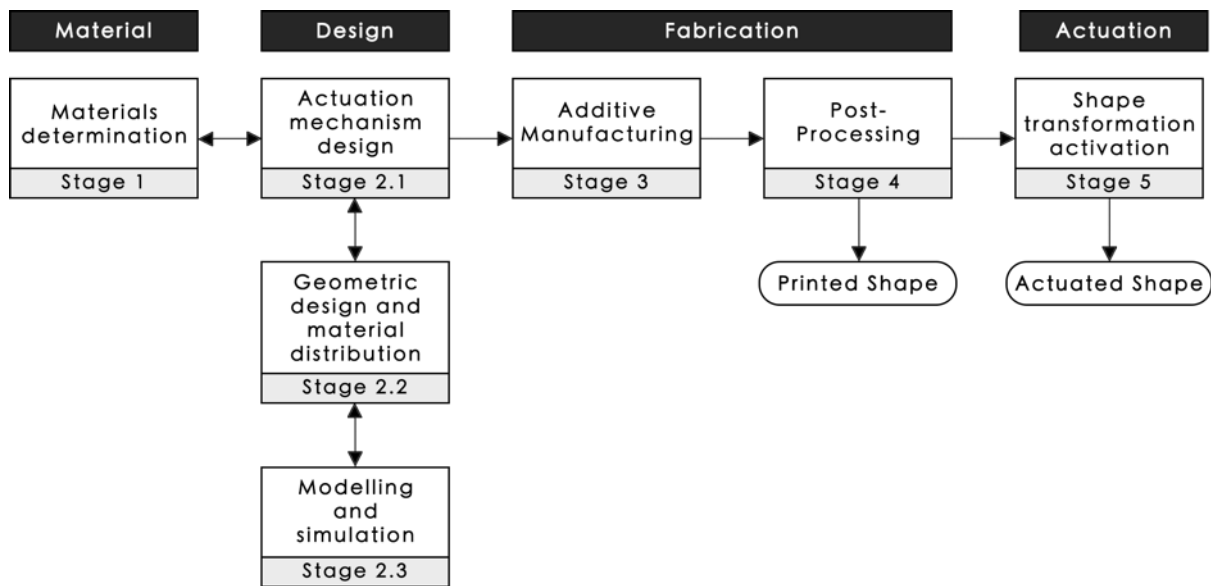


Figure 3.15. 4DP process flow showing the four major phases.

Table 3.9. Manufacturing methodology of 4DP.

Phases	Stage		Process	Ref
Material	1	Materials determination	List of SRMs Material characterisation Functional element selection (for multi-material 4DP) Synthesis and quantification Principal material selection	Chapter 3.2.2
Design	2.1	Actuation mechanism design	Analyse the object property Determine the functional properties Design the actuation characteristic Design of deformation mechanism (for shape-memory actuation)	Chapter 3.2.3
	2.2	Geometric design and material distribution	Definition of the main part Design of active structure for AM Determine the material orientation, allocation and distribution (for multi-material 4DP)	
	2.3	Modelling and Simulation	Model construction Design simulation Testing and optimisation	Chapter 3.2.4
Fabrication	3	AM	AM process selection	

			Manufacturing strategy and process plan Process control and monitoring		Chapter 3.2.1
	4	Post-processing	Part removal Support structures removal Cleaning Surface treatment		(Redwood, Schöffner and Garret, 2017)
Actuation	5	Shape transformation actuation	Self-actuated shape change	Self-assembly, self-folding, self-bending or other shape-shifting behaviours.	Chapter 3.5
			Shape memory	One-way, two-way or triple-way SME.	

There is no definite sequence in the process flow of the 4DP design framework as some processes are tightly intertwined and should be processed simultaneously, especially in Stage 1 and 2 (2.1, 2.2. and 2.3). This was suggested in the study by Sossou *et al.* (2018) that the determination of materials should be carried out alongside the design of the 4DP component. Though, the multi-functional SMP design framework proposed by Jian *et al.* (2018) suggested otherwise. Jian *et al.* (2018) advised that the material selection should come after the design of the actuation mechanism when the functional properties of the 4DP component are determined.

### 3.4. The Advancement of 4DP

AM provides greater possibilities in manufacturing SMP structures that were restricted and beyond the limits of traditional manufacturing methods (i.e., situ polymerisation, extrusion and casting), particularly in increasing product design freedom, no extra cost for complexity and on-demand production in batches of one (Campbell, Tibbits and Garrett, 2014).

By leveraging on AM of SRMs, 4DP offers unique advantages over conventional AM (3DP) in several aspects. The printed structures are no longer static. They are dynamic, exhibit multi-functionality and evolve in a certain sequence under an appropriate amount of time when the right stimulus is introduced. 4DP structures can be programmed for actuation without the need for external power sources or electromechanics (Pei, Loh and Nam, 2020). Hence, the need for expensive, complex, energy-consuming and failure-prone electro-mechanical systems such as motors, sensors can be removed or minimised (Tibbits *et al.*,

2014; Bakarich *et al.*, 2015; Pei and Loh, 2018b). As it moves towards the goal of dynamic self-assembly objects, 4DP can also reduce the materials and the number of components in an object, decrease energy cost, the fabrication and assembly time, minimise manufacturing complexities and printing restrictions (i.e., printing scales and post-processing support structures). 4DP can eliminate post-fabrication assembly. Structures are no longer constrained by the size or volume of the print bed. They can be printed in two-dimensional (2D) shapes or in simpler geometries to be activated to self-assembly or reconfiguration into a more complex three-dimensional (3D) assembly at post-fabrication. Self-construction structures pave the way for novel flat-pack design solution which can help to reduce volume for storage and transportation (Ge, Qi and Dunn, 2013; Kuang, Roach, *et al.*, 2018). The components can also be further programmed for self-disassembly. Abuzied *et al.* (2020) and Chiodo and Jones (2012) suggested that self-disassembly can be used for active product or joints disassembly at their end of life for effective recycling.

### **3.4.1. 4D Printing Applications**

4DP paves the way to novel performance-driven applications ranging from nanoscale to macroscale, pioneering aerospace and defence, automotive, biomedical and healthcare, followed by construction, manufacturing and infrastructure (Campbell, Tibbits and Garrett, 2014; Knowledge Sourcing Intelligence, 2020). 4DP is predominantly researched for fabricating responsive structures for soft robotics and printable actuators at the moment (Bakarich *et al.*, 2015). The use of the 4DP strategy is expected to become significantly widespread with more applications across different industries in the future, such as packaging, food equipment, sports products, toys, fashion and textiles. The applications can be categorised according to their capabilities, which are self-assembly, self-adaptability and self-repair.

#### **3.4.1.1. Self-assembly**

Self-assembly would be specifically useful for micro and macroscale applications with less accessible areas or harsh environment with minimum human involvement. Researchers have planned several interesting ideas for self-assembly structures. For instance, Soldini *et al.* (2020) developed an origami solar sail that can change its local surface reflectivity for the next generation of self-reconfigurable small satellites (CubeSats). Other potential self-

assembly aerospace applications include lightweight deployable structures like ground-based mirrors, panels, morphing aircraft wings, space antennae and satellites (Tibbits, 2014; Sun *et al.*, 2016; Bashir, Lee and Rajendran, 2017). The same concept can be applied to automotive applications like tuneable automotive brackets and automobile actuators.

As an alternative to using shape-memory fibres, yarns and fabrics, direct ME of SRMs onto conventional textiles would be an approach to create SRMs-textile composites (Pei, Shen and Watling, 2015; Loh, Sotayo and Pei, 2021). 4DP will potentially open up new opportunities in fashion and textile innovation with the production of programmable textiles, smart wearables and related products that can self-transform and shape change when subjected to temperature change, water or humidity sensitivity (Leist *et al.*, 2017; Zapfl, 2019). Other promising applications include self-interlocking safe boxes and lockers (Zhang, Demir and Gu, 2019).

#### **3.4.1.2. Self-adaptability**

Self-adaptable and multifunctional applications using biocompatible and biodegradable SRMs would be a novel breakthrough for the biomedical and healthcare sectors, especially in supporting minimally invasive surgery and the fabrication of personalised medical devices. The anticipated applications include controlled drug release system, microactuators for clot removal, surgical sutures, stents (Figure 3.16) and self-anchoring implants (Neffe *et al.*, 2009; Wykrzykowska, Onuma and Serruys, 2009; Wischke and Lendlein, 2010; Xu and Song, 2011; Zarek *et al.*, 2017). Adaptive infrastructures proposed by Campbell, Tibbits and Garrett (2014) are another striking application of 4DP.

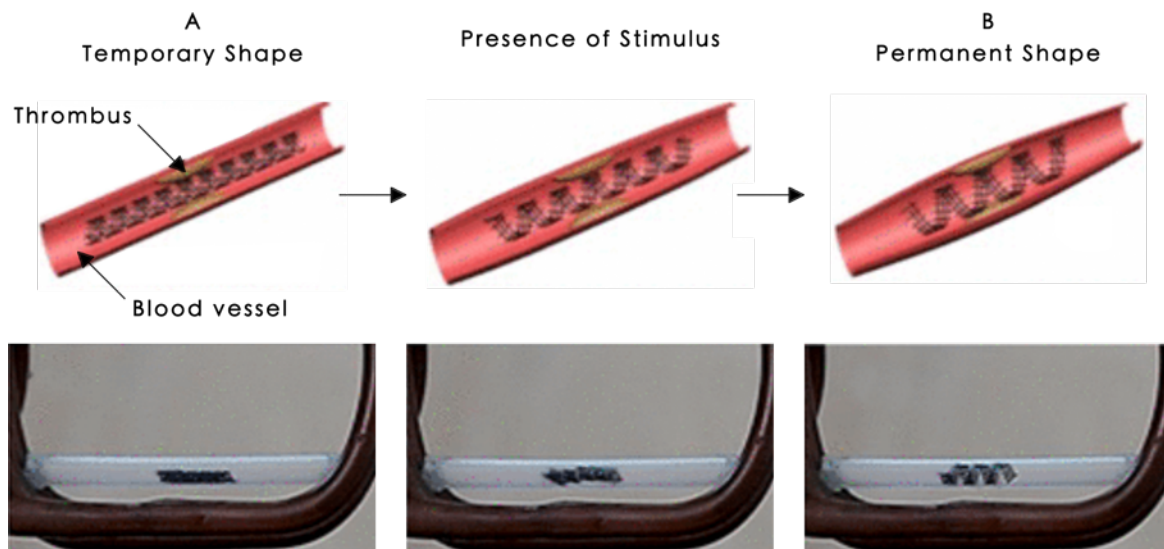


Figure 3.16. Magnetic stent adapted by Wei *et al.*, (2017). (A) the temporary shape for deployment and (B) the permanent shape for performance.

### 3.4.1.3. Self-repair

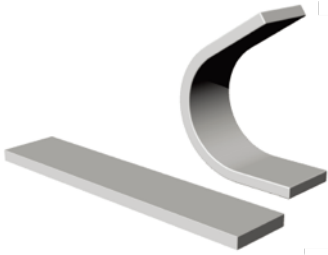
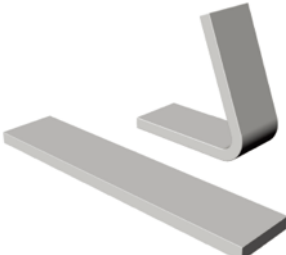
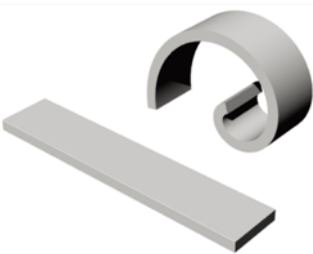
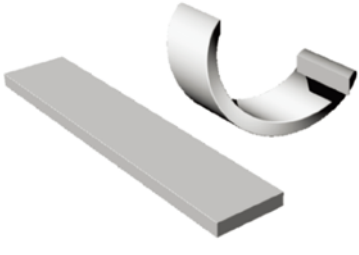
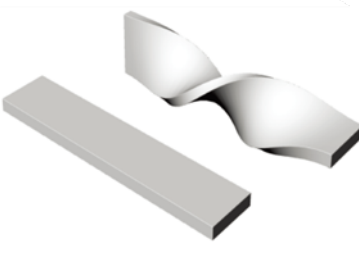
4DP structures can also be designed to error-correct and self-repair a mechanical damage using shape memory assisted self-healing materials (Taylor and Panhuis, 2016). The ability of self-restoration by bringing the crack surfaces closer together enhances the reliability and extends a product's service life. Kuang, Chen, *et al.* (2018) exploited a material system capable of repeated crack healing post-UV-assisted DIW printing, which can potentially pave a new way for the development of novel vascular repair devices. Browne and Johnson (2009) developed an automotive tire capable of autonomously repair a structural anomaly (i.e., crack and puncture) and remove a surface anomaly such as foreign objects that adhered to or lodged in the tire. Other proposed applications include flexible healing pipe by Campbell, Tibbits and Garrett (2014), soft robotics and wearable soft robotic skins for assisted health technologies using self-healing hydrogel (Taylor and Panhuis, 2016).

## 3.5. Types of Shape-Shifting Behaviours and Shape Transformation Actuation

Table 3.10 lists other primary basic shape-shifting behaviours which include, but not limited to, curving, rolling, helixing, twisting, waving, expansion or contraction as proposed by Nam and Pei (2019). Different shape-shifting behaviours can be combined to create complex shape transformation (Table 3.11). In reviewing the recent experimental and theoretical

literatures, it has been clear that bending and folding are the fundamental shape-shifting behaviour applied for 4DP structure. Bending and folding have also been widely used to characterise the shape memory cycle of SMPs. The studies by Groeger, Chong Loo and Steimle (2016) and Ryu *et al.* (2014) emphasised the importance to characterise the differences between bending and folding before investigating other shape-shifting behaviours and self-assembly behaviours.

Table 3.10. Basic shape-shifting behaviours.

<p style="text-align: center;"><b>Bending</b></p> 	<p style="text-align: center;"><b>Folding</b></p> 
<p>Bending is a global deformation associated with a smooth distributed curvature.</p>	<p>Folding is sharp angle deformation with a crease hinge at a pre-defined location, while the surrounding areas are left undeformed.</p>
<p style="text-align: center;"><b>Curving</b></p> 	<p style="text-align: center;"><b>Rolling</b></p> 
<p>Curving is a surface deviation from a plane surface without sharp breaks or angularity.</p>	<p>Rolling is moving by turning over and over on its own axis.</p>
<p style="text-align: center;"><b>Helixing</b></p> 	<p style="text-align: center;"><b>Twisting</b></p> 
<p>Helixing a type of smooth space curve with tangent lines at a constant angle to a fixed axis.</p>	<p>Twisting is turning the two ends of the part in the opposite direction from another.</p>

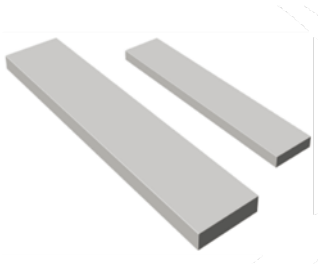
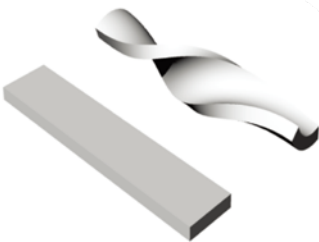
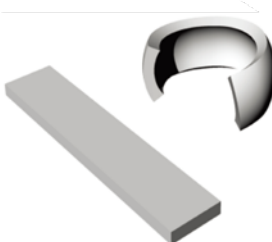
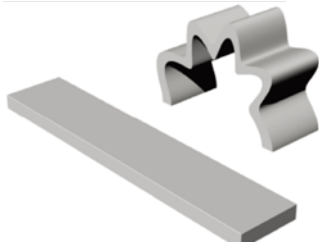
<p style="text-align: center;"><b>Waving</b></p> 	<p style="text-align: center;"><b>Expansion or Contraction</b></p> 
<p>Waving is to bend alternately in opposite directions forming an undulating form.</p>	<p>Expansion is an action of becoming larger while the contraction is becoming smaller in shape, volume or area of the material.</p>

Table 3.11. Examples of combined shape-shifting behaviours.

<p style="text-align: center;"><b>Bending and Twisting</b></p> 	<p style="text-align: center;"><b>Bending and Curving</b></p> 	<p style="text-align: center;"><b>Bending and Waving</b></p> 

The temporal shape-shifting behaviour, geometrical, shape-shifting characteristics, the mechanical stiffness and load-carrying capacity of a 4DP structure can be strategically controlled through the gradient distribution, varying the spatial position of material (i.e., lattices) or changing the build parameters of AM, particularly the printing speed, print patterns, fill angle ( $0^\circ$ ,  $90^\circ$  or  $45^\circ$  /  $-45^\circ$  orientation) and infill density (Mao *et al.*, 2015; Rajkumar and Shanmugam, 2018). The research by Nam and Pei (2020) demonstrated the integration of mixed print patterns and infill density within a ME structure to control the recovery speed and to perform asymmetrical shape change (Figure 3.17). Using material jetting, Yu *et al.* (2015) utilised the placement of SMP hinges with different graded material distributions to control and vary the shape recovery profile to perform sequential folding recovery (Figure 3.18). J. Wu *et al.* (2018) have introduced a grayscale 4DP method for DLP to create dissimilar rate of shape-changing at different positions within a structure (Figure 3.19). The sliced grayscale pattern controls and varies the light intensity distribution of a projected pattern, leading to a different degree of cure and crosslinking densities within the photopolymerized sample.

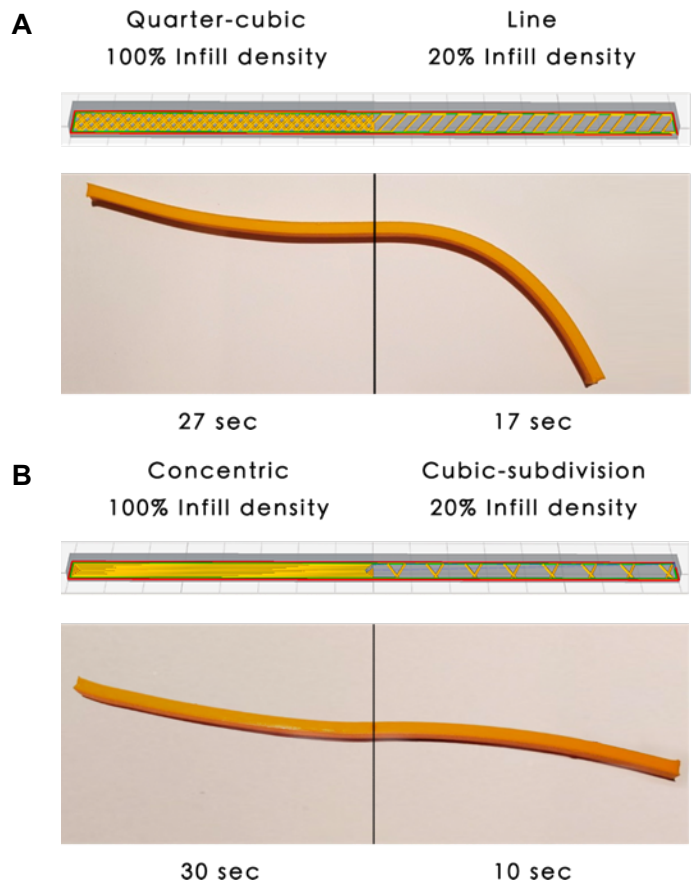


Figure 3.17. Introducing varied recovery speed and asymmetrical shape change within a printed structure using different print patterns and infill density (A and B) by Nam and Pei (2020).

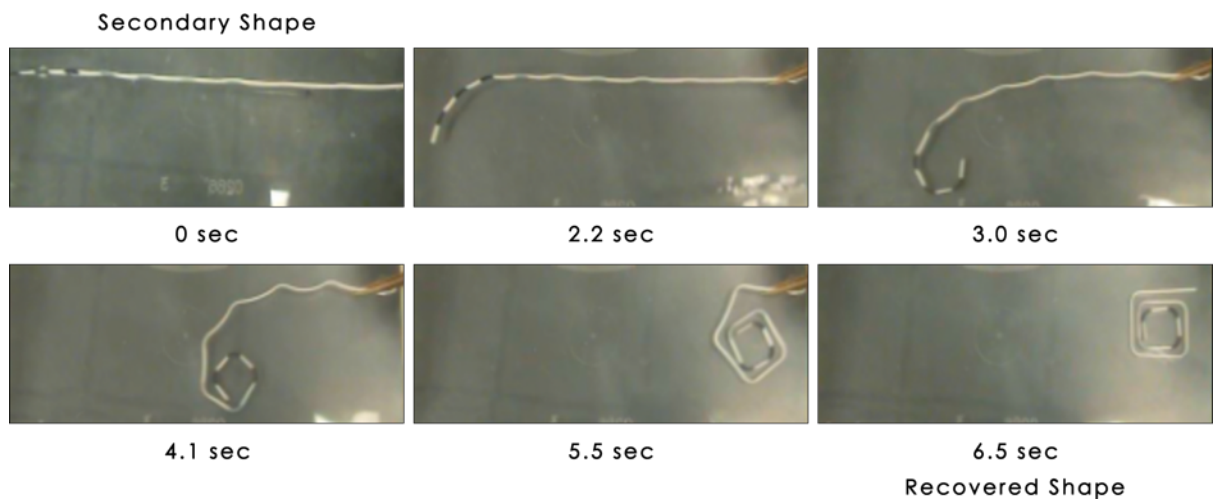


Figure 3.18. Helical line with graded hinge sections to perform sequential folding recovery adapted by Yu *et al.* (2015).

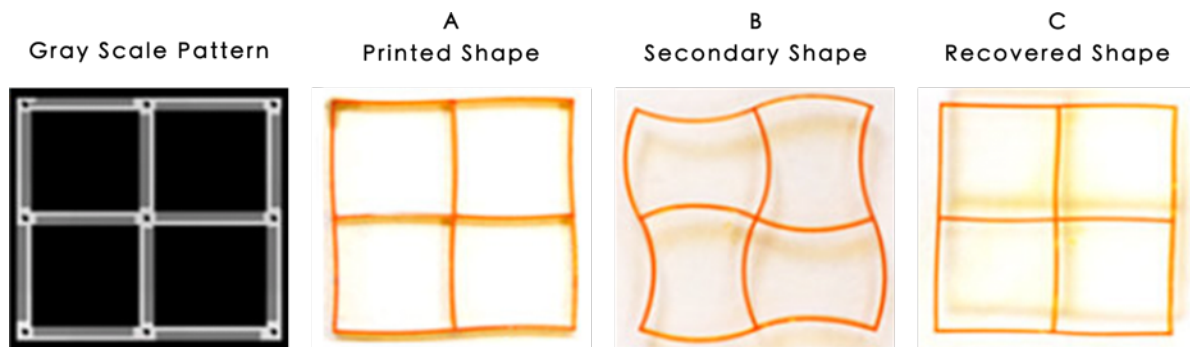


Figure 3.19. Grayscale 4DP method for DLP to introduce different degree of cure and crosslinking densities within a photopolymerized sample proposed by J. Wu et al. (2018).

The literature revealed limited focus on distinguishing the types of shape transformation actuation and programmable behaviours. The shape transformation actuation of 4DP structures can be divided into self-actuated shape change and shape-memory (Table 3.12).

Self-actuated shape change is an automatic shape changing without a shape programming step. It is usually exploited using SCM as a single material or a multi-material composite combining (1) a passive material with an active material, or (2) multiple active materials. SMP heating up to its  $T_g$  can also evoke shape-change actuation. The shape-shifting behaviour of a single SMP is usually limited to bending and curving (Rajkumar and Shanmugam, 2018). SMP combined with a passive material can create self-assembly active origami, controlled sequential folding or self-bending mechanism. On the other hand, SMP combined with another active material can create reversible shape transformations. A reversible actuating component is usually an effect of deformation mismatch of two active materials in a bilayer actuator. Each material reacts differently to the stimuli or stimulus, thereby shape switching between two configurations in a controllable manner without the need for mechanical loading or unloading.

In contrast to self-actuated shape change, shape-memory actuation requires a shape programming and recovery process by submitting the structure to a thermo-mechanical cycle. The printed structure needs to be deformed through a programming and shape fixation process to obtain its secondary shape. The desired shape would be restored through a recovery process.

The dimensional shape change can be classified into 1D to 1D, 2D to 3D or 3D to 3D. The various possible mechanisms, materials and printing methods and potential applications are specified accordingly. In reviewing the studies in literature, it is clear that water is the widely

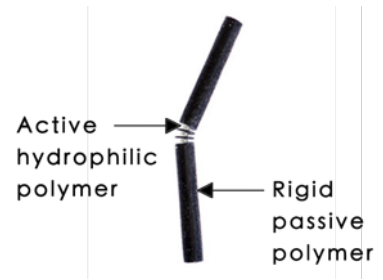
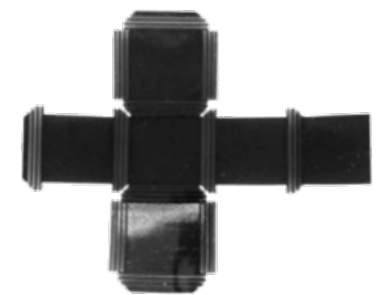
used stimulus to actuate self-actuated shape change transformation, while heat is largely used for shape-memory transformations.

Table 3.12. Types of shape transformation actuation.

Types of shape transformation actuation	Materials	Composition		Concept	Reversible	Types of shape-shifting behaviours	Refer To
Self-actuated shape change	SCM	Single material		Printed shape $\leftrightarrow$ Actuated shape	Yes (When stimulus is removed)	Homogeneous swelling	Chapter 3.2.2.1
		Multi-material	SCM and passive material		Yes (When stimulus is removed)	Self-assembly active origami, controlled sequential folding or self-bending mechanism	Table 3.13
			SCM and active material	Configuration A $\leftrightarrow$ Configuration B	Yes (Through stimulus variation)	Reversible or two-way actuation switching between two configurations	Table 3.14
	SMP	Single material		Printed shape $\rightarrow$ Actuated shape	No	Bending or curving	Rajkumar and Shanmugam (2018)
		Multi-material	SMP and passive material	Printed shape $\rightarrow$ Actuated shape	No	Self-assembly active origami, controlled sequential folding or self-bending mechanism	Table 3.15

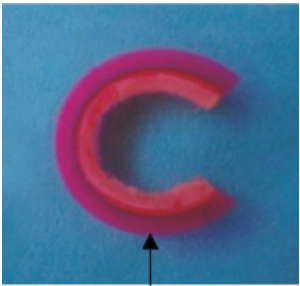
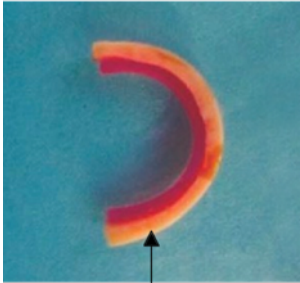
			SMP and active material	Printed shape ↔ Actuated shape	Yes	Reversible or two-way actuation switching between two configurations	Table 3.16
Shape-memory	One-way SMP (Figure 3.10)	Single material		Printed shape → Secondary shape → Recovered shape	No (Reprogramming required)	Determine by the deformation mechanism	Table 3.17
		Multi-material	Active and active				Table 3.18
	Two-way SMP (Figure 3.11)	Single material		Configuration A ↔ Configuration B	Yes (Through stimulus variation)	Determine by the deformation mechanisms and switching between two configurations	Table 3.19

Table 3.13. Examples of self-actuated shape change (Multi-material mechanism: SCM and passive material).

Shape-shifting Behaviours	Types of Responsive Structures	Stimuli	Fabrication		Design			Ref
			Material	Manufacturing Process (Printer)	Concept	Printed Shape	Actuated Shape	
Folding (1D to 2D)	Angle joints	Water	Active hydrophilic polymer (hydrogel) and static UV curable polymer (Material type not disclosed)	Material jetting (Stratasys Connex)	The active hydrophilic polymer swells in water resulting in the fold. The rigid passive material gives the structure and acts as a limiter that controls the fold angle to achieve the final state configuration.			(Tibbits, 2014; Tibbits <i>et al.</i> , 2014)
Self-folding assembly (2D to 3D)	Truncated Octahedron							
Self-folding assembly (2D to 3D)	Cube							

Curving (2D to 3D)	Curve-crease origami							
-----------------------	----------------------	--	--	--	--	---	---	--

Table 3.14. Examples of self-actuated shape change (Multi-material mechanism: SCM and active material).

Shape-shifting Behaviours	Types of Responsive Structures	Stimuli	Fabrication		Design			Ref
			Material	Manufacturing Process (Printer)	Concept	Configuration A	Configuration B	
Switchable bending (2D to 2D)	Bilayer hydrogels actuator	pH level	RH hydrogel and NRG hydrogel	Manufacturing process not disclosed.	Reversible bidirectional bending caused by hydrogels laminate of different pH responsivity.	<p>pH high (pH= 7)</p>  <p>RH hydrogel</p>	<p>pH low (pH= 2)</p>  <p>NRG hydrogel</p>	(Ma <i>et al.</i> , 2014)

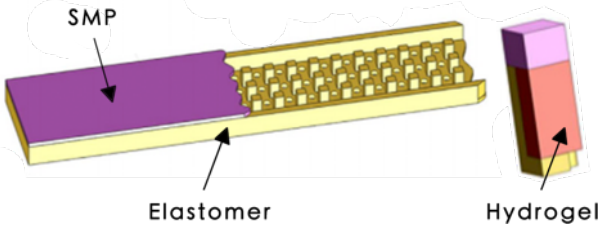
<p>Buckling, expansion and contraction (2D to 3D)</p>	<p>Lego hydrogels</p>					<p>pH high (pH= 7)</p> 	<p>pH low (pH= 2)</p> 		
<p>Bending to flat (2D to 3D)</p>	<p>Reversible actuation component</p>	<p>Water and heat</p>	<p>Active hydrophilic polymer (hydrogel), SMP (Grey60) and elastomer (Tango Black)</p>	<p>Material jetting (Stratasys Objet260 Connex)</p>	<p>A reversible actuation component where the hydrogel is confined by the SMP and the elastomer layers.</p>		<p>(Mao <i>et al.</i>, 2016)</p>		
									

Table 3.15. Examples of self-actuated shape change (Multi-material mechanism: SMP and passive material).

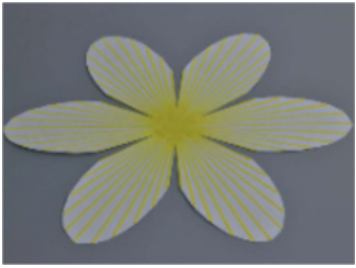
Shape-shifting Behaviours	Types of Responsive Structures	Stimuli	Fabrication		Design			Ref
			Material	Manufacturing Process (Printer)	Concept	Printed Shape	Actuated Shape	
Bending (2D to 3D)	3D flower	Heat	PLA and paper	ME (Printer not disclosed)	Bending caused by the mismatching CTE of composite materials.			(Zhang <i>et al.</i> , 2015)
Bending (3D to 3D)	3D flower	Heat	SMP and elastomer (Material type not disclosed)	VP (Printer not disclosed)	The printing time of petals is varied to introduce a different degree of curvatures.			(Ding <i>et al.</i> , 2017)

Table 3.16. Examples of self-actuated shape change (Multi-material mechanism: SMP and active material).

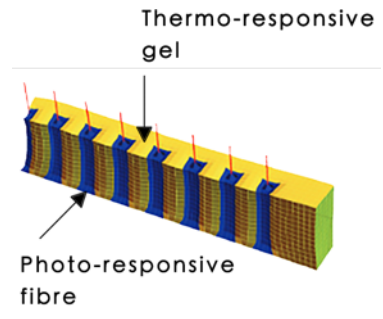
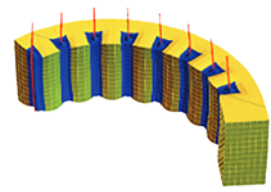
Shape-shifting Behaviours	Types of Responsive Structures	Stimuli	Fabrication		Design			Ref
			Material	Manufacturing Process (Printer)	Concept	Printed Shape	Actuated Shape	
Bending and shrinkage (3D to 3D)	Gel–fiber composite	Heat and light	Thermo-responsive gels and photo-responsive fibres	ME (Direct Ink Writing)	The structure anchored to a surface bend in the presence of light and shrink in the opposite direction when heated.			(Kukse nok and Balazs, 2016)

Table 3.17. Examples of one-way shape-memory transformation.

Types of Responsive Structures	Shape-Memory Function	Stimuli	Fabrication		Design			Ref
			Material	Manufacturing Process (Printer)	Printed Shape	Secondary Shape	Recovered Shape	
Heart shaped cup (3D to 3D)	One-way SME	Heat	PLA	ME (MakerBot Replicator 2)				(Zhou <i>et al.</i> , 2015)
Distorted shape (2D to 2D)	One-way SME	Heat	PU	Manufacturing process not disclosed.				(Huang, 2012)
Spiral spring (2D to 3D)	One-way SME	Heat	PLA	ME (MakerBot Replicator 2)				(Zhou <i>et al.</i> , 2015)

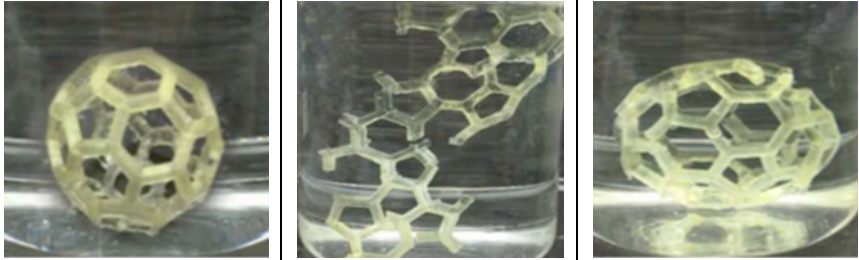
Bucky-ball (2D to 3D)	One-way SME	Heat	Epoxy resin with tBA-co- DEGDA network	VP (DigitalWax System 029X)		(Choong <i>et al.</i> , 2017)
Self- tightening staple (3D to 3D)	One-way SME	Heat	PLA	ME (MakerBot Replicator 2)		(Yang <i>et al.</i> , 2014)
Distorted shape (3D to 2D)	One-way SME	Heat	ABS	N/A (Filament)		(Zhou <i>et al.</i> , 2015)

Table 3.18. Examples of multi-material one-way shape-memory transformation.

Types of Responsive Structures	Shape-Memory Function	Stimuli	Fabrication		Design			Ref
			Material	Manufacturing Process (Printer)	Printed Shape	Secondary Shape	Recovered Shape	
Multi-material gripper (3D to 3D)	One-way SME	Heat	Photo curing methacrylate-based SMPs (own developed materials)	VP (Projection Microstereolithography (P $\mu$ SL))				(Ge <i>et al.</i> , 2016)

Table 3.19. Examples of two-way shape-memory transformation.

Types of Responsive Structures	Shape-Memory Function	Stimuli	Fabrication		Design			Ref
			Material	Manufacturing Process (Printer)	Concept	Configuration A	Configuration B	
Reversible bidirectional SMP (3D to 3D)	Two-way SME	Heat	Multiphase Copolyesters urethane network PPD-PCL ( $\mu$ PCL)	Manufacturing process not disclosed.	The two-way SME occurred as reversible shift between configuration A at T high (50°C) and configuration B at T low (0°C).	T high (50°C) 	T low (0°C) 	(Behl <i>et al.</i> , 2013)
Two-way SMP gripper (3D to 3D)								

### 3.6. Challenges, Research Gaps and Future Work

4DP is still mainly researched within academia rather than industry. There are many research gaps and existing limitations that need to be tackled and overcome in a holistic approach to unveil the full potentials for widespread commercial adoption of 4DP. As 4DP research is interdisciplinary, extensive collaborations between scientists and engineers from various fields are required to move from laboratory-scale research to full-scale research and production.

#### 3.6.1. Materials

The investigation of SRMs for 4DP is still in infancy. According to research findings, there are a few prominent issues limiting the materials practical applicability as a product. The predominant factors are their functionality (shape change or shape memory properties), processability, predictability, adaptability, reliability, and durability. The repeatability and reversibility of the materials are also underexplored. Regarding water-responsive SCMs, their swelling kinetics and response velocity are slow and limited by the diffusion of water inside the polymer network (Ionov, 2013). Though Zhao *et al.* (2009) have designed a method to control the pore size and distributions of the hydrogels using polyvinyl alcohol (PVA) to improve and optimise their response properties. The majority of swelling mechanisms are still limited by mass diffusion. As a result, SCMs usually could not support large deformations. Besides, the actuated shape may not be stable due to the volatility of the water. Some SCMs are quite brittle and can undergo mechanical degradation and mass loss during repeated wetting and drying cycles, leading to short shape change cycle life (Raviv *et al.*, 2014; J. J. Wu *et al.*, 2018).

As for SMPs, Díaz Lantada *et al.* (2010) emphasised that the mechanical and thermo-mechanical properties of SMPs have not yet been fully characterised. More research is needed to extend the knowledge in the properties of SMPs and their complete characterisation process. Zhang, Demir and Gu (2019) further identified other challenges such as inaccurate actuation accuracy and lack of control of intermediary states of deformation. Additional factors that still need to be compromised in 4DP especially for a single material mechanism include low recovery stress, low deformation speed, poor cycle life and weak material stability (Teoh, 2018). SMP undergoes functional fatigue during repeated actuation through mechanical or thermal loading. Lee, An and Chua, (2017) explained that the increased accumulation of irrecoverable strain has a large effect on the

functionality, durability and service life of SMP. Kong and Xiao (2016) highlighted that a high cycle life is crucial especially to applications that require repetitive shape transformation actuation. Comprehensive test methods to examine the cycle life and the mechanical degradation of materials need to be established.

Another major constraint is material availability. The available thermo-responsive SMPs include polytetrafluoroethylene (PTFE), PLA, ethylene-vinyl acetate (EVA) and Polyurethane (PU). However, not all of them are additive manufacturable. The current list of commercial SMPs for AM is very limited and expensive, hence, only a small range of materials was investigated. Works of literature have exploited the use of commercial thermoplastic filaments PLA and ultraviolet (UV) cured thermoset polymer VeroWhitePlus RG835 used in PolyJet Technology as potential SMPs (Zhou *et al.*, 2015; Zarek *et al.*, 2016; Leist *et al.*, 2017; Monzón *et al.*, 2017; Invernizzi *et al.*, 2018; Roudbarian *et al.*, 2019). However, most SMPs found in the literature are often laboratories-based developed materials that cannot be easily purchased or obtained, or their product names and sources are kept confidential. 3M (2020) has recently developed the first PTFE for AM using vat polymerisation, but its SME is yet to be studied. Rajkumar and Shanmugam (2018) have demonstrated the use of Acrylonitrile butadiene styrene (ABS) and High Impact Polystyrene (HIPS). However, their study has only proven the thermally actuated SCE of the materials, not SME. Some researchers develop their own printable SMP blend such as ABS with maleic anhydride graft (SEBS-g-MA) by Chávez *et al.* (2019), PLA/TPU blend by Lai and Lan (2013) and ABS/TPU blend by Memarian, Fereidoon and Ghorbanzadeh Ahangari (2018). In general, little work has been done to support designers in exploiting the materials for 4DP. There is a lack of a benchmark process to initiate the process of selecting the most suitable materials for 4DP and detecting the strength and limitations of a material choice.

Despite the physical fundamentals of SMP are well understood, using them by non-experts is still very challenging. The education and commercial materials libraries have shown interest in SMPs for 4DP, but it is still in the early stage. Current material selection tools, such as Granta Design CES do not describe the material specification, energy-transforming functions, properties or behaviour change of SMPs (Lefebvre *et al.*, 2014). There is a need for “a library of future materials” that can effectively inform and deliver the fundamental physical knowledge of “active” and “adaptive” materials for designers and non-experts to model and simulate their designs. The limitation regarding the design, modelling and simulation will be discussed in the following section.

### 3.6.2. Design, Modelling and Simulation

Up to date, there is no feasible design framework and standardised programming protocols to aid designers to design and develop smart 4DP structures. There is a lack of design guidelines that inform a particular design solution, taking account of the material characterisation, material structure design, corresponding working mechanism, constitutive behaviour modelling and the fabrication process. Although Nam and Pei (2019) have presented the taxonomy of shape-shifting behaviour for 4DP structure, their study did not advise the design methods to achieve those shape-shifting behaviours. This may be somewhat limited by the uncertainty in identifying the properties and function of SMPs in a 4DP working mechanism, especially in a multi-material composition when combined with other materials, such as wood, carbon or textiles. Different materials have different programming and activation methods with respect to the number of materials, specific materials combination, the type of deformation mechanism, the structure intended to build, and the fabrication process. The overall response to a stimulus may not be the same. Greater efforts are needed to fill in the gaps of knowledge in designing and fabricating 4DP structures so they can be activated into intended transformation by an energy source. Other design scopes that have been rarely investigated include the design of sequential transformation according to the types of hinge, geometry and pattern design, and understanding the communication of 4DP design among product designers and manufacturing engineers (Azhar and Pei, 2019).

4DP software is still very limited as this AM strategy and technology are still a novelty. Currently, there are numerous complications in modelling and simulation for shape transformation prediction. Although FEM may be an accurate method for modelling material behaviour and matter dynamics, Sossou *et al* (2018) described that this approach is cumbersome and too computationally costly when simulating and predicting the controlled sequential shape-changing behaviour and final configuration of a multi-material structure. As a result, this makes it not worthwhile, particularly at the beginning of the design process.

Owing to insufficient self-transformation data on the SRMs and environments, Pei *et al.* (2020), Chung, Song and Cho (2017) emphasised that one of the current challenges is to acquire sophisticated software that can carry out the designated functions of simulation, modelling, design and control, at a particular stage and for the entire 4DP process. There is a need for software that can communicate the material properties, taking account of the material and fabrication constraints, predict and control the shape transformation, and capture the actual behaviour of the modelled 4DP structure so that the physical structure can perform the same preset effect.

In the future, there is a need for a platform allowing designers to explore the design space and expedite the design process using SRMs. For instance, design framework and tutorials to inform the design, modelling, simulation methods and AM settings to reproduce a particular shape-shifting behaviour, instructing the method of patterning the arrangement and distribution of the materials for a particular type of self-assembly.

### **3.6.3. AM Processes**

One of the main technological limitations is the compatibility of AM technology for the specified input material selection (SRMs). Current AM technologies are limited to printing single form feedstock materials or supply phase (i.e., filament, powder or resin) and one type of processing method, either melt extrusion, light polymerisation, continuous liquid interface production or sintering (Kumbhar and Mulay, 2018). For instance, VP SLA can only process liquid photopolymers cured by UV light. Whilst powder bed fusion SLM can only process powder-form metallic materials fused by laser. The material has to satisfy the processing criteria of the printer for fabrication. Concerning multi-material AM machines, they cannot simultaneously print multi-material structure from different material types, not even to mention different material groups, such as polymer with metal (Zhang, Demir and Gu, 2019). This narrowed down the possible SRMs combination for multi-material 4DP structure.

Current AM processes are still highly prone to systemic issues, contributing to printer-associated, deposition-associated and print quality problems as discussed in chapter two (Loh et al., 2020). Another general limitation would be post-processing difficulties like support structures removal, especially at inaccessible internal sections (Zhang, Demir and Gu, 2019). Precise printing is still a challenge for the most widely used extrusion-based method. Most machines would struggle to print part at a small dimension as limited by the nozzle diameter and print resolution. Although, there are some AM technologies like direct ink writing (DIW) that has introduced a microscale nozzle for high-resolution printing (Zhou et al., 2017). Printing two different materials types (i.e., combining commodity and high-performance materials) requires different nozzle and build platform temperature, fan power and heated chamber settings. The distinct changes in the print parameters contribute to poor interlayer adhesion between two materials hence affecting the mechanical properties of the produced part (Loh et al., 2020). According to Yap, Sing and Yeong (2020), the printed materials of VP and material jetting tend to have a low ultimate strain and poor fatigue properties.

### 3.7. Comparison of FGAM and 4DP

Taken together, the findings of chapter two and three answers the first research objective in clarifying the state of the art of FGAM and 4DP, and identifying the key characteristics and aspects that separate and bridge the two AM strategies. Table 3.20 clarifies the distinct differences and association between FGAM and 4DP. This provides important insights into selecting the right AM strategy to answer the subsequent research aim and objectives.

Table 3.20. FGAM versus 4DP.

Category	FGAM	4DP
Definition	A layer-by-layer fabrication process that involves gradationally varying the material organisation within a component to achieve an intended function.	The use of AM to produce a freeform stimulus-responsive component that can sense and actuate in response to an appropriate stimulus over time, without the reliance on power-source, robotics or electro-mechanical devices.
Features	The printed structure has graded functionalities, on-demand or site-specific properties through porosity, microstructural or chemical composition change.	The printed structure is capable of self-adaptability, self-assembly and self-repair.
Product state	Passive and static. The printed structure is the final form.	Active and dynamic when stimuli introduced. The printed structure is not the final form.
Key bases	Material composition, gradient distribution, mathematical modelling, AM process and build strategies.	SRMs, stimuli, smart structure design, mathematical modelling and AM process.

The findings revealed that 4DP is the SRMs-driven AM strategy that allows actuated products to be created from the base materials alone. The key bases of 4DP give the active properties to be built in the printed structure so that it can self-transform and morph from one form to another when subjected to appropriate stimuli. Whilst FGAM is a process of modifying material organisation within a component to achieve graded functionalities, on-demand or site-specific properties. The key bases of FGAM do not principally integrate SRMs to offer smartness in a printed structure. As a result, 4DP is the selected AM strategy to answer the research objectives to create shape-changing thermo-responsive textiles.

Whilst the study on FGAM was not extended in this research. Hence the research title "4D Printing of 4D printed shape-changing thermo-responsive textiles".

However, it is foreseen in the future that FGAM and 4DP can be combined to fabricate functionally graded stimuli-responsive structures. SRMs could be printed using the FGAM strategy to have functionally graded properties (Figure 3.20). Varied densification FGAM allow the tailoring of microstructural properties of 4DP structures, controlling the density and directionality of SRMs to perform more complicated shape-shifting behaviours. The gradual variation in porosity modifies the strength-to-weight ratio and introduces varied activation speed, rate of transformation or recovery in different regions of the printed part. The majority of 4DP structures are made up of multiple materials. However, they are printed using conventional multi-material AM (MMAM), having discrete changes of material properties (as illustrated in Figure 2.3).

Multi-material FGAM can expand the portfolio of multi-material 4DP structure as it opens greater opportunities to combine and organise different types of materials. It enables seamless integration of materials in a single print using dynamically composed gradient or morphology. Functionally graded chemical compositional change helps to overcome the shortcomings of MMAM, such as delamination and cracks, especially when involving active interaction between materials of different properties, CTE rates, strain or degree of swelling.

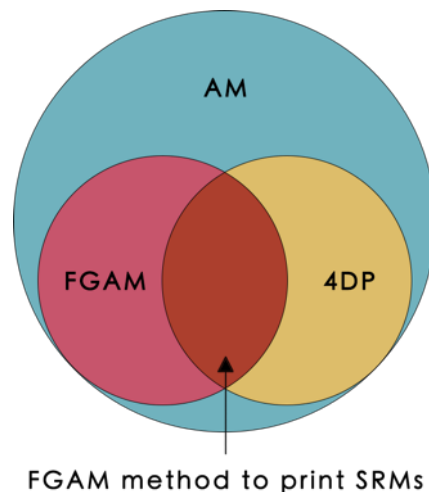


Figure 3.20. The relationship of FGAM and 4DP in AM.

### **3.8. Chapter Summary**

This chapter has discussed the concept, process flow, advancement, potential applications, materials, printing methods and various possible actuation mechanisms design of 4DP. In summary, 4DP is a highly investigated topic but it is still in its early development stage. Despite the promising advancement of 4DP, it is still currently challenging to commercialise products. Research is still limited on the development of a fundamental framework or methodology to establish complete and standardised processing stages for 4DP. The findings from the literature reviews clarified the differences between 4DP and FGAM and suggested that 4DP would be the right AM strategy to answer the research objectives to create thermo-responsive textiles. Therefore, the study on FGAM was not extended in this research. This is because 4DP is SRMs-driven which allows actuated products to be created from the base materials alone. The key bases of 4DP give the active properties to be built in the polymer-textile composite so that it can self-transform and morph from one form to another when subjected to heat. Whilst FGAM is a process of modifying material organisation within a component to achieve graded functionalities, on-demand or site-specific properties. The key bases of FGAM do not principally integrate SRMs to offer smartness in a printed structure. Although, it can be foreseen that FGAM can be incorporated with 4DP to create variable-property 4D printed structures with strategically tailored compositions or microstructure. However, this is beyond the scope of this research. The next chapter discusses the development of a material selection process to confirm the material characteristics that are suitable for 4DP. The framework is created to select the most suitable SMP for material extrusion to produce the thermo-responsive textile.

## Chapter 4

### **A Framework for Selecting Thermo-Responsive Shape Memory Polymers for 4D Printing**

Chapter four proposes a material selection framework to discover, define and select commercially available thermoplastics as potential SMPs for use in material extrusion 4DP. A systematic material selection process is designed to test, qualitatively and quantitatively measure the shape fixity, response rate and shape memory effect of an SMP. This chapter also describes the basic theoretical and practical knowledge to create a single-material thermo-responsive dual-state mechanism (DSM) active structure, including design, fabrication, and experimental procedure for programming-recovery characterisation. The shape memory properties of the materials in filament-form and post printed form when activated by different shape recovery temperatures ( $T_r$ ) are investigated and analysed in this chapter.

#### **4.1. Introduction**

4D Printing (4DP) is a material-driven design process in which stimuli-responsive materials (SRMs) play a fundamental role to satisfy the functionalities and reconfigurability of the printed structure when subjected to a defined stimulus. Nevertheless, the growth of 4DP is still at an early stage. There are currently no standardised design method and benchmark process workflow to guide the development and manufacturing of 4DP structures. Most academic and research publications concentrate on advanced theory and algorithms of shape-memory polymer (SMP) with little information tailored for non-technical audiences (Monzón *et al.*, 2017; Rosales *et al.*, 2019; Momeni and Ni, 2020). Furthermore, the availability of SMP for 4DP in the commercial market is very limited and expensive. Most SMPs found in the literature are often laboratories-based developed materials that cannot be easily purchased or obtained, or their product names and sources are kept confidential. There is also a lack of methodology in selecting and detecting the strength and limitations of a material choice. The current material libraries (i.e., Granta Design CES) do not describe the shape memory properties and energy-transforming function data of SMPs. A designer requires adequate theoretical knowledge about the shape memory properties and functionalities of SMPs as a system and have wider access to materials to exploit the full potential of 4DP.

To overcome some of the limitations, a material selection framework to select potential commercially available thermoplastics as SMPs for use in material extrusion (ME) thermo-responsive 4DP is proposed. It is a systematic explorative process to test, quantitatively measure and analyse the shape fixity, response rate and shape memory effect of an SMP. This chapter also describes the theoretical knowledge and practical approach to create a thermo-responsive dual-state mechanism (DSM) active structure including design, fabrication and experimental procedure for programming and recovery characterisation to complete a shape memory cycle. Discovering the suitable SMP can be time-consuming and difficult. This framework can increase the list of inexpensive and easily accessible commercial filament material options for 4DP. The goal is to allow designers to have greater access to materials for 4DP to envision new applications and research outputs. The framework can also be practically used in general and educational settings to train and educate about 4DP.

## **4.2. Material Selection Process Framework**

The material selection framework presented in Figure 4.1 has been developed by the author, generated from literature findings in chapter three followed by verification and validation with target users through workshops (Chapter 4.5.1) and semi-structured interviews (Chapter 4.5.2). This framework is designed to be used at the front-end phase of the design process to discover, define and select potential commercial filament thermoplastics as SMPs for use in ME 4DP. The shape fixity, response rate and cycle life of the material are the most important characteristics of the shape memory effect (SME) for evaluation (Ashby, 2017; Jose *et al.*, 2020; Parameswaranpillai *et al.*, 2020). These factors determine the functionality and transformation efficiency of a thermo-responsive 4DP structure react upon activation. They are quantitatively defined and analysed through thermo-rheological characterisation which includes programming (Process 1) and recovery testing (Process 2) by submitting the material to a thermo-mechanical cycle. Shape fixity is defined as the extent of a temporary shape being fixed (Thakur and Hu, 2017), the response rate refers to the time taken for an SMP to self-actuate and transforms into a predetermined shape when subjected to a defined stimulus. The cycle life represents the number of consecutive shape memory cycles that SMP can achieve without noticeable decrease in shape recovery and shape fixity (Kong and Xiao, 2016). Whilst the SME represents the ability of an SMP to recover to its original shape from a temporary configuration (Teoh, 2018).

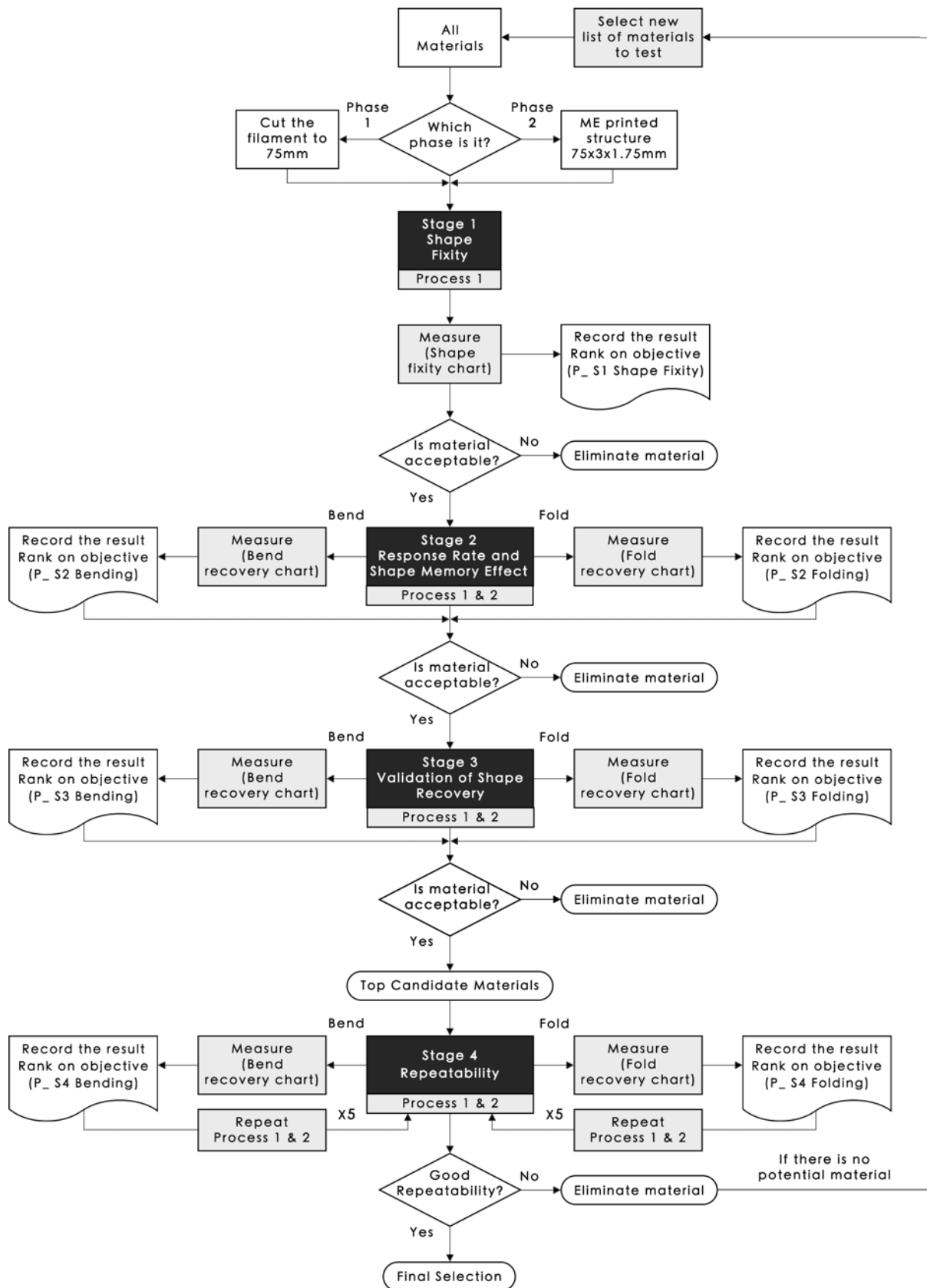


Figure 4.1. The material selection process workflow.

The material selection process can be investigated from two phases, Phase 1 in the filament state and Phase 2 in ME printed structure to examine and compare the shape memory properties of SMP in different forms (Figure 4.1). Both phases comprise the same process workflow to progressively filter the list of materials through four experimental stages. The experimental stages are labelled according to their phase number and stage number. For example, Phase 1 Stage 1 is labelled as P1 S1. The objectives of each experimental stage are described before Table 4.1. The interaction mechanisms investigated in this study are bending and folding. Three measuring charts are created to use as a guide to measure and rate the shape fixity and recovery of the material (Table 4.5).

**Stage 1 – Shape Fixity:** Stage 1 examines the ability of the material to be successfully fixed or retained at its programmed shape.

**Stage 2 – Response Rate and SME:** Stage 2 observes the differences in the response rate, which include the rate of shape morphing activation ( $T_a$ ) and the time taken for complete shape recovery, as well as the SME of the material when activated at different shape recovery temperatures ( $T_r$ ).

**Stage 3 – Validation of Shape Recovery:** Stage 3 analyses *five* specimens per material to observe the consistency and calculate the average value of shape memory properties. *Five* specimens are a recommended average, although more (or less) samples could be tested by users which determines the accuracy of the results.

**Stage 4 – Repeatability:** Stage 4 investigates the changes in shape memory properties of the material after going through multiple shape memory cycles. *Five* memory cycles are a recommended average, although more (or less) cycles could be tested by users which determines the accuracy of the results.

Table 4.1. The material selection process.

Experimental Stages		Phase 1 Filament	Phase 2 ME Printed Structure	Number of specimens required per test	Number of tests required per specimen	Measuring chart
Stage 1	Shape fixity	P1 S1 Shape fixity	P2 S1 Shape fixity	One	One	Shape fixity (Bend)

						Fold Recovery (Fold)
Stage 2	Response Rate and SME	P1 S2 Bending	P2 S2 Bending	One	One	Bend recovery
		P1 S2 Folding	P2 S2 Folding	One	One	Fold recovery
Stage 3	Validation of shape recovery	P1 S3 Bending	P2 S3 Bending	Five	One	Bend recovery
		P1 S3 Folding	P2 S3 Folding	Five	One	Fold recovery
Stage 4	Repeatability	P1 S4 Bending	P2 S4 Bending	One	Five	Bend recovery
		P1 S4 Folding	P2 S4 Folding	One	Five	Fold recovery

The evaluation criteria and the recommended number of top candidate materials to be carried forward for each experimental stage are suggested below but can be regulated by users.

Stage 1 – Shape Fixity: Only materials with shape fixity rating R:10 could be carried forward to Stage 2.

Stage 2 – Response Rate and SME: The materials would be ranked according to the sum of their shape recovery ratings across the selected optimum range of Tr. *Five* top candidate materials with the lowest grand total of shape recovery rating would be carried forward to Stage 3.

Stage 3. The recovery rating of the material for each Tr should not exceed R:3 to be considered as a potential material. For example, if three sets of Tr (i.e., 60°C, 65°C and 70°C) were tested, the sum of recovery rating of the material should not exceed nine points.

Stage 3 – Validation of Shape Recovery: The materials would be ranked according to the sum of their shape recovery percentages across the selected optimum range of Tr. *Three* top candidate materials with the highest grand total of shape recovery percentages would be carried forward to Stage 4.

Stage 4 – Repeatability: The final selection material should have the highest grand total of shape recovery percentages, best repeatability and most consistent in shape recovery over consecutive shape memory cycles.

Although not all experimental stages are indispensable for every study, it is advised to follow all four experimental stages of the material selection process as to comprehensively discover and define the shape memory properties of a material (unless the performance or functionality of the material was not met and eliminated). On the contrary, the material selection process can be adjusted and processed from three different angles, (1) the required material is not known – carry out Phase 1 and 2, (2) the required material is known – proceed directly to Phase 2 or (3) a specific interaction mechanism is known– pursue the specific programming condition.

### 4.3. Methods

#### 4.3.1. Materials and Fabrication of Test Specimens

Works of literature have demonstrated the use of thermoplastic filaments as SMPs (Zarek et al., 2016; Leist et al., 2017; Monzón et al., 2017; Invernizzi et al., 2018; Roudbarian et al., 2019). 21 commercially available Polylactic acid (PLA) of similar molecular weights, one Polycaprolactone (PCL), seven Thermoplastic polyurethane (TPU), four Polyurethane (PU) with Polyvinyl acetate (PVA) and one Polypropylene (PP) are selected for this study (Table 4.2). The extrusion and platform temperatures for the materials were suggested by their respective manufacturers.

Table 4.2. The material list with their tradenames and printing temperatures.

Polymer Type	No.	Brand	Extrusion Temperature (°C)	Platform Temperature (°C)
PLA	1	RepRapper Tech Ltd	190 – 240	60
	2	Reprepper Tech Ltd	190 – 240	60
	3	MakerBot	230	60
	4	Flashforge	210 – 220	60
	5	Haydale and Amphilogic Ltd.	200	58

	6	Pxmalion	210	60
	7	Prusa	215	60
	8	Filaprint	180 – 210	60
	9	Ultraline 3D	190 – 220	30 – 50
	10	Fiberlogy	200 – 220	50 – 70
	11	Filamentum	190 – 210	40 – 50
	12	3Dom	180 – 220	0 – 60
	13	Qidi Tech	190 – 220	0 – 50
	14	PM	200 – 220	0 – 60
	15	3DJake	195 – 215	Not necessary
	16	ColorFabb	195 – 220	0 – 60
	17	Bq	210 – 220	Not necessary
	18	Polymaker	190 – 220	Not necessary
	19	KOBO	195 – 210	0 – 55
	20	Filament PM	200 – 220	20 – 60
	21	Filament PM	200 – 220	20 – 60
PCL	22	eSUN	80 – 110	45
TPU	23	eSUN	210 – 230	Not necessary
	24	eSUN	220 – 240	30 – 50
	25	eSUN	210 – 230	40 – 60
	26	Ninjatek	210 – 225	15 – 50
	27	Ultraline 3D	190 – 230	50 – 80
	28	Filament PM	210 – 230	20 – 60
	29	Filament PM	220 – 240	20 – 60
PU – PVA	30	Kai Parthy CC Products	225 – 235	Not necessary
	31	Kai Parthy CC Products	220 – 230	Not necessary
	32	Kai Parthy CC Products	200	50
	33	Kai Parthy CC Products	225 – 235	Not necessary

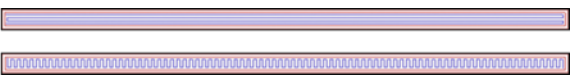
PP	34	Filament PM	210 – 230	70 – 90
----	----	-------------	-----------	---------

Phase 1 filament and Phase 2 ME printed test specimens were prepared based on the dimensions stated in Table 4.3. The CAD design of the ME printed specimen was created using SolidWorks, exported as an STL. file, imported into Slic3r for slicing and fabricated using an Original Prusa i3 MK3S Printer, using the ME fabrication settings specified in Table 4.4. All of the specimens should be fabricated on the same day to ensure constant processing parameters and minimum deviation in environmental variables (i.e., print environment temperature, humidity level) that would influence the test results.

Table 4.3. The dimensions for the filament and ME printed structure test specimen.

Phase	Form	Dimensions
Phase 1	Filament	75mm (L)
Phase 2	ME printed structure	75mm x 3mm x 1.75mm (L x W x H)

Table 4.4. The fabrication settings for ME printed specimen.

Print Parameters	Settings	Refer To
Layer height	0.15mm	
Fill density	100%	
Fill Pattern	Rectilinear	
Fill angle	0° and 90° 	(An <i>et al.</i> , 2018)
Extrusion width	0.45mm	
Nozzle temperature	As instructed by the manufacturer	Table 4.2
Platform temperature	As instructed by the manufacturer On a side note, the platform temperature usually represents the glass transition temperature (T <sub>g</sub> ) of the material (Rajkumar and Shanmugam, 2018).	Table 4.2

First layer speed	20mm/s	
-------------------	--------	--

### 4.3.2. Tools and Equipment

To enable the widest uptake of this material selection framework, the tools and equipment have to be affordable, widely available and simple to calibrate for use. The experiment would require a heated water bath, a thermometer, tweezers (to grip the specimen), stopwatch, cloth, forming jigs (for shape programming) and the measuring charts (shape fixity, bend recovery and fold recovery charts).

The forming jigs for fold and bend programming (Figure 4.2 and Figure 4.3) were created using SolidWorks and fabricated using an Original Prusa i3 MK3S Printer with Polyethylene terephthalate glycol (PETG) filament. Their technical drawings can be found in Figure 4.35 and Figure 4.36. A 25mm diameter circular bend was chosen to represent the standard diameter of a plastic bottle neck. If the fabrication of forming jigs were unavailable or inaccessible, a plastic bottle with  $\pm 25\text{mm}$  neck could be used for circular bend programming, while a solid right-angle cube or table corner for  $90^\circ$  fold programming (Figure 4.4). The height of both programming jigs is designed at 32mm for a better grip of the jig during fixing and to accommodate material specimen with width up to 30mm. Though, the height can be adjusted.

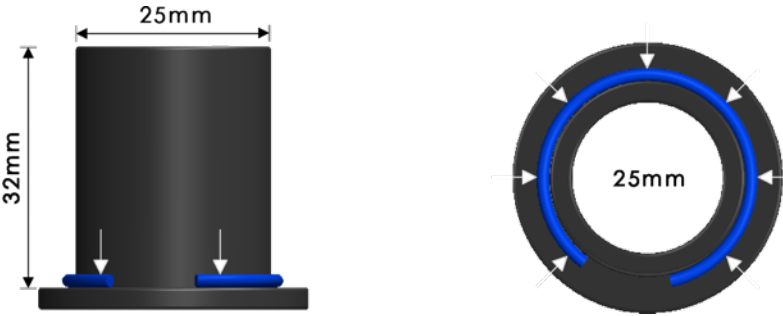


Figure 4.2. The forming jig to program the material specimen into a 25mm diameter circular bend.

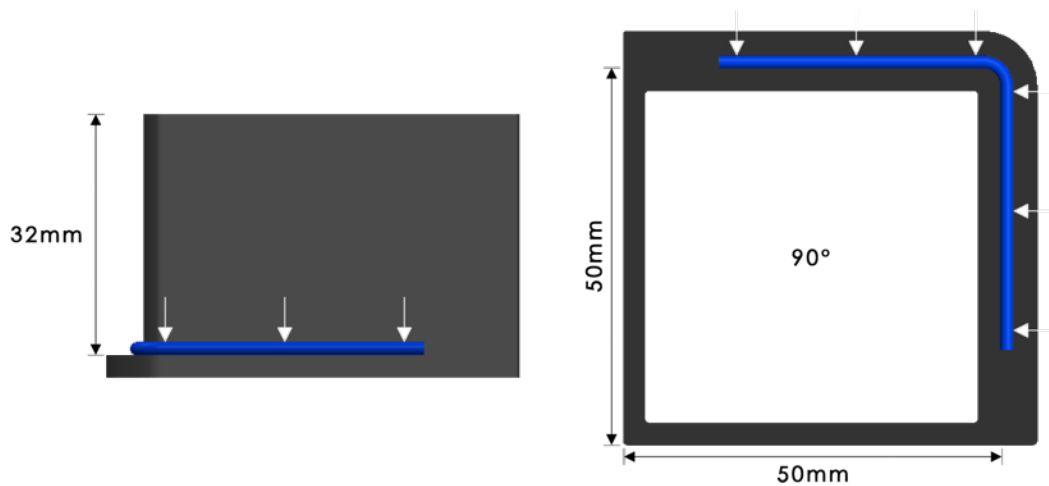


Figure 4.3. The forming jig to program the material specimen into a 90° fold.

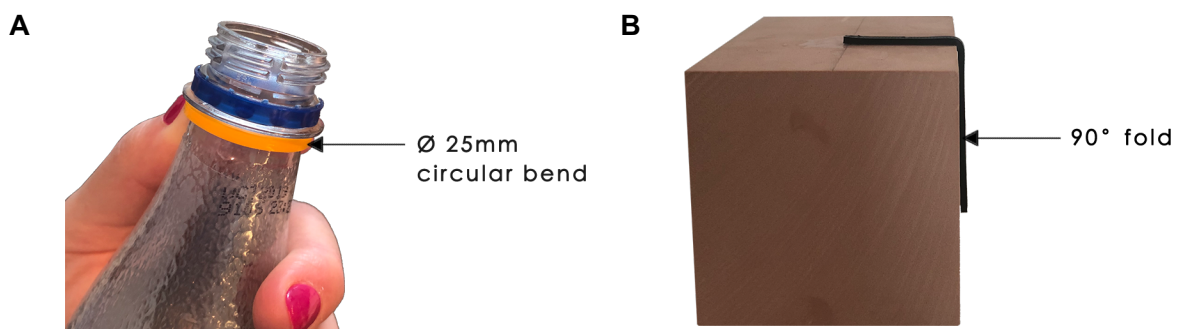


Figure 4.4. Objects that can be used as alternative forming jigs. (A) plastic bottle (B) right-angle cube.

A thermal immersion circulator was utilized for its precision performance and convenience over manual heating of the water bath (Figure 4.5). It allowed the water temperature to be easily adjusted, fixed and monitored with a precision of 0.1°C. It also has a built-in stirring mechanism to circulate the water bath to ensure a consistent temperature and to reduce heat loss from the surrounding air that could decrease the ambient temperature of the specimen (Teoh, 2018). An external thermometer was also used to validate the temperature reading of the water bath.



Figure 4.5. Experiment set up.

### 4.3.3. Experimental Procedures for Thermo-rheological Characterisation

The thermo-rheological characterisation (also known as the programming-recovery characterisation) entails the thermo-mechanical processing of SMPs to form a full shape memory cycle. It consists of two processes: thermomechanical programming (Process 1) and shape recovery testing (Process 2). A single-material DSM heat-induced SMP comprises three stages of material shape, which are the original printed shape, programmed (temporary) shape, and recovered shape (Figure 4.6) (Sobota *et al.*, 2017; Sun *et al.*, 2019). Every experimental stage involved Process 1 followed by Process 2, except for Stage 1 (Shape fixity) which involved only Process 1 to study the ability of a material to be effectively fixed at a programmed shape. In line with Pretsch (2010), a significant precondition of shape memory behaviour is the successful application of shape programming.

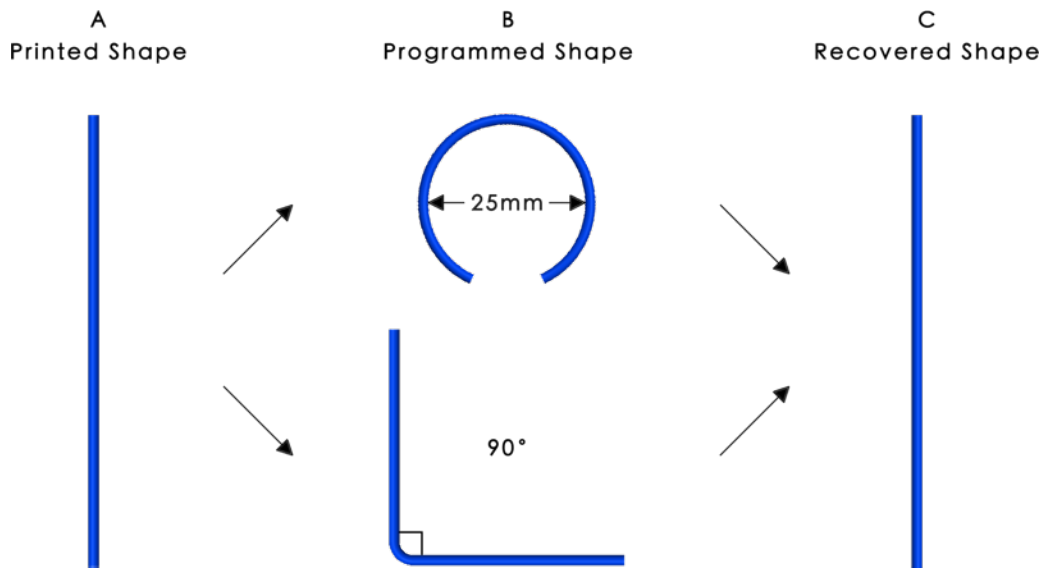


Figure 4.6. The three stages of DSM heat induced SMP. (A) printed shape, (B) programmed (temporary) shape and (C) recovered shape.

#### 4.3.3.1 Process 1: Thermomechanical Programming Process

This process involves constrained thermo-mechanical programming to deform the material (SMP) into a desired temporary configuration. The thermomechanical programming process for a one-way SME structure entails shape deformation and fixation, followed by the removal of constraint to achieve a programmed secondary shape.

1. The material specimen is immersed in the heated water bath at its shape deforming temperature ( $T_d$ ) (may be equal or above their  $T_g$ ) for *one* minute to change the material from a glass state to a rubbery state. (The time taken for transition from the glass to rubber state are for recommendation. The value may differ according to the material type and characteristics).
2. The softened material specimen is removed from the water bath for shape programming (phase fixation). It is moulded immediately using the respective forming jig with applied downward force to form a 25mm diameter circular bend (Figure 4.2) or a 90° fold (Figure 4.3).
3. The material specimen is unloaded from the forming jig when it has returned to its glass state. The deformed shape is the programmed shape.

### 4.3.3.2 Process 2: Shape Recovery Process

The shape recovery process starts from the programmed shape (Process 1) and ends at a recovered shape (Process 2), ideally at its original configuration.

1. The programmed material specimen is immersed into the heated water bath at shape recovery temperature ( $T_r$ ) to release the stored strained energy to trigger shape recovery.
2. The rate of shape morphing activation ( $T_a$ ) and the duration for complete shape recovery is recorded using a stopwatch. The stopwatch is stopped when there is no further shape recovery. Alternatively, the response time can be taken through videography for more accurate results.
3. The material specimen is removed from the water bath, and the cloth is used to remove any excess water.
4. The shape recovery of the material is measured using the respective measuring chart.

### 4.3.4. Measuring and Recording of Results

Three measuring charts were designed to simplify the process of measuring the material specimens and replace the use of complex calculations and algorithm (Table 4.5). The two programming conditions are the circular bend and 90° fold configurations.

Table 4.5. Types of measuring charts.

Measuring Charts	To measure results from	Descriptions	Evaluation Criteria	Refer To
Shape fixity chart	Process 1	To measure the ability of the material to be successfully fixed at its programmed shape from its original printed shape.	Programmed bend at R:9 or below should be reconsidered or eliminated.	Figure 4.7
Bend recovery chart	Process 2	To measure the recovered shape of the material from a bend deformation.	A potential SMP must be able to recover to its original shape at R:1, or within the preferred	Figure 4.8

Fold recovery chart	Process 2	To measure the recovered shape of the material from a fold deformation.	range (R:2). Recovered shape above R:3 should be reconsidered or eliminated.	Figure 4.9
---------------------	-----------	---	--	------------

The degree and rating of the shape fixity or shape recovery can be evaluated by placing and aligning the material specimen over the shaded area on the charts to match the corresponding shapes. Each chart has a rating system and is colour coded to suggest if the material is “preferred”, “acceptable”, “for consideration” or “under-performing”, with the latter two eliminate from subsequent experimental stages. The measuring charts should be printed in actual size (A4) with a scale of 1:1. It is important to place the measuring charts on a flat surface for accurate measurement of the results.

The degree of bend gathered on the shape fixity and bend recovery charts were analysed and mapped based on the recovered frequency from over 250 bend inputs. The angle of fold recovery was measured and rated using a 360° protractor concept. Concerning the rating system on the folding chart (Figure 4.9), the degree range for R:1 and R:2 was minimised to five for each rating (0° to 5°; 6° to 10°) to increase the precisions in differentiating the level of recovery among the preferred range.

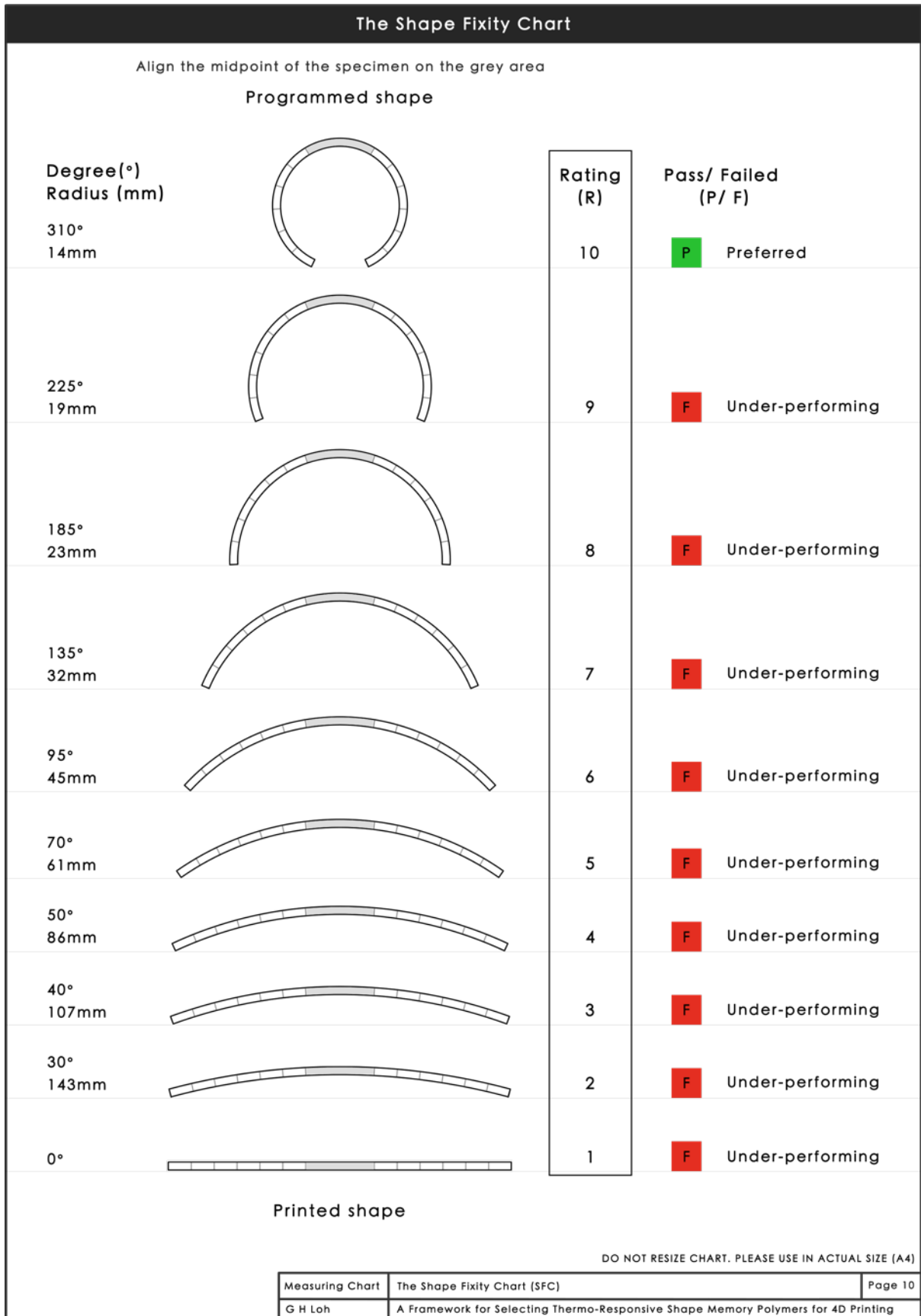


Figure 4.7. The shape fixity chart (not in actual size).

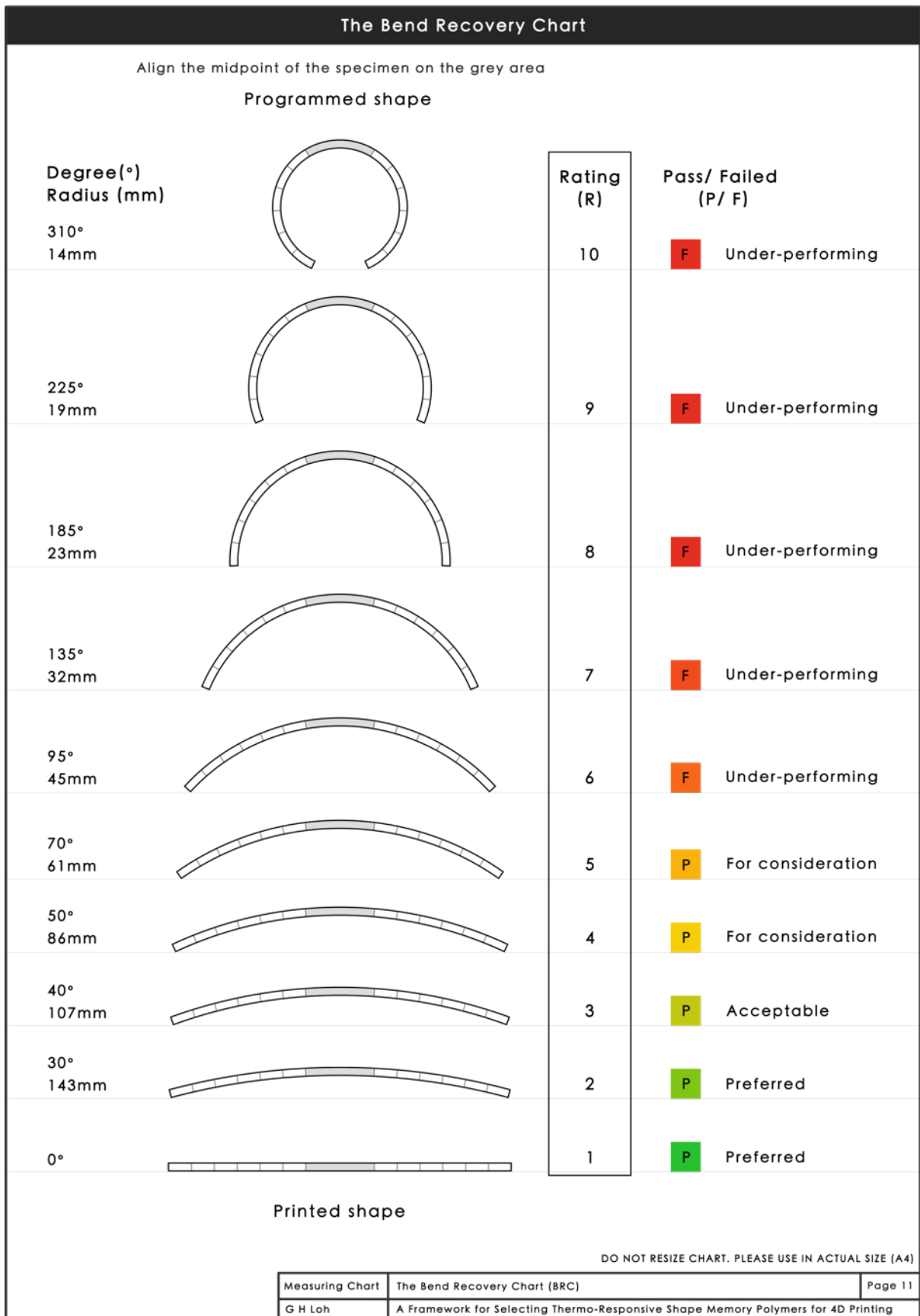


Figure 4.8. The bend recovery chart (not in actual size).

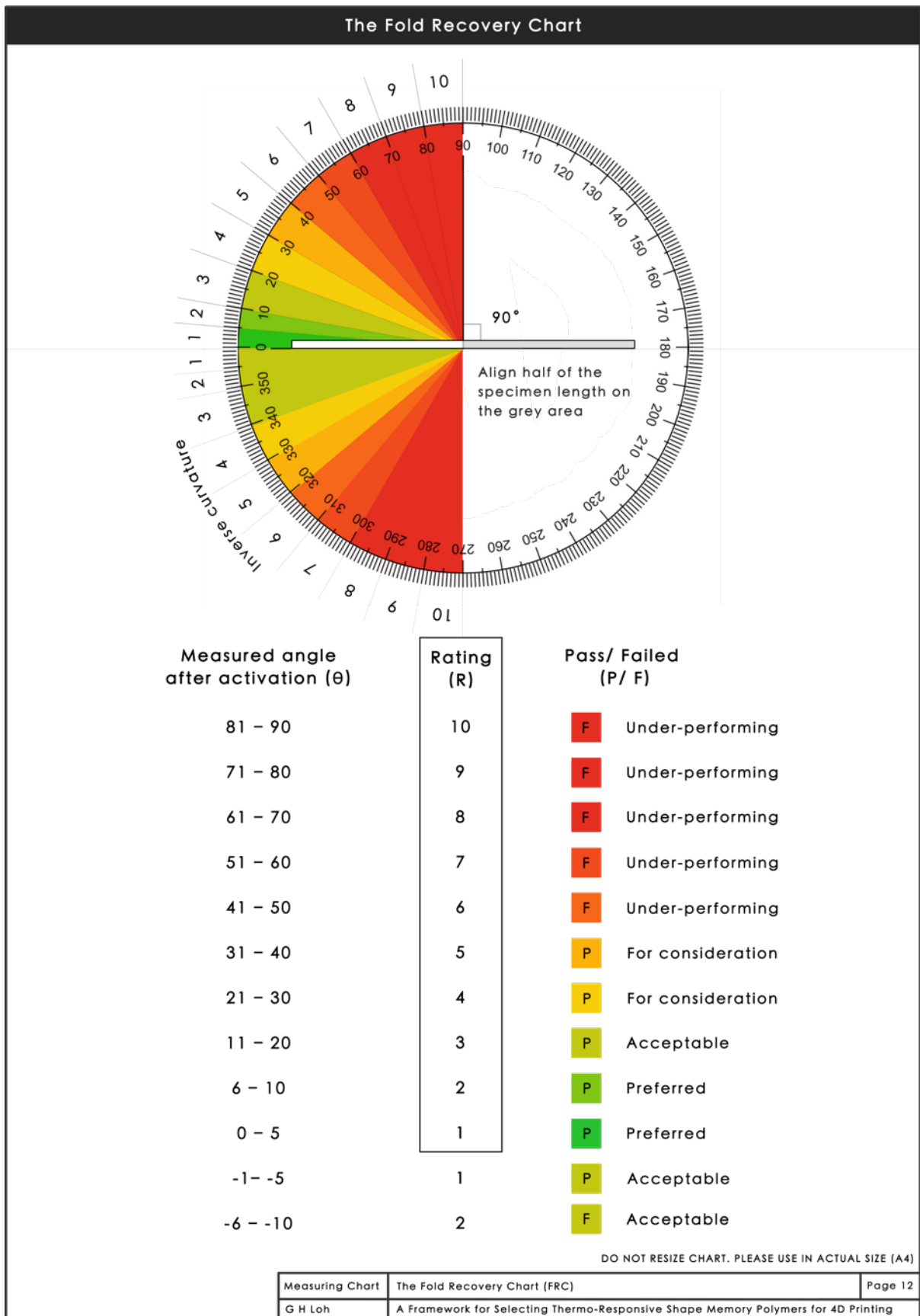


Figure 4.9. The fold recovery chart (not in actual size).

The percentage for shape recovery ( $R_r$ ) was calculated using a ratio of the initial programmed displacement (angle or degree) to the recovered displacement after activation (Equation 1) explained by Thakur and Hu (2017).

$$R_r = \frac{\varepsilon - \varepsilon_{\text{recovery}}}{\varepsilon} \times 100\%$$

$\varepsilon$  = The initial displacement (angle or degree) of the programmed shape.

$\varepsilon_{\text{recovery}}$  = The recovered displacement (angle or degree) after activation.

Equation 1. The shape recovery percentage.

## **4.4. Results and Discussions**

In this section, the quantified results obtained from the thermo-rheological characterisation are analysed and ranked according to the objective of each experimental stage. The results were also used as a proof-of-concept.

### **4.4.1. Phase 1 Filament**

Phase 1: Stage 1 Shape Fixity

Stage 1 Shape Fixity study revealed that not all commercial filaments have the ability to be fixed at a programmed shape despite belonging to the same polymer type. The shape fixing efficiency of filament thermoplastics can be affected by the Td followed by the duration of fixation (loading). The difference in Td would result in a difference in the molecular stability of the material under the same deformation condition. This temperature is especially important as it affects the overall performance of the SMP (Basit, 2016). Zhou *et al.* (2015) emphasized that it is important to not overheat the materials, particularly PLA, as it induces crystallisation, and the shape will become virtually permanent. The Td and Tr would vary according to the material type (i.e., commodity, flexible) and characteristics (Loh *et al.*, 2020). Therefore, the Tr for shape recovery process must be adjusted coherently by referencing to the Td and Tg of the material.

Most of the regular PLA filament specimens were able to achieve rubbery state at 80°C and be fixed easily and effectively into the programmed shape (R:10). However, PLA with infused or reinforced material, such as material No. 18 with enhanced mechanical properties, require higher Td (greater than 80°C) to change into a rubber state due to its higher Tg. On the contrary, PCL (material No.22) required lower Td for shape fixation, around 60°C due to lower material Tg. Concerning the flexible materials (TPU, PU, PVA, and PP), their shape fixity was rather poor despite testing with a range of Td (60°C, 70°C, 80°C and 90°C). The shape fixity results at 80°C of the materials can be compared in Figure 4.10. According to Kačergis, Mitkus and Sinapius (2019), the room temperature is above the Tg of TPU. As a result, the TPU can only bend and slightly elongated. Flexible elastomers, typically TPU, are used as passive materials in multi-material 4DP structure. The passive layer (i.e., TPU) would be resistant to the shortening of the active layer (i.e., PLA) within the multi-material mechanism to transform into a particular shape-changing behaviour (Kačergis, Mitkus and Sinapius, 2019). Based on the results in Table 4.6, the PLAs (material No. 1-17, 19-21) passed with shape fixity rating (R:10) at Td 80°C were carried forward to the following stage (Stage 2).

Table 4.6. P1 S1 Shape fixity.

Polymer Type	Material No.	Shape deforming temperature (°C)	Shape fixity Rating (1 – 10; Poor – Excellent)	Pass (P)/ Failed (F)
PLA	1-17, 19-21	80	10	P
	18	> 80	5	F
PCL	22	60	10	P
TPU	23	80	3	F
	24	80	2	F
	25	80	4	F
	26	80	6	F
	27	80	8	F
	28	80	3	F
	29	80	3	F
PU; PVA	30	80	7	F
	31	80	9	F

	32	80	8	F
	33	80	7	F
PP	34	80	6	F

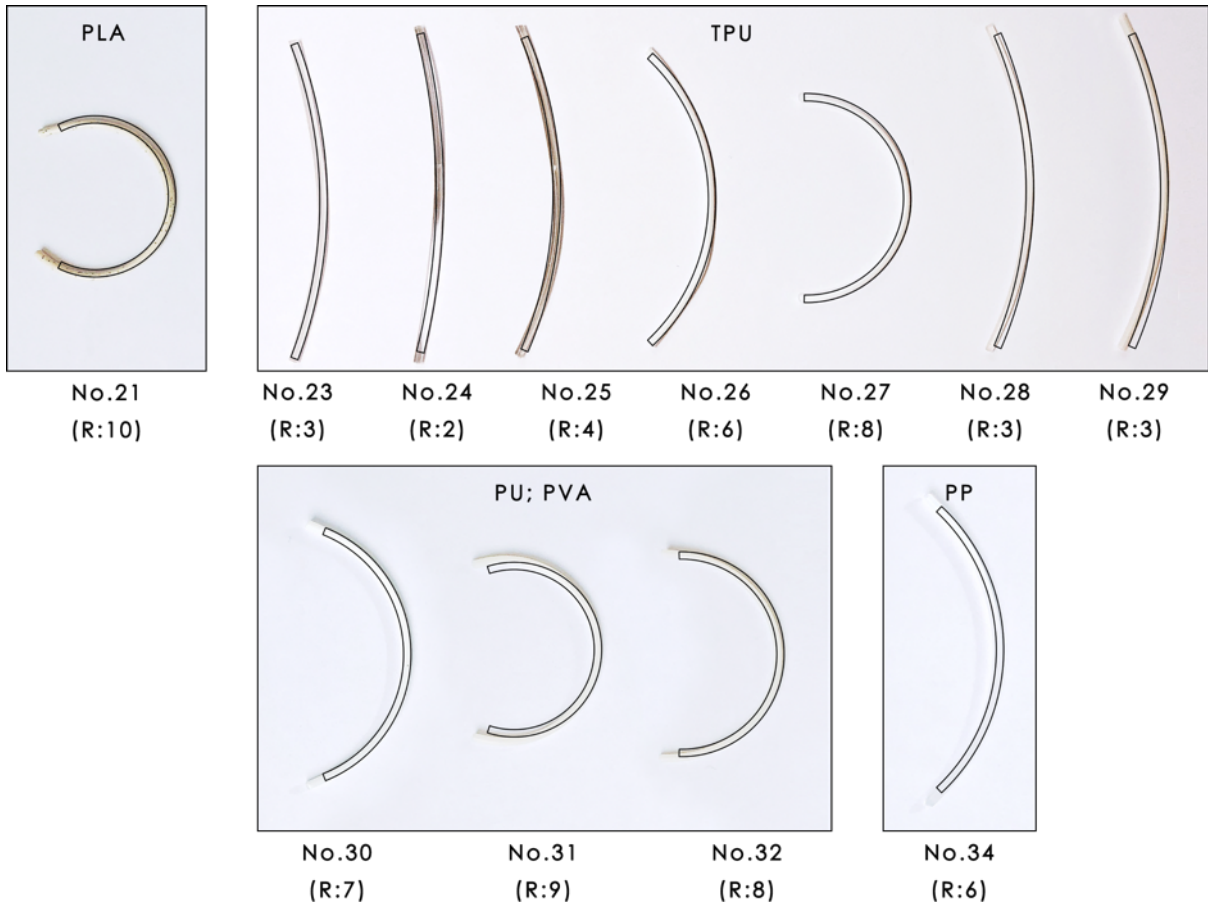


Figure 4.10. The shape fixity of materials specimens of different polymer types.

#### Phase 1: Stage 2 Response Rate and SME

The response rate and SME of the filament specimens (material No. 1-17, 19-21) from bending and folding deformation activated by heated water at Tr of 55°C, 60°C, 65°C, 70°C and 75°C were examined and compared. The results revealed that the materials exhibited different behaviours, differing from example, by the strength of recovery and the response time despite belonging to the same polymer type. About 80% of PLAs did not recover completely from a high level of deformation back to its original shape. The study also revealed that the Tr had a significant effect on the response rate and the SME.

The results from both programmed shapes, bending (Table 4.7) and folding (Table 4.8), showed that an increase in the  $T_r$  led to shorter response rate and improved SME. At the minimum  $T_r$  of 55°C, the  $T_a$  was the longest. The time taken for a complete shape recovery was predominantly at one minute and above, while the recovery rating of most materials was at R:6 and above. At the maximum  $T_r$  of 75°C, the  $T_a$  was the shortest. The time taken for a complete shape recovery were less than 10s. More than half of the materials were able to recover to their original shape at R:1 unless specified otherwise (Table 4.7). Although a  $T_r$  of 75°C offered the best shape recovery performance, 75°C may be too high as a thermal stimulus, as the temperature is not ideal for conventional 4DP applications. The recommended  $T_r$  for regular PLA is between 60°C to 70°C, which can provide a relatively fast response and recovery time of 10s to 30s, and equally good shape recovery result (within preferred and acceptable range of R:1 to 3). The materials were screened and ranked according to their quantified grand total (only considering  $T_r$  60°C–70°C), which is the sum of their shape recovery rating across the three  $T_r$  (60°C, 65°C and 70°C). The grand total was limited to maximum of 9 points to be considered as a potential SMP. Nearly 80% of PLAs from the list were not able to recover completely from deformation. The top nine materials with grand total value no greater than 9 were carried forward for P1 S2 folding experiment (Table 4.8).

Table 4.7. P1 S2 Bending.

P1 S2 Bending											
No.	55°C		60°C		65°C		70°C		75°C		Grand Total (60°C–70°C)
	T (s)	R	T (s)	R	T (s)	R	T (s)	R	T (s)	R	
1	90	7	46	5	11	6	10	5	7	3	16
2	90	7	43	5	10	6	10	5	7	3	16
3	90	6	21	5	13	6	7	5	7	5	16
4	90	9	30	4	9	2	8	1	8	1	7
5	90	6	29	6	18	6	9	6	8	6	18
6	90	9	30	6	15	6	14	5	8	5	17
7	90	8	30	4	12	4	6	1	8	1	9
8	90	7	19	5	19	2	8	1	8	1	8
9	90	6	18	5	13	5	5	5	5	5	15
10	90	9	42	5	20	2	8	1	4	1	8
11	90	7	22	4	11	1	6	1	6	1	6
12	26	7	12	5	12	4	7	4	5	1	13
13	90	7	31	6	9	4	9	4	7	4	14
14	50	9	33	5	13	2	9	2	4	1	9
15	90	7	29	5	32	4	15	3	9	2	12
16	90	10	40	9	24	8	14	8	7	8	25
17	90	9	37	3	11	3	5	1	6	1	7
19	25	6	24	5	12	3	5	1	5	1	9
20	90	7	25	5	18	3	7	2	5	1	10
21	90	8	45	2	17	2	9	2	7	1	6

Table 4.8. P1 S2 Folding.

P1 S2 Folding																
No.	55°C			60°C			65°C			70°C			75°C			Grand Total (60°C–70°C)
	T (s)	$\theta^\circ$	R													
4	90	51	7	47	11	3	14	4	1	8	1	1	7	1	1	5
7	76	56	7	31	5	1	16	6	2	5	1	1	7	5	1	4
8	71	50	6	27	12	2	15	10	2	12	5	1	9	3	1	5
10	55	60	7	25	1	1	16	3	1	4	1	1	8	1	1	3
11	13	41	6	36	5	1	16	3	1	8	1	1	5	1	1	3
14	90	57	7	18	10	2	7	12	3	5	1	1	4	1	1	6
17	41	66	8	15	20	4	6	5	1	5	5	1	5	5	1	6
19	20	11	3	11	4	1	9	4	1	7	6	2	5	1	1	4
21	90	35	5	18	15	3	7	6	2	5	12	3	5	4	1	8

The results from Table 4.7 and Table 4.8 presented no significant differences in response rate and SME from a fold deformation and a bend deformation. The average time taken for complete shape recovery were 28s, 13s and 7s when activated at Tr of 60°C, 65°C and 70°C respectively. Figure 4.11 shows the ranking of materials based on their shape recovery ratings, ranging from the highest to the lowest (left to right), for both programmed shapes (bending and folding). By comparing the material arrangements, the results revealed that the shape recovery performance of a material (SMP) varied according to the programming condition. For instance, material No. 21 was the second-best candidate material for bend recovery but was ranked at ninth for the fold recovery. The list of potential materials was narrowed down further. The top six candidate materials (material no. 4, 7, 8, 10, 11 and 19 were carried forward to Stage 3 (validation of shape recovery).

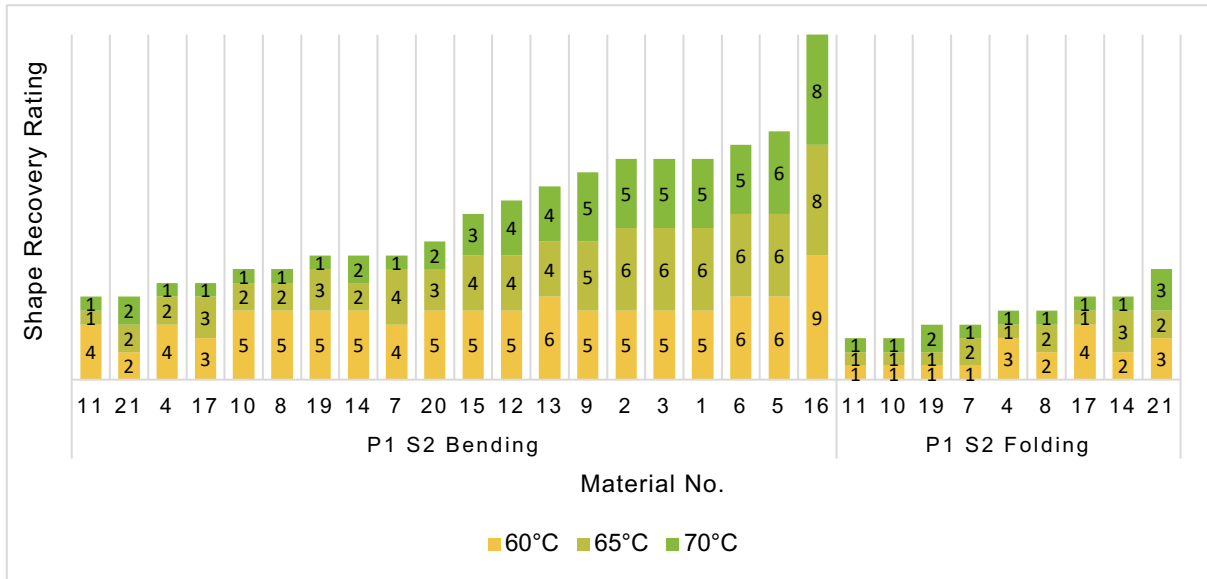


Figure 4.11. The ranking of materials based on their shape recovery ratings, ranging from the highest to the lowest, from left to right, for both programming conditions (bending and folding).

#### Phase 1: Stage 3 Validation of Shape Recovery

The  $T_a$  and the shape recovery percentage ( $R_r$ ) (calculated using Equation 1) were used to characterise the shape recovery performance of the materials. P1 S3 Bending result from the five specimens of each material displayed close proximity in the R values. While P1 S3 Folding results displayed several oscillations in the recovery angle ( $\theta^\circ$ ). There were several fluctuated values which appeared to be much higher or lower compared to the results obtained among the same set. For example, material No. 4 (Test 1 at 65°C), material No. 7 (Test 1 at 60°C) and material No. 11 (Test 4 at 65°C).

Table 4.9. P1 S3 Bending.

P1 S3 Bending														
No.	Ta (s)			Test Number	60°C			65°C			70°C			Grand Total (%)
	60°C	65°C	70°C		T (s)	R	Rr (%)	T (s)	R	Rr (%)	T (s)	R	Rr (%)	
4	8	8	3	Test 1	45	3	86	25	2	91	9	2	91	268
				Test 2	39	3	86	18	1	100	9	1	100	286
				Test 3	37	3	86	19	1	100	10	1	100	286

				Test 4	47	3	86	17	2	91	10	1	100	277
				Test 5	48	4	85	17	1	100	12	1	100	285
				Average	43	3	86	19	2	96	10	2	98	280
7	7	5	4	Test 1	35	3	86	18	3	86	9	1	100	272
				Test 2	34	3	86	18	2	91	9	1	100	277
				Test 3	35	3	86	18	2	91	9	1	100	277
				Test 4	34	2	91	14	2	91	10	2	91	273
				Test 5	35	3	86	15	2	91	9	2	91	268
				Average	35	3	87	17	3	90	9	2	96	273
8	7	5	4	Test 1	37	4	85	17	3	86	10	2	91	262
				Test 2	37	4	85	15	3	86	9	3	86	257
				Test 3	32	5	77	18	3	86	11	1	100	263
				Test 4	38	4	85	14	4	85	10	3	86	256
				Test 5	34	5	77	18	3	86	9	3	86	249
				Average	36	5	82	16	3	86	10	3	90	258
10	9	5	4	Test 1	40	4	85	16	1	100	8	1	100	285
				Test 2	40	4	85	17	1	100	9	1	100	285
				Test 3	41	3	86	12	2	91	8	1	100	277
				Test 4	41	2	91	18	1	100	9	1	100	291
				Test 5	45	3	91	16	1	100	10	1	100	291
				Average	41	3	88	16	2	98	9	1	100	286
11	8	4	4	Test 1	35	2	91	12	1	100	9	1	100	291
				Test 2	28	2	91	10	1	100	8	1	100	291
				Test 3	29	2	91	13	1	100	8	1	100	291
				Test 4	38	1	100	18	1	100	7	1	100	300
				Test 5	35	1	100	11	2	91	9	1	100	291
				Average	33	2	95	13	2	98	8	1	100	293
19	3	3	3	Test 1	12	3	86	6	1	100	7	3	86	272

				Test 2	11	4	85	7	1	100	7	1	100	285
				Test 3	12	2	91	8	1	100	7	3	86	277
				Test 4	10	2	91	6	2	91	7	2	91	273
				Test 5	12	2	91	7	1	100	7	2	91	282
				Average	11	3	89	7	2	98	7	2	91	278

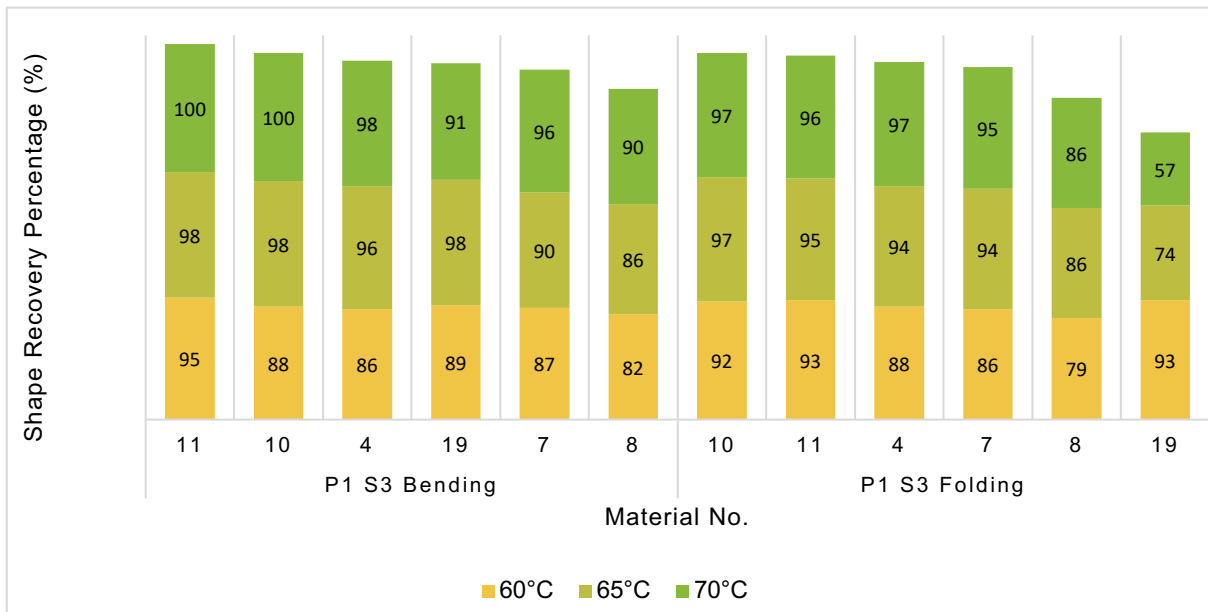


Figure 4.12. The ranking of materials based on their shape recovery ratings, ranging from the highest to the lowest, from left to right, for both programming conditions (P1 S3 bending and folding).

Table 4.10. P1 S3 Folding.

P1 S3 Folding																	
No.	Ta (s)			Test Number	60°C				65°C				70°C				Grand Total (%)
	60°C	65°C	70°C		T (s)	$\theta^\circ$	R	Rr (%)	T (s)	$\theta^\circ$	R	Rr (%)	T (s)	$\theta^\circ$	R	Rr (%)	
4	8	5	3	Test 1	53	18	3	80	23	12	3	87	9	5	1	94	261
				Test 2	43	11	3	88	27	6	2	93	9	3	1	97	278
				Test 3	43	6	2	93	19	2	1	98	9	2	1	98	289
				Test 4	40	8	2	91	21	2	1	98	8	3	1	97	286
				Test 5	40	10	2	89	20	4	1	96	8	2	1	98	283
				Average	44	11	3	88	22	5	1	94	9	3	1	97	279
7	7	4	3	Test 1	24	22	4	76	21	6	2	93	9	5	1	94	263
				Test 2	40	9	2	90	16	8	2	91	8	5	1	94	275
				Test 3	47	11	3	88	12	4	1	96	8	4	1	96	280
				Test 4	42	10	2	89	20	4	1	96	10	5	1	94	279
				Test 5	37	12	3	87	12	3	1	97	11	5	1	94	278
				Average	38	13	3	86	16	5	1	94	9	5	1	95	275
8	7	4	3	Test 1	27	17	3	81	25	15	3	83	14	15	3	83	247

				Test 2	38	18	3	80	24	10	2	89	14	12	3	87	256
				Test 3	31	19	3	79	16	12	3	87	11	15	3	83	249
				Test 4	29	21	4	77	13	12	3	87	11	7	2	92	256
				Test 5	33	21	4	77	22	12	3	87	11	12	3	87	251
				Average	32	19	3	79	20	12	3	86	12	12	3	86	251
10	9	5	4	Test 1	54	11	3	88	15	4	1	96	10	3	1	97	281
				Test 2	50	6	2	93	21	1	1	99	10	5	1	94	286
				Test 3	56	5	1	94	21	5	1	94	10	3	1	97	285
				Test 4	60	9	2	90	17	4	1	96	9	1	1	99	285
				Test 5	54	5	1	94	16	1	1	99	10	2	1	98	291
				Average	55	7	2	92	18	3	1	97	10	3	1	97	286
11	8	4	3	Test 1	40	9	2	90	12	5	1	94	7	1	1	99	283
				Test 2	31	4	1	96	14	2	1	98	11	5	1	94	288
				Test 3	41	9	2	90	10	1	1	99	11	5	1	94	283
				Test 4	32	1	1	99	18	10	2	89	11	3	1	97	285
				Test 5	46	9	2	90	16	4	1	96	11	4	1	96	282
				Average	38	6	2	93	14	4	1	95	10	4	1	96	284
19	3	3	2	Test 1	13	5	1	94	11	8	2	91	9	Curl	10	0	185

				Test 2	11	5	1	94	12	5	1	94	8	5	1	94	282
				Test 3	13	2	1	98	12	6	2	93	7	3	1	97	288
				Test 4	14	8	2	91	12	Curl	10	0	10	Curl	10	0	91
				Test 5	14	10	2	89	11	5	1	94	8	5	1	94	277
				Average	13	6	2	93	12	6	3	74	8	4	5	57	224

The response rate of the materials from both programming conditions (Table 4.9 and Table 4.10) were nearly similar, with an average  $T_a$  of 8s, 6s to 4s at  $T_r$  60°C, 65°C and 70°C respectively. With a 10°C increase in  $T_r$  from 60°C to 70°C, the overall shape recovery percentages were increased by at least 7%. The average time taken to complete shape recovery decreased from 50s to 10s. From the results in Figure 4.12, it was relatively straightforward to identify the top candidate materials. The top three candidate materials (material No. 4, 10 and 11) were selected to the Stage 4 to examine any changes in shape memory properties after going through multiple shape memory cycles. The filament specimens of material No. 19 failed by curling inward when thermally activated at 65°C and 70°C. Therefore, material No. 19 was eliminated despite having the shortest response time and highest SME.

#### Phase 1: Stage 4 Repeatability

The results from both programming conditions (bending and folding) indicated no increase in the response rate for the shape recovery (Table 4.11 and Table 4.12). However, there was a slight reduction in the shape recovery rating and shape recovery percentage in all tested materials after each thermo-mechanical cycle (Figure 4.13).

Table 4.11. P1 S4 Bending.

P1 S4 Bending														
No.	Ta (s)			Test Number	60°C			65°C			70°C			Grand Total (%)
	60°C	65°C	70°C		T (s)	R	Rr (%)	T (s)	R	Rr (%)	T (s)	R	Rr (%)	
4	5	3	2	Test 1	37	4	85	17	2	91	6	2	91	267
				Test 2	23	3	86	12	6	70	12	6	70	226
				Test 3	21	4	85	15	6	70	11	6	70	225
				Test 4	24	5	77	13	6	70	10	6	70	217
				Test 5	17	5	77	11	6	70	8	7	56	203
				Average	24	5	82	14	6	74	9	6	71	227
10	6	3	2	Test 1	48	2	91	15	2	91	7	1	100	282

				Test 2	27	3	86	15	2	91	11	5	77	254
				Test 3	22	3	86	17	2	91	10	5	77	254
				Test 4	27	4	85	15	2	91	12	6	70	246
				Test 5	20	5	77	11	3	86	8	6	70	233
				Average	29	4	85	15	3	90	10	5	79	254
11	4	3	2	Test 1	35	2	91	11	1	100	10	2	91	282
				Test 2	15	2	91	15	2	91	15	3	86	268
				Test 3	21	1	100	16	2	91	6	3	86	277
				Test 4	26	3	86	10	2	91	8	2	91	268
				Test 5	20	2	91	10	3	86	6	3	86	263
				Average	23	2	92	12	2	92	9	3	88	272

Table 4.12. P1 S4 Folding.

P1 S4 Folding																	
No.	Ta (s)			Test Number	60°C				65°C				70°C				Grand Total (%)
	60°C	65°C	70°C		T (s)	$\theta^\circ$	R	Rr (%)	T (s)	$\theta^\circ$	R	Rr (%)	T (s)	$\theta^\circ$	R	Rr (%)	
4	6	4	3	Test 1	36	12	3	87	14	7	2	92	10	3	1	97	276
				Test 2	32	7	2	92	15	12	3	87	11	10	2	89	268
				Test 3	18	18	3	80	12	5	1	94	11	10	2	89	263
				Test 4	29	18	3	80	12	8	2	91	10	4	1	96	267
				Test 5	22	20	3	78	10	18	3	80	7	15	3	83	241
				Average	27	15	3	83	13	10	2	89	10	8	2	91	263
10	5	4	3	Test 1	40	10	2	89	14	4	1	96	7	2	1	98	283
				Test 2	27	30	4	67	14	19	3	79	10	11	3	88	234
				Test 3	42	42	6	53	15	8	2	91	12	11	3	88	232
				Test 4	37	49	6	46	14	10	2	89	11	9	2	90	225
				Test 5	22	53	7	41	13	13	2	86	8	15	3	83	210
				Average	34	37	5	59	14	11	3	88	10	10	2	89	236
11	5	4	2	Test 1	48	11	3	88	8	1	1	99	8	10	2	89	276

				Test 2	11	18	3	80	12	10	2	89	12	5	1	94	263
				Test 3	21	19	3	79	12	5	1	94	14	12	3	87	260
				Test 4	26	9	2	90	10	1	1	99	6	5	1	94	283
				Test 5	16	11	3	88	9	10	2	89	8	5	1	94	271
				Average	24	14	3	85	10	5	1	94	10	7	2	92	271

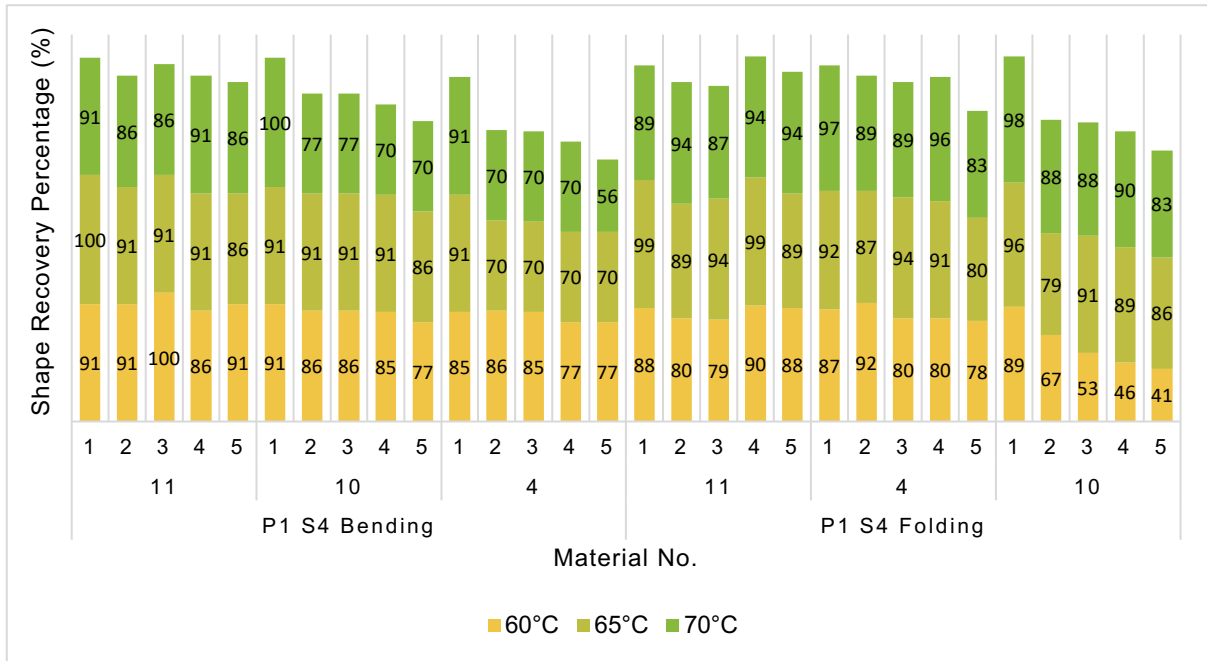


Figure 4.13. The shape memory properties of materials in five repetitive thermo-mechanical cycle.

Figure 4.13 also shows that the shape recovery percentage of the materials subjected to a circular bend reduced more significantly than the 90° fold after five thermo-mechanical cycles. Filament (No. 11) showed the least reduction compared No. 4 and No. 10 after the five thermo-mechanical cycles. Therefore, based on the results and comparison of Phase 1 (filament) experiments, No. 11 was the most suitable SMP for ME 4DP. It had the highest and most consistent shape recovery performance, capable of repetitive shape memory cycles with the least reduction in the SME. The same material selection process workflow was implemented for Phase 2. The five top candidate materials from P1 S3 were selected to investigate the shape memory properties of the materials in ME printed form.

#### 4.4.2. Phase 2 ME Printed Structure

##### Phase 2: Stage 1 Shape Fixity

All the ME printed specimens (material No. 4, 7, 8, 10 and 11) attained the preferred programmed shape at R:10 at a Td of 80°C (Table 4.13).

Table 4.13. P2 S1 Shape Fixity.

Polymer Type	Material No.	Shape deforming temperature (°C)	Shape fixity Rating (1 – 10; Poor – Excellent)	Pass (P)/ Failed (F)
PLA	4, 7, 8, 10, 11	80	10	P

#### Phase 2: Stage 2 Response Rate and SME

The results showed no changes in Ta and relatively similar time was taken for the complete shape recovery for the ME printed structures and filaments at 65°C and 70°C. However, the Ta decreased by approximately 3s from 8s to 5s, and the overall time taken for complete shape recovery reduced by 7s at Tr 60°C (Table 4.14 and Table 4.15). In general, the shape recovery ratings of the PLA materials were significantly improved when being ME manufactured (Figure 4.14).

Table 4.14. P2 S2 Bending.

P2 S2 Bending													
No.	Ta (s)			60°C			65°C			70°C			Grand Total (%)
	60°C	65°C	70°C	T (s)	R	Rr (%)	T (s)	R	Rr (%)	T (s)	R	Rr (%)	
4	5	4	3	77	2	91	12	1	100	9	1	100	291
7	5	4	3	44	1	100	14	1	100	12	1	100	300
8	5	4	3	44	2	91	10	1	100	8	1	100	291
10	5	4	3	34	1	100	11	1	100	7	1	100	300
11	5	4	3	30	1	100	8	1	100	7	1	100	300

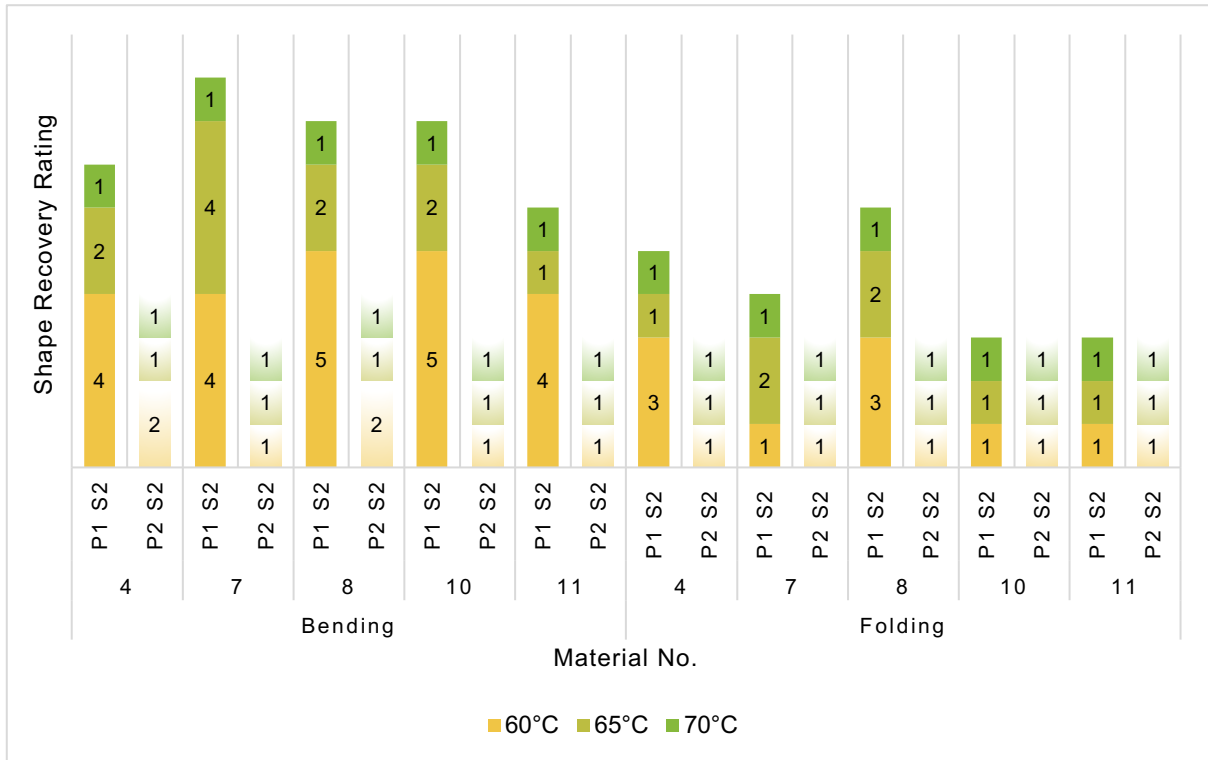


Figure 4.14. The shape memory properties of materials in filament form (P1 S2) versus ME printed structure (P2 S2).

All ME printed specimens recovered to their original shape from fold deformation, shown as rating “1” and “2” in Figure 4.14 and Table 4.15. However, it was observed that the fold recovery of several ME printed specimens would surpass its original configuration and retrieved into an inverse curvature as visualised in Figure 4.15.

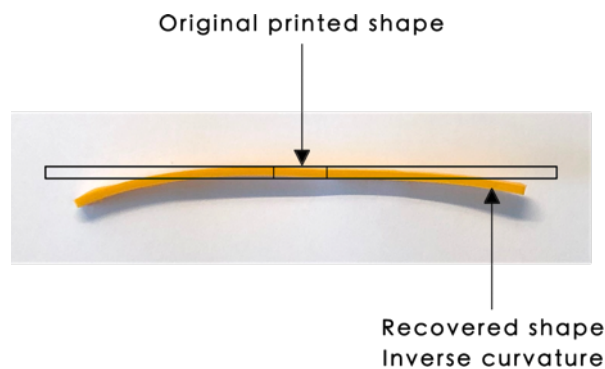


Figure 4.15. An inverse curvature shape recovery from fold deformation.

Goo, Hong and Park (2020) explained that these results are likely to be related to the double extrusion processes and the differences in residual stresses caused by the printing direction. In Phase 2, the materials underwent two series of extrusion processes, first was the filament production process, followed by the ME manufacturing process. Due to these extrusion processes, the ME printed structure became highly oriented along its longitudinal direction with tensile residual stress along its length and compressive residual stress along its cross-section. The relaxation and recovery of these residual stresses during activation led to the effect shown in Figure 4.15. It was not due to the  $T_r$  being too high for the material. What is surprising is that this particular behaviour appeared only from a fold recovery. Another possible explanation for this might be due to a higher stress concentration formed at the  $90^\circ$  crease fold. On the other hand, the stress formed was distributed more evenly on the smooth curvature of a bend deformation. Further research can be undertaken to investigate the cause of this phenomenon. From the semi-structured interviews findings, the experts in 4DP explained that an inverse curvature was not a sign of bad shape memory or recovery but was due to the recovery of internal stresses within the ME structure. Therefore, an inverse curve within acceptable range of  $-1^\circ$  to  $-20^\circ$  is acceptable (Figure 4.9).

Table 4.15. P2 S2 Folding.

P2 S2 Folding																
No.	Ta (s)			60°C				65°C				70°C				Grand Total (%)
	60°C	65°C	70°C	T (s)	R	$\theta^\circ$	Rr (%)	T (s)	R	$\theta^\circ$	Rr (%)	T (s)	R	$\theta^\circ$	Rr (%)	
4	5	4	3	54	1	0	100	17	1	0	100	8	1	0	100	300
7	5	4	3	30	1	0	100	14	1	0	100	9	1	0	100	300
8	5	4	3	21	1	0	100	10	1	0	100	8	1	0	100	300
10	5	4	3	34	1	0	100	15	1	0	100	10	1	0	100	300
11	5	4	3	22	1	0	100	11	1	0	100	8	1	-17	100	300

## Phase 2: Stage 3 Validation of Recovery

The shape recovery results indicated that the ME printed structures were better and showed more consistent results than the filaments. There were fewer fluctuations in the response time and R values among the same set. Figure 4.16 showed an inverse trend of results compared to Phase 1, where the bend recovery was higher than fold recovery. In P2 S3, the shape recovery percentage from a fold deformation were slightly higher than bend deformation for each material.

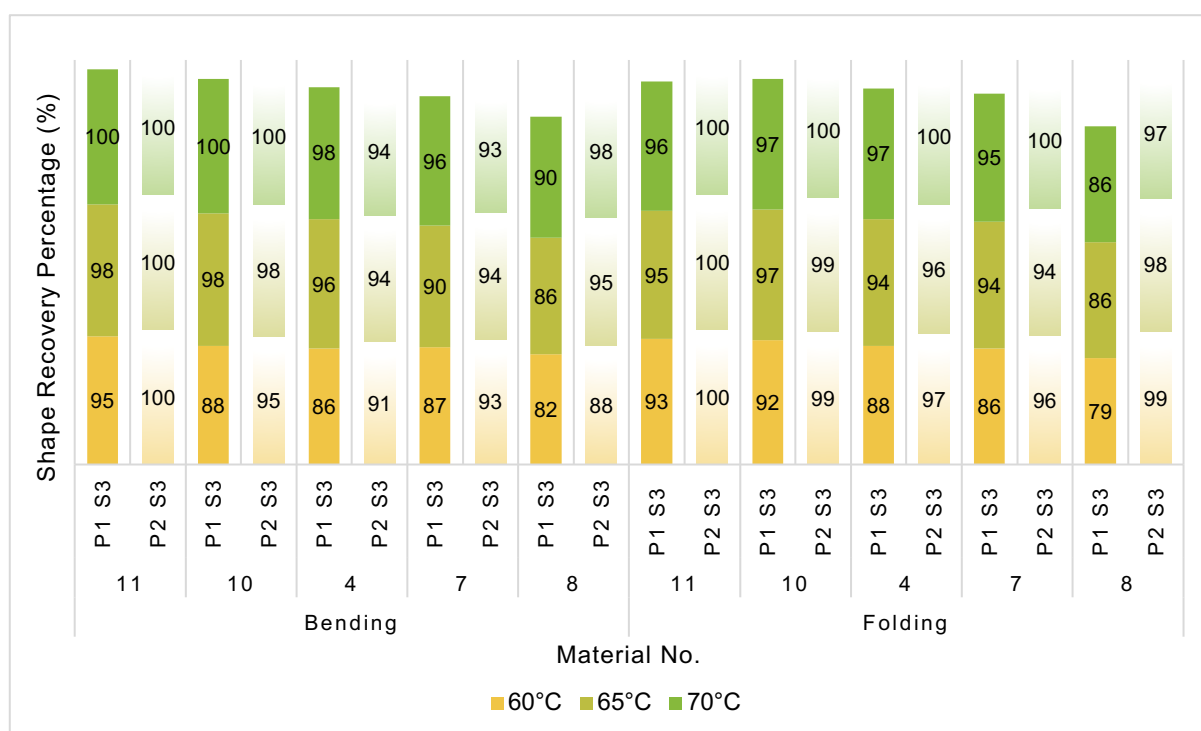


Figure 4.16. Comparison of the shape recovery percentages of the filaments (P1 S3) with the ME printed structures (P2 S3) for both programming conditions (bending and folding).

The order of the best performing materials remained the same as Phase 1 (P1 S3). Material No.11 was the best SMP which have coherently accomplished 100% full recovery in five tests from each programming condition. Material No.10 came second with an average Rr of 98.5%, followed by material No. 4 with 95%. However, it should be noted that the shape recovery performance of each material (SMP) would vary based on the programming condition and the processing parameters.

Table 4.16. P2 S3 Bending.

P2 S3 Bending														
No.	Ta (s)			Test Number	60°C			65°C			70°C			Grand Total (%)
	60°C	65°C	70°C		T (s)	R	Rr (%)	T (s)	R	Rr (%)	T (s)	R	Rr (%)	
4	6	5	4	Test 1	34	2	91	12	1	100	15	1	100	291
				Test 2	33	2	91	19	2	91	15	3	86	268
				Test 3	32	2	91	25	2	91	12	1	100	282
				Test 4	36	2	91	21	1	100	10	2	91	282
				Test 5	35	2	91	23	3	86	12	2	91	268
				Average	34	2	91	20	2	94	13	2	94	279
7	6	4	4	Test 1	44	1	100	14	1	100	12	1	100	300
				Test 2	42	3	86	11	1	100	12	2	91	277
				Test 3	40	1	100	11	1	100	7	2	91	291
				Test 4	49	3	86	14	3	86	10	2	91	263
				Test 5	41	2	91	21	3	86	12	2	91	268
				Average	43	2	93	14	2	94	11	2	93	280
8	5	4	4	Test 1	44	2	91	10	1	100	8	1	100	291
				Test 2	34	5	77	12	1	100	9	1	100	277
				Test 3	31	2	91	18	2	91	13	1	100	282
				Test 4	29	2	91	15	2	91	10	1	100	282
				Test 5	33	2	91	18	2	91	10	2	91	273
				Average	34	3	88	15	2	95	10	1	98	281
10	6	5	4	Test 1	34	1	100	11	1	100	7	1	100	300
				Test 2	35	1	100	15	1	100	13	1	100	300
				Test 3	35	2	91	14	2	91	9	1	100	282
				Test 4	38	1	100	16	1	100	11	1	100	300
				Test 5	35	3	86	15	1	100	9	1	100	286

				Average	35	2	95	14	2	98	10	1	100	293
11	6	5	4	Test 1	30	1	100	8	1	100	7	1	100	300
				Test 2	23	1	100	10	1	100	8	1	100	300
				Test 3	22	1	100	12	1	100	9	1	100	300
				Test 4	25	1	100	10	1	100	7	1	100	300
				Test 5	26	1	100	10	1	100	7	1	100	300
				Average	25	1	100	10	1	100	8	1	100	300

Table 4.17. P2 S3 Folding.

P2 S3 Folding																	
No.	Ta (s)			Test Number	60°C				65°C				70°C				Grand Total (%)
	60°C	65°C	70°C		T (s)	$\theta^\circ$	R	Rr (%)	T (s)	$\theta^\circ$	R	Rr (%)	T (s)	$\theta^\circ$	R	Rr (%)	
4	6	5	5	Test 1	54	0	1	100	17	0	1	100	8	0	1	100	300
				Test 2	57	0	1	100	16	10	2	89	9	-17	1	100	289
				Test 3	48	4	1	96	14	0	1	100	10	-15	1	100	296
				Test 4	49	5	1	94	24	9	2	90	14	0	1	100	284
				Test 5	52	3	1	94	23	0	1	100	10	-17	1	100	294
				Average	52	2	1	97	19	4	1	96	10	-10	1	100	293
7	7	5	4	Test 1	30	0	1	100	14	0	1	100	9	0	1	100	300
				Test 2	34	0	1	100	13	5	1	94	9	0	1	100	294
				Test 3	36	12	3	87	14	1	1	99	10	0	1	100	286
				Test 4	43	4	1	96	17	11	3	88	11	0	1	100	284
				Test 5	38	6	2	98	20	8	2	91	9	0	1	100	289
				Average	36	4	2	96	16	5	2	94	10	0	1	100	290
8	6	5	5	Test 1	21	0	1	100	10	0	1	100	8	0	1	100	300

				Test 2	29	3	1	100	11	0	1	100	14	8	2	91	291
				Test 3	32	2	1	100	15	0	1	100	7	-10	1	100	300
				Test 4	27	12	3	97	28	10	2	89	7	-10	1	100	286
				Test 5	26	0	1	100	18	1	1	99	8	4	1	96	295
				Average	27	3	1	99	16	2	1	98	9	-8	1	97	294
10	8	6	5	Test 1	34	0	1	100	15	-12	1	100	10	0	1	100	300
				Test 2	37	6	2	98	16	-15	1	100	10	-15	1	100	298
				Test 3	35	8	2	98	22	0	1	100	8	0	1	100	298
				Test 4	32	0	1	100	17	-13	1	100	8	-12	1	100	300
				Test 5	40	0	1	100	25	6	2	93	9	0	1	100	293
				Average	36	3	1	99	19	-7	1	99	9	-5	1	100	298
11	6	5	4	Test 1	22	-14	1	100	11	-12	1	100	8	-17	1	100	300
				Test 2	24	-15	1	100	13	-15	1	100	8	-18	1	100	300
				Test 3	23	-17	1	100	13	-12	1	100	8	-17	1	100	300
				Test 4	39	-18	1	100	16	-15	1	100	11	-15	1	100	300
				Test 5	26	-14	1	100	14	16	1	100	7	-15	1	100	300
				Average	27	-16	1	100	13	-14	1	100	8	-16	1	100	300

## Phase 2: Stage 4 Repeatability

High shape memory cycle life is important for SMP to ensure that the repeatability and durability of the 4DP structure without failure. Based on Figure 4.17, the ME printed structures showed more consistent and better results compared to the filaments, when subjected to consecutive shape memory cycles. The results showed no delay in response time and no sign of apparent deterioration or failure in the SME. The response rate of the material from both programming conditions (Table 4.18 and Table 4.19) were almost similar, with an average  $T_a$  of 6s, 5s, 4s, and 22s, 11s, 8s for complete shape recovery at  $T_r$  of 60°C, 65°C and 70°C respectively. Therefore, based on the experiments and results, Material No. 11 was the most suitable commercially available thermoplastic for ME thermo-responsive 4DP.

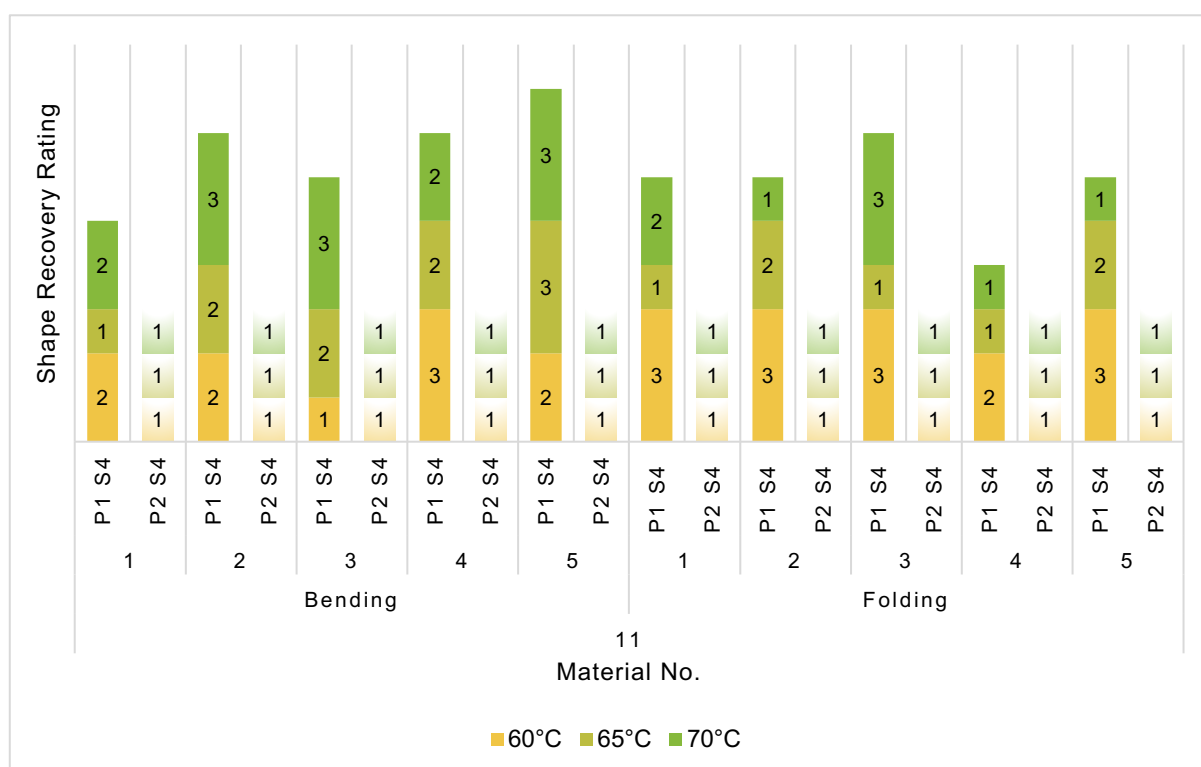


Figure 4.17. Comparison of the shape recovery ratings of Material No. 11 filaments (P1 S4) with the ME printed structures (P2 S4) after five repetitive thermo-mechanical cycles.

Table 4.18. P2 S4 Bending.

P1 S4 Bending														
No.	Ta (s)			Test Number	60°C			65°C			70°C			Grand Total (%)
	60°C	65°C	70°C		T (s)	R	Rr (%)	T (s)	R	Rr (%)	T (s)	R	Rr (%)	
11	6	4	4	Test 1	25	1	100	10	1	100	8	1	100	300
				Test 2	17	1	100	8	1	100	7	1	100	300
				Test 3	26	1	85	9	1	100	7	1	100	285
				Test 4	17	1	100	10	1	100	8	1	100	300
				Test 5	14	1	100	12	1	100	7	1	100	300
				Average	20	2	97	10	1	100	7	1	100	297

The final selection material suggested from Phase 1 and Phase 2 were identical. Material No. 11 was nominated as the most potent commercial thermoplastic for use in material extrusion (ME) thermo-responsive 4DP. It had the highest shape memory performance and transformation efficiency among the list of materials.

Table 4.19. P2 S4 Folding.

P2 S4 Folding																	
No.	Ta (s)			Test Number	60°C				65°C				70°C				Grand Total (%)
	60°C	65°C	70°C		T (s)	$\theta^\circ$	R	Rr (%)	T (s)	$\theta^\circ$	R	Rr (%)	T (s)	$\theta^\circ$	R	Rr (%)	
11	6	5	4	Test 1	27	-14	1	100	13	-15	1	100	8	-15	1	100	300
				Test 2	30	-14	1	100	12	-17	1	100	9	-17	1	100	300
				Test 3	21	-10	1	100	10	-15	1	100	8	-15	1	100	300
				Test 4	20	-18	1	100	10	-18	1	100	8	-18	1	100	300
				Test 5	19	-15	1	100	12	-15	1	100	8	-15	1	100	300
				Average	23	-14	1	100	11	-16	1	100	8	-16	1	100	300

## **4.5. Framework Validation**

This material selection framework was subjected to a two-phase validation. The first phase involved a pilot workshop to test and revise the developed framework through its practical application with target beneficiaries. The second phase involved one-to-one online interviews with experts in 4DP for validation and feedback to improve the framework. At the end of both each activity, the participants were asked to complete a questionnaire survey to provide quantitative and qualitative feedback about the completeness, effectiveness and usability of the framework.

Both workshop and interviews were conducted in line with the research ethics policy of the College of Engineering, Design and Physical Sciences at Brunel University London. The BREO approval letter can be found in Appendix IV. All participants were briefed about the nature of the activities. The Participant Information Sheet can be found in Appendix V. The identities and organisations of the participants were kept anonymous. The participants were referenced with an Alphanumeric ID when mentioned rather than their names. Their background, discipline, and level of knowledge on 4DP of the participants were labelled accordingly (Table 4.22).

### **4.5.1. Workshops**

The developed framework was applied and tested by three doctoral researchers from design and engineering background currently investigating different areas of 4DP. A one-to-one participant observation approach was used. Each workshop was organised to bring mutual benefits to the doctoral researchers and the author. The participants can learn the process workflow for selecting the best performing SMP, receive theoretical and practical knowledge to create a DSM active structure. Whilst the collect data allowed the author to identify the applicability of the developed framework by recognising the strengths and weaknesses of the workflow.

Before each workshop, the participants were given a material selection framework user guide which contained information about the material selection process workflow, the objective and description of the experimental stages, the thermo-mechanical cycle process workflow, the experimental procedure for each stage (which can be found in Appendix VI), together with the measuring charts, containing the shape fixity, bend and fold recovery charts.

Prior to the practical task, the research background including the current findings, aims and objectives of the workshop were clarified to the participants. The processes and steps identified in the user guide were carefully explained to the participant. The filament materials, tools and equipment required for the experiment were provided. The items remained constant for all workshops. However, the participants were allowed to include their own choice of filament materials for the study if requested. The methods of preparing the material specimens and the experiment setup were demonstrated (Figure 4.18). Later, the participants were given as much time to undertake their experiments (Figure 4.19). The length of each workshop took an average of three days, approximately five hours a day. The author acted as an active observer at the research site in order to take notes of the participant behaviour during the study. The author would identify whether the practical exercise was easy for participants to follow, or whether there were difficulties on the exercise.

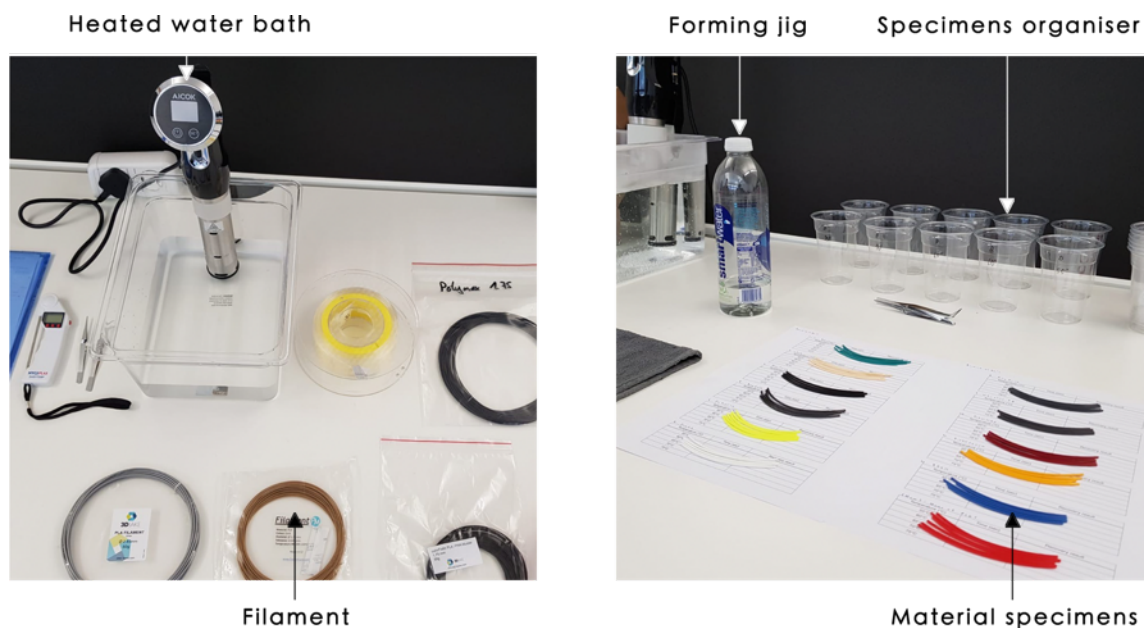


Figure 4.18. The experiment setup and prepared material specimens by a participant.



Figure 4.19. Participant conducting the practical task.

At the end of the workshop, a questionnaire survey via Google Form was shared immediately to each participant to record their most recent experiment experience and allowed for any feedback. The questionnaire survey comprised six closed-ended questions (CE), four open-ended questions (OE) and four sets of Likert scale questions (LS). Likert scale 1 (Table 4.20) for the material selection process and Likert scale 2 (Table 4.21) for the three measuring charts. The five-point Likert-scale questions allow the participant to rate their responses clearly according to very poor, poor, neutral, good and excellent (1 to 5). The questions were:

#### 1) General Background

Q1 (CE) Please identify which category of discipline do you belong to?

Q2 (CE) Which level best describes your knowledge and background in 4DP?

#### 2) Framework-specific Questions

Q3 (CE) Are you aware of any framework for selecting thermo-responsive materials for 4DP currently available?

- Q4 (CE) Do you agree with the tools and equipment used?
- Q5 (CE) Do you agree with the procedure in Process 1 and 2 to complete the shape memory cycle of a dual-state mechanism (DSM) heat-induced structure?
- Q6 (CE) Based on the four experimental stages discussed, do you agree with the structure of this framework?
- Q7 (OE) Are there any stages to add, reduce or require improvement?
- Q8 (OE) Based on your opinion, what are the advantages and drawbacks of this material selection framework?
- Q9 (OE) Please provide any other general feedback.
- Q10 (OE) Please kindly recommend an expert in 4DP to expand this research study.

Table 4.20. Likert Scale 1 for the material selection process.

	<b>1</b> Very Poor	<b>2</b> Poor	<b>3</b> Neutral	<b>4</b> Good	<b>5</b> Excellent
Concept	<input type="checkbox"/>				
Easy to understand	<input type="checkbox"/>				
Easy to use	<input type="checkbox"/>				
Accuracy	<input type="checkbox"/>				
Usefulness	<input type="checkbox"/>				

Table 4.21. Likert Scale 2 for the measuring charts.

	<b>1</b> Very Poor	<b>2</b> Poor	<b>3</b> Neutral	<b>4</b> Good	<b>5</b> Excellent
Easy to understand	<input type="checkbox"/>				
Easy to use	<input type="checkbox"/>				
Accuracy	<input type="checkbox"/>				

A collective discussion on the open-ended questions was carried out with the participants to share insights about the ease and difficulties faced during the practical task. Their comments and recommendations were recorded, which were later gathered to identify the refinements and improvements needed for the framework.

#### **4.5.2. Semi-structured Interviews**

Five experts in the field of 4DP were invited for interviews to evaluate the completeness (concept), effectiveness, and usability of the framework. They were two doctoral researchers, two academic professionals from different universities and one industry professional from an engineering simulation software industry. Potential interviewees were contacted via email and invited to take part in the one-to-one online interview hosted through Zoom. The interviews were conducted individually as opposed to group interview to avoid influence in decision-making and minimise bias between participants. The Participant Information Sheet was shared with the interviewees in advance, providing them sufficient time to understand the details and prepare for the upcoming interview. All interviews were conducted with the same interviewer and subjected to the same process and interview questions.

Each interview session was pre-arranged with a duration of an hour to allow sufficient time for the interviewer to deliver a short presentation introducing the material selection framework, asking the interview questions, followed by informal discussion. The interview was conducted using a semi-structured approach which included closed-ended questions, Likert scales and open-ended questions. The questions were identical to the questionnaire survey used in the workshop in order to collect consistent data about the same aspects of the framework. The interview script can be found in Appendix VII. During the informal conversational discussions, the second set of questions was introduced depending on the

expertise of the interviewees. The questions were raised to validate the literature review findings as well as contribute to the information which has not been previously identified from the literature. The interviewees were also encouraged to provide additional information as supporting data when required. The interviews were recorded to refine and improve the framework. Some of the additional questions included:

Q11 (OE) Based on your opinion, why would an inverse curvature occur?

Q12 (OE) Why did an inverse curvature occur only in the fold recovery but not in the bend recovery?

Q13 (OE) Would it be due to the nature of the material that contributes to an inverse curvature?

Q14 (OE) Do you agree that five specimens are a recommended average of samples to be tested to determine the accuracy of the results?

### 4.5.3. Framework Validation Findings

The results from the workshops and semi-structured interviews were analysed for formal validation. The nine participants belong to three main disciplines, which were designer, engineer, and material scientist (Figure 4.20). The descriptions of each participant were listed in Table 4.22.

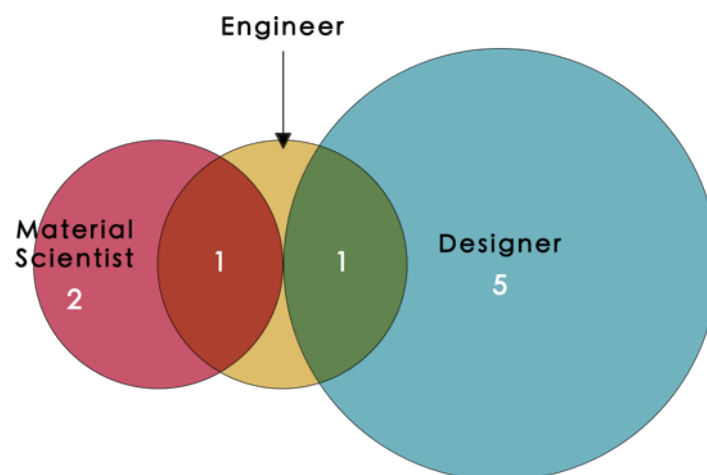


Figure 4.20. The disciplines of the participants.

Table 4.22. The general background of participants and the validation phase involved.

Validation Phase	Participants	Professions	Disciplines	Knowledge level in 4DP
Workshop	A	Doctoral researcher	Designer	Intermediate
	B	Doctoral researcher	Designer	Intermediate
	C	Postgraduate student	Material scientist	Intermediate
Semi-structured Interview	D	Postdoctoral researcher	Designer	Intermediate
	E	Doctoral researcher	Designer	Intermediate
	F	Doctoral researcher	Engineering designer	Intermediate
	G	Academic professional	Engineer and material scientist	Advanced
	H	Academic professional	Designer	Advanced
	I	Industry professional	Material scientist	Intermediate

All participants from the workshops and semi-structured interviews acknowledged that there is currently no existing material selection framework for 4DP. Overall, the participants declared that very little was found in the literature to demonstrate the practical workflow to create thermo-responsive 4DP structures. They recognised that this framework could help to reduce the gap in knowledge where limited material filament options and no standardised process workflow for 4DP exist.

None of them had objections to the tools and equipment used for the experiments. Eight out of nine participants gave a positive response when asked if they agree with the procedures for thermo-rheological characterisation to complete the shape memory cycle of a DSM heat-induced structure. Whilst Participant G raised concerns for (step 2) shape deformation and (step 3) phase fixation for Process 1; *“Why didn’t you deform the part in the hot water?”*. Participant G was concerned that having the specimen removed and deformed out of the water would cause a 5 °C to 10°C decrease in deforming temperature. As a consequence,

the exact Td value used for the particular deformation would be lower than the pre-set Td and difficult to predict. The author agreed to the statement by Participant G that the ideal method would be deforming the specimen in the heated water bath. However, both understood that the current limitations were (1) the rigid specimen could not fit into the forming mould before softening at Td, and (2) the temperature at 80°C was too hot for manual deformation underwater. The author has suggested an alternative method which involved heating the specimen at Td, removal from the water bath for phase fixation and re-immersing the specimen in its forming jig back into the heated water bath. However, this applied cycle of heating, cooling and reheating the specimen would affect the shape memory and recovery properties of the material. After considering all the factors, Participant G came to an agreement with the initially proposed method and clarified that “as long as the Td is within the range for the material, this is acceptable”.

The first Likert question asked the participants to evaluate the completeness, effectiveness and usability of the material selection process by rating its concept, easy to understand, easy to use, accuracy and usefulness (Table 4.23).

Table 4.23. Quantitative feedback collected from the participants to evaluate the completeness, effectiveness and usability of the material selection process.

The Material Selection Process						
	<b>1 Very Poor</b>	<b>2 Poor</b>	<b>3 Neutral</b>	<b>4 Good</b>	<b>5 Excellent</b>	<b>Average (Out of 5)</b>
Concept	0	0	0	5	4	4.4
	0%	0%	0%	56%	44%	
Easy to understand	0	0	0	5	4	4.4
	0%	0%	0%	56%	44%	
Easy to use	0	0	1	5	3	4.2
	0%	0%	11%	56%	33%	
Accuracy	0	1	3	4	1	3.6
	0%	11%	33%	44%	11%	
Usefulness	0	0	3	1	5	4.2
	0%	0%	33%	11%	56%	

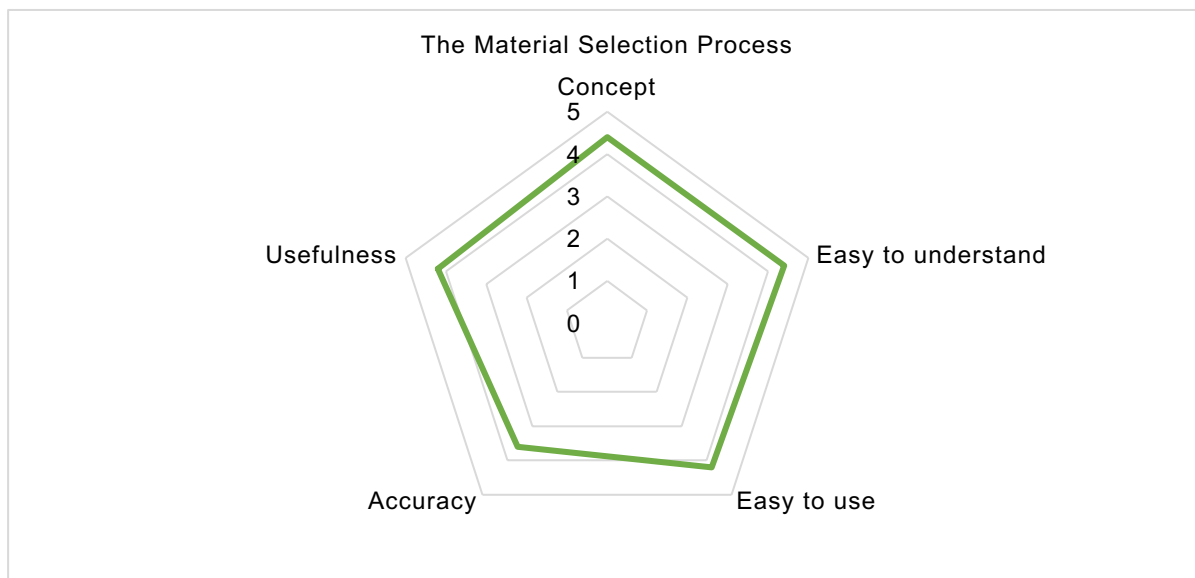


Figure 4.21. The average rating for the material selection process.

The average score for each element was calculated and illustrated using a radar chart in Figure 4.21. Most factors of the material selection process received rating between good to excellent with average scores of 4 and above. However, the accuracy was rated neutral with an average score of 3.6 (Table 4.23). Based on the four experimental stages discussed, all participants agreed to the concept and structure of this framework. 56% rated good for the concept and 44% rated excellent. No participant voted neutral, poor or very poor (Table 4.23). The majority of participants have no suggestions when asked if there are any stages to add or reduce. Though, Participant F suggested that the investigation on the moisture absorption properties of the materials can be added in the material selection process. Additional pre-processing stage includes instructing the methods of drying thermoplastics with high moisture sensitivity before fabrication (i.e., thermally conditioned in an oven and dried). This may be relatively crucial, predominantly for shape memory polyurethane (SMPU) as the effect of moisture trapping within the thermoplastics has a significant influence on the ME process (i.e., poor print quality, rough surface finishing, an increment of voids in the manufactured part), and the SME of the material. Moisture trapping will downgrade the end product performance (Garces *et al.*, 2019).

56% described that the framework was simple and relatively easy to understand, while 44% voted for very easy. With respect to the usability, three felt that the framework was very easy to use, five responded easy and one responded neutrally. Two out of three participants from the workshop were able to follow the process, complete and achieve their goals using the user guide provided without additional support. They responded positively about the

framework without identifying any difficulties to understand the process. However, Participant A criticised that the pass and failure criteria for materials in Stage 2 were unclear. The number of top candidate materials to be carried forward to the following stage was not specified clearly in the material selection process workflow. Participant I also commented that the evaluation criteria are important and need to be explicit; “*it was hard to know what is acceptable or not in your model*”. For this reason, a concise statement on the evaluation criteria and the number of top candidate materials to be carried forward for each experimental stage would be identified in the material selection process workflow. The grand total ranking system used in evaluating the results for Phase 1 Stage 2 will be added and highlighted in the user guide to notify the user about the subsequent action.

Regarding the accuracy of the framework, four participants responded good (44%), three responded neutral (33%), one responded excellent (11%) and one responded poor (11%). The respondent who voted for poor explained that this decision was associated with the accuracy of the measuring charts. In general, most participants felt that this framework is purposeful for the exploration and early development of 4DP. The participants signified that the guide would help to make the experiments for selecting materials significantly easier.

Table 4.24. Quantitative feedback collected from the participants to evaluate the effectiveness and usability of the shape fixity chart.

The Shape Fixity Chart (SFC)						
	<b>1 Very Poor</b>	<b>2 Poor</b>	<b>3 Neutral</b>	<b>4 Good</b>	<b>5 Excellent</b>	<b>Average (Out of 5)</b>
Easy to understand	0	0	1	2	6	4.6
	0%	0%	11%	22%	67%	
Easy to use	0	0	3	0	6	4.3
	0%	0%	33%	0%	67%	
Accuracy	0	2	1	2	4	3.9
	0%	22%	11%	22%	45%	

The second Likert question sought to determine the effectiveness, usability and accuracy of the shape fixity chart (Table 4.24). These aspects were rated at an average of 4.6, 4.3 and 3.9 respectively. 67% described that the process of measuring the programmed shape was

very easy to understand, 22% responded easy, while 11% responded neutrally. The majority of the participants described the chart was very easy and relatively straightforward to use, suitable for a broad range of users with different background and knowledge level in 4DP. Over half of those surveyed responded positively about the accuracy of the shape fixity chart. However, two participants voted for poor as they felt that the measuring charts “*were not scientific enough*”. However, Participant E defended that a simpler version of measurement tailored for designers was essential. Participant G agreed that the present methodology was useful and efficient enough to provide users with adequate theory and technical details to understand the materials. The expert suggested that a profile projector or gradiometer can be used as add-on instrument for an advanced investigation to obtain scientific measurement at the highest accuracy. On the other hand, Participant H advised that “*it is important to mention that the chart has to be placed on a flat surface*”. The expert also suggested that a coloured or highlighted area on the chart to initiate the placement and alignment of the specimen would be beneficial. Some given instructions or visual guide to initiate the correct use of measuring charts can also be added in the user guide to improve their usability.

Table 4.25. Quantitative feedback collected from the participants to evaluate the effectiveness and usability of the bend recovery chart.

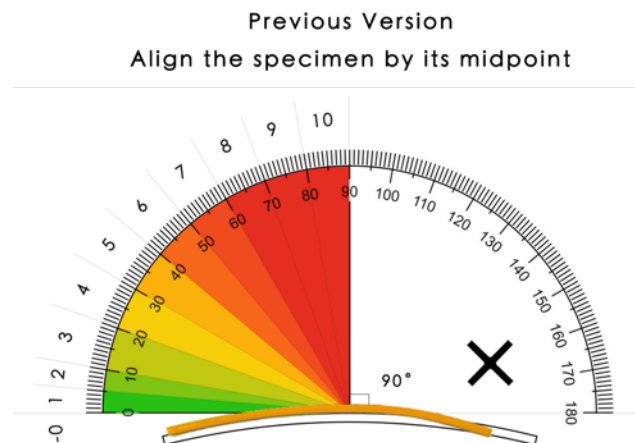
The Bend Recovery Chart (BRC)						
	<b>1 Very Poor</b>	<b>2 Poor</b>	<b>3 Neutral</b>	<b>4 Good</b>	<b>5 Excellent</b>	<b>Average (Out of 5)</b>
Easy to understand	0	1	0	2	6	4.4
	0%	11%	0%	22%	67%	
Easy to use	0	0	3	0	6	4.3
	0%	0%	33%	0%	67%	
Accuracy	0	2	1	2	4	3.9
	0%	22%	11%	22%	45%	

Table 4.26. Quantitative feedback collected from the participants to evaluate the effectiveness and usability of the fold recovery chart.

The Fold Recovery Chart (FRC)						
	<b>1 Very Poor</b>	<b>2 Poor</b>	<b>3 Neutral</b>	<b>4 Good</b>	<b>5 Excellent</b>	<b>Average (Out of 5)</b>
Easy to understand	0	0	1	2	6	4.6
	0%	0%	11%	22%	67%	
Easy to use	0	0	3	0	6	4.3
	0%	0%	33%	0%	67%	
Accuracy	0	1	2	3	3	3.9
	0%	11%	22%	33%	33%	

For the fold recovery chart, Participant H pointed out that the method used for measuring an inverse curvature was incorrect (Figure 4.22A). The expert instructed that the correct method to measure an inverse curvature would be placing half of the specimen length as flat as possible at 0° to capture the true degree (< 0°) of the recovered inverse curvature (Figure 4.22B). In addition, the degree of the protractor on the fold recovery chart should change from 180° to 360° to capture the negative degree of recovered inverse curvature. Other than that, the overall feedback for the bend recovery chart (Table 4.25) and the fold recovery chart (Table 4.26) were closely similar to the shape fixity chart. Therefore, the same suggested design refinements and improvements were applied.

**A**



**B**

Updated Version  
Align half of the specimen length on the grey area

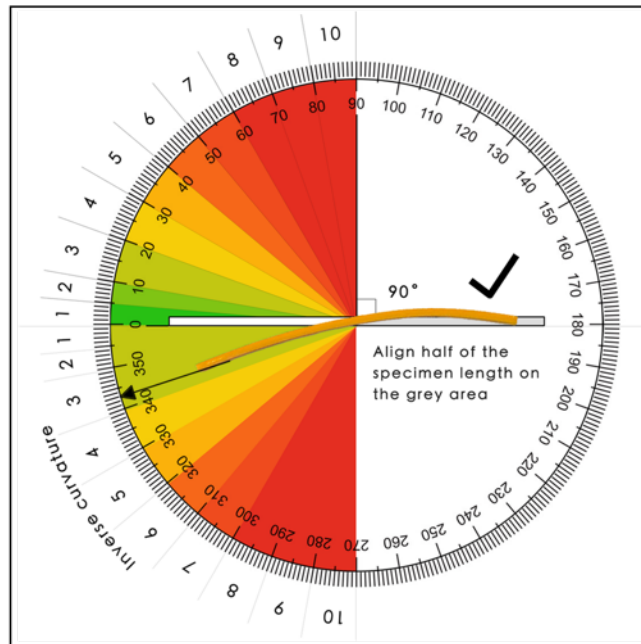


Figure 4.22. The corrected method to measure an inverse curvature using the fold recovery chart. (A) previous version and (B) updated version.

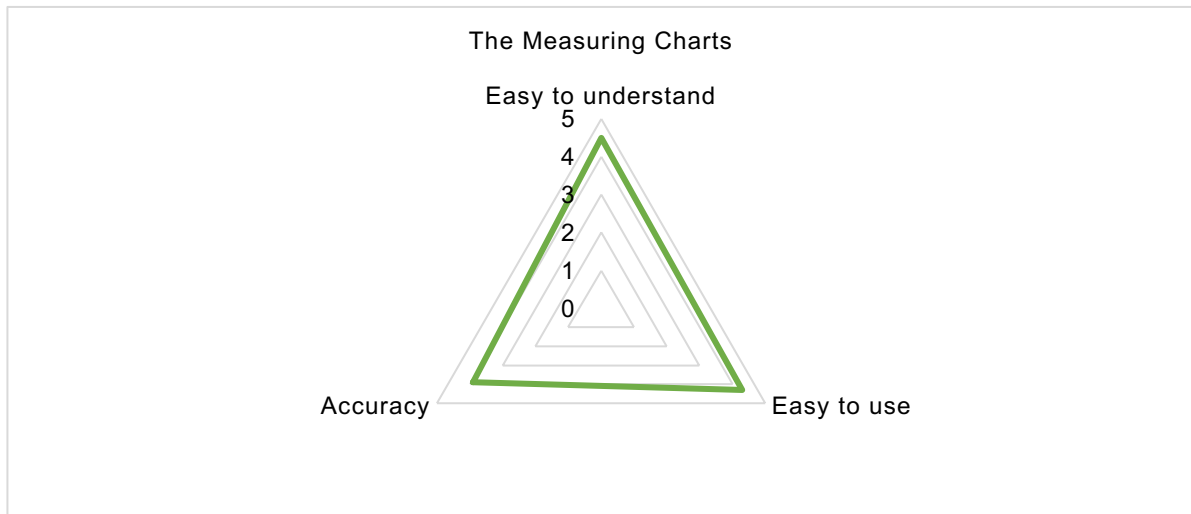


Figure 4.23. The average rating for the measuring charts.

Figure 4.23 summarises the rating for the measuring charts as a whole. In summary, all participants from the workshop and semi-structured interviews gave a positive response to the material selection framework. There were no supplementary comments from the participants when asked to provide other general feedback.

#### 4.5.4. Design Refinements to The Framework

The final version of the material selection framework was created based on the feedback received from the validation study. The key changes applied include specifying the evaluation criteria and the recommended number of top candidate materials to be carried forward for each experimental stage, adding an introductory section to give some general information to the user before presenting the particular subject. Instead of relying solely on the infographics, detailed descriptions were added to explain the thermo-rheological characterisation processes, experimental procedures and evaluation criteria and the measuring and recording of results.

To improve the accuracy of the result measurements, the instructions on how to use the measuring charts were visualised in the user guide to ensure correct methods were used. Coloured areas were made on the measuring charts to specify the correct placement and alignment of the material specimen (Figure 4.24 and Figure 4.25 B). The initial label “-0” to classify an inverse curvature was replaced by the rating system R:1 to R:10 to advise if the material is acceptable or for consideration (Figure 4.25 A). But for the inverse curvature rating system, R:1 to R:2 is labelled as “acceptable” because they were not preferred results. An ideal material should recover to its original shape.

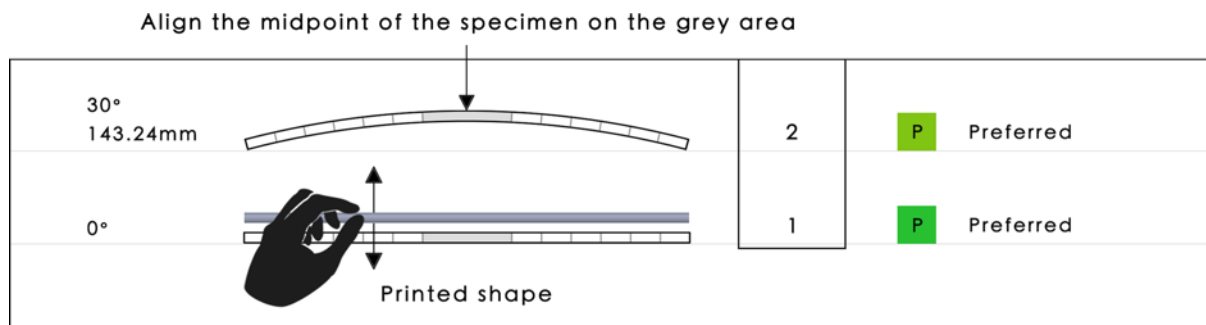


Figure 4.24. The correct placement and alignment of the material specimen on the shape fixity and shape recovery charts.

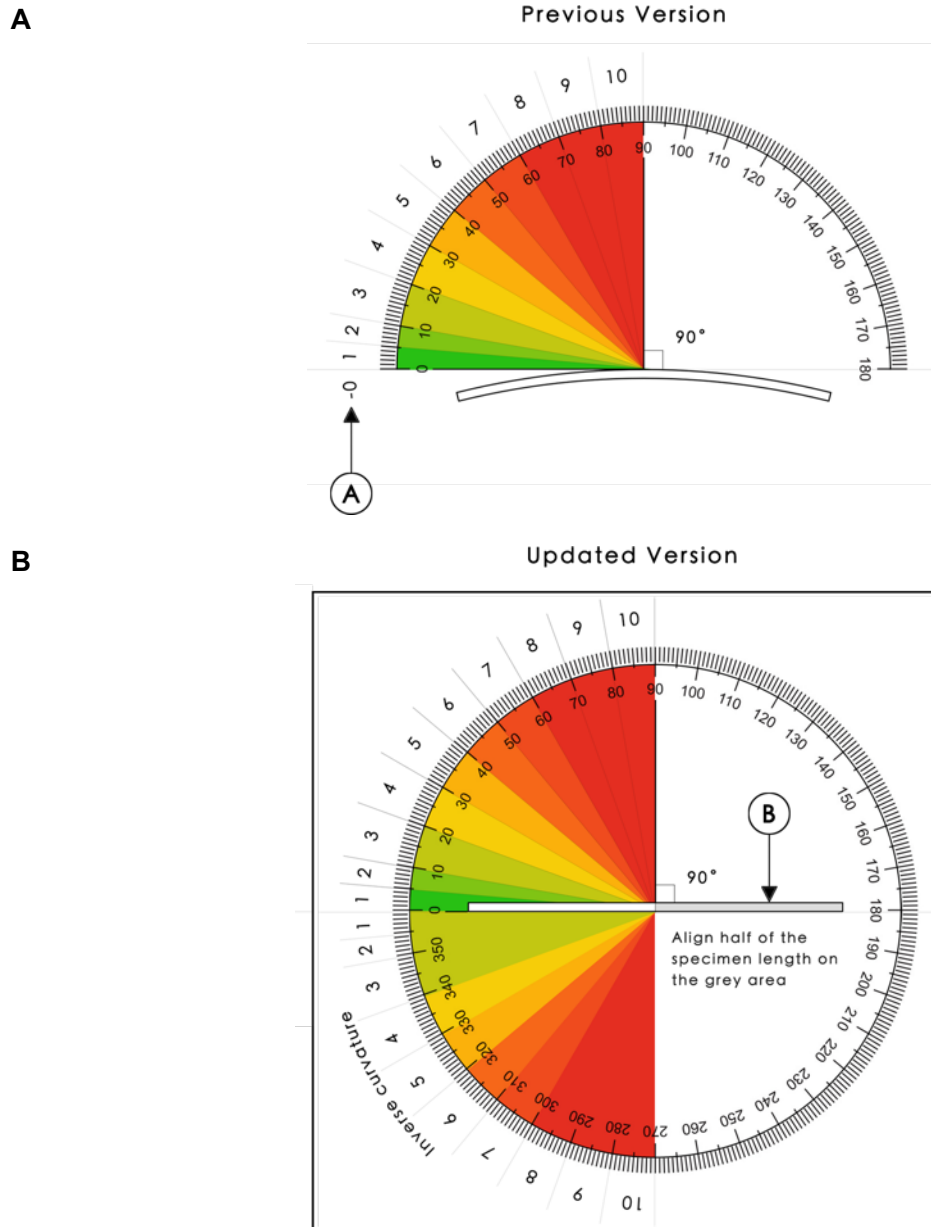


Figure 4.25. The design refinements to the fold recovery chart. (A) previous version, the initial label “-0” was modified into the rating system and (B) highlighted area was added to initiate the placement and alignment of the specimen.

#### 4.5.5. User Guide

The refined user guide consists of 14 pages as specified in Table 4.27.

Table 4.27. User guide contents.

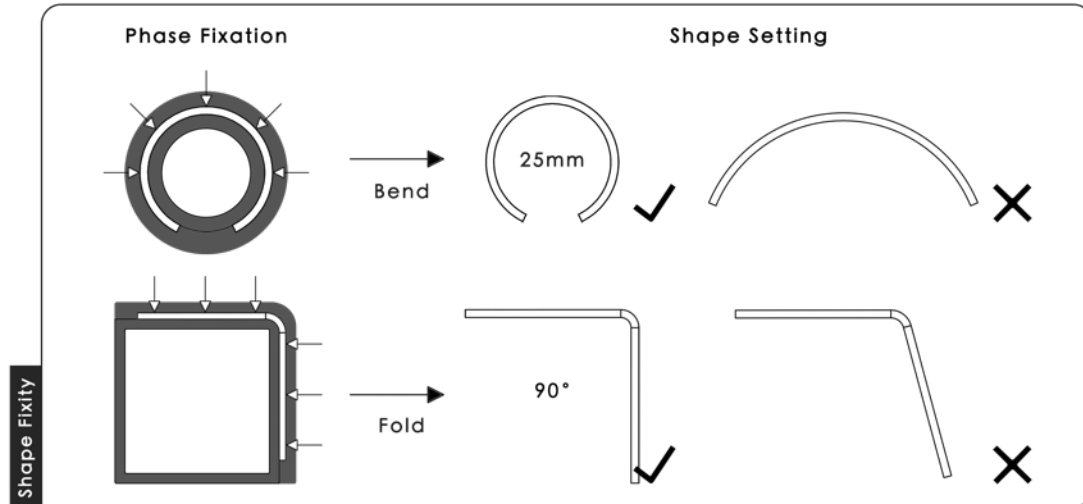
1. Introduction to The Material Selection Framework	Figure 4.26
2. Fabrication of Material Specimens, Tools and Equipment	Figure 4.27

3. Thermo-Rheological Characterisation: Process 1	Figure 4.28
4. Thermo-Rheological Characterisation: Process 2	Figure 4.29
5. The Material Selection Process Workflow	Figure 4.30
6. The Material Selection Process Flowchart	Figure 4.31
7. Experimental Procedures and Evaluation Criteria (Stage 1 and 2)	Figure 4.32
8. Experimental Procedures and Evaluation Criteria (Stage 3 and 4)	Figure 4.33
9. Measuring and Recording of Results	Figure 4.34
10. The Shape Fixity Chart (SFC)	Figure 4.7
11. The Bend Recovery Chart (BRC)	Figure 4.8
12. The Fold Recovery Chart (FRC)	Figure 4.9
13. Technical Drawing of the Circular Bend Forming Jig	Figure 4.35
14. Technical Drawing of the 90° Fold Forming Jig	Figure 4.36

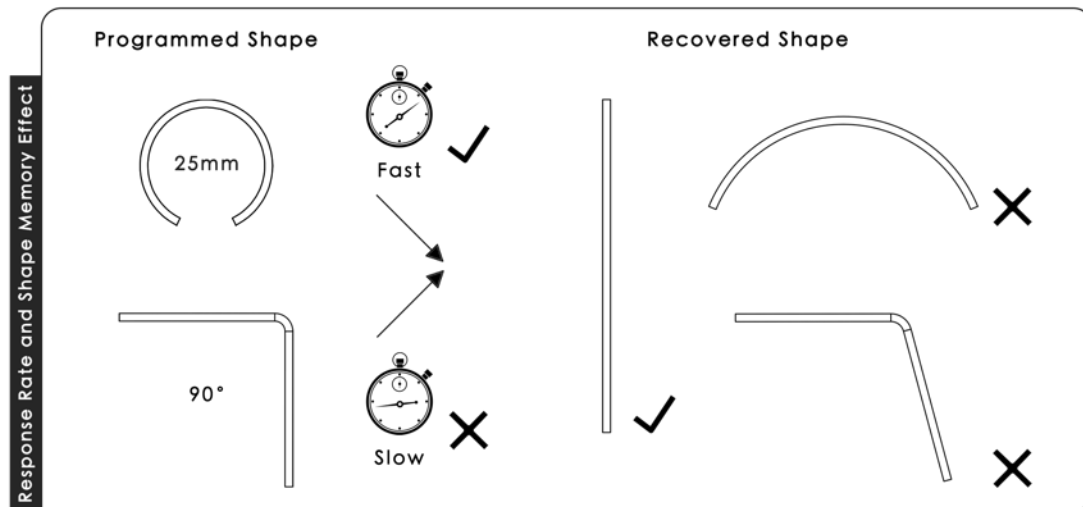
## The Material Selection Framework

This material selection framework is designed for designers to discover, define and select potential commercially available thermoplastics as Shape Memory Polymers (SMPs) for material extrusion (ME) thermo-responsive 4D Printing.

It involves a systematic explorative process to test, quantitatively define and analyse the shape fixity, response rate and shape memory effect of material through thermo-rheological characterization.



A potential material must be able to be successfully fixed at its programmed (temporary) shape.



The time taken for shape morphing activation and complete shape recovery should be fast. The material must have the ability to recover to its original (printed) shape when activated.

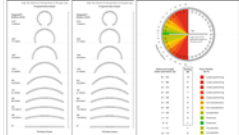
Framework	The Material Selection Framework	Page 1
G H Loh	A Framework for Selecting Thermo-Responsive Shape Memory Polymers for 4D Printing	

Figure 4.26. Introduction to the material selection framework.

## Fabrication of Material Specimens

<p><b>Phase 1</b></p> <p><b>1</b></p> <p>Filament</p> <p>75mm</p>  <p>Ø 1.75mm</p>	<p><b>Phase 2</b></p> <p><b>2</b></p> <p>ME Printed Structure</p> <p>75mm x 3mm x 1.75mm</p> <div style="display: flex; justify-content: space-around;"> <div style="text-align: center;"> <p>0°</p>  </div> <div style="text-align: center;"> <p>90°</p>  </div> </div>																		
<table border="1" style="width: 100%; border-collapse: collapse;"> <thead> <tr> <th style="text-align: left;">Print Parameters</th> <th style="text-align: left;">Settings</th> </tr> </thead> <tbody> <tr> <td>Print Quality</td> <td>0.15mm</td> </tr> <tr> <td>Fill Density</td> <td>100%</td> </tr> <tr> <td>Fill Pattern</td> <td>Rectilinear</td> </tr> <tr> <td>Fill Angle</td> <td>0°, 90°</td> </tr> <tr> <td>Extrusion Width</td> <td>0.45mm</td> </tr> <tr> <td>Nozzle Temperature</td> <td>As instructed by manufacturer</td> </tr> <tr> <td>Bed Temperature</td> <td>As instructed by manufacturer</td> </tr> <tr> <td>First Layer Speed</td> <td>20mm/s</td> </tr> </tbody> </table>		Print Parameters	Settings	Print Quality	0.15mm	Fill Density	100%	Fill Pattern	Rectilinear	Fill Angle	0°, 90°	Extrusion Width	0.45mm	Nozzle Temperature	As instructed by manufacturer	Bed Temperature	As instructed by manufacturer	First Layer Speed	20mm/s
Print Parameters	Settings																		
Print Quality	0.15mm																		
Fill Density	100%																		
Fill Pattern	Rectilinear																		
Fill Angle	0°, 90°																		
Extrusion Width	0.45mm																		
Nozzle Temperature	As instructed by manufacturer																		
Bed Temperature	As instructed by manufacturer																		
First Layer Speed	20mm/s																		

## Tools and Equipment

					
Heated water bath	Thermometer	Tweezer	Forming jigs See Page 13 · 14	Stopwatch	Measuring charts See Page 10, 11, 12

If the fabrication of forming jigs were unavailable or inaccessible, a plastic bottle with  $\pm 25\text{mm}$  neck could be used for circular bend programming, while a solid right-angle cube or table corner for 90° fold programming.

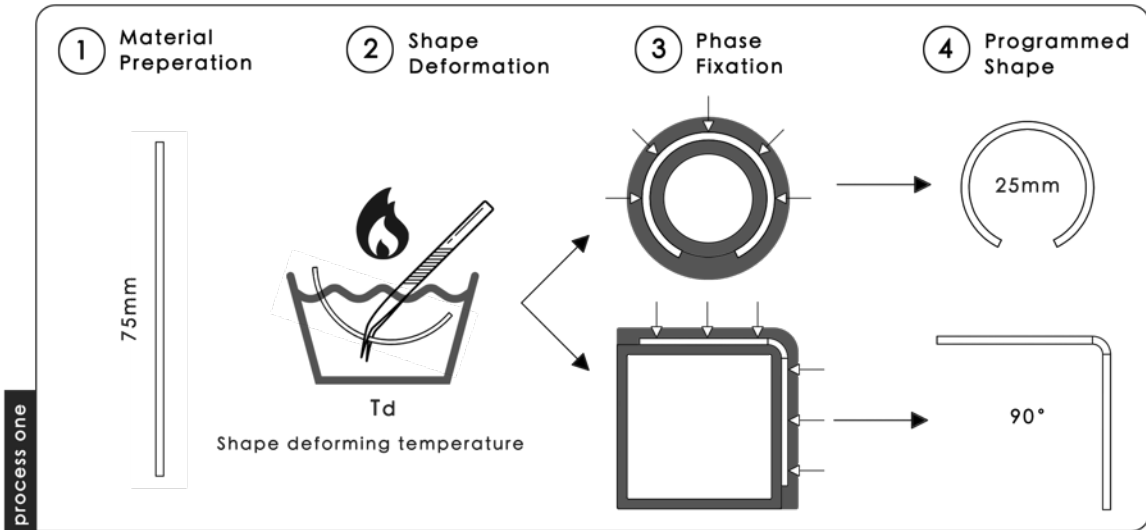
Figure 4.27. Fabrication of material specimens, tools and equipment.

Thermo-rheological characterization includes (Process 1) thermomechanical programming and (Process 2) shape recovery by submitting the material to a thermomechanical cycle.

Process

1

Thermomechanical Programming



process one

1. Prepare the material specimen according to the specified dimensions.
2. The material specimen is immersed in the heated water bath at its shape deforming temperature ( $T_d$ ) (may be equal, below or above their  $T_g$ ) for one minute\* to change the material from a glass state to a rubber state.  
  
(\*The time taken for the transition from the glass to rubber state are a recommendation. The value may differ according to the material type and characteristics).
3. The softened material specimen is removed from the water bath for shape programming (phase fixation). It is moulded immediately using the respective forming jig with applied downward force to form a 25mm diameter circular bend or a 90° fold.
4. The material specimen is unloaded from the forming jig when it has returned to its glass state. The deformed shape is the programmed shape.

Measure the degree of the programmed <i>bend</i> using The Shape Fixity Chart	See Page 10
Measure the angle of the programmed <i>fold</i> using The Fold Recovery Chart	See Page 12

Procedures	The Thermo-rheological Characterization: Process 1	Page 3
G H Loh	A Framework for Selecting Thermo-Responsive Shape Memory Polymers for 4D Printing	

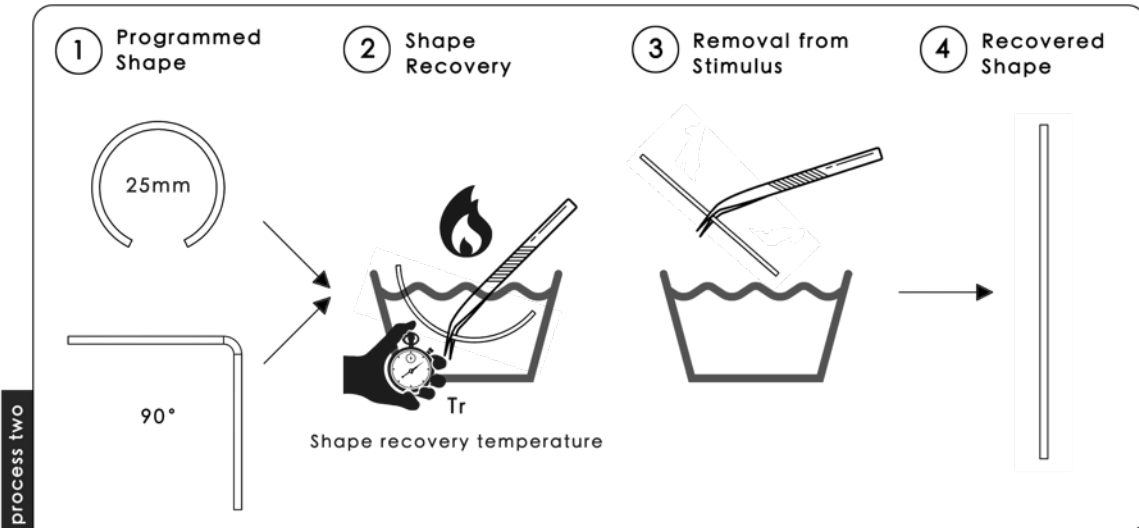
Figure 4.28. Thermo-rheological characterisation: Process 1.

Thermo-rheological characterization includes (Process 1) thermomechanical programming and (Process 2) shape recovery by submitting the material to a thermomechanical cycle.

Process

2

Shape Recovery



1. The programmed material specimen is immersed into the heated water bath at shape recovery temperature ( $T_r$ ) to release the stored strained energy to trigger shape recovery.
2. The rate of shape morphing activation ( $T_a$ ) and the duration for complete shape recovery is recorded using a stopwatch. The stopwatch is stopped when there is no further shape recovery. Alternatively, the response time can be taken through videography for more accurate results.
3. The material specimen is removed from the water bath, and the cloth is used to remove any excess water.
4. The shape recovery of the material is measured using the respective measuring chart.

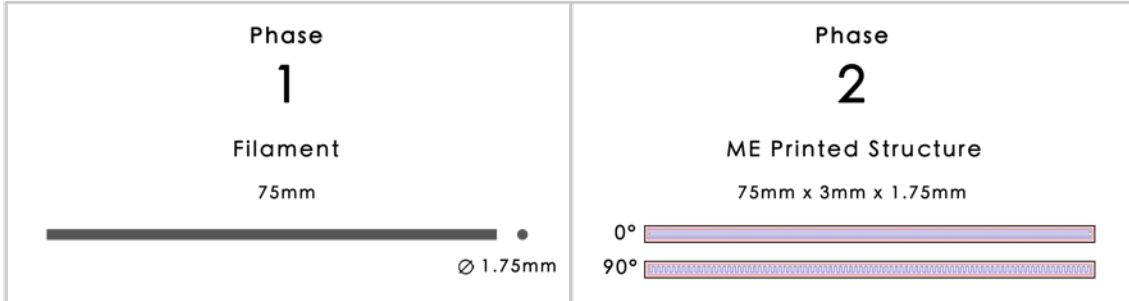
Measure the degree of the recovered <i>bend</i> using The Bend Recovery Chart	See Page 11
Measure the angle of the programmed <i>fold</i> using The Fold Recovery Chart	See Page 12

Procedures	The Thermo-rheological Characterization: Process 2	Page 4
G H Loh	A Framework for Selecting Thermo-Responsive Shape Memory Polymers for 4D Printing	

Figure 4.29. Thermo-rheological characterisation: Process 2.

## The Material Selection Process Workflow

The material selection process can be investigated from two phases, Phase 1 (P1) in the filament state and Phase 2 (P2) in ME printed structure to examine and compare the shape memory properties of SMP in different forms.



The materials would be progressively filtered through four experimental stages to determine the most potential material. The experimental stages are labelled according to their phase number and stage number.

For example, Phase 1 Stage 1 is labelled as P1 S1.

(SFC: Shape Fixity Chart; BRC: Bend Recovery Chart; FRC: Fold Recovery Chart)

Experimental Stages		Phase		No. of specimens required per test	No. of tests required per specimen	Measuring Chart
		Phase 1	Phase 2			
Stage 1	Shape Fixity	P1 S1 Shape Fixity	P2 S1 Shape Fixity	One	One	SFC <i>Bend</i> FRC <i>Fold</i>
Stage 2	Response Rate and Shape Memory Effect	P1 S2 Bending	P2 S2 Bending	One	One	BRC
		P1 S2 Folding	P2 S2 Folding	One	One	FRC
Stage 3	Response Rate and Shape Memory Effect	P1 S3 Bending	P2 S3 Bending	One	One	BRC
		P1 S3 Folding	P2 S3 Folding	One	One	FRC
Stage 4	Repeatability	P1 S4 Bending	P2 S4 Bending	One	One	BRC
		P1 S4 Folding	P2 S4 Folding	One	One	FRC

Figure 4.30. The material selection process workflow.

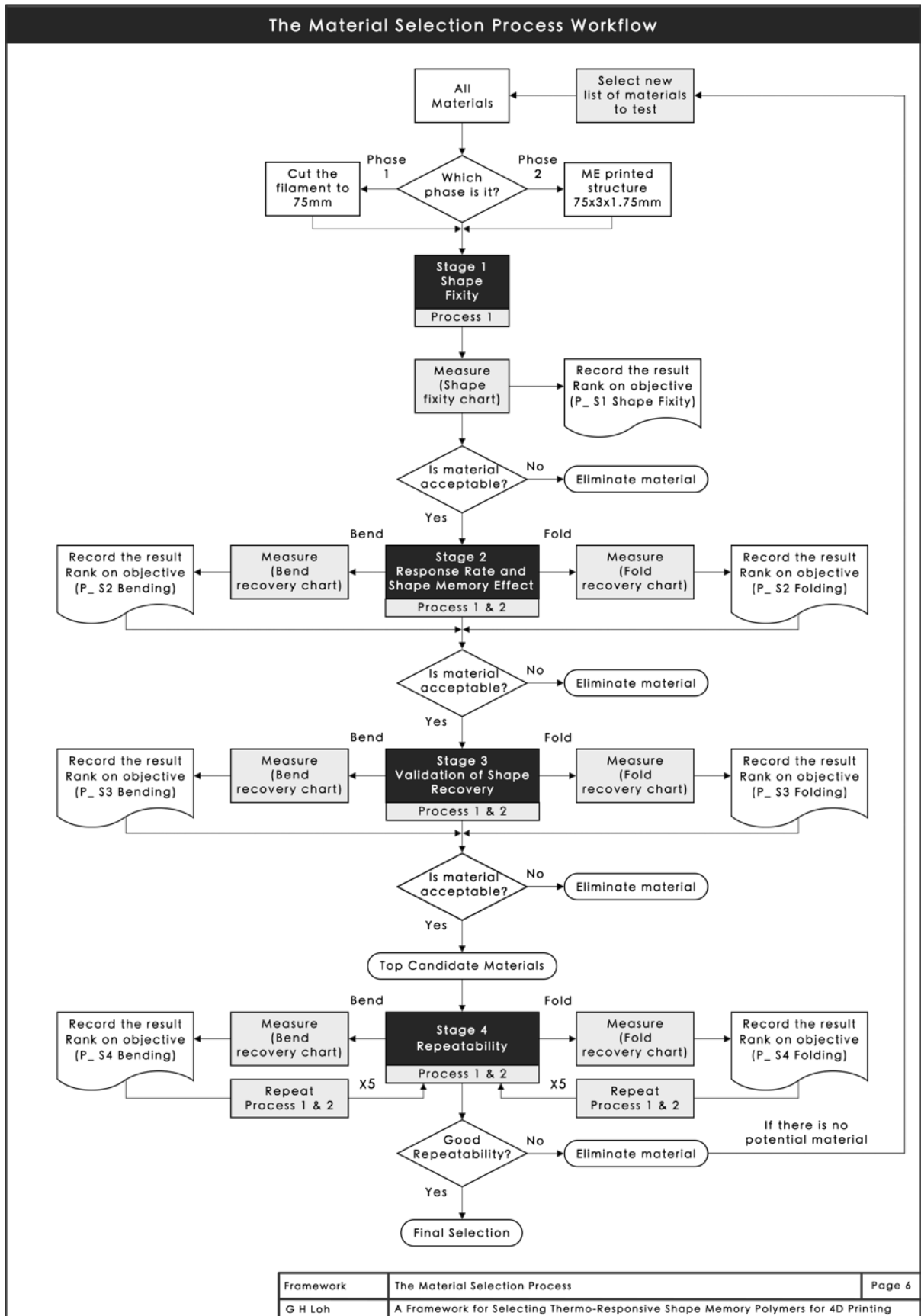
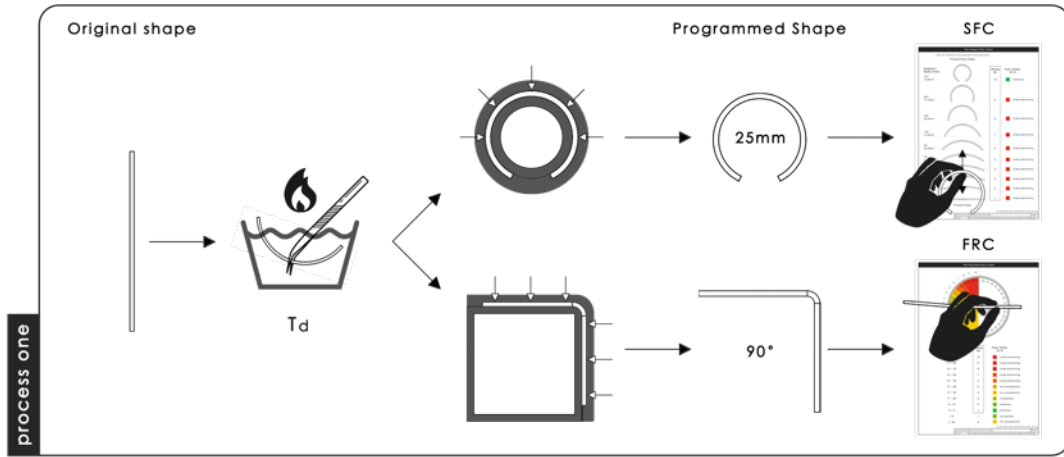


Figure 4.31. The material selection process flowchart.

### 1 Shape Fixity

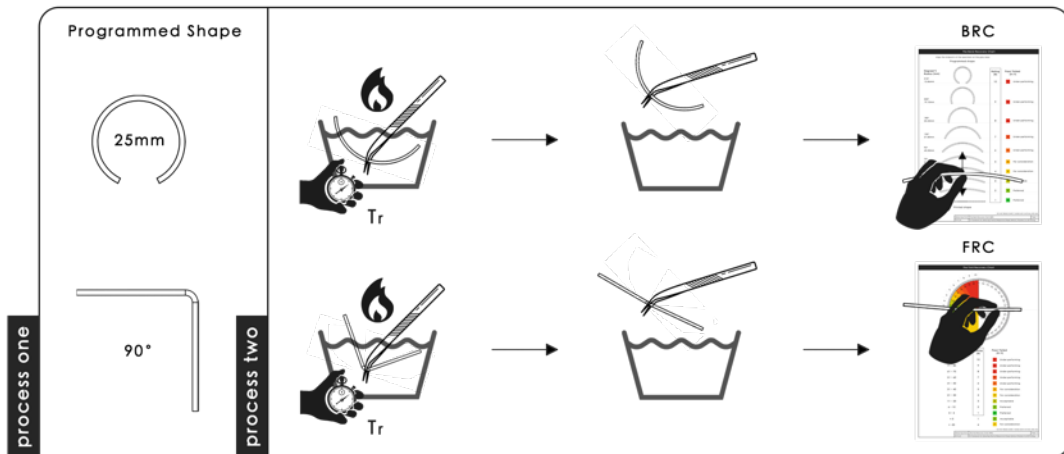
Stage 1 examines the ability of the material to be successfully fixed or retained at its programmed shape.



Only materials with shape fixity rating R:10 could be carried forward to Stage 2.

### 2 Response Rate and Shape Memory Effect

Stage 2 observes the differences in the response rate, which include the rate of shape morphing activation ( $T_a$ ) and the time taken for complete shape recovery, as well as the shape memory effect of the material when activated at different shape recovery temperatures ( $T_r$ ).



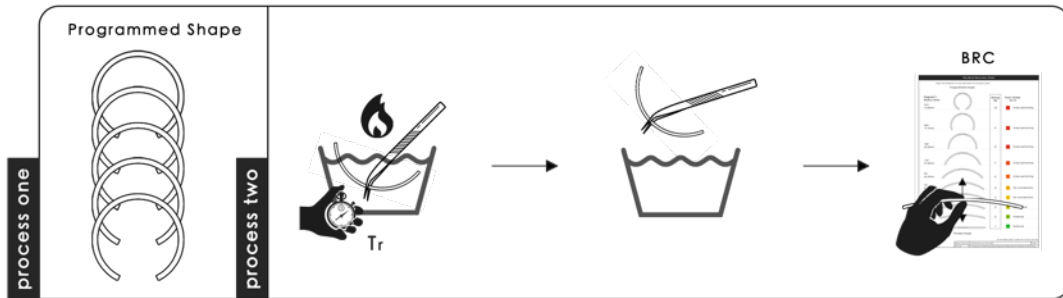
The materials would be ranked according to the sum of their shape recovery ratings across the selected optimum range of  $T_r$ . Five top candidate materials with the lowest grand total of shape recovery rating would be carried forward to Stage 3. The recovery rating of the material for each  $T_r$  should not exceed R:3 to be considered as a potential material. (For example, if three sets of  $T_r$  were tested, the sum of recovery rating of the material should not exceed nine points).

Procedures	The Experimental Procedures and Evaluation Criteria	Page 7
G H Loh	Material selection process for 4D printing through physical programming	

Figure 4.32. Experimental procedures and evaluation criteria (Stage 1 and 2).

### 3 Validation of Shape Recovery

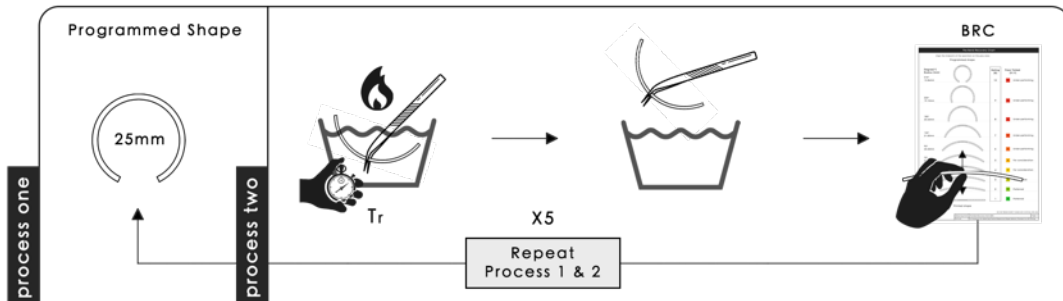
Stage 3 analyses five specimens per material to observe the consistency and calculate the average value of shape memory properties. *Five specimens* are a recommended average, although more (or less) samples could be tested by users which determines the accuracy of the results.



The materials would be ranked according to the sum of their shape recovery percentage (%) across the selected optimum range of  $T_r$ . *Three* top candidate materials with the highest grand total of shape recovery percentage would be carried forward to Stage 4.

### 4 Repeatability

Stage 4 investigates the changes in shape memory properties of the material after going through multiple shape memory cycles. *Five* memory cycles are a recommended average, although more (or less) cycles could be tested by users which determines the accuracy of the results.



The final selection material should have the highest grand total of shape recovery percentages, best repeatability and most consistent in shape recovery over consecutive shape memory cycles.

Procedures	The Experimental Procedures and Evaluation Criteria	Page 8
G H Loh	Material selection process for 4D printing through physical programming	

Figure 4.33. Experimental procedures and evaluation criteria (Stage 3 and 4).

## The Measuring Charts

Three measuring charts were designed to quantitatively measure and rate the shape fixity and recovery of the materials. Each chart has a rating system and is colour coded to suggest if the material is preferred, acceptable, for consideration or under-performing for elimination.

Types of Charts	To Measure Results From	Descriptions	Evaluation Criteria
The Shape Fixity Chart (SFC)	Process 1	To measure the ability of the material to be successfully fixed at its programmed shape from its original printed shape.	Programmed shape at R:9 or below should be reconsidered or eliminated.
The Bend Recovery Chart (BRC)	Process 2	To measure the recovered shape of the material from a bend deformation.	A potential material must be able to recover to its original shape at R:1, or within the preferred range R:2. Recovered shape above R:3 should be reconsidered or eliminated.
The Fold Recovery Chart (FRC)	Process 2	To measure the recovered shape of the material from a fold deformation.	

## Measuring and Recording of Results

### 1 Match and Align The Shape

### 2 Measurement and Record

Bend Fixity & Recovery

30°  
143mm



2	P	Preferred
1	P	Preferred

Bend Fixity & Recovery

0°



Printed shape

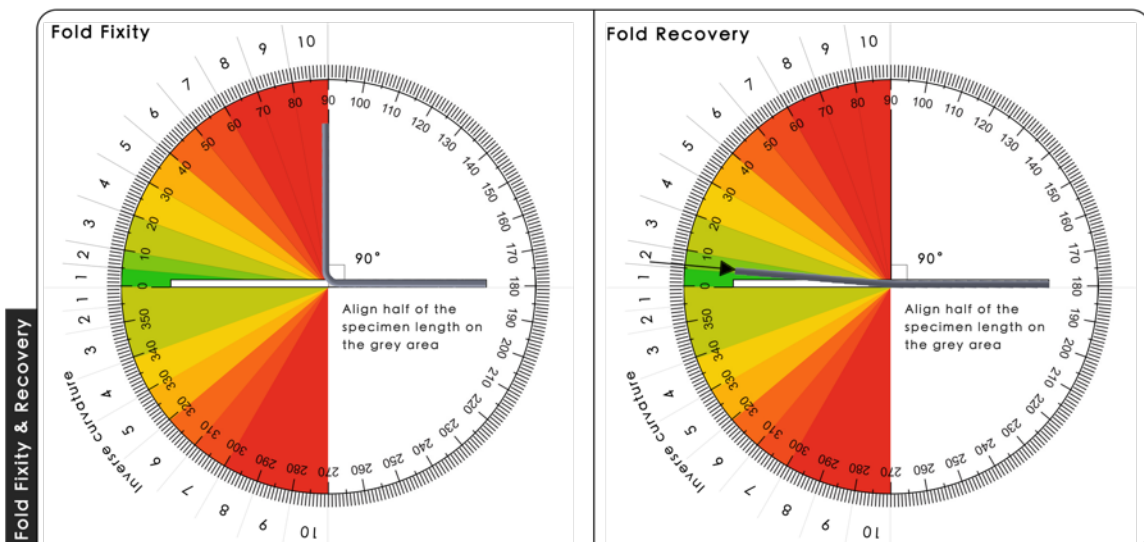
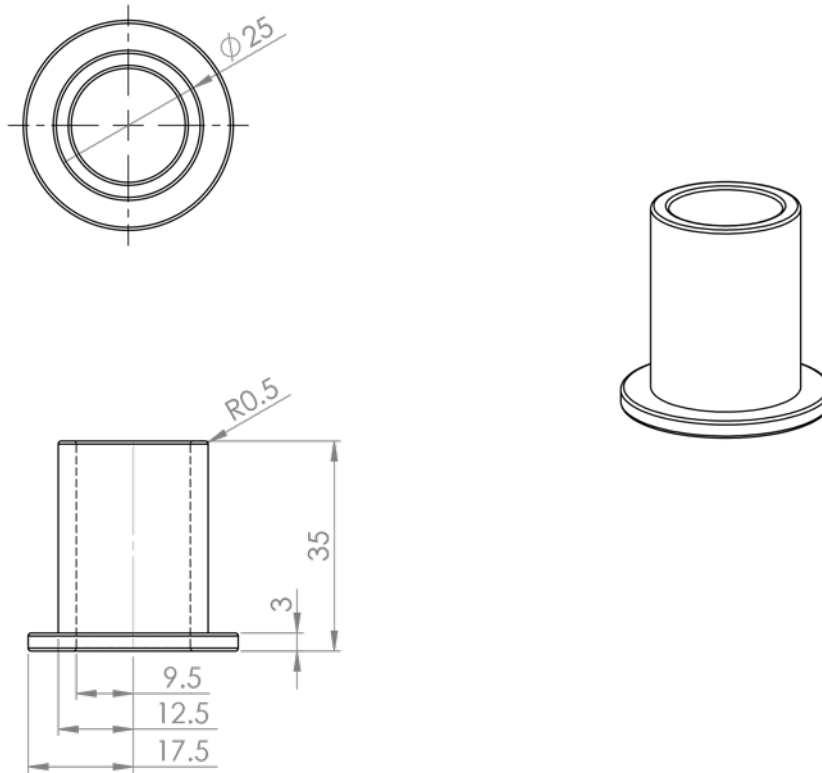
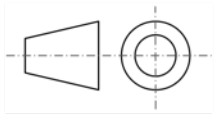


Figure 4.34. Measuring and recording of results.

## The Circular Bend Forming Jig

The forming jig to program the material specimen into a 25mm diameter circular bend.



Print Parameters	Settings	
Print Quality	0.15mm	
Fill Density	25%	
Fill Pattern	Rectilinear	
Fill Angle	45°	
Extrusion Width	0.45mm	Dimensions are in millimeters unless otherwise specified Tolerances: ±0.5mm Material Type: PETG
Nozzle Temperature	230°C	
Bed Temperature	80°C	
First Layer Speed	20mm/s	

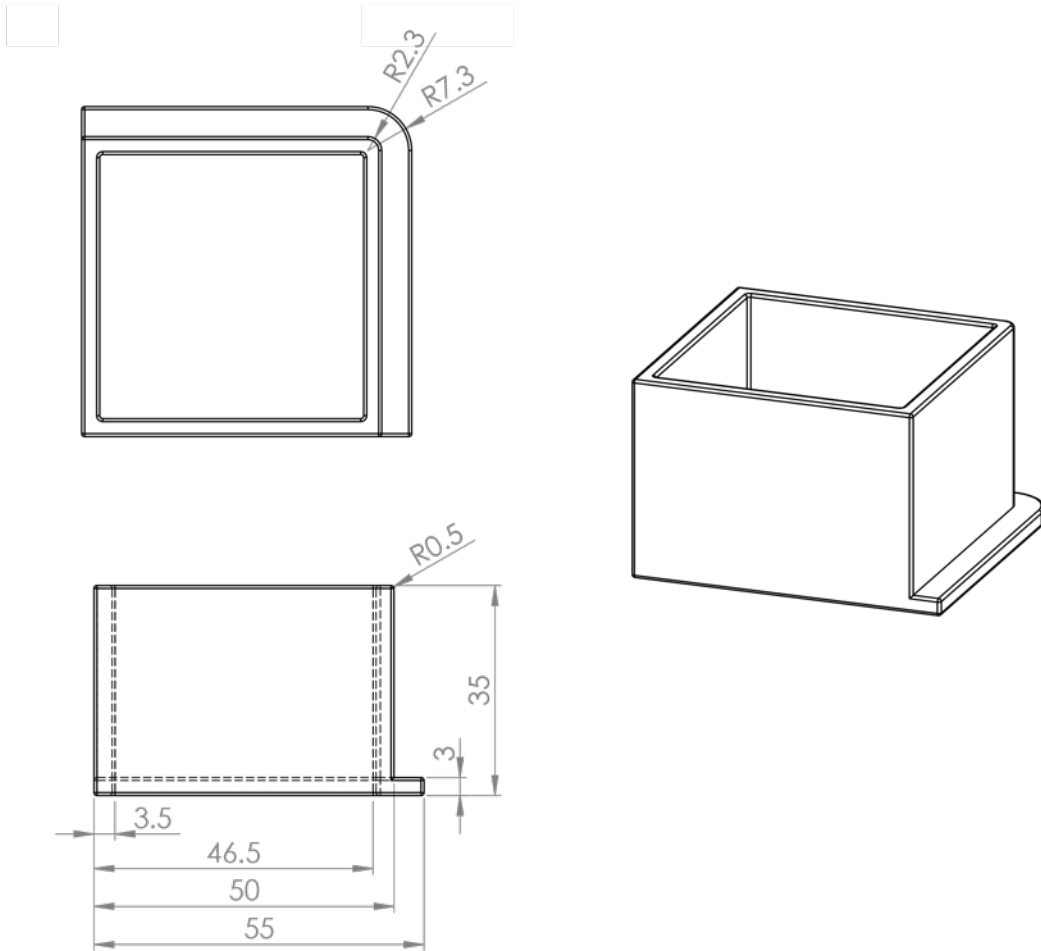
SCALE 1:1 DO NOT RESIZE CHART. PLEASE USE IN ACTUAL SIZE (A4)

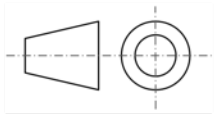
Technical Drawing	The Circular Bend Forming Jig	Page 13
G H Loh	A Framework for Selecting Thermo-Responsive Shape Memory Polymers for 4D Printing	

Figure 4.35. Technical drawing of the circular bend forming jig (not in actual size).

## The 90° Fold Forming Jig

The forming jig to program the material specimen into a 90° fold.



Print Parameters	Settings	
Print Quality	0.15mm	
Fill Density	25%	
Fill Pattern	Rectilinear	
Fill Angle	45°	
Extrusion Width	0.45mm	Dimensions are in millimeters unless otherwise specified Tolerances: ±0.5mm
Nozzle Temperature	230°C	
Bed Temperature	80°C	
First Layer Speed	20mm/s	
		Material Type: PETG

SCALE 1:1 DO NOT RESIZE CHART. PLEASE USE IN ACTUAL SIZE (A4)

Technical Drawing	The 90° Fold Forming Jig	Page 14
G H Loh	A Framework for Selecting Thermo-Responsive Shape Memory Polymers for 4D Printing	

Figure 4.36. Technical drawing of the 90° fold forming jig (not in actual size).

#### **4.5.6. Limitations of the Validation Study and the Framework**

The reliability of the framework was strengthened by conducting qualitative and quantitative research to collect feedback from doctoral researchers and experts with at least intermediate knowledge in 4DP. Despite achieving positive results from the validation, this study was not without limitations. The validation was limited to small sample size with only nine respondents. The author encountered several challenges in inviting the right participants to participate in this study owing to a limited number of experts specialised in 4DP, poor response and high refusal rate due to their tight schedule. The workshop was conducted with the doctoral researcher at Brunel University only and the number of researchers involved in 4DP were limited. A higher number of participants from different universities or backgrounds were anticipated.

Another limitation of this validation study was time constraints. The duration for conducting the one-to-one workshop was long and time consuming. Each workshop has to be organised based on the schedule of the participants. As a result, the time invested in this study has to be distributed throughout the course of a year. There was a limited timeframe for this research to ensure equal amount of time were assigned to answer the other research questions. An additional uncontrolled factor was COVID-19. No further face-to-face workshop can be conducted due to limited access of university facilities and the restrictions during the pandemic. The study was also limited by the lack of in-depth response from the participants. The overall feedback for the open-ended questions contributed by participants were very brief. It would be interesting to obtain more comprehensive insight from the participants.

The framework was presented at the 2020 Design Doctoral Symposium and AM Open Day organised by Brunel University London with nearly 80 attendees, aimed to obtain feedback from the audiences as further validation study. Unfortunately, there were no questions raised, nor feedback given by the audiences during the Q&A session.

Concerning the limitation of this material selection framework, this framework was developed mainly for material characterisation and functional elements selection. It was not a general 4DP orientated framework that informs the entire product design and development process of an active structure, covering the actuation mechanism and geometric design, modelling and simulating (Jian *et al.*, 2018). This framework was limited to quantifying one-way shape memory properties of single material SMP structure using a heated water bath for activation. This framework could be further developed to test the folding and unfolding, bending and unbending of multi-material 4DP structures. The multi-material 4DP structure

could be a combination of rigid and semi-rigid materials, two different active SMPs (i.e., PLA and PLA), or active SMP and passive material (i.e., PLA and TPU). The shape memory properties of materials were studied using specimens of fixed dimensions and ME fabricated settings. The framework aimed to be made available online in the future to increase accessibility and wider adoption by designers, practitioners, academics and students interested in 4DP. To ensure the tool and equipment were cost-effective, highly accessible for the widest uptake of this framework, the measuring charts system were employed to substitute the use of specialist equipment. As regards, measurement standard and traceability could not be fulfilled. Though, specialist measuring system for SMPs characterisation and scientific calculations for SME can always be introduced at the next stage of the investigation. The design and content of the framework will be updated according to future finding and forthcoming user feedback.

#### **4.6. Chapter Summary**

A material selection framework was developed as a tool and reference guide for designers to discover, define and select potential commercially available thermoplastics as SMPs in ME thermo-responsive 4DP. The basic theoretical knowledge and practical process workflow for the developing a single-material DSM thermo-responsive SMP structure were explained and demonstrated. The methodology to test, qualitatively measure and analyse the shape fixity, response rate and SME of the materials were introduced.

The shape memory properties of a list of commercial material filaments, predominantly PLA in filament and post printed form when activated by different shape recovery temperatures ( $T_r$ ) were investigated and analysed in this study. The results revealed that not all materials exhibit thermo-responsive SME despite belonging to the same material type. Only three out of 21 PLAs have the ability to effectively recover their original shapes from deformations without noticeable depreciation in their shape memory cycle life. The results also indicated that the shape recovery performance of SMP would vary according to the type of programming condition. Thus, the proper selection of material must be evaluated carefully upon the programming parameters and the profile of the intended application. Flexible materials in general have poor shape fixity. As a result, they are typically used as passive material to create resistance to the shortening of the active layer in the multi-material 4DP structure.

The  $T_d$  for shape fixation and  $T_r$  for shape recovery process varied according to the material type and characteristics (Loh et al., 2020). The response time reduced, while the shape recovery rating improved, as the  $T_r$  increased. The response rate in filament form and ME printed structure are closely similar. However, the shape recovery results of the materials improved significantly and were more consistent when ME manufactured. In terms of repeatability, the SME of a material in filament form depreciated faster from a bending deformation over folding deformation. In general, there was no observable deterioration in response time and SME over five consecutive shape memory cycles in the ME printed structures. The top candidate materials and final selection material suggested from Phase 1 and Phase 2 were identical. This reflected the accuracy and effectiveness of the framework. The material selection framework was tested, refined and validated by experts and doctoral researchers through workshops and semi-structured interviews to confirm its completeness, effectiveness and usability.

Further investigation involved identifying why an inverse curvature only occurred on ME printed specimens when recovered from a fold deformation. Different fold programming angles (i.e.,  $45^\circ$ ,  $145^\circ$ ) could be tested to investigate whether the angle of deformation is the main influence on this effect. Furthermore, the number of sequential shape memory cycle tests can be increased to examine the maximum shape memory cycle life of the material. This framework can be used to investigate the influences of different geometric parameters and fabrication settings such as infill patterns on the response rate and SME of the materials. The next chapter shall discuss the development and testing of polymer-textile composites using PLA filaments on synthetic mesh fabrics using direct ME.

## Chapter 5

### **Development and Testing of Material Extrusion Additive Manufactured Polymer-Textile Composites**

Chapter five presents the development and testing of polymer-textile composites using PLA filaments on synthetic mesh fabrics using direct ME. This chapter highlights the appropriate combination of printing material, textile substrate and printer settings to achieve excellent polymer-textile adhesion. Details of the printing process to create polymer-textile composites, the interfacial strength results of the T-peel tests and the observed failure modes post-testing are described. The peel strengths for different ME bonded polymer-textile composites are examined and used to identify the compatibility of materials. The polymer-textile orientation with the highest relative peel resistance is then be applied for the creation of 4D printed shape-changing thermo-responsive textiles in Chapter 6.

#### **5.1. Introduction**

The rise in the adoption of Additive Manufacturing (AM) has also led to a significant transformation of the fashion and textile industry through innovation and technology. One of the pioneers of this adoption is the influential designer, Iris Van Herpen. In 2010, she showcased her first 3D printed dress, which led to greater awareness and exploitation of the technology being employed in the fashion industry (Van Herpen, 2010). The role of AM has continually evolved with increasing awareness and interest in the technology from researchers and designers. The number of research publications on “3D Printing Textiles” has continuously increased over the past few years with over 4700 publications on Google Scholar in 2020. This figure shows that AM will potentially open up new opportunities in fashion and textile innovation, promoting localised production of on-demand and personalised garments, allowing smaller batches or home production to compete in the market. Fashion designers can utilise AM technologies to rethink and reinterpret knit, weave and prints with futuristic vision and new functionalities that cannot be achieved by the conventional textile fabric itself. The combination of digital manufacturing techniques provides the possibility for a textile to be three-dimensionally manufactured without tedious labour work, complex pattern-cutting, stitching, or the use of a specific mould. This approach also promotes a more environmentally conscious and sustainable future for materials used in the fashion industry (Van der Velden, Kuusk and Köhler, 2015; Mageean, 2018; Flynt, 2019; Kim *et al.*, 2019; Zapfl, 2019). However, the production of AM textiles is machine-

intensive which require extensive understanding of the materials, the design and modelling programs, and the printing production process.

3D printed textiles can be classified into two distinct types, (a) fully AM fabricated structure and (B) AM polymer-textile composite. Fully AM fabricated structure is solely made out of printing material. It uses shapes and patterns of “chain-link” or interlocking structures to resemble the fluidity and flexibility of cloth (Figure 5.1). On the other hand, AM polymer-textile composite involves direct printing of thermoplastics onto conventionally manufactured textile fabric substrates (Figure 5.2). The free movement and aesthetics of a traditional textile fabric can be preserved. This novel material-joining technique highlights the synergy between conventional manufacturing processes and AM process to encourage a new vision of polymer-textile functionalisation and innovative aesthetic print techniques in the textile industry.

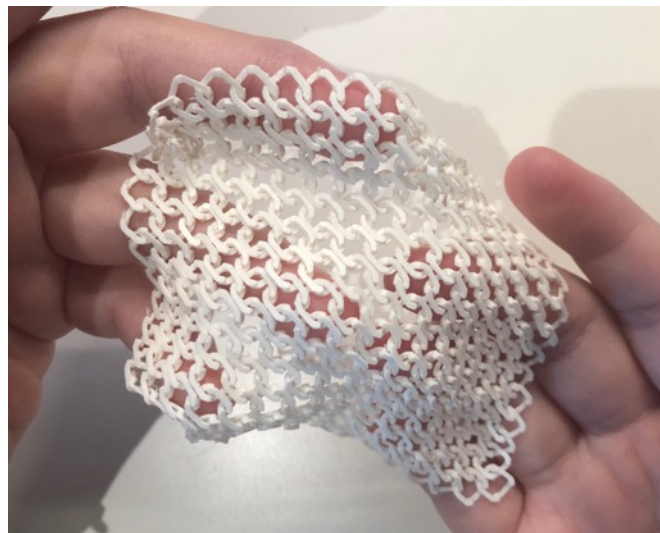


Figure 5.1. Fully AM fabricated structure.

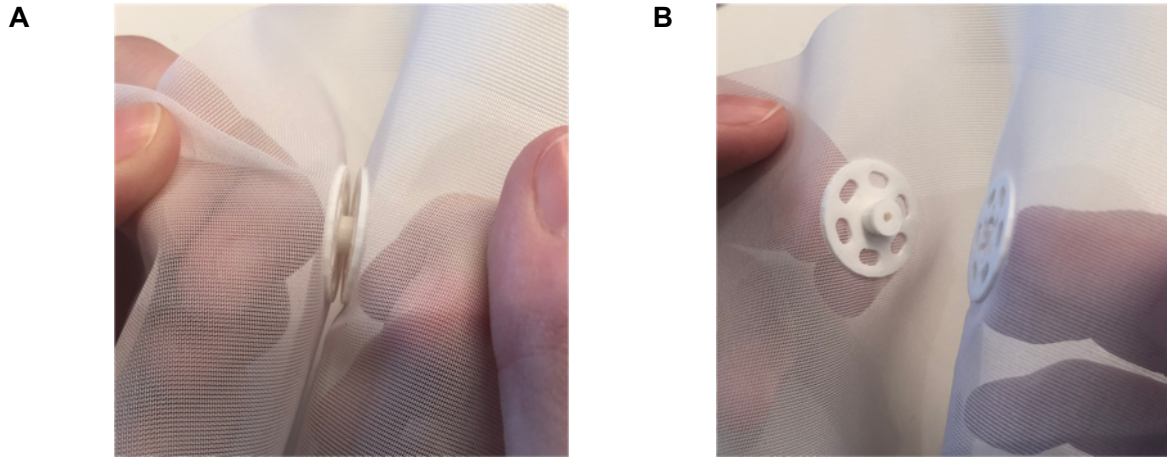


Figure 5.2. AM polymer-textile composite snap fastener demonstration. (A) secured and (B) open.

This research focuses on the development and testing of material extrusion (ME) additive manufactured polymer-textile composites. This study can provide helpful information for designers and researchers to develop new applications and facilitate future research development in textile design (Table 5.1). Novel AM strategy such as Functionally Graded Additive Manufacturing (FGAM) with the integration of digital materials using PolyJet technology can offer sophisticated localised graded colours and different properties on a single piece of textile by varying the material organisation at a precisely defined area (Oxman, 2011; Bader *et al.*, 2016; Loh *et al.*, 2018). New materials such as shape-memory materials can be used to create programmable or stimulus-responsive textiles that can transform or morph from one form to another when subjected to an external stimulus, known as 4D Printing (Leist *et al.*, 2017; Pei and Loh, 2018b).

This chapter discusses three key interconnected factors (i.e., printing material, textile substrate and printer settings) affecting the production and overall quality of the polymer-textile composites. It also gives details of the design process, manufacturing process, as well as the experimental setup, procedures and analysis techniques used to quantify the adhesion properties for different orientations of bonded ME printed polymer-textile composites. An objective of this study is to identify the effect of varying textile substrate parameters (i.e., different fibre types, structure, and weights) on the polymer-textile adhesion force. The printing material and ME printing parameters were kept constant. Different combinations of ME printed polymer-textile composites using PLA (printing material), Nylon and Polyester (textile substrates) were manufactured to evaluate their manufacturing feasibility and assess their mechanical properties. The manufacturing demonstration and experimental results add to the current limited knowledge of developing and testing of ME

printed polymer-textile, which provides useful information for designers and researchers to facilitate further research and increased uptake towards industry-wide applications.

Table 5.1. Examples of applications and future research direction for ME polymer-textile composite.

Development	Application	Brand/ Subject	Description	Ref
Product	Wearables	LabeledBy; Tamicare	Personalised, localised, and sustainable garments and fabrics.	(Labeledby, 2020; Lopez, 2020; Tamicare, 2020)
	Mounting or Embossing Elements	Braille on textiles	Modifications of textile surface properties to support blind people.	(Kreikebaum <i>et al.</i> , 2017)
	Orthopaedic devices	Glove; Knee Brace	Customised orthopaedic devices.	(Uysal and Stubbs, 2019; Ahrendt and Karam, 2020)
Research	Programmable or stimulus-responsive textiles	Hybrid Textiles	Polymer – elastic textiles composite: The elastic textile is pre-stretched prior to printing, the stored energy in the textile material prior to printing causes a change in form when the energy is released.	(Papakonstantinou, 2015; Narula <i>et al.</i> , 2018)
		Shape change and self-assembly	Stimulus-responsive polymer – textile composite: Stimulus-responsive textiles that can self-transform or morph from one form to another when subject to an external stimulus.	(Leist <i>et al.</i> , 2017; Momeni <i>et al.</i> , 2017; Zapfl, 2019)
	Textile-based sensors or electronics	Self-sensing or actuator	Conductive materials or biohybrid materials – textile composite: Sensing body and sensing element.	(BioLogic, 2015; Gehrke <i>et al.</i> , 2019; Kumar, Chen and Ren, 2019)

## 5.2. Factors affecting ME Printed Polymer-Textile Composites

ME as a category of AM process described in ISO-ASTM 52900 (ISO/ASTM 52900, 2017), often known as “Fused Deposition Modelling (FDM)” and “Fused Filament Fabrication (FFF)” is the predominant method of manufacturing polymer-textile composites (Chatterjee and Ghosh, 2020). The AM process involves the material from a spool of filament loaded into the printer, melted above its glass transition temperature ( $T_g$ ) for amorphous polymers and above its melt temperature ( $T_m$ ) for semi-crystalline polymers. The polymer is then selectively dispensed through the heated extrusion nozzle and deposited onto the build platform at a predetermined location (Redwood, Schöffner and Garret, 2017; Loh et al., 2020). This technology of additively building up material by selectively dispensing through a nozzle or orifice allows AM parts to be built directly on the surface of the textile substrate. Sanatgar et al. (2017) described it as a thermal welding method for joining of the printing material (adhesive) and the textile substrate (adherent) during the ME process (see Figure 5.3).

There are three major interconnected factors that affect the fabrication, polymer-textile adhesion and the overall quality of ME polymer-textile composites reported in the literature by Melnikova, Ehrmann and Finsterbusch (2014), Pei, Shen and Watling (2015), Loh and Pei, (2019) and Sanatgar, Campagne and Nierstrasz (2017).

- (a) Printing material,
- (b) Textile substrate, and
- (c) Printer settings.

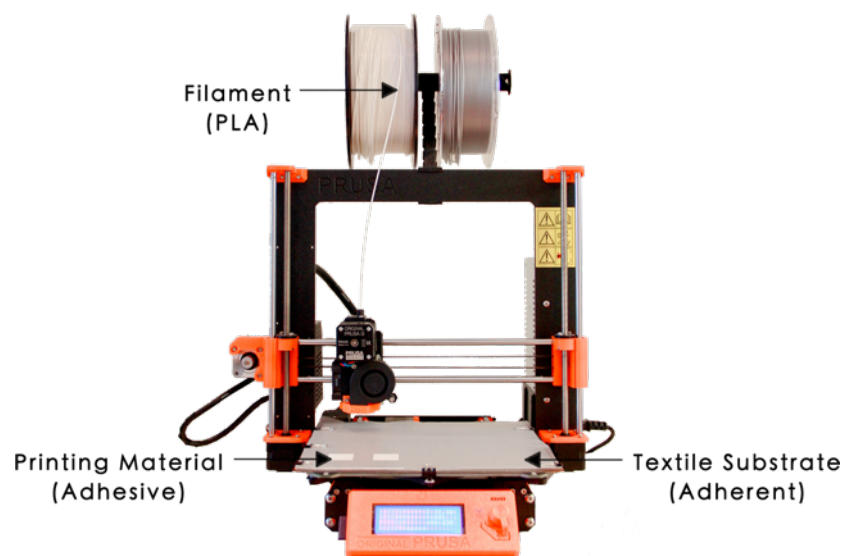


Figure 5.3. Desktop ME printer (Original Prusa i3 MK3S 3D Printer) setup for ME onto the textile substrate.

### 5.2.1. Printing Material

ME makes use of thermoplastics in the form of filaments, which are typically 1.75 mm or 3 mm in diameter (Redwood, Schöffner and Garret, 2017). ME processes allow a wide variety of materials with diverse characteristics and properties to be used, ranging from commodities, engineering, to high-performance thermoplastics, composites and functional materials (Loh *et al.*, 2020). Table 5.2 presents some of the common thermoplastics used in ME, their key material characteristics, cost as well as their printing parameters including the nozzle and build platform temperature. The printing temperature, performance and cost of the materials increase through each material category from PLA to Polyetherimide (PEI) (Redwood, Schöffner and Garret, 2017; Rigid.Ink, 2019). According to Redwood, Schöffner and Garret (2017), the better the engineering properties of thermoplastics, the higher the temperature required to heat the material to a deformable state and therefore, the more difficult the material is to print. This suggests that the use of materials with lower printing temperature is recommended to avoid damaging or burning the textile substrate during direct deposition of the polymer.

Table 5.2. Common thermoplastics used in ME and their properties.

Material Type	Filament Material	Material Characteristics	Cost (£/KG)	Nozzle Temperature (°C)	Build Platform Temperature (°C)	Ref
Commodity	PLA	Biopolymer, lower impact strength and temperature resistance.	32	180 – 210	20 – 45	(Rigid.Ink, 2019; Tyson, 2020c)
	PLA Plus+	Very durable biopolymer, vibration absorbing and less brittle version of PLA.	37	220 – 230	50 – 60	(Rigid.Ink, 2019; Gregurić, 2020)
	Flexible PLA	Flexible and durable biopolymer, good vibration dampening.	37	240 – 250	30 – 60	(Griffin, 2019; Rigid.Ink, 2019)
	ABS	Strong and durable, good temperature resistance but susceptible to warping.	32	230 – 250	90 – 95	(Rigid.Ink, 2019; Tyson, 2020e)
Engineering	PETG	Extremely durable, high impact and chemical resistance, low shrinkage.	40	220 – 245	70 – 80	(Rigid.Ink, 2019; Tyson, 2020b)
	TPU	Flexible and rubber-like, stretchy properties with good elongation but difficult to print accurately.	49	210 – 240	20 – 70	(Rigid.Ink, 2019; Tyson, 2020d)
	Nylon (PA 12)	Extremely durable, flexible, low friction for high impact and high stress prints.	38	255 – 275	100 – 110	(Rigid.Ink, 2019; Tyson, 2020a)
High performance	PEI	Excellent strength to weight, fire, and chemical resistance.	250	355 – 390	120 – 160	(3D4Makers, 2020)

## 5.2.2. Textile Substrate

Table 5.3 describes the variables of the textile substrates that affect the polymer-textile adhesion of ME printed polymer-textile composites. These properties include, but not limited to, the types of fibres, fabric weight, weave pattern, weft density and surface properties. These variables determine the type of print structure layout appropriate for the chosen textile substrate proposed in Table 5.4.

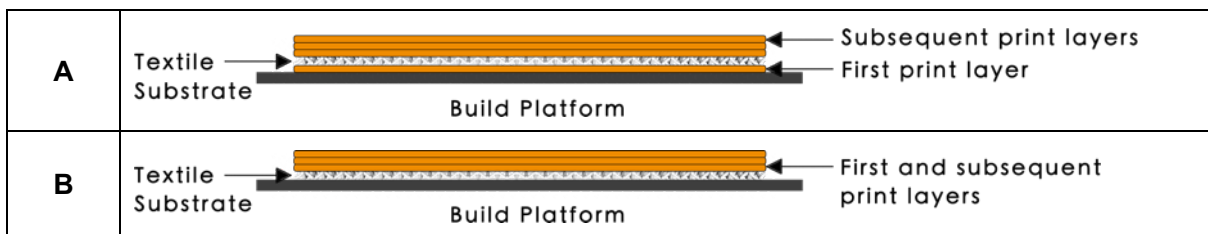
Table 5.3. Different variables of textile substrates that can affect the polymer-textile adhesion.

Textile Substrate Properties and Structure	List of Variables	Options	Characteristics or Descriptions	Ref
Fibre Types	Plant	Cotton	Cool, soft and comfortable; absorbs and releases respiration quickly; durable but wrinkles easily.	(Elliot, 2015; Pei, Shen and Watling, 2015; Korger <i>et al.</i> , 2016; Mpofu <i>et al.</i> , 2019)
		Linen	Woven from the stems of flax; two-times stronger than cotton; absorbs and releases perspiration quickly; lightweight; non-stretchable and wrinkles easily.	
	Animal	Wool	Ranges from scratchy to very soft; absorbs 30% of its weight in moisture; absorbs and releases moisture quickly; dirt and flame resistant; stronger when dry; performs as an insulator.	
		Silk	Versatile, soft and comfortable; strongest natural fibre; absorbs and releases perspiration quickly; easily dyed; retains shape and drapes well but weakened by sunlight and perspiration.	
	Synthetic	Rayon	Strong; extremely absorbent; soft and comfortable; made in a variety of qualities and weights but wrinkles easily.	
		Acetate	Crisp and soft; suitable for dyes and prints; shrink, moth and mildew resistant; low moisture absorbency and fast drying.	
		Nylon	Strong, lightweight, stretchable and durable; dries quickly; easy to clean;	

			resistant to abrasion and chemicals; does not absorb moisture well.	
		Acrylic	Lightweight, soft and warm; dyes to bright colours; absorbs and releases moisture quickly; retain shape and resists shrinkage and wrinkles; hold pleats; resistant to moths, oils and chemical, and sunlight degradation.	
		Polyester	Strong, stretchable, and durable; does not wrinkle; dries quickly; does not absorb moisture.	
Weight	Denier	Low denier count	Denier is a method for measuring the fineness of fibres, defined by the mass in grams per one strand of 9000m fibre. High denier count fabrics tend to be thick, sturdy, and durable while low denier count fabrics tend to be sheer, soft, and silky.	(Hindman, 2013a; Standard Fiber, 2020)
		High denier count		
	Stitch density	Low stitch density	Stitch density is a measurement of the number of stitches per inch (SPI) of fabric as it passes from the entrance of a needle loom to the exit.	(Hindman, 2013b)
		High stitch density		
	Weft density	Low weft density	Warp and weft are the two basic components used in weaving to turn thread or yarn into fabric. The adhesion force decreases when weft density increase.	(Malengier <i>et al.</i> , 2017; Narula <i>et al.</i> , 2018; Mpofu <i>et al.</i> , 2019, 2020)
		High weft density		
	Warp linear density	Low warp linear density	The adhesion force increases when the linear density increase.	
		High warp linear density		
	Pore properties	Fine	The pore properties include the pore size, pore size distribution, pore shape, and porosity determined by the fibre properties and structural properties, such as setting and weave type.	(Ragab <i>et al.</i> , 2017; Eutionnat-Diffo <i>et al.</i> , 2019)
		Large		
Surface	Finish	Mechanical	Squished, Circe' finish, brushed or knapped.	(Korger <i>et al.</i> , 2016; Unger <i>et al.</i> , 2018; Meyer,
		Chemical	Polymer coating (i.e., PMMA coating), plasma treatment.	

		Washing	Washing agent, enzyme amylase.	Döpke and Ehrmann, 2019)
	Texture	Surface appearance	Texture is defined by the surface appearance, structure, and thickness of the fabric. Texture is created by the fibre type, by weaving or knitting process, or by fabric finishes. Examples of textures include fuzzy, furry, soft, shiny, dull, bulky, rough, crisp, smooth, and sheer.	(Sew Guide, 2020)
		Structure		
		Thickness		

Table 5.4. Types of print layout. (A) polymer – textile substrate – polymer and (B) polymer – textile substrate.



Print layout A involves embedding the textile substrate between two print layers to form a laminated composite, while print layout B involves a one-sided print, deposited directly on the textile substrate. Preliminary tests were carried out to investigate the adhesion force of deposited polymer on selected textile substrates to select the appropriate print layout. The results for print layout A showed good diffusion between two subsequent polymeric layers. In contrast, the printed component using print layout B can be peeled off easily from both net and voile textile substrates using a small amount of manual force (Figure 5.4). Agreeing with Meyer, Döpke and Ehrmann (2019), print layout A is suitable for printing on “open” mesh or perforated textile substrates, whereas print layout B is suitable for “closed” tightly woven textile substrates, as revealed by (Pei, Shen and Watling, 2015).

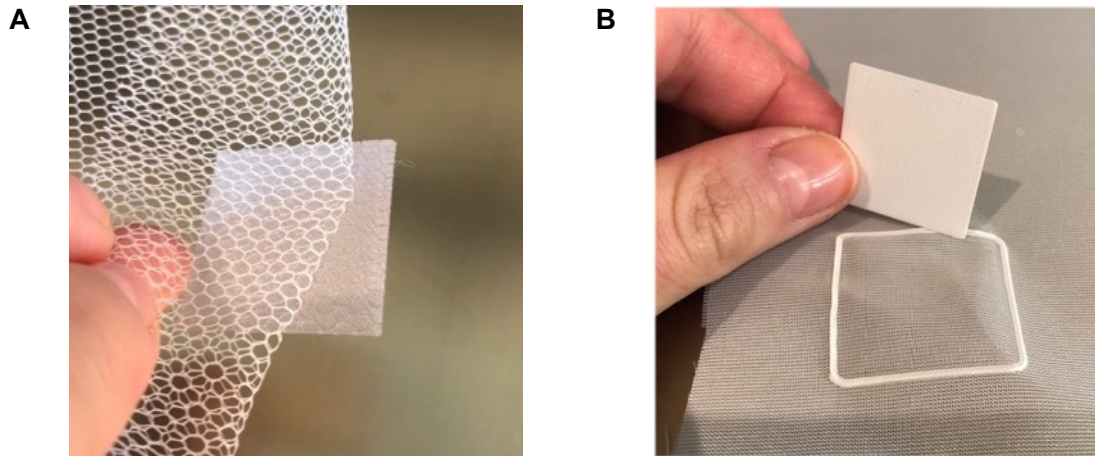


Figure 5.4. Print layout B. (A) PLA printed on net textile substrate and (B) PLA printed on voile textile substrate.

### 5.2.3. Printer Settings

Desktop Cartesian ME printer uses a system of X-Y-Z coordinates to determine the location of the extrusion nozzle, which allows direct ME onto the textile substrate. The setup is shown in Figure 5.3 using an Original Prusa i3 MK3S ME machine with a single extruder. ME machines with multiple extruders can be used to create multi-material AM components, achieved by swapping the filament materials at a predetermined location or between layer changes.

Table 5.5 identifies some of the ME processing parameters taken into consideration and the settings used during the fabrication of polymer-textile composites. These results are based on preliminary tests and literature review. The processing parameters include the Z-distances, printing temperature (Table 5.2), layer height, printing speed, fill settings, extrusion width, flow rate as well as build platform surface. The printer settings have a great impact on the visual and haptic finishing of the printed structure (Pei, Shen and Watling, 2015). The Z-distance has a significant effect on the adhesion of polymers to the textile substrate and quality of the print. An increment in Z-distance (build platform to extrusion nozzle adding fabric thickness) must be applied while printing on mid-weight to heavy-weight or textured textile substrate to compensate the fabric thickness. An optimum Z-distance adjustment should prevent the extruder nozzle from getting caught on the fabric but close enough to press the extruded polymer into the textile substrate with no gaps between deposited parameters. Table 5.6 illustrates several scenarios that may indicate the Z-distance was set too high, including print with sparse infill and visible gaps between perimeters, filament dragging, or the print being caught on the nozzle when being lifted. In

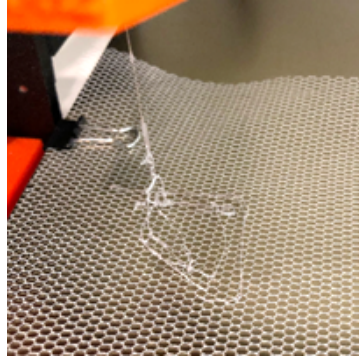
line with an optimum Z – Distance between the nozzle and the build platform used, 0.1mm and 0.2mm layer height can usually provide a good linear surface finishing with no scars on the top surface, messy first layer or gaps between infill and outline (Loh et al., 2020). A layer height greater than 0.2mm exhibited a negative effect on dimensional accuracy and adhesion force (Spahiu *et al.*, 2017). The printing temperature and printing speed have the largest effect on the adhesion force (Sanatgar, Campagne and Nierstrasz, 2017). High nozzle temperature can reduce the material viscosity, allowing deeper and stronger material penetration into the textile substrate (Spahiu *et al.*, 2017). For printing taller or larger components, the nozzle temperature can be adjusted back to the suggested temperature after five print layers on top of embedded textile to prevent overheating. Although Sanatgar et al. (2017) claimed that the build platform temperature does not affect the adhesion force, an optimum build platform temperature can provide a better first layer adhesion to build platform and prevent warping. The extrusion width should be set at 100% or 150% greater than the default nozzle diameter (> 0.4mm) in order to generate enough material to penetrate into the textile fabric (Spahiu *et al.*, 2017). The study by Spahiu et al. (2017) also revealed that increasing the printing speed and polymer flow rate showed no substantial effect on the polymer-textile adhesion.

Table 5.5. The list of ME printer settings taken into consideration during the fabrication of the polymer-textile composites.

<b>Printer Parameters</b>	<b>List of Variables</b>	<b>Settings or Suggestions</b>	<b>Ref</b>
Z – Distance	Build platform to extrusion nozzle	Calibrate the optimum Z–height through first layer calibration.	(Grimmelsmann <i>et al.</i> , 2018; Prusa3D, 2018)
	Build platform to extrusion nozzle <i>adding</i> fabric thickness	Multiple first layer calibration and preliminary printing tests results given that the optimum Z–height increment is by adding halved of the fabric thickness. (i.e., increment between +0.05mm to +0.07mm for fabric thickness of 0.15mm). This is applicable when using mid-weight to heavy-weight and textured textile substrates.	(Sanatgar, Campagne and Nierstrasz, 2017; Spahiu <i>et al.</i> , 2017)
Printing Temperature	Nozzle temperature	Increase 5°C to 10°C on top of suggested temperature by manufacturer.	
	Build platform temperature	As suggested by manufacturer.	

Layer Height	First layer	0.2mm	
	Subsequent layer	0.1mm	
Printing Speed	First layer	20mm/s	
	Perimeters	45mm/s	
Fill	Pattern	Rectilinear	
	Angle	0°; Solid infill threshold area 90°	
	Density	100%	
Extrusion Width (Nozzle diameter: 0.4mm)	First layer	0.42mm	
	Subsequent layer	0.45mm	
Flow Rate	N/A	100%	
Surface	Build platform	PEI Sheet, Blue Painter's Tape, Build Tak, Flex Plate, Magigoo or Heated Glass.	(Loh <i>et al.</i> , 2020)

Table 5.6. Scenarios that indicate the Z-distance was set too high.

		
Sparse bottom fill, gaps between infill and perimeters.	Poor adhesion of the layer causing the dragging of filament.	The print stuck on the nozzle when being lifted.

### 5.3. Methods

#### 5.3.1. Materials and AM Process

This work explains the procedure of direct ME off-the-shelf PLA on selected mesh fabrics using print layout A. Three different combinations of Polymer – Textile – Polymer composites were produced as shown below:

- (a) PLA – Nylon (net structure) – PLA,
- (b) PLA – Polyester (voile structure) – PLA, and
- (c) PLA – Nylon (voile structure) – PLA.

The printing material was Prusa PLA filament with a diameter of 1.75 mm. PLA is cost-effective and relatively easier to print at a lower nozzle and build platform temperature, without burning the textile substrates. This is because PLA has a melting point of 260 to 270°C (Callister and Rethwisch, 2018). It has relatively low warping and stringing properties, leading to high detail finishing and better overall aesthetical quality (Tyson, 2020c). The three different types of textiles substrates used were namely Nylon (net structure), Polyester (voile structure) and Nylon (voile structure). Table 5.7 lists the properties of the three lightweight mesh fabrics. The woven Polyester (F2) and Nylon voile (F3) shared relatively similar properties, comprising fabric thicknesses, non-stretch properties, fine pore sizes with smooth and sheer surface texture. On the other hand, the knitted Nylon net fabric (F1) had larger thicknesses (almost double), stretchable horizontally, relatively larger pore sizes of approximately 2 x 1.5 mm with rough surface texture. The three textile substrates have the same melting point between 260°C to 270°C, adapted from Callister & Rethwisch (2018).

Table 5.7. Properties of the three textile substrates (mesh fabrics) used for the ME polymer-textile composites.

Fabric No.	Name	Structure	Process	Thickness (mm)	Pore Size	Stretch
F1	Nylon	Net	Knitted	0.25	Large	One-directional (horizontally)
F2	Polyester	Voile	Woven	0.13	Fine	Non-stretch
F3	Nylon	Voile	Woven	0.14	Fine	Non-stretch

Adhesion affects the durability and quality of the final product (i.e., polymer-textile composite). Therefore, it was deemed appropriate to investigate the mechanical properties of the bonded ME polymer-textile composites, to determine the optimum printing material and textile substrate combination and orientation. The T-Peel test was chosen as it is the most suitable adhesion test method to determine the relative peel resistance of adhesive bonds between thin flexible-to-flexible assemblies. The similar test method was demonstrated in several published journal articles by Narula *et al.* (2018), Sanatgar, Campagne and Nierstrasz (2017) and Spahiu *et al.* (2017) but all of their works only focused on the adhesion test of a single-sided deposited polymer layer on the textile substrate (Print layout B). A previous study by Sabantina *et al.* (2015) has conducted a separation test conducted on polymer – textile – polymer composites (print layout A) using similar standard ISO DIN 53530. However, the experiment did not provide any evidence on the adhesives design tool kits. The design process, types of joint used and the specimen dimension were not explained. Furthermore, another source of uncertainty is that the printed test samples shown appeared to be different and not designed according to the referenced standard BS EN ISO 11339 (2010).

For this study, the ME polymer-textile composites designed for the T-Peel test were in line with British Standards (BS) EN ISO 11339 (2010) (Figure 5.5). To manufacture the polymer-textile composites using ME, the CAD design of the printed structure (L x W x H of 200mm x 150mm x 0.5mm) was created using SolidWorks, exported as an STL file, imported into Slic3r for slicing and exported as a G-code for printing. The polymer-textile composites were manufactured using an Original Prusa i3 MK3S 3D Printer with a 250 mm by 230 mm build platform and a nozzle diameter of 0.4 mm, using the printer settings specified in Table 5.5. The nozzle temperature to print Prusa PLA was 220°C, while the build platform temperature was set at 60°C.

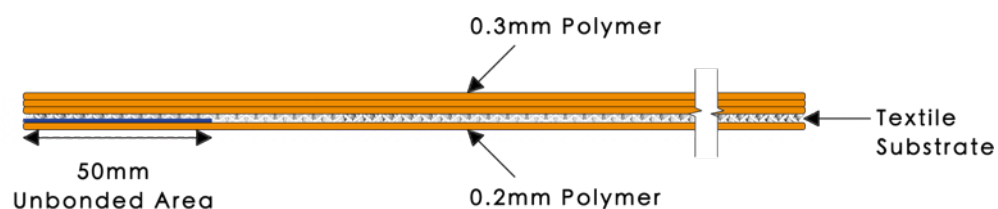


Figure 5.5. Illustration of the ME polymer-textile composite for the T-Peel test panel.

As far as the printing procedure for ME polymer-textile composites (print layout A) was concerned, the first or base PLA layer (0.2mm layer height) was printed on the build platform

using the calibrated Z –distance between build platform to the extrusion nozzle. While the first layer print was almost complete, the nozzle height was increased to a new Z –distance to offset the fabric thickness. The printer was paused immediately once the first layer was completed. The Z –axis will automatically be lifted from the build platform by the system (Table 5.8A). To create the T-Peel test panel, a section of blue tape was applied on the surface of PLA layer to create a 50mm unbonded area, separating with the subsequent print layers during the printing process (Table 5.8B). Thereafter, the textile substrate, which was cut prior, to match the size of the build platform was placed above the blue tape separator, secured, and tensioned using binder clips to remove any wrinkles or crease. It is extremely important to position the clips carefully to prevent any obstruction in the path (top–bottom and both sides of the built platform). Afterwards, the printer was resumed to complete the print (Table 5.8C).

The T-Peel test panel was printed as a whole sheet, then cut into six individual strips in 200 mm (L) x 25 mm (W) x 0.5 mm (H). Six T-Peel test panels for each polymer-textile combination were created, producing a total of 18 specimens to be tested. The unbonded area was pull separated by hand to form a “T” angle for the T-Peel specimen to be fixed to the top and bottom clamps on the testing machine for the T-peel test (Figure 5.6). The adhesion value of the separated section will not be considered in the result as the unbonded area of the T-Peel test panel was designed to be clamped on the universal testing machine. Therefore, the net structure belonging to the upper or lower part of the unbonded area would not affect the adhesion result of this experiment.

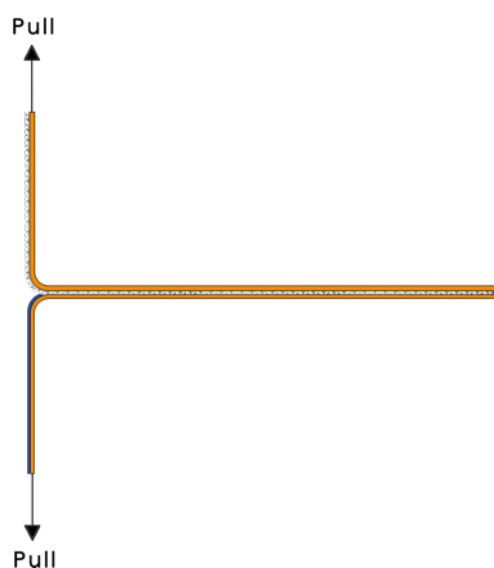
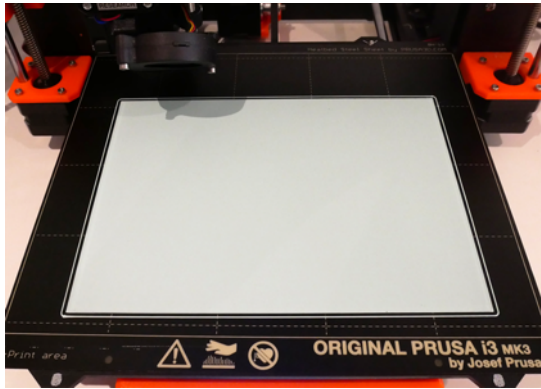
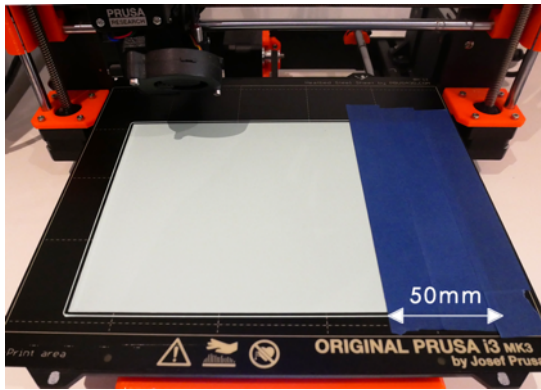
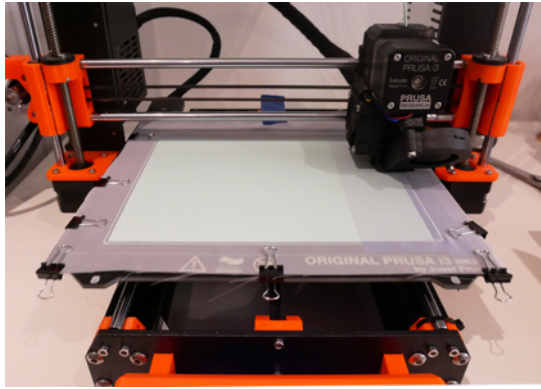
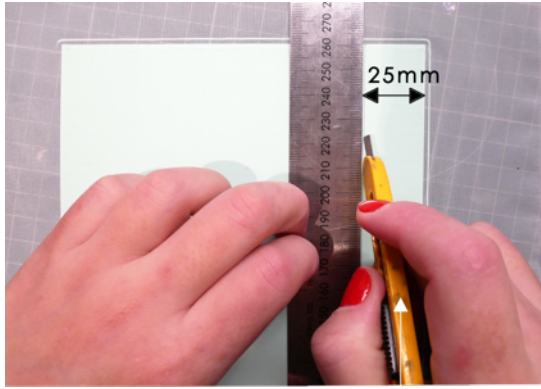


Figure 5.6. T-Peel test specimen (not drawn to scale).

Table 5.8. The printing procedure involved in manufacturing ME polymer-textile composite (print layout A) to create T-Peel test panel.

A		<ol style="list-style-type: none"> <li>1. First layer calibration for optimum Z-distance between the build platform to the extrusion nozzle.</li> <li>2. Print the first or base PLA layer using 0.2mm layer height.</li> <li>3. Add nozzle height increment while the first layer print was almost complete.</li> <li>4. Pause the printer immediately once the first layer was completed.</li> </ol>
B		<ol style="list-style-type: none"> <li>5. Apply blue tape on the printed PLA layer (50mm width).</li> </ol>
C		<ol style="list-style-type: none"> <li>6. Place and secure the textile substrate above the printed layer using binder clips.</li> <li>7. Resume the printer to complete the subsequent print layers.</li> </ol>
D		<ol style="list-style-type: none"> <li>8. Cut the T-Peel panel into six individual 25mm wide strips.</li> </ol>

### 5.3.2. Test Procedures

T-peel tests were carried out on the bonded ME printed polymer-textile composites to determine the peel force and peel strength required to separate the bonded polymers. Figure 5.7 shows a schematic diagram and dimensions of the bonded ME printed polymer-textile composites in line with BS EN ISO 11339 (2010).

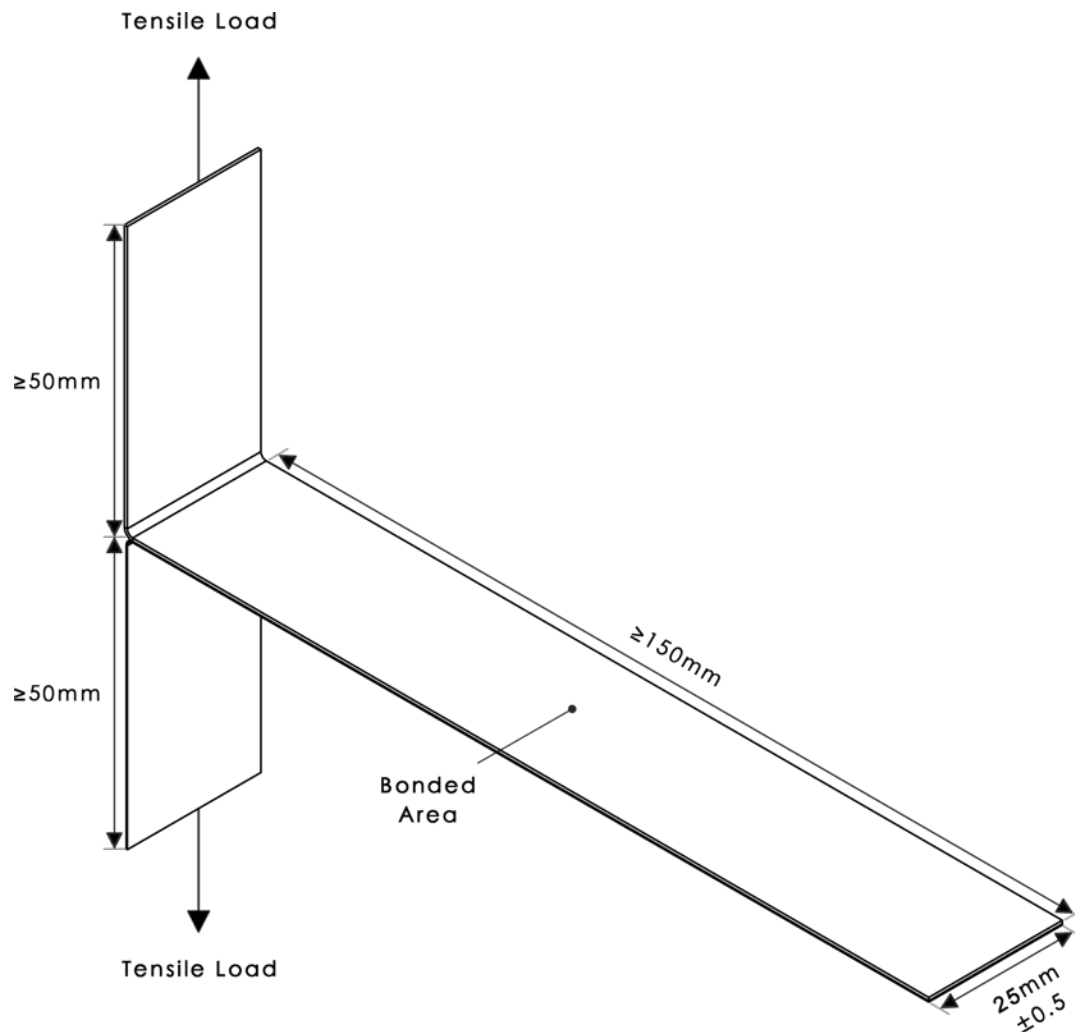


Figure 5.7. Technical drawing of the T-Peel test specimen in line with BS EN ISO 11339 (2010).

All the specimens had the same nominal dimensions. The peel force was divided by the width (25 mm), to compute the peel strength. The tests were carried out using a universal testing machine (Instron 5969), which had a maximum load capacity of 500 N. The grips of the machine were used to secure the ends of the specimens so that they were subjected to uniform tension. It is important to ensure that the bonded area of the specimen remained perpendicular to the applied load. The test specimen was bent backwards 180° and peeled.

The crosshead displacement was applied at a rate of 10 mm/min, based on the guideline given in BS EN ISO 11339 (2010). A digital camera was used to monitor the failure modes of the specimens. Six specimens were tested from each batch of material.

#### **5.4. Results and Discussion**

PLA in general printed well on Polyester and Nylon textile substrate with good linear and haptic finishing. Due to a limited volume of turquoise coloured Prusa PLA filament, a white coloured Prusa PLA filament was used to create the remaining test specimens. The material properties remained the same whilst the material colour would not have an impact on the T-Peel test results.

Figure 5.8, Figure 5.9 and Figure 5.10 show the test setup on and failure modes of PLA – Nylon (net structure) – PLA, PLA – Polyester (voile structure) – PLA and PLA – Nylon (voile structure) – PLA orientations, respectively. The six tested T-peel specimens for each orientation were presented alongside to further visualise the failure modes. The samples were labelled according to their fabric number and specimen number (i.e., F1-1). The failure mode classification was based on BS EN ISO 10365 (1995). For the two orientations with Nylon net structure (Figure 5.8C) and voile structure (Figure 5.10C), both were the failure of an adherend, caused by the fracture of printed PLA layer (cohesive substrate failure). On the other hand, the orientation with Polyester voile structure showed an adhesion failure mode, delamination of printed PLA layer (substrate) from the textile, shown in Figure 5.9C.

PLA – Nylon (net structure) – PLA orientation

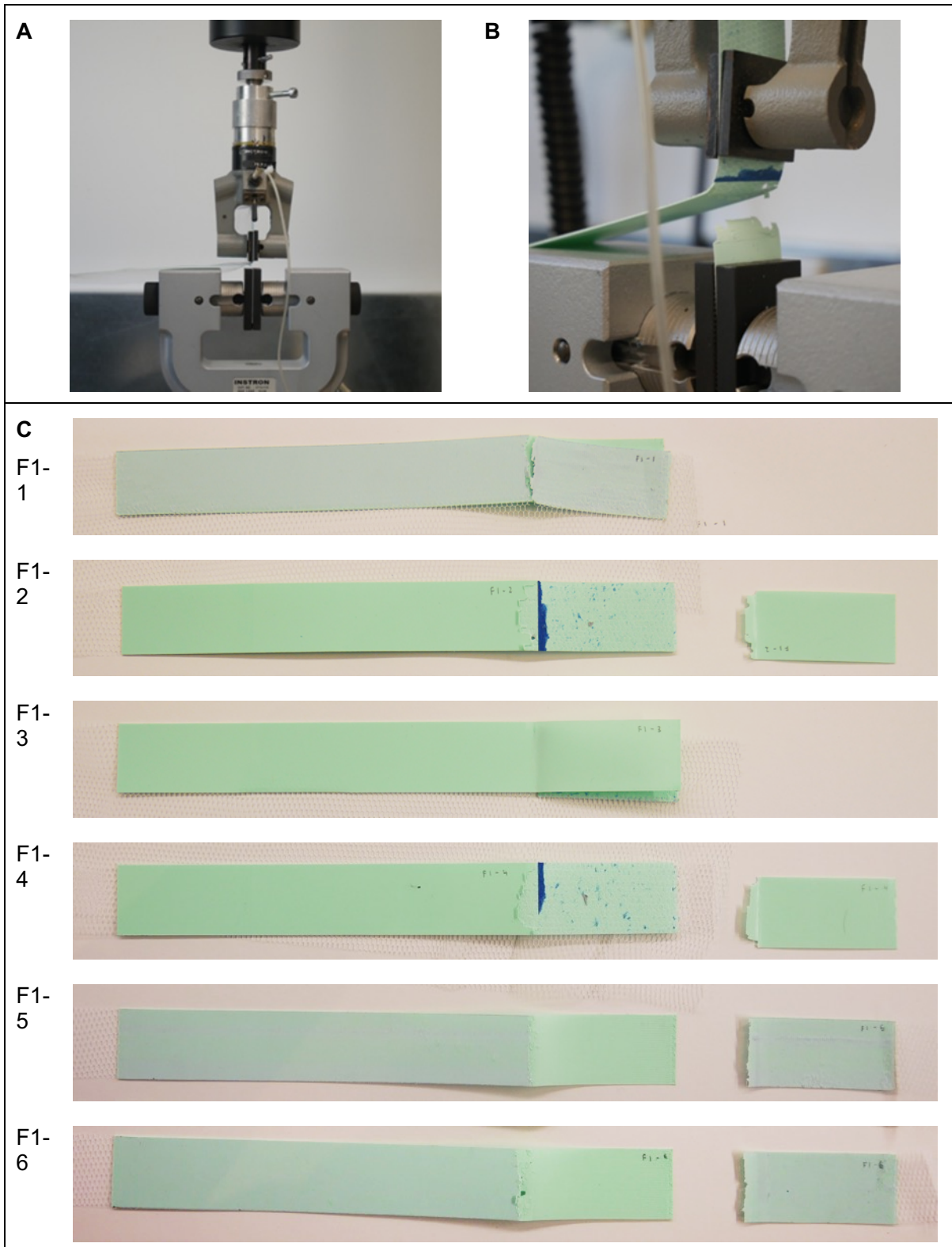


Figure 5.8. (A) Test setup, (B) failure mode for the PLA – Nylon (net structure) – PLA orientation and (C) failure of an adherend (cohesive substrate failure). (F1-1 to F1-6= sample label).

PLA – Polyester (voile structure) – PLA orientation

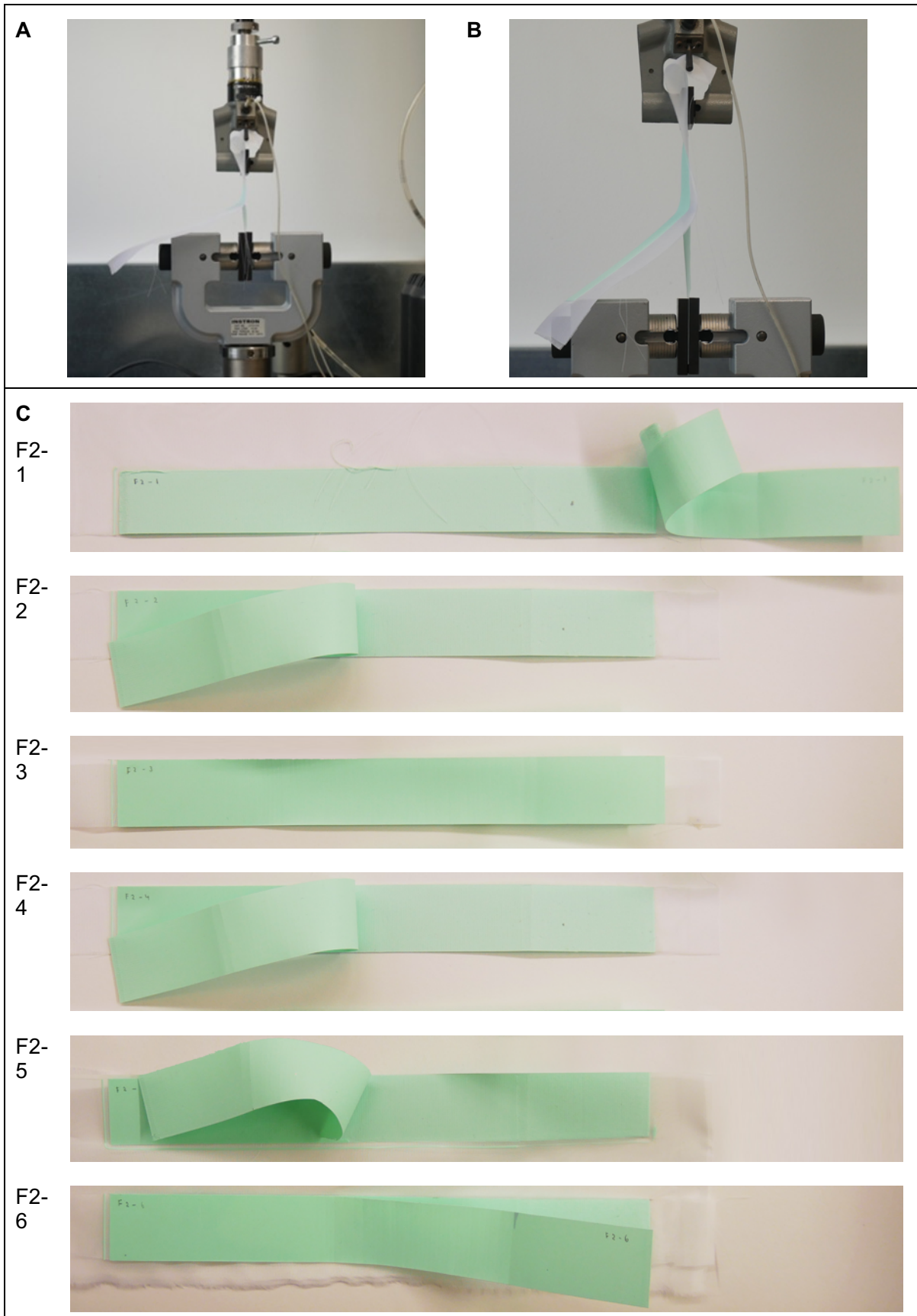


Figure 5.9. (A) Test setup, (B) failure mode for the PLA – Polyester (voile structure) – PLA orientation and (C) adhesion failure (delamination). (F2-1 to F2-6= sample label).

PLA – Nylon (voile structure) – PLA orientation

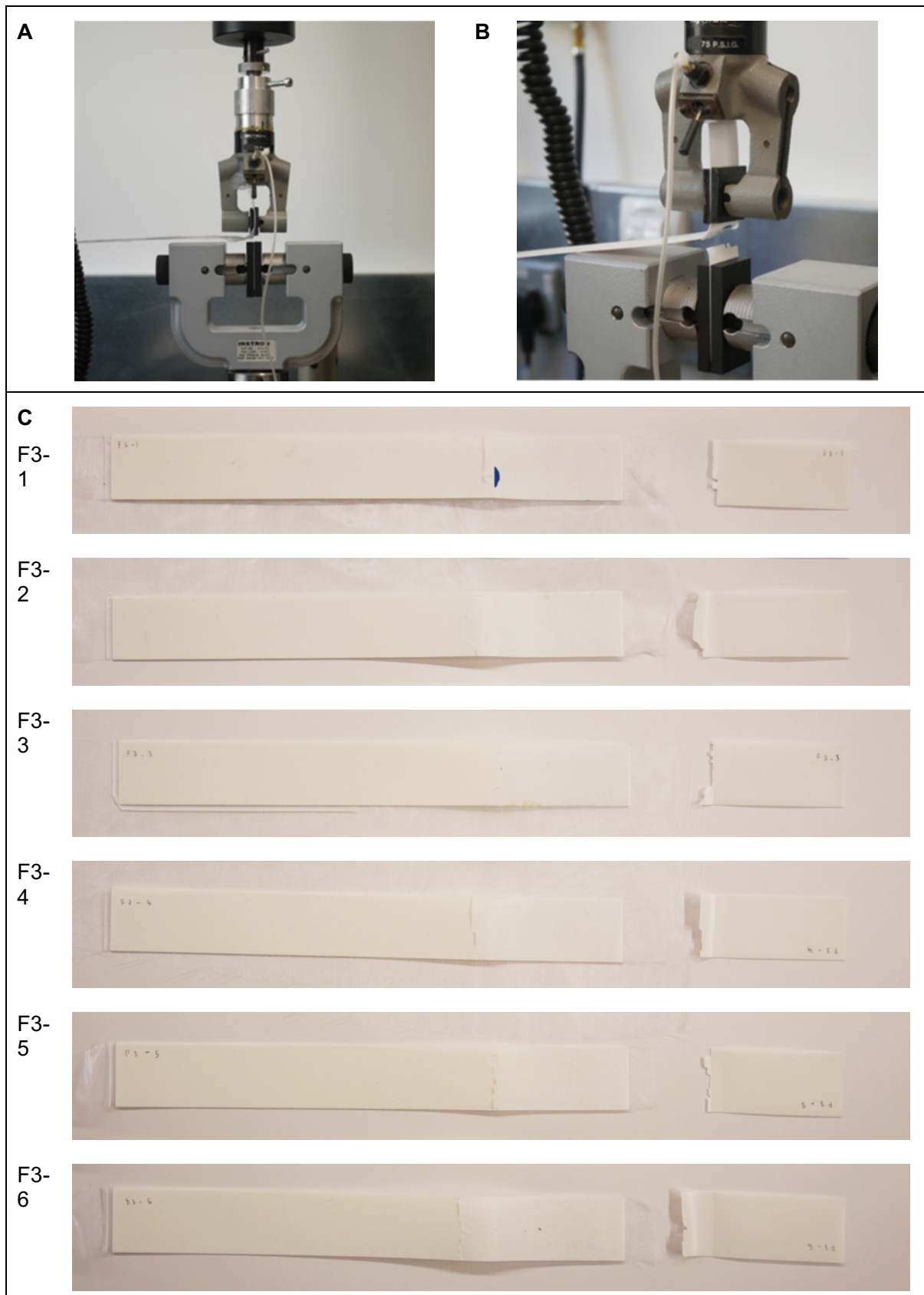


Figure 5.10. (A) Test setup, (B) failure mode for the PLA – Nylon (voile structure) – PLA orientation and (C) failure of an adherend (cohesive substrate failure). (F3-1 to F3-6= sample label).

Figure 5.11, Figure 5.12 and Figure 5.13 show the force versus extension responses for the six specimens for the three different combinations of polymer-textile composites, (a) PLA – Nylon (net structure) – PLA, (b) PLA – Polyester (voile structure) – PLA, and (c) PLA – Nylon (voile structure) – PLA. Table 5.9, Table 5.10 and Table 5.11 record the peel forces and strength for the six specimens of each orientation. The average peel force and peel strength value, the standard deviation and coefficient of variation were calculated. Following the recommendation given in BS EN ISO 6133 (2015), the average peel force was determined based on the midpoint of the minimum and maximum peak force values, whilst ignoring the initial rise at the start of the test. It was worth noting that the test data for specimen F3-3 (highlighted in red in Table 5.11) was discarded and not included in the analysis because of inaccurate results caused by misalignment of the specimen in the testing machine.

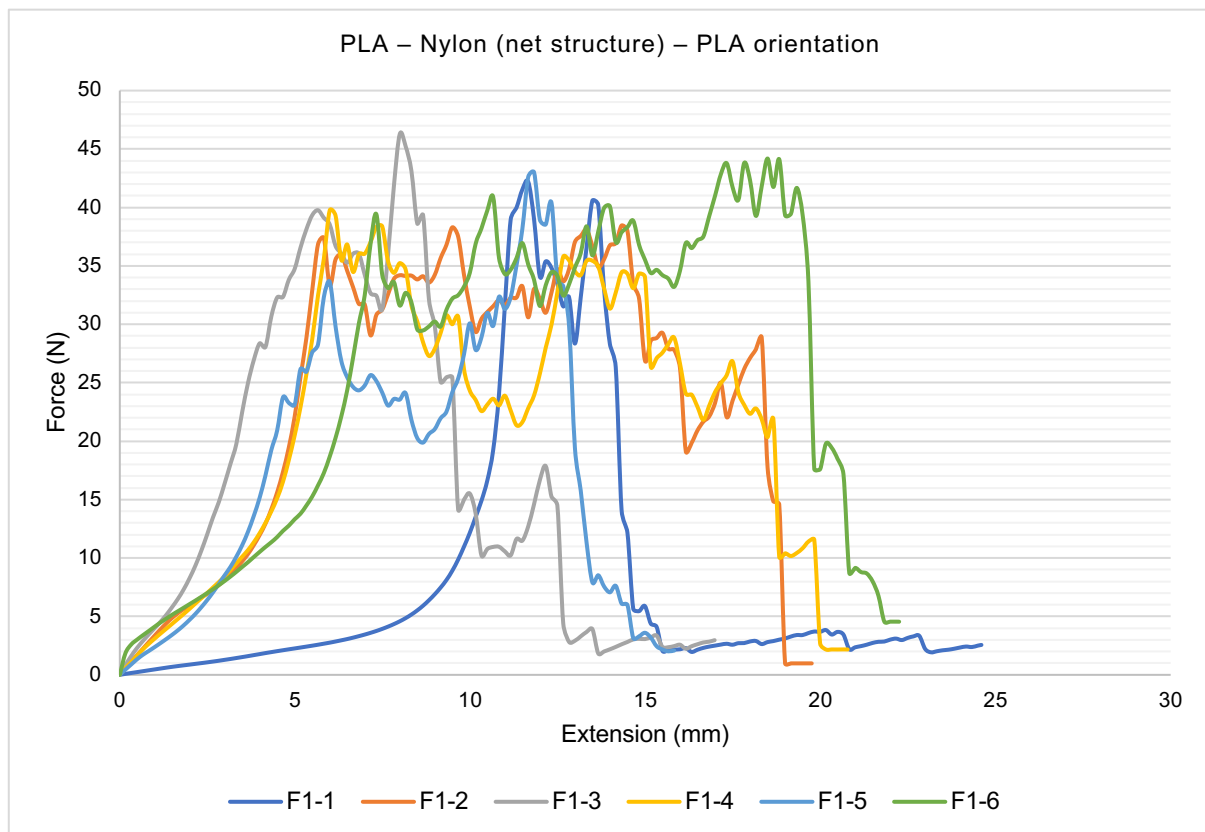


Figure 5.11. Force versus extension plots for six specimens with the PLA – Nylon (net structure) – PLA orientation.

Table 5.9. The peel forces and strength, standard deviation and coefficient of variation for the six specimens with the PLA – Nylon (net structure) – PLA orientation.

<b>Sample Label</b>	<b>Minimum peel force (N)</b>	<b>Maximum peel force (N)</b>	<b>Average peel force (N)</b>	<b>Minimum Peel Strength (N/mm)</b>	<b>Maximum Peel Strength (N/mm)</b>	<b>Average Peel Strength (N/mm)</b>
F1-1	28.3	42.2	35.3	1.1	1.7	1.4
F1-2	19.1	38.0	28.6	0.8	1.5	1.1
F1-3	31.3	46.3	38.8	1.3	1.9	1.6
F1-4	21.3	39.3	30.3	0.9	1.6	1.2
F1-5	19.9	43.0	31.5	0.8	1.7	1.3
F1-6	29.5	44.2	36.9	1.2	1.8	1.5
<b>Average</b>	24.9	42.2	33.5	1.0	1.7	1.3
<b>Lowest</b>	19.1	38.0	28.6	0.8	1.5	1.1
<b>Highest</b>	31.3	46.3	38.8	1.3	1.9	1.6
<b>Standard deviation</b>	5.4	3.1	4.0	0.2	0.1	0.2
<b>Coefficient of variation</b>	22%	7%	12%	22%	7%	12%

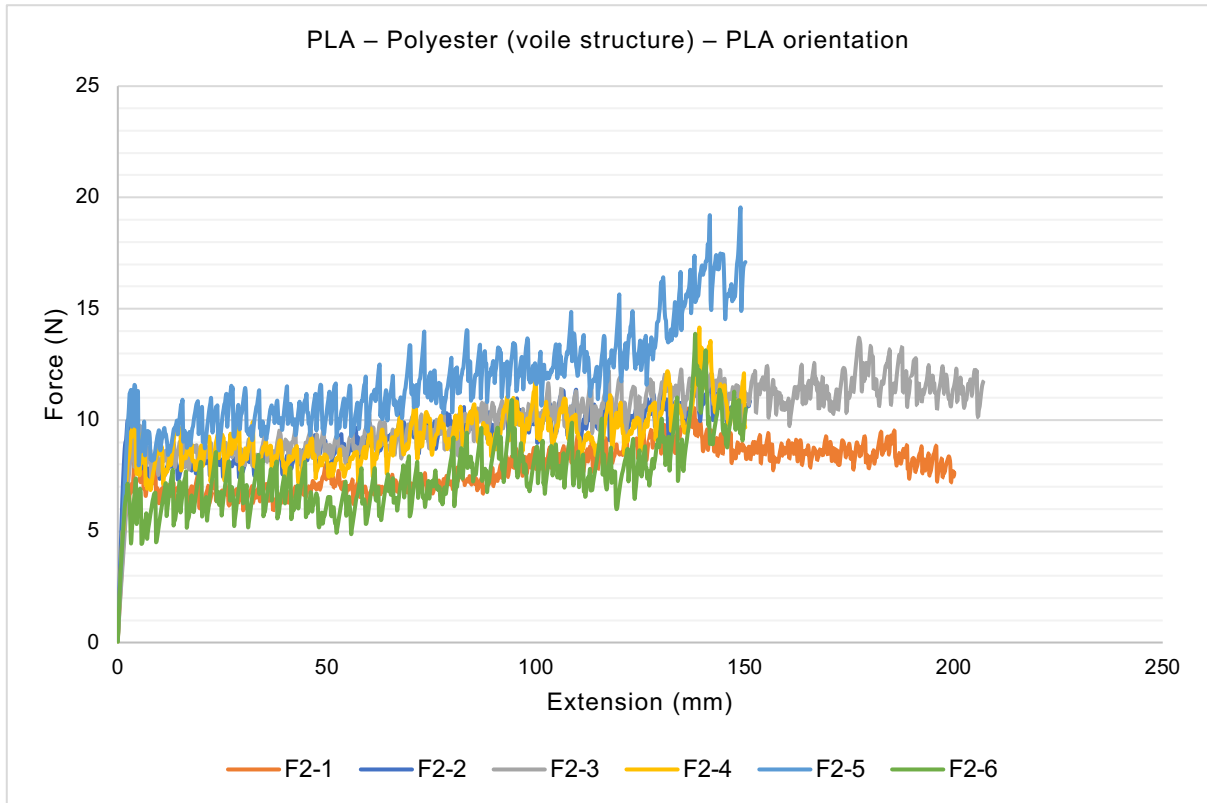


Figure 5.12. Force versus extension plots for six specimens with the PLA – Polyester (voile structure) – PLA orientation.

Table 5.10. The peel forces and strength, standard deviation and coefficient of variation for the six specimens with the PLA –Polyester (voile structure) – PLA orientation.

Sample Label	Minimum peel force (N)	Maximum peel force (N)	Average peel force (N)	Minimum Peel Strength (N/mm)	Maximum Peel Strength (N/mm)	Average Peel Strength (N/mm)
F2-1	5.9	9.4	7.7	0.2	0.4	0.3
F2-2	7.4	11.4	9.4	0.3	0.5	0.4
F2-3	7.8	12.1	10.0	0.3	0.5	0.4
F2-4	7.1	12.0	9.6	0.3	0.5	0.4
F2-5	9.1	15.6	12.4	0.4	0.6	0.5
F2-6	4.9	10.9	7.9	0.2	0.4	0.3
<b>Average</b>	7.0	11.9	9.5	0.3	0.5	0.4
<b>Lowest</b>	4.9	9.4	7.7	0.2	0.4	0.3
<b>Highest</b>	9.1	15.6	12.4	0.4	0.6	0.5

<b>Standard deviation</b>	1.5	2.1	1.7	0.1	0.1	0.1
<b>Coefficient of variation</b>	21%	17%	18%	21%	17%	18%

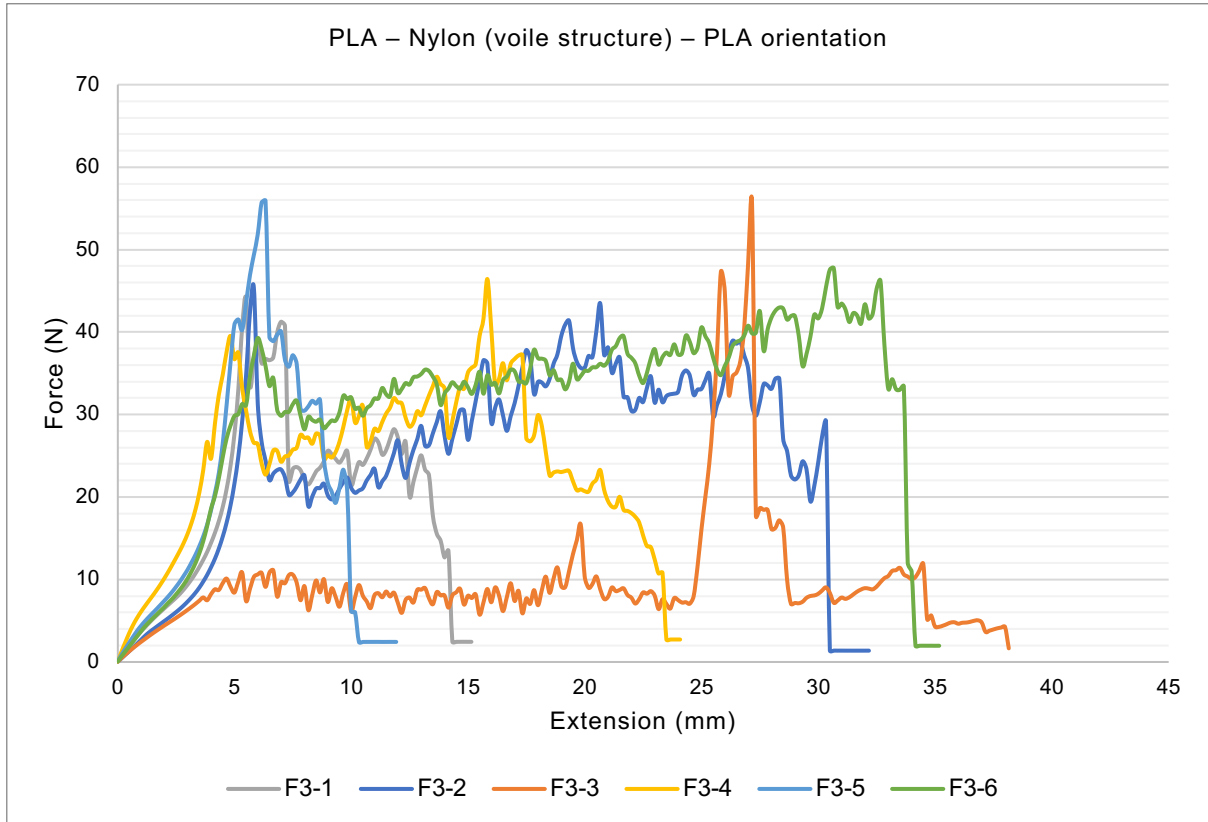


Figure 5.13. Force versus extension plots for six specimens with the PLA – Nylon (voile structure) – PLA orientation.

Table 5.11. The peel forces and strength, standard deviation and coefficient of variation for the six specimens with the PLA – Nylon (voile structure) – PLA orientation.

Sample Label	Minimum peel force (N)	Maximum peel force (N)	Average peel force (N)	Minimum Peel Strength (N/mm)	Maximum Peel Strength (N/mm)	Average Peel Strength (N/mm)
F3-1	20.1	44.1	32.1	0.8	1.8	1.3
F3-2	18.9	45.4	32.2	0.8	1.8	1.3
<b>F3-3</b>	5.7	55.6	30.7	0.2	2.2	1.2
F3-4	18.8	46.4	32.6	0.8	1.9	1.3

F3-5	19.3	55.9	37.6	0.8	2.2	1.5
F3-6	28.2	47.7	38.0	1.1	1.9	1.5
<b>Average</b>	21.1	47.9	34.5	0.8	1.9	1.4
<b>Lowest</b>	18.8	44.1	32.1	0.8	1.8	1.3
<b>Highest</b>	28.2	55.9	38.0	1.1	2.2	1.5
<b>Standard deviation</b>	4.0	4.7	3.0	0.2	0.2	0.1
<b>Coefficient of variation</b>	19%	10%	9%	19%	10%	9%

For an overall comparison, Figure 5.14 shows a representative force versus extension responses for the three different combinations of polymer-textile composites. Similar to their failure modes, the force versus extension responses for PLA on Nylon net structure and voile structure were similar, far better results as compared to Polyester. Their initial force exceeded 40 N and included a few force peaks, up to a maximum extension of about 20 mm, which subsequently dropped leading to failure of the PLA polymer, reflecting a relatively stronger bond compared to PLA on Polyester textile. The average peel forces for both PLA – Nylon composites were closely similar at 24.9N and 21.1N at minimum, and 42.2N and 47.9N at maximum respectively.

In comparison, the force versus extension responses for the PLA – Polyester (voile structure) composite showed an initial linear response until about 7 N. After that, there were several force peaks (i.e., undulating curve), reflecting the gradual separation of the Polyester textile from the PLA polymer, until the end of the test. For all the PLA – Polyester (voile structure) – PLA T-Peel specimens, there was no damage to both printed polymer layer and textile substrate (Figure 5.9). The average peel force was the lowest among the three orientations with 7.0N at minimum and 11.9N at maximum.

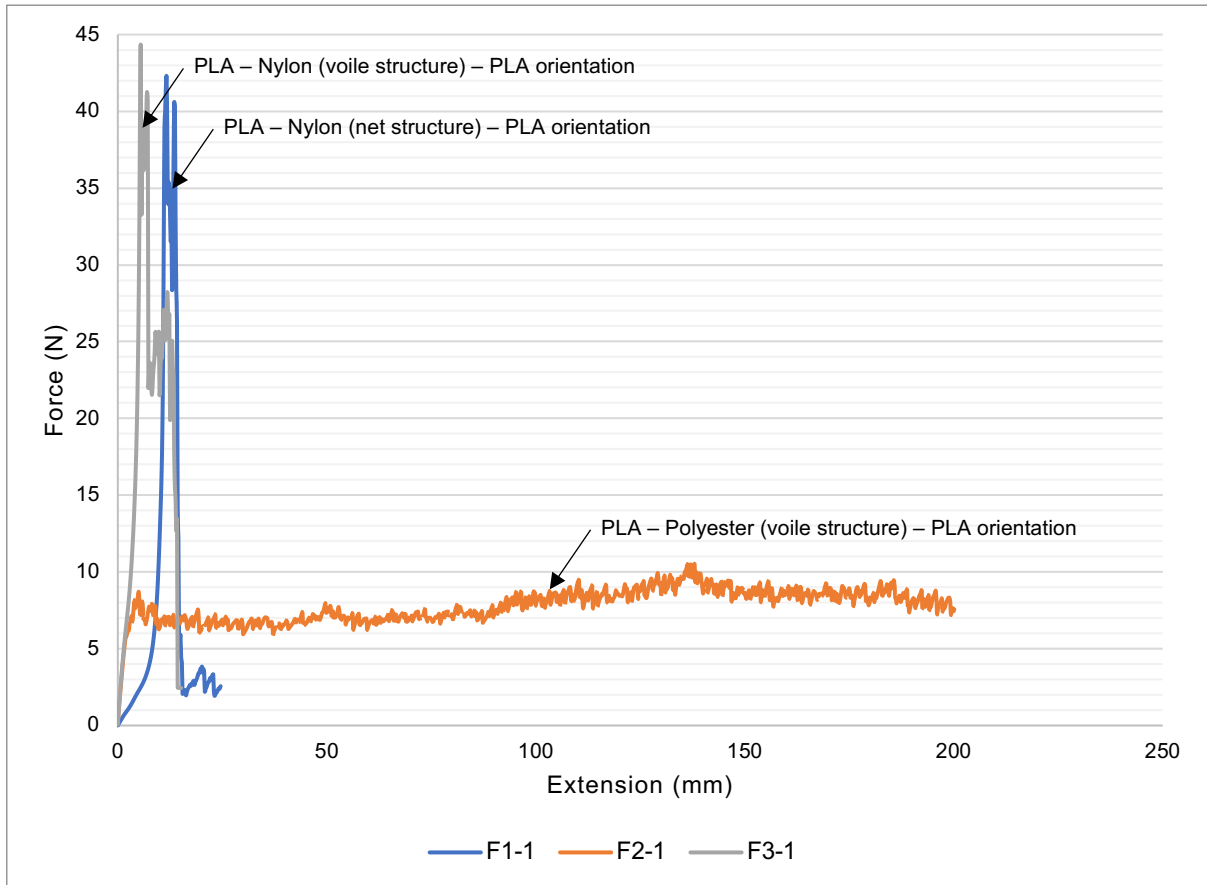


Figure 5.14. Comparison of the force versus extension plots for the three bonded ME printed polymer-textile composites.

Table 5.12 summarises the average peel forces, peel strengths and coefficients of variation for the three bonded ME printed polymer-textile composites. The peel strengths for the PLA – Nylon (net structure) – PLA, PLA – Polyester (voile structure) – PLA and PLA – Nylon (voile structure) – PLA polymer-textile composites were 1.3 N/mm, 0.4 N/mm and 1.4 N/mm, respectively.

Table 5.12. Average peel forces and strengths and coefficients of variation for the three bonded ME printed polymer-textile composites.

Orientation	Peel force		Peel strength	
	Average (N)	Coefficient of variation (%)	Average (N/mm)	Coefficient of variation (%)
PLA – Nylon (net structure) – PLA	33.5	12	1.3	12

PLA – Polyester (voile structure) – PLA	9.5	18	0.4	18
PLA – Nylon (voile structure) – PLA	34.5	9	1.4	9

The results showed that PLA – Nylon (voile structure) – PLA has the highest relative peel resistance. The average peel forces and strengths for both PLA – Nylon composites (net and voile structure) were about three times greater than PLA – Polyester composite (voile structure), which explained the breaking of the deposited layer at the beginning of extension in all samples during the T-Peel test. The statistical analysis show that the PLA – Nylon (voile structure) – PLA orientation had the lowest coefficient of variation of 9% and the PLA – Polyester (voile structure) – PLA orientation had a coefficient of variation of 18%, representing a relatively larger variation across the tested specimens.

PLA printed on Polyester textile did not show high peel strength result, which revealed that both materials were less compatible. According to the diffusion theory, the fine pore properties of voile structure decrease the amount of infiltration between the two polymer layers for polymer–polymer adhesion. As a result, the deposited polymer cannot protrude through the textile layer to create a form-locking connection (Sabantina *et al.*, 2015; Unger *et al.*, 2018; Eutionnat-Diffo *et al.*, 2019). However, their theory was challenged when comparing the results obtained from both voile structures and the two PLA – Nylon composites. Despite both nylon textiles having different mesh structure (net and voile), weave type, thickness and pore sizes, there were no substantial differences on their peel force and strength. It can be concluded that the fibre type has a predominant effect on the interfacial bonding strength between the printing material and textile substrate due to the chemical nature of both and interpolymer polar interactions (Van der Waals dipole-dipole inter-actions) across phase boundaries as explained by Sanatgar *et al.* (2017). The compatibility between the printing material and the textile substrate fibre type has a significant effect on the polymer-textile adhesion. Regarding the textile stretchability, there was no direct and substantial effect of the textile stretch on the peel resistance, nevertheless, working with low level or non-stretch textile substrate improves the ease of printing process. It can be equally stretched in both vertical and horizontal directions to be secured on the build platform and no pre-strain to cause irregular pore circularity and pore area which will cause an inconsistent amount of infiltration of the printed polymer at the time of printing, which will correspondingly affect the peel strength (Narula *et al.*, 2018).

Concerning the limitations of this study, the ME printing production process was demonstrated and tailored for Cartesian XZ hot end, Y bed ME desktop printer (i.e., Prusa i3 MK3S). Although the manufacturing concept is similar, there will be slight differences in the calibration and printing steps to accommodate the function of each ME printers, such as the Cartesian XY hot end, Z bed ME desktop printer (i.e. Ultimaker) (3D Printing Beta, 2020). This study examined the mechanical and adhesion properties of ME polymer-textile composites using basic structure design to meet the standards' requirement BS EN ISO 11339 (2010). Future work could explore printing different geometrical structures on more variety of textile substrates of different properties (i.e., weight and texture). PLA with different performance, mechanical properties and flexural characteristics mentioned in Table 5.2 can be explored. For instance, PLA Plus+ can be used for greater mechanical performance and resistance than regular PLA and has lower printing temperature compared to ABS and PETG (Gregurić, 2020). Flexible PLA can be used to create soft and flexible prints that can drape according to the fluidity of the textile fabric (Griffin, 2019).

## **5.5. Chapter Summary**

In this chapter, the three key interconnected factors (the printing material, textile substrate and printer settings) which affect the production, printed quality and adhesion strength of the polymer-textile composites were discussed. The experimental setup, procedures and analysis techniques to quantify the adhesion properties of polymer-textile composites have been described, and the results were compared and discussed.

This study investigated the influence of varying textile substrate parameters using different fibre types, structure and weight on polymer-textile adhesion force. The printing material and ME printing parameters used were kept constant. Different ME printed polymer-textile composites were manufactured using PLA (printing material) and Nylon and Polyester (textile substrates) to evaluate their manufacturing feasibility and assess their mechanical properties. The ME printed polymer-textile composites included (a) PLA – Nylon (net structure) – PLA; (b) PLA – Polyester (voile structure) – PLA; and (c) PLA – Nylon (voile structure) – PLA. Based on the results from the T-peel tests, it can be concluded that the compatibility between the printing material and the textile substrate fibre type has a dominant effect on the peel resistance of ME polymer-textile composite. The average peel forces and strengths for both printed PLA on Nylon textiles composites were nearly three times stronger than Polyester textile despite the differences in their mesh structures, pore properties and weave type.

Finally, the work reported in this chapter has not only added to the current limited knowledge of developing polymer-textile composite using ME but also demonstrated the appropriate mechanical testing method to determine the relative peel resistance of adhesive bonds between thin flexible adherends. Chapter six uses the polymer-textile orientation with the highest relative peel resistance (PLA – Nylon (voile structure) – PLA) to extend the concept of direct ME of polymers onto textile fabrics as a material-joining technique for the development of thermo-responsive textiles.

## Chapter 6

### **4D Printed Shape-Changing Thermo-responsive Textiles**

The top-performing material and the polymer-textile orientation with the highest relative peel resistance, discovered in chapters four and five respectively, were applied for the 4DP of thermo-responsive textiles. Chapter six discusses the design, fabrication, heating activation test and characterisation methods for the 4D printed shape-changing thermo-responsive textile. This chapter investigates the potential for controlling shape deformation to produce varieties of shape-shifting behaviours using the geometrical dimensions and structural arrangements of the printed SMP structure on the textile substrate. The optimum geometric parameters to achieve the most predictable and accurate deformation are analysed, and the structural arrangements to achieve particular shape-shifting patterns are reported. The findings serve as a design parameter selection guide for designers and researchers to create relevant shape transformations, develop new applications or facilitate future research development. This chapter concludes by providing insight into the potential applications and the limitations in creating 4D printed shape-changing thermo-responsive textiles.

#### **6.1. Introduction**

4D Printing (4DP) can provide direct functionality to conventionally manufactured textile fabrics, offering a new vision of Additive Manufacturing (AM) for fashion and textile innovation. It can be used to develop active smart textiles that are stimuli-responsive and can be programmed to dynamically change shape. 4D printed shape-changing textiles are grouped under the second generation of smart textiles as they comprise both sensor and actuator functions to perform aesthetic and feature augmentations when exposed to external stimuli (Zhang and Tao, 2001; Leist *et al.*, 2017).

Thermo-responsive textiles are a class of stimuli-responsive textiles that respond to temperature stimulation. The class incorporates thermo-responsive shape-memory polymer (SMP) or shape-changing polymer, which provide the functional and active properties required to sense, self-actuate and undergo controllable shape change in an appropriate manner and time frame when exposed to the correct temperature (Hu and Chen, 2010). Joule heating directly from the water is a widely used temperature-based actuation method. The difference of coefficient of thermal expansion (CTE) between the continuous fibres and flexible matrix stimulates the shape transformation of the thermo-responsive textiles (Q.

Wang *et al.*, 2018). There was a clear difference in the thermally induced shape-changing behaviour when the SMP was printed on its own and onto a textile substrate (Figure 6.1), with a curvature of R:7 and R:10, respectively.

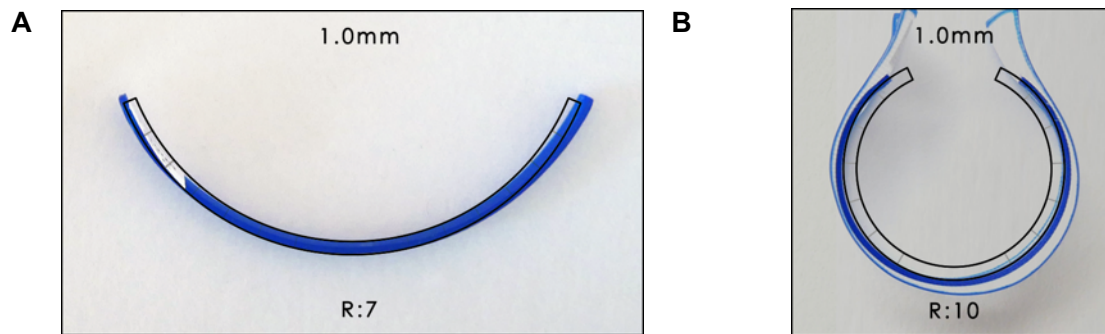


Figure 6.1. The differences in thermally induced shape-changing behaviour. (A) SMP printed on its own and (B) SMP printed onto a textile substrate.

Shape-changing textiles are conventionally synthesised using shape memory fibres produced by wet spinning, melt spinning and electrospinning, woven or knitted using SMP yarn, or coating of SMP material (i.e. Polyurethane) onto conventionally manufactured textile fabrics (Zhu *et al.*, 2006; Hu and Chen, 2010; Leist *et al.*, 2017). This research details the development of shape-changing thermo-responsive textile using direct material extrusion (ME) of thermo-responsive SMP onto nylon mesh fabric. As discussed in Chapter 3.2.2.3, a material may behave as shape-change material (SCM) or shape-memory material (SMM) depending on the working condition. In this study, the selected thermo-responsive SMP is designed to perform self-actuated shape change, permitting the thermo-responsive textiles to undergo an automatic shape change from the printed (primary) shape to an actuated (secondary) shape without a shape programming step. Whilst the textile substrate is a passive material serving as a structural material. As the material system consists of only a single active material, the shape-shifting behaviours are limited to bending and curving (Rajkumar and Shanmugam, 2018). The process of stimulated deformation would be single-driven and non-reversible.

Work by Rajkumar and Shanmugam (2018) has demonstrated the ability to control the shape-shifting behaviour changing of 4DP structure by changing the variables of design elements, such as the geometric shape and dimensions. By extending the concept, this research aims to investigate the opportunity to create particular shape-shifting behaviours and achieve accurate programmable deformation by modifying the geometrical dimensions

and structural arrangements of the printed thermo-responsive SMP on the textile substrate. The results from the shape transformation studies are established into a design parameter selection guide as a starting point for designers and researchers to create a wide range of shape transformations. This work can also be used to facilitate future research development or extended to create potential applications, particularly transformable wearables or accessories.

## **6.2. Shape Transformation Studies**

Table 6.1 lists the experiments for the shape transformation studies of 4D printed shape-changing thermo-responsive textiles which are divided into two parts, (I) geometrical dimensions and (II) structural arrangements. Part one systematically studies the influences of geometrical dimensions, namely thickness, width and length of the printed structure on the shape transformation behaviour. An additional variable, shape recovery temperature ( $T_r$ ), is studied in the first experiment to investigate the differences in the response rate and shape-change effect (SCE) when activated at different  $T_r$ , 60°C and 65°C, and to determine the optimal actuation temperature for the following experiments. 60°C and 65°C were used as they were the recommended  $T_r$  range for the chosen material based on the findings from chapter four. The optimal dimensions that provide the most accurate and controllable deformation are selected for use in Part two experiments to discover different shape-shifting behaviours achieved by changing the structural arrangements of the printed SMP on the textile substrate. In all experiments for Part two, three structural widths (1.0, 2.0 and 3.0mm) were tested for each configuration to determine the optimal parameter for the particular shape transformation, unless specified otherwise. Each experiment would also examine the response rate and the SCE of the samples. The assessment for the SCE comprised the shape change rating (R), the controllability and accuracy of deformation of the actuated shape. The studies would reveal the parameters to achieve particular shape transformation. Three specimens are created for each configuration for testing to obtain the average result.

Table 6.1. List of experiments to study the shape transformation of 4D printed shape-changing thermo-responsive textiles.

Experiment Type	No.	Experiment	Objective	Outcome	Manipulated Variables	Constant Variables	Refer To
Geometrical dimensions	1	Structural thickness and Tr	<ol style="list-style-type: none"> <li>To examine the effect of structural thickness on the shape transformation behaviour.</li> <li>To investigate the differences in the response rate and SCE when activated at different Tr.</li> </ol>	<ol style="list-style-type: none"> <li>Define the optimal structural thickness to achieve the most accurate and controllable deformation.</li> <li>Determine the optimal actuation temperature.</li> </ol>	Structural thickness and Tr	Structural width and length	Figure 6.2
	2	Structural width and length	<ol style="list-style-type: none"> <li>To examine the effect of structural width and length on the shape transformation behaviour.</li> </ol>	<ol style="list-style-type: none"> <li>Define the optimal structural width and length to achieve the most accurate and controllable deformation.</li> </ol>	Structural width and length	Structural thickness and Tr	Figure 6.3
Structural arrangements	3	Single column and multiple rows	<ol style="list-style-type: none"> <li>To examine the shape-shifting behaviour when printed in a single column and multiple rows.</li> <li>To investigate whether increasing the number of rows can lead to a higher deformation accuracy.</li> </ol>	<ol style="list-style-type: none"> <li>Discover the shape-shifting behaviour.</li> <li>Define the method to achieve accurate and controllable deformation by increasing the number of printed rows without modifying the structural width.</li> </ol>	Structural width and number of rows	Structural thickness, length and row spacing	Table 6.2

	4	Multiple columns and single row	<ol style="list-style-type: none"> <li>1. To examine the shape-shifting behaviour when printed in multiple columns and a single row.</li> <li>2. To examine the effect of structural width and length on the shape transformation behaviour.</li> </ol>	<ol style="list-style-type: none"> <li>1. Discover the shape-shifting behaviour.</li> <li>2. Define the optimal structural width and length to achieve the most accurate and controllable deformation.</li> </ol>	Structural width and length	Structural thickness, number of rows and columns	Figure 6.4
	5	Multiple columns and rows	<ol style="list-style-type: none"> <li>1. To examine the shape-shifting behaviour when printed in multiple columns and rows.</li> <li>2. To investigate whether increasing the structural width can lead to a higher deformation accuracy.</li> </ol>	<ol style="list-style-type: none"> <li>1. Discover the shape-shifting behaviour.</li> <li>2. Define the optimal structural width to achieve the most accurate and controllable deformation.</li> </ol>	Structural width and number of rows	Structural thickness, length, number of columns, row and column spacings	Figure 6.5
	6	Varied row arrangements	<ol style="list-style-type: none"> <li>1. To examine the shape-shifting behaviour when the row arrangements are varied.</li> </ol>	<ol style="list-style-type: none"> <li>1. Determine the optimal row arrangements for the shape-shifting behaviour.</li> </ol>	Row arrangement and spacing	Structural thickness, width and length, number of columns and column spacing	Table 6.3
	7	Print configuration	<ol style="list-style-type: none"> <li>1. To examine the shape-shifting behaviour when printed on different sides of textile substrates.</li> <li>2. To investigate whether increasing the structural</li> </ol>	<ol style="list-style-type: none"> <li>1. Discover the shape-shifting behaviour.</li> <li>2. Define the optimal structural width to achieve the most</li> </ol>	Structural width	Print placement, structural thickness, length and column spacing	Table 6.4

			width can lead to a higher deformation accuracy.	accurate and controllable deformation.			
	8	Print configuration with varied row arrangements	1. To examine the shape-shifting behaviour when the row arrangements are varied.	1. Determine the optimal row arrangements for the shape-shifting behaviour.	Row arrangement and spacing	Print placement, structural thickness, width, length, number of columns and column spacing	Table 6.5

For Experiment 1, the SMP structure was printed on the textile substrate in six different thicknesses, namely 0.5, 0.6, 0.7, 0.8, 0.9 and 1.0mm. This range of thickness was selected because 0.5mm was the most minimum structural thickness that can be achieved while maintaining a good polymer-textile adhesion (as identified in chapter five). Whilst 1.0mm builds a rigid three-dimensional structure that would not be too thick, bulky and heavy for textile application. In Experiment 1, the structural length and width were kept constant at 75mm and 3mm, respectively (Figure 6.2). The optimal structural thickness that provides the most accurate and controllable deformation is defined and applied for Experiment 2.

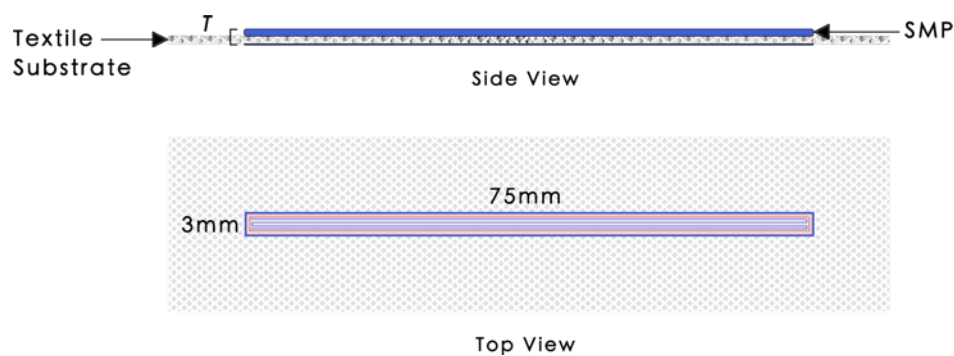


Figure 6.2. Experiment 1 Structural thickness manipulation.

Experiment 2 extends the study by manipulating the structural width and length (Figure 6.3). Six different structural width were printed, namely 1.0, 1.5, 2.0, 2.5, 3.0 and 3.5mm, paired with seven different structural length of 15, 25, 35, 45, 55, 65 and 75mm. A total of 42 samples were created from the width and length combinations. The optimal structural thickness of 1.0mm resulting from Experiment 1 was used.

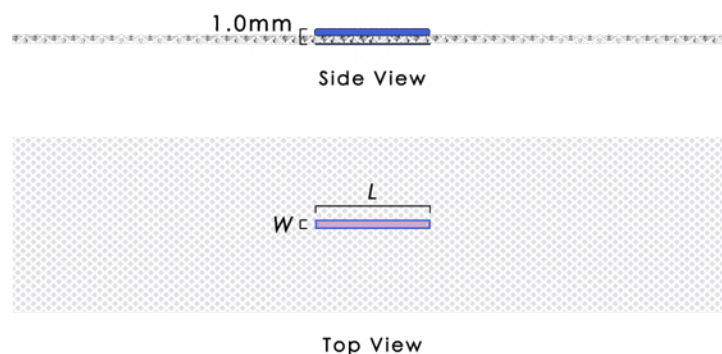
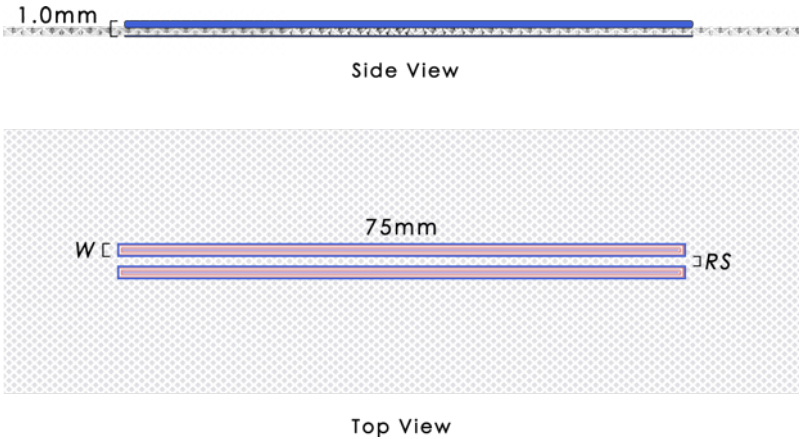
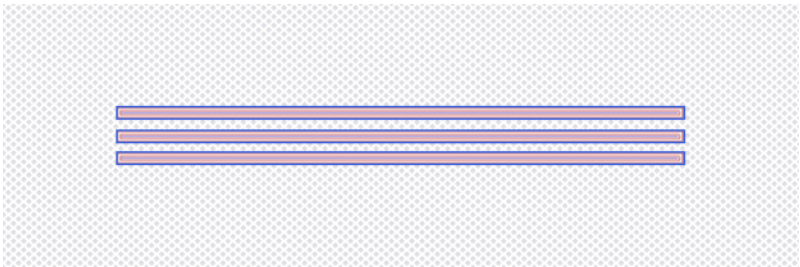
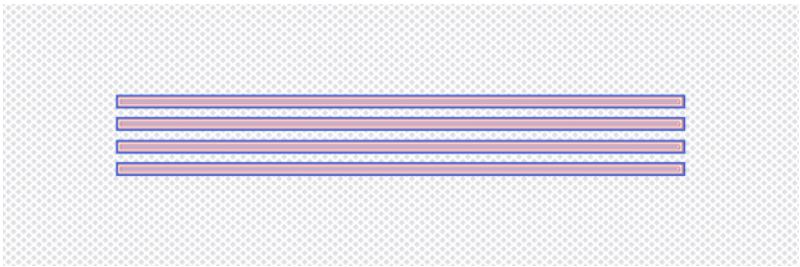
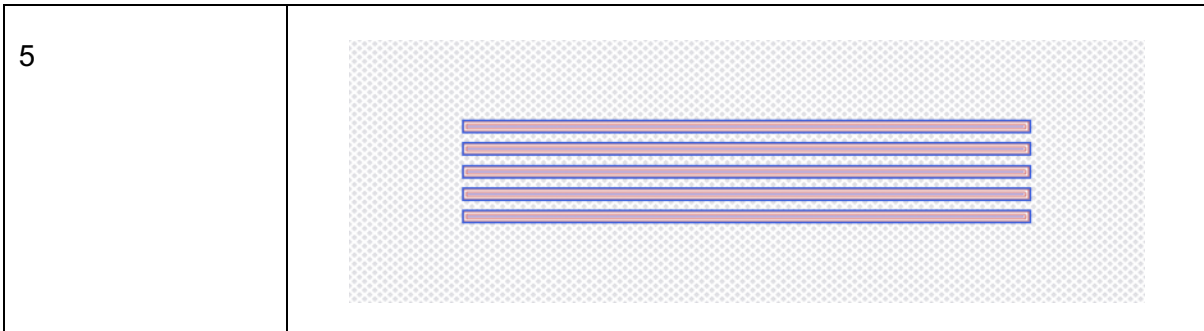


Figure 6.3. Experiment 2 Structural width and length manipulation.

For Experiment 3, the SMP structure of five different sets of structural width, namely 1.0, 1.5, 2.0, 2.5 and 3.0mm (extended from Experiment 2) was printed on the textile substrate in two, three, four and five rows separately. A total of 20 combinations were created. The row spacing between the printed structures changed according to the structural width ( $RS=W$ ). The structural thickness and length were kept constant at 1.0mm and 75mm, respectively. Experiment 3 did not test specimens with a single printed row as they were tested in Experiment 2.

Table 6.2. Experiment 3 Structural width and number of rows manipulation.

Number of Rows	Figure
2	 <p>The figure for 2 rows consists of two parts. The top part is a 'Side View' showing a single horizontal bar with a thickness of 1.0mm. The bottom part is a 'Top View' showing two parallel horizontal bars, each 75mm long. The distance between the centers of the two bars is labeled 'RS'.</p>
3	 <p>The figure for 3 rows is a 'Top View' showing three parallel horizontal bars of equal length, stacked vertically with equal spacing between them.</p>
4	 <p>The figure for 4 rows is a 'Top View' showing four parallel horizontal bars of equal length, stacked vertically with equal spacing between them.</p>



For Experiment 4, the SMP structures were printed in five columns and a single row, in three different structural widths (1.0, 2.0 and 3.0mm), paired with two different structural lengths (35 and 45mm), as shown in Figure 6.4. A total of six samples were created from the width and length combinations. The structural width of 1.5mm and 2.5mm were no longer being tested because the results from Experiment 3 showed a very slight difference in SCE between an increment of 0.5mm. On the other hand, structural widths of 35mm and 45mm were used as they resulted in different types of shape-shifting patterns as discovered in Experiment 2 (Table 6.9). 35mm creates a circular bend while 45mm creates a semi-circle bend. A 0.5mm column spacing was used to provide tolerance between the printed structures for shape transformation and to maintain the flexibility and movement of the textile substrate. The optimal structural length to achieve the most accurate and controllable deformation for the shape-shifting behaviour is defined and applied for Experiment 5.

Experiment 5 extends the study by introducing multiple rows and modifying the row spacing from 0.5mm to 35mm (Figure 6.5). The SMP structures were also printed in three different widths (1.0, 2.0 and 3.0mm) to select the optimal structural width that provides the most accurate and controllable deformation. As the width of the textile substrate was fixed at 38mm, the number of printed rows depend on the width setting of the printed structure. Structural widths of 1.0, 2.0 and 3.0mm can fit in 11 rows, 9 rows and 7 rows respectively on the textile substrate.

Table 6.3 shows the six different configurations tested in Experiment 6 to examine the shape-shifting behaviour when the row arrangements are varied. The optimal structural width of 1mm defined in Experiment 5 was used. The specimens were printed in five columns with 10mm spacing between each column.

Experiment 7 alternates the print placement or location by changing the side of SMP deposition onto the textile substrate. The CAD models were split into two sets, identified as Set A and B, to be printed on both sides of the textile substrate (side A and side B) as shown

in Table 6.4. The fabrication of the specimens involved two printing processes to print on both sides of the textile substrate, which will be discussed in Table 6.6.

Using the same concept and the optimal structural width of 1mm defined in Experiment 7, Experiment 8 examines the shape-shifting behaviour of different row arrangements. Table 6.5 presents the four different configurations tested.

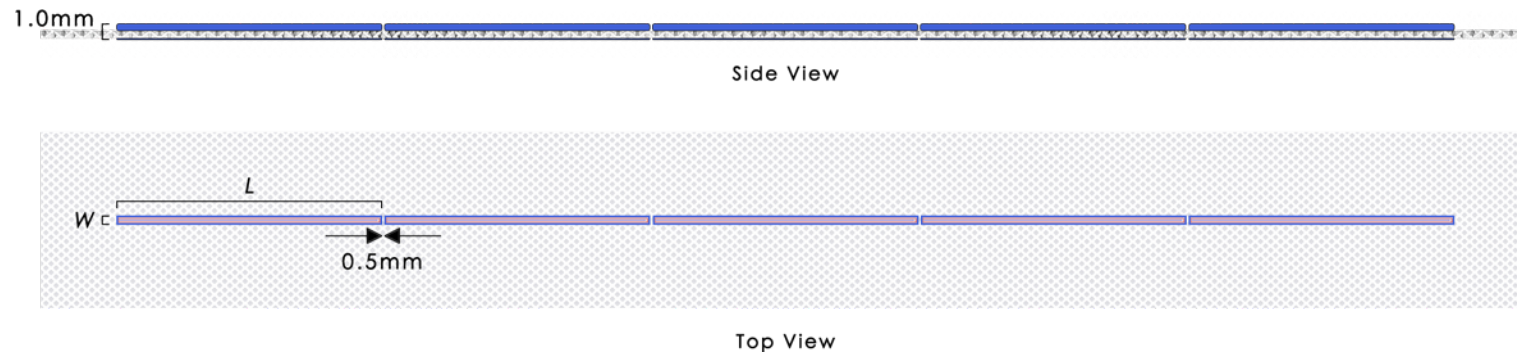


Figure 6.4. Experiment 4 Multiple columns and single row with structural width and length manipulation.

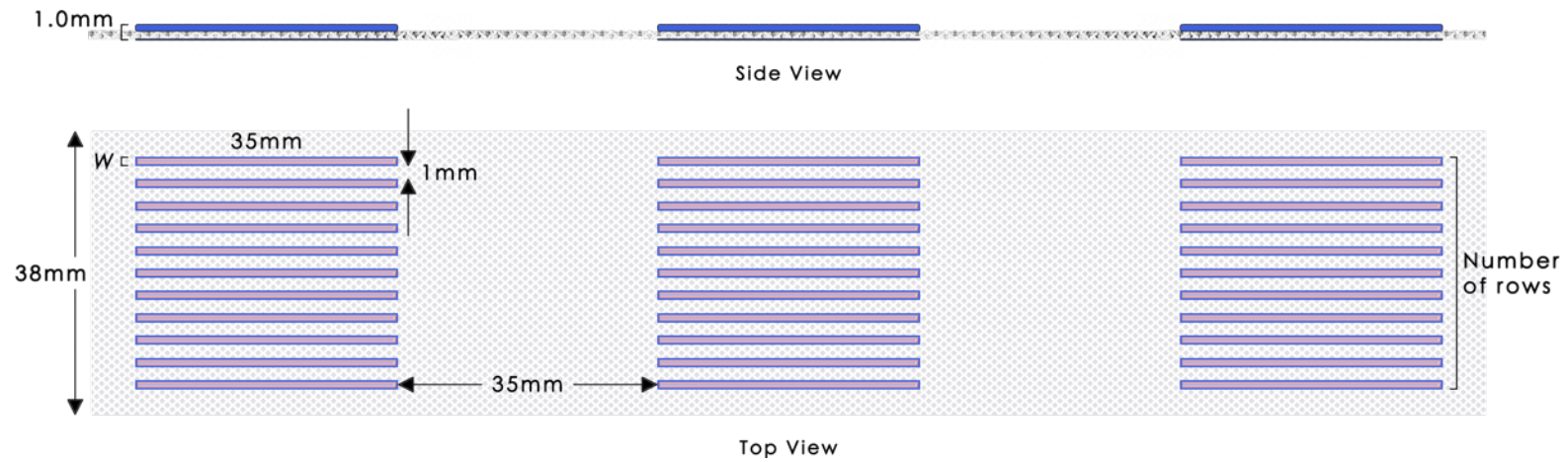
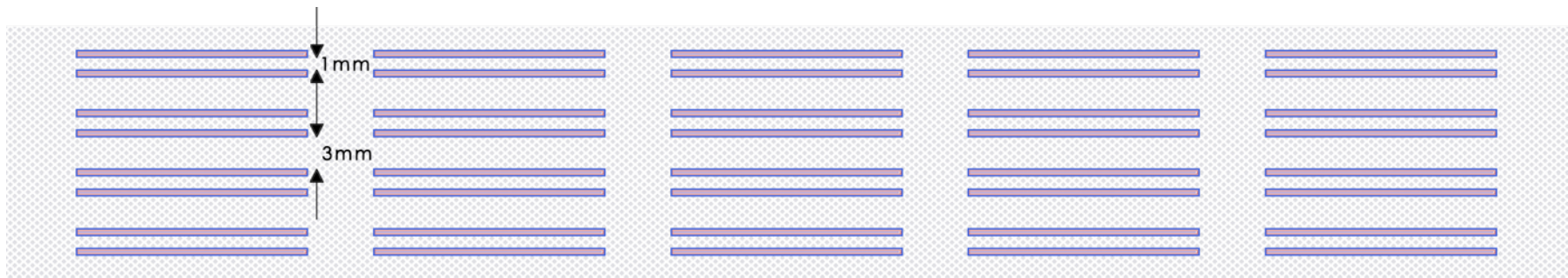


Figure 6.5. Experiment 5 Multiple columns and rows manipulation.

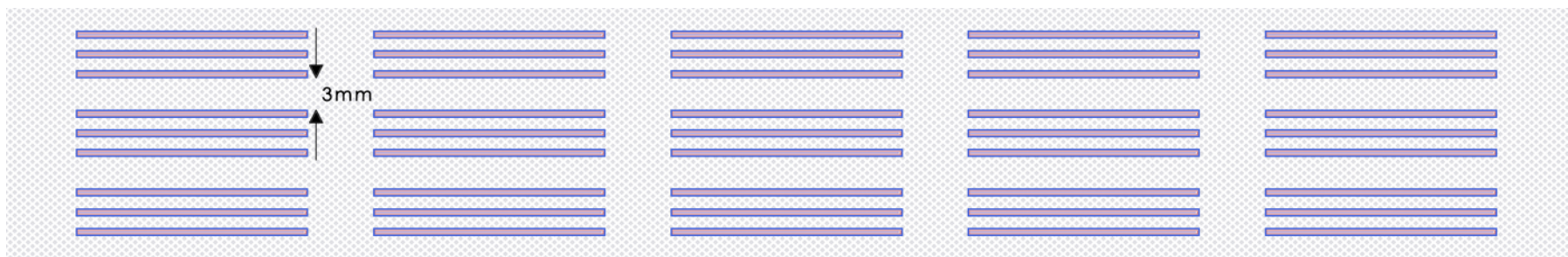
Table 6.3. Experiment 6 Varied row arrangements.



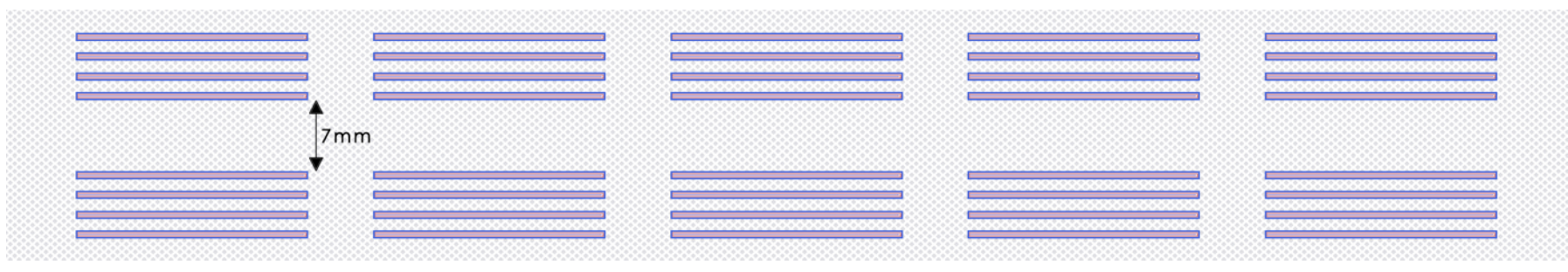
3



4



5



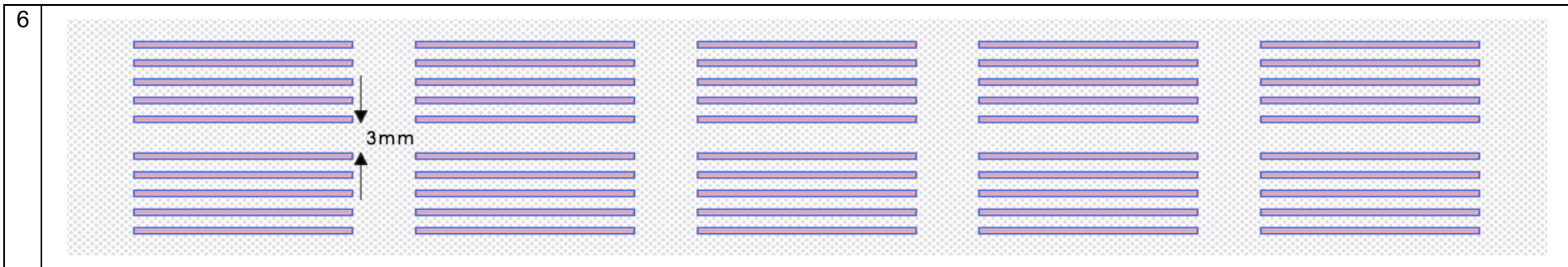
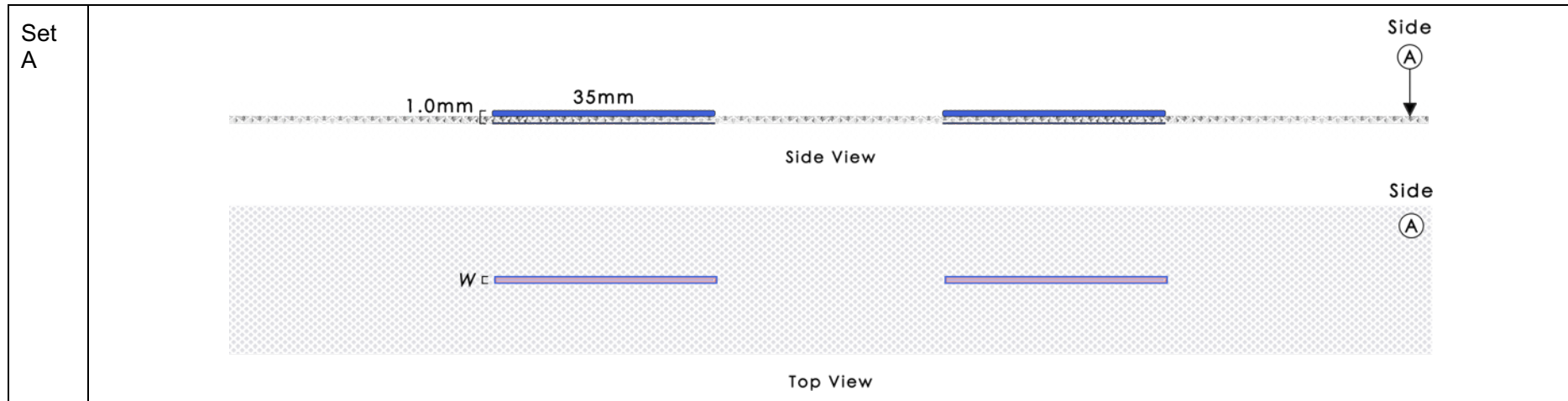


Table 6.4. Experiment 7 Print configuration.



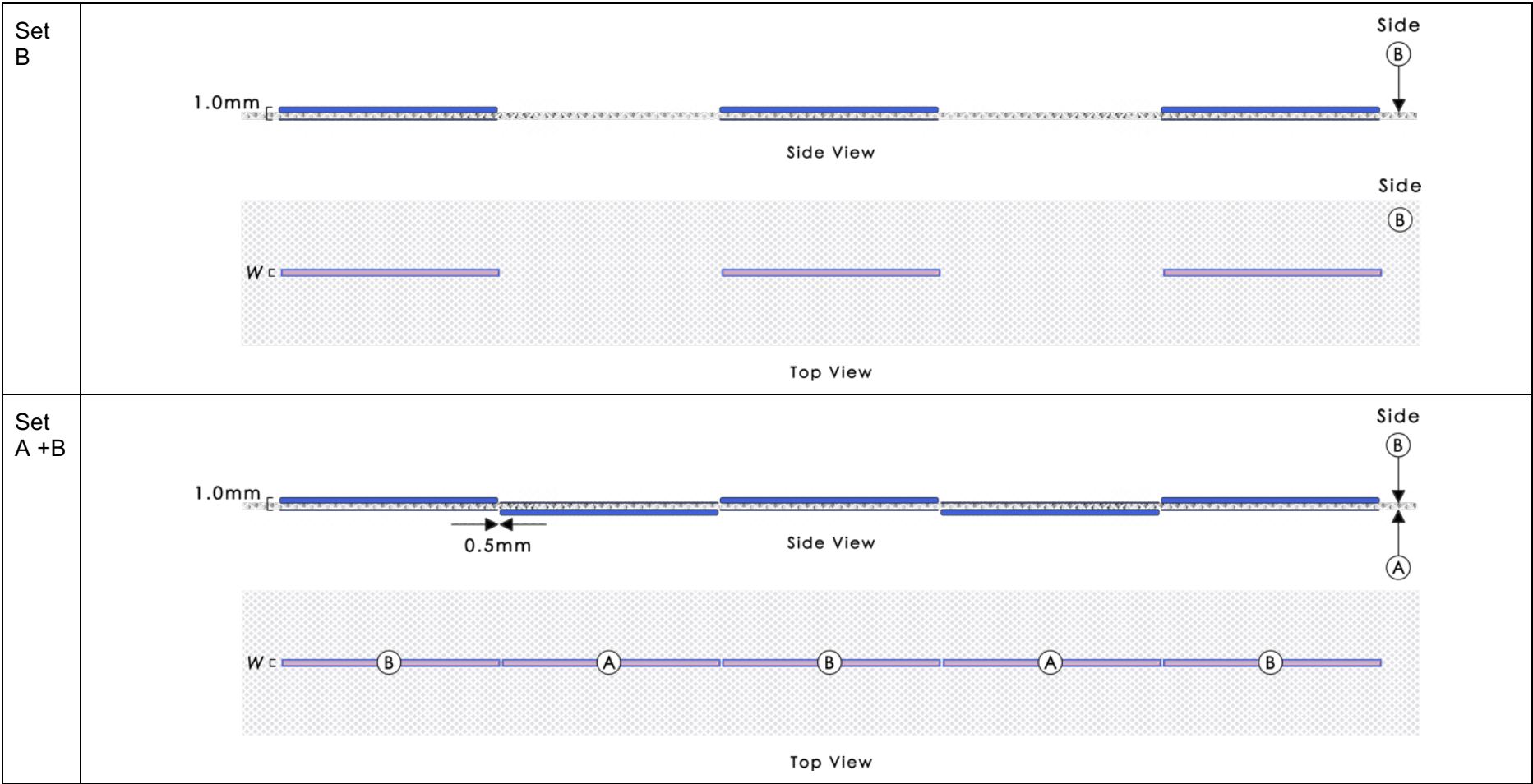
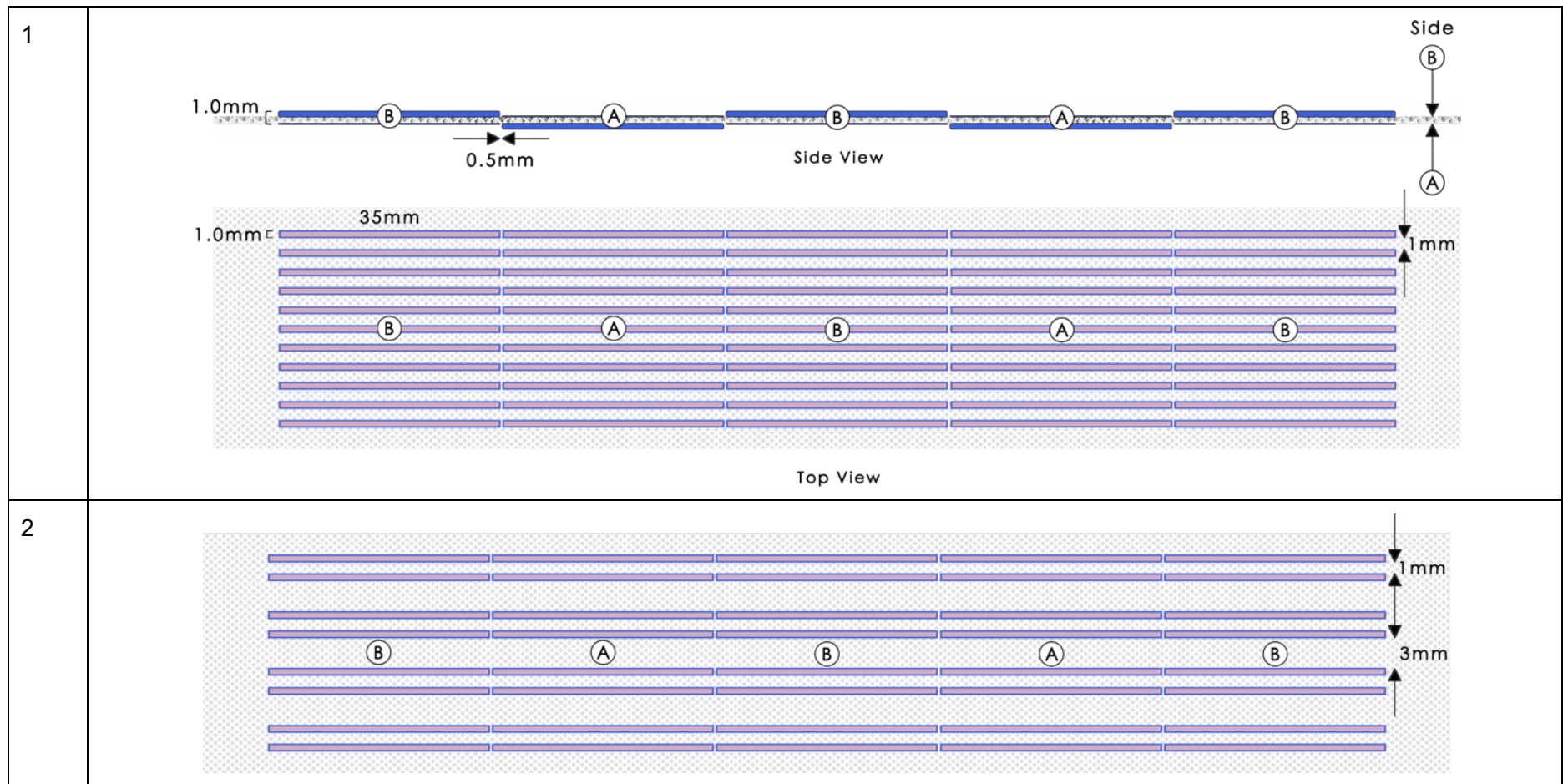
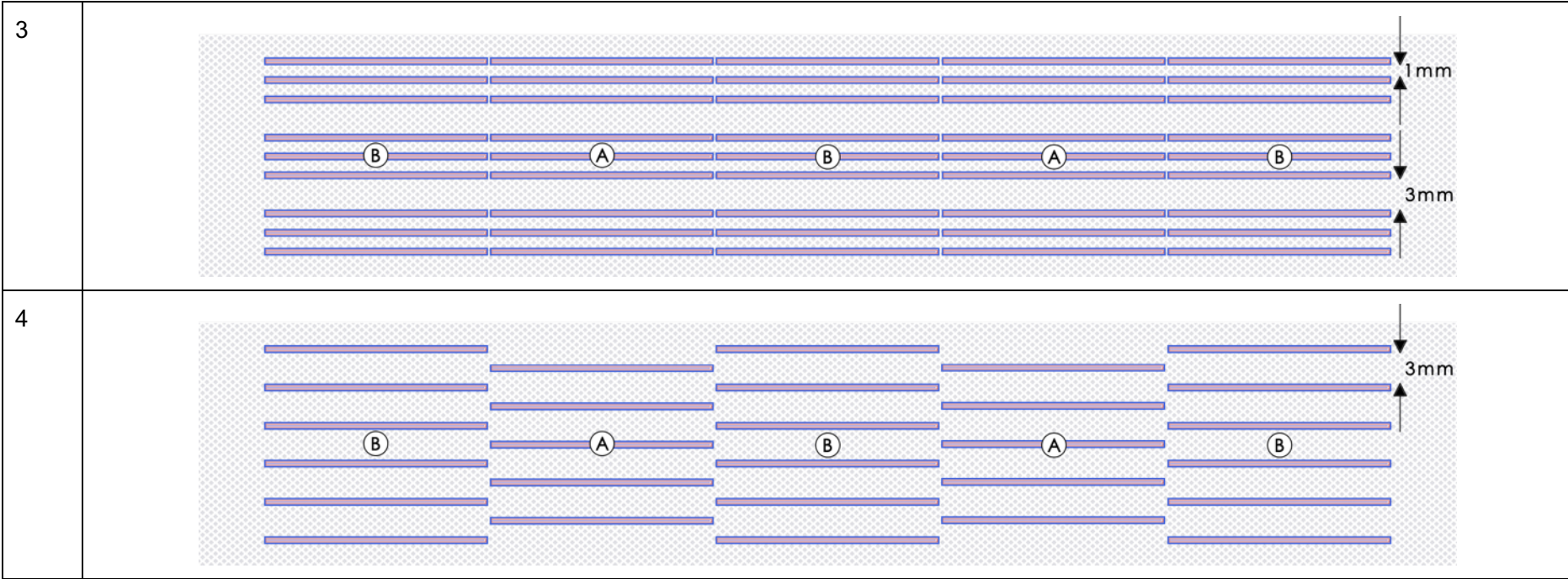


Table 6.5. Experiment 8 Print configuration with varied row arrangements.





## 6.3. Methods

### 6.3.1. Materials and AM Processes

The method of direct ME of polymers onto textile fabrics (presented in Chapter 5.3) was used to produce the thermo-responsive textile specimens. In this work, the printing material (thermo-responsive SMP) used was Filamentum PLA (material No.11 from Chapter four) and the textile substrate was Nylon (voile structure). Detailed parameters of these materials can be found in Table 4.2 and Table 5.7 respectively.

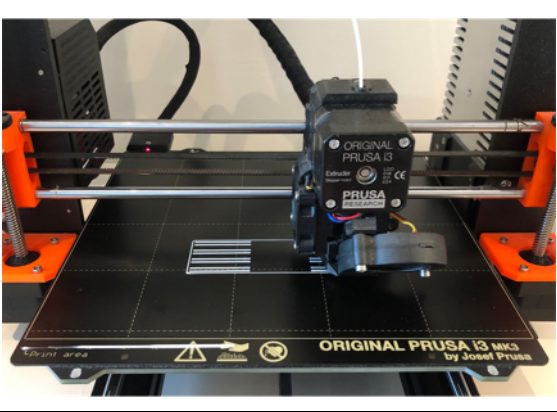
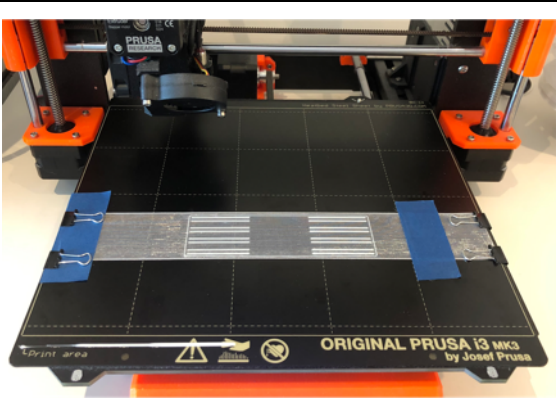
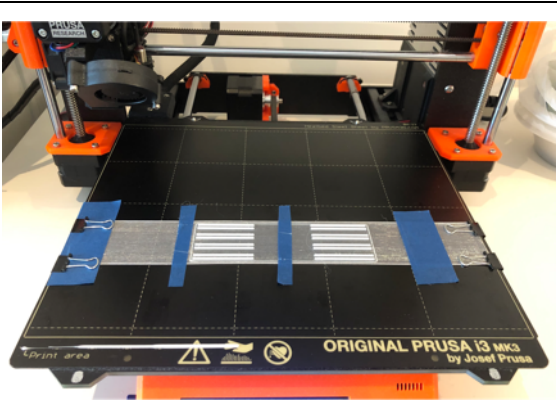
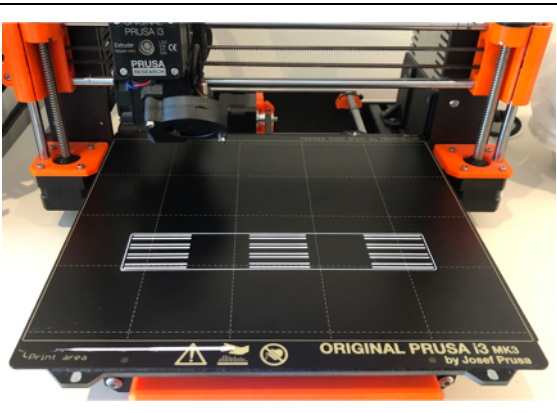
The CAD design of the printed structures for each experiment (listed in Chapter 6.2) were created using SolidWorks, exported as an STL file, imported into Slic3r for slicing and exported as a G-code for printing. All specimens were fabricated by ME using an Original Prusa i3 MK3S 3D Printer with a 250 mm by 230 mm build platform and a nozzle diameter of 0.4 mm, using the same print settings and parameters specified in Table 5.5. The printing material, textile substrate and ME printing parameters used were kept constant in all experiments.

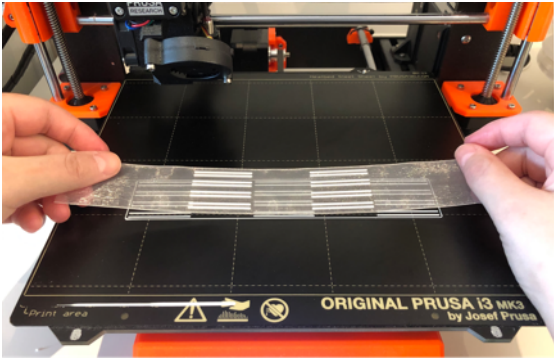
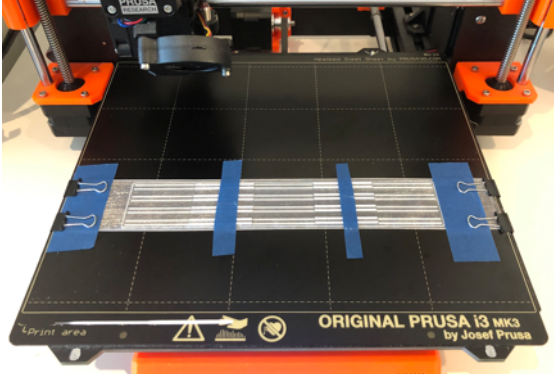
Print layout A was used to create the polymer-textile composite with Filamentum PLA - Nylon (voile structure) – Filamentum PLA orientation (Figure 6.6). All specimens were produced using the printing procedure presented in Chapter five (Table 5.8) or Table 6.6 (Procedure A to C), except for the specimens for Experiments 8 and 9. Table 6.6 describes the printing procedure for Experiments 8 and 9 specimens, which involved two printing processes to print on both sides of the textile substrate.



Figure 6.6. Direct ME of polymers onto textile fabrics using print layout A.

Table 6.6. The printing procedure for Experiments 8 and 9 specimens.

A		<ol style="list-style-type: none"> <li>1. First layer calibration for optimum Z-distance between the build platform to the extrusion nozzle.</li> <li>2. Print the first layer of Set A using 0.2mm layer height.</li> <li>3. Add nozzle height increment (+0.05mm) while the first layer print was almost complete.</li> <li>4. Pause the printer immediately once the first layer was completed.</li> </ol>
B		<ol style="list-style-type: none"> <li>5. Place and secure the textile substrate (Side A) above the printed layer using binder clips and blue tape.</li> </ol>
C		<ol style="list-style-type: none"> <li>6. Resume the printer to complete the subsequent print layers.</li> <li>7. Remove the panel from the build platform when the print was completed.</li> </ol>
D		<ol style="list-style-type: none"> <li>8. Print Set B by repeating the steps in procedure A.</li> </ol>

E		<p>9. Place and secure the textile substrate (Side B) above the printed layer using binder clips and blue tape.</p> <p>(The base layer from Set A should be facing up when printed on the opposite side of the fabric).</p>
F		<p>10. Resume the printer to complete the subsequent print layers.</p>

During the printing process, it is important to ensure that the subsequent print layers (printed above the textile substrate) adhered well to the bottom layer. An unbonded area would cause the print structure to lift and curl upwards when responded to nozzle heat during the printing process as shown in Figure 6.7. This scenario must be avoided, and the specimen needs to be reprinted.

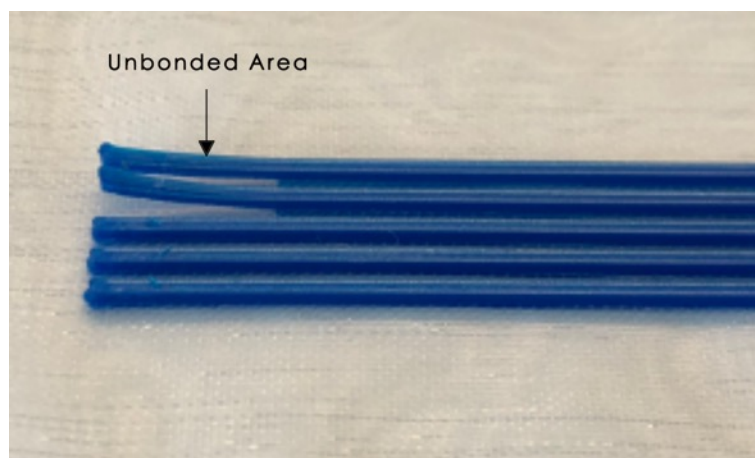


Figure 6.7. Lifting and curling of the printed structure when did not bond properly with the previous layer.

As woven types of fabric fray easily, a single-line border can be printed to embed the textile substrate between two print layers to prevent soft fringing on the edges when the fabric was cut. It also enables the specimens to be cut into the same size (Figure 6.8). The offset distance was set at 15mm from the printed structure(s) for this study. This value can be changed as long as the printed border remained narrow (suggested at 0.42mm wide and 0.3mm thick) to ensure that it has no impact on the shape change behaviour of the 4D printed thermo-responsive textiles.

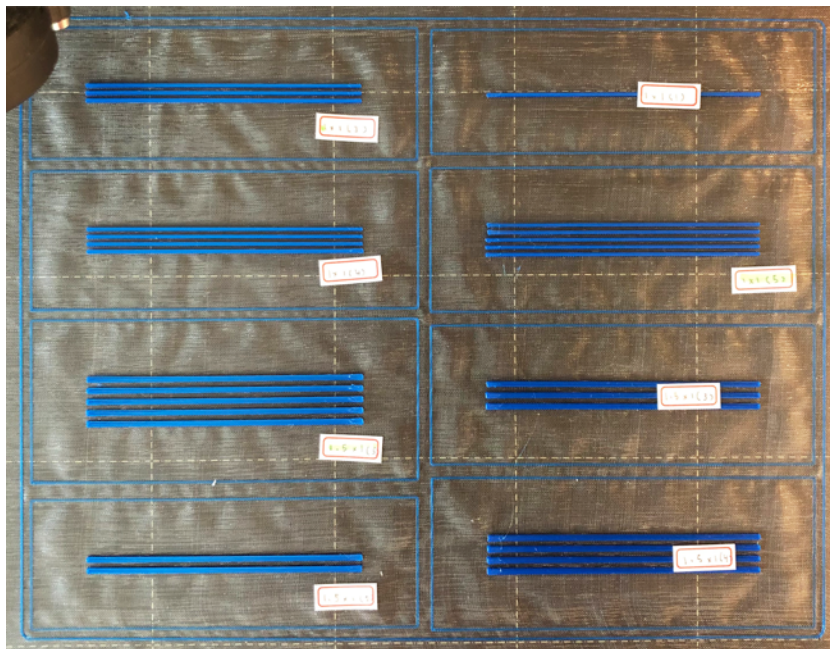


Figure 6.8. Printed single-line border to prevent frayed edges when the fabric was cut and to enable the specimens to be cut into the same size.

### 6.3.2. Experimental Procedures

The shape change behaviour of the 4D printed thermo-responsive textiles was actuated through joule heating directly from the water. This method was used because it was abundant and can ensure consistent and uniform heating on all areas of the specimen. This type of thermal triggering means resembles soaking and washing of the textiles in heated standing water. The tools and equipment used, and the experiment set-up was the same as detailed in Chapter 4.3.2, excluding the forming jigs, which were not required in this study. In this study, all specimens were activated three days after fabrication to eliminate the influence of duration to heating activation on the response rate and SCE.

The shape-changing process starts from the printed shape (primary shape) and ends at an actuated shape (secondary shape), as shown in Figure 6.9. The response time was taken using a stopwatch and videography for more accurate results.

1. The printed specimen is immersed into the heated water bath at  $T_r$  to actuate shape change.
2. The  $T_a$  and the duration for complete shape change is recorded using a stopwatch. The stopwatch is stopped when there is no further shape change. Alternatively, the response time can be taken through videography for more accurate results.
3. The specimen is removed from the water bath and allowed to cool to room temperature. A cloth can be used to remove any excess water. The actuated shape of the printed structure rehardens at room temperature. The secondary form is maintained.
4. The shape change rating (R), the controllability and accuracy of deformation of the actuated shape are measured using the respective bend recovery measuring chart.

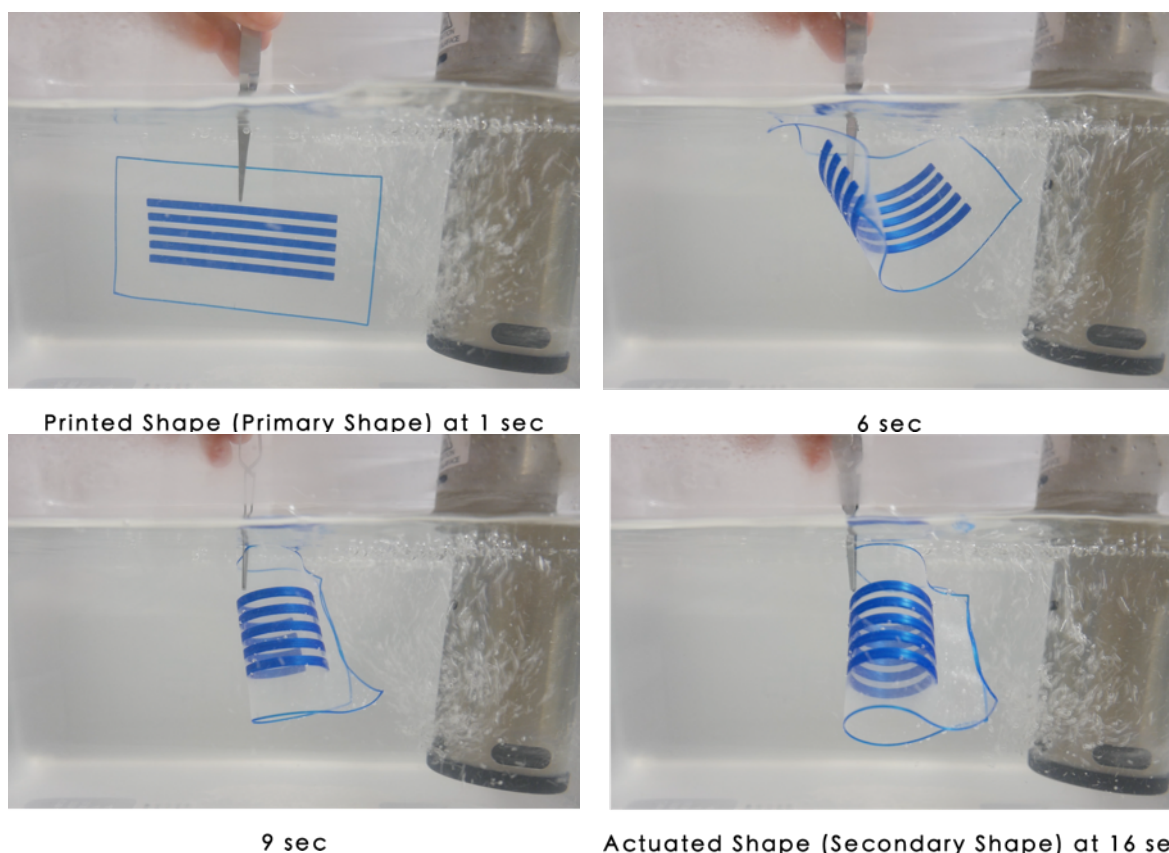
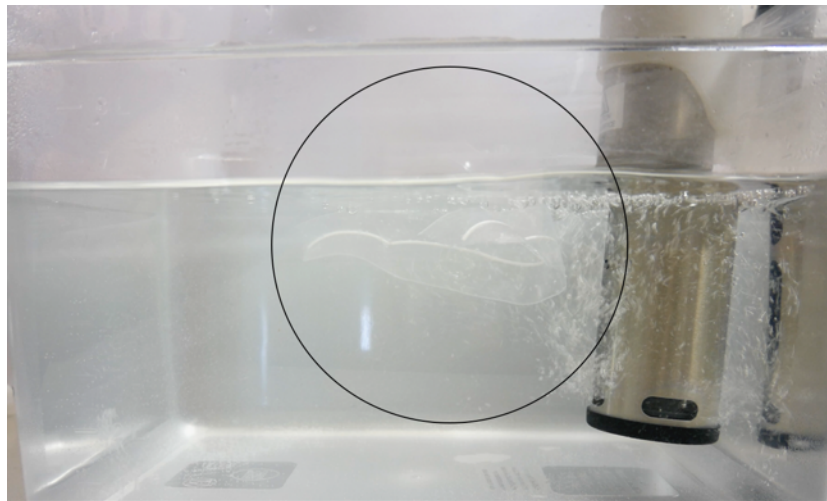


Figure 6.9. The specimen immersed in the heated water undergoing shape transformation into a circular bend.

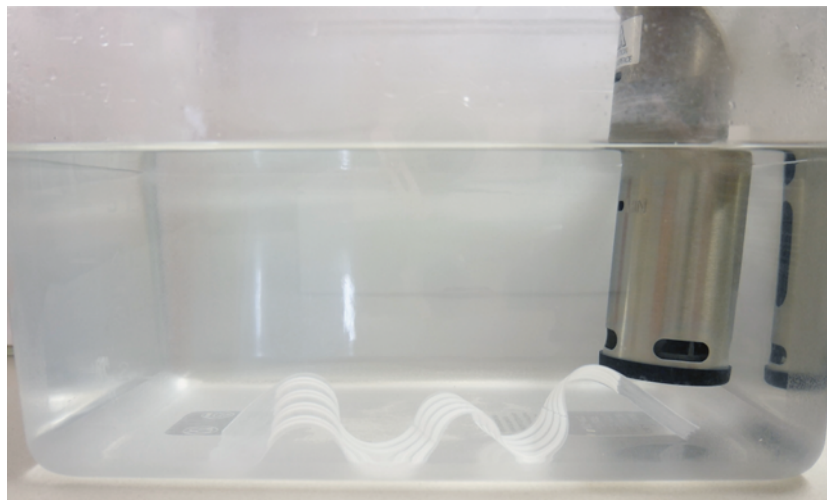
During the heating activation test, it was observed that the water circulation generated by the thermal immersion circulator would cause the specimens to float and move about actively in the water bath, consequently affecting the shape change of the specimen (Figure 6.10A). The actuated shape was disturbed and altered by the water force led to irregular shape deformation. It was also difficult to capture the duration for complete shape change. These particularly impacted specimens with the printed structure of 1mm width or 0.5mm thickness as they were not strong enough to retain their actuated shape. As a solution, it was suggested to switched off the thermal immersion circulator to actuate the specimen in a standing water environment at  $T_r$  (Figure 6.10B). Wan *et al.* (2019) explained that the shape change could occur at a close rate even if the water temperature fell slightly below the optimum  $T_r$ .

**A**



The thermal immersion circulator was switched on

**B**



The thermal immersion circulator was switched off

Figure 6.10. The impact of the water circulation generated by the thermal immersion circulator on shape transformation.

Two bend recovery charts were designed to measure the shape change rating (R), the controllability and accuracy of deformation of the actuated shape. The same bend recovery chart introduced in chapter four (Figure 4.8) was used to measure the bend deformation of specimens. Another bend recovery chart (as presented in Figure 6.12) was created to measure the deformation results of smaller diameters, which were more applicable for specimens with printed structural lengths between 15mm to 45mm. The pass and failure feature on the bend recovery chart (in Figure 4.8) did not apply to this experiment.

The controllability and accuracy of the bend deformation were determined by comparing the actuated curvature with the illustration on the measuring charts. The deformation classification was rated into three categories, (I) least, (II) average and (III) most controllable and accurate. Figure 6.11 specifies the three different colours assigned for easier differentiation of the deformation results (applied in Table 6.7, Table 6.9 and Table 6.11).

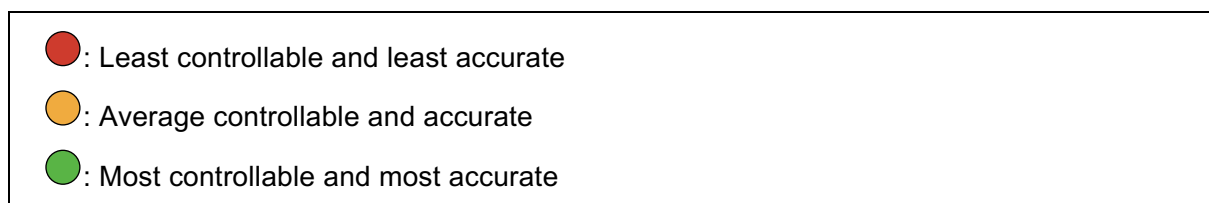


Figure 6.11. Deformation classifications and their assigned colour codes.

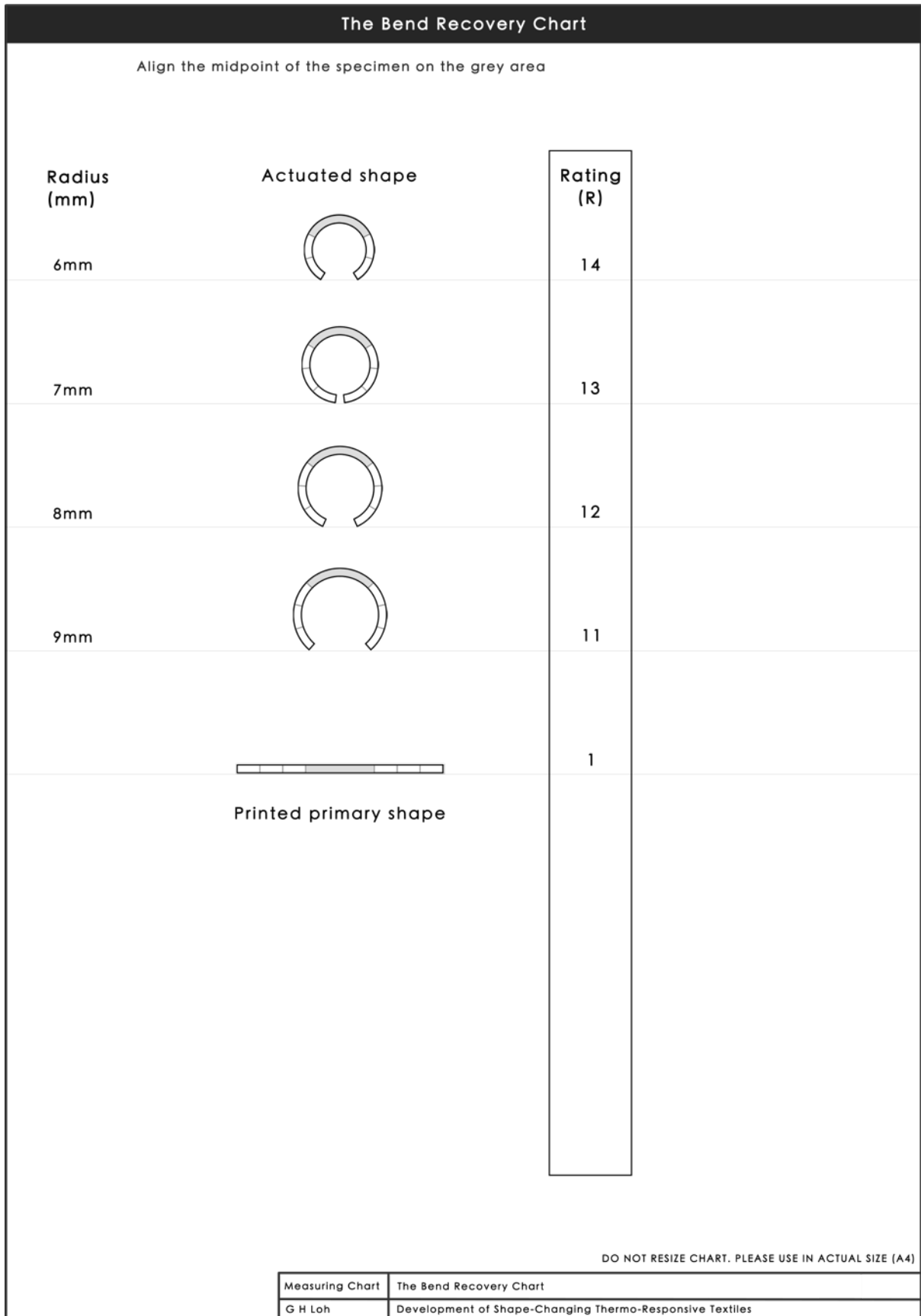


Figure 6.12. The bend recovery chart (15mm - 45mm).

## 6.4. Results and Discussion

The release of internal stresses and strains stored in the SMP structure during the ME deposition induced the shape change when responded to the appropriate temperature ( $T_r$ ). The results showed that the deformation mechanism for Filamentum PLA – Nylon (voile structure) – Filamentum PLA orientation is bending. It can be found that the curvature transformed in an opposite direction to the first print layer (Figure 6.13). This revealed that the bending direction of the 4D printed shape-changing thermo-responsive textiles is influenced by the position of the first SMP layer.

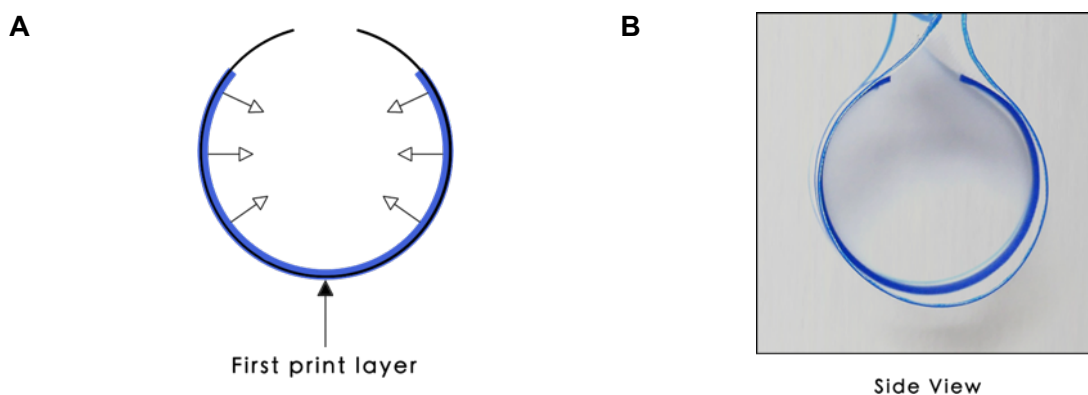


Figure 6.13. Bend occurred in an opposite direction to the first print layer. (A) schematic diagram and (B) photograph of specimen.

The following sections discuss the effect of the geometrical dimensions and structural arrangements on the shape change behaviour of the 4D printed thermo-responsive textiles. The recorded results for each category were an average value calculated from three specimens. The results from each experiment were qualitatively and quantitatively analysed and presented comparatively to reveal the shape transformation that can be achieved using particular design parameters. The optimum geometric parameters to achieve the most predictable and accurate deformation were also reported.

### 6.4.1. Geometrical Dimensions

#### 6.4.1.1. Experiment 1: Effect of $T_r$ and Structural Thickness

Experiment 1 disclosed the response time and SCE of the different printed structural thicknesses when exposed to two different actuation temperatures of water (Tr at 60°C and 65°C). The results in Table 6.7 and Figure 6.14 reveal that Tr of 65°C provided a faster response rate than 60°C. The Ta and time taken for complete shape transformation decreased by at least 60% when the Tr was raised by 5°C. The overall response time also reduced gradually as the structural thickness increased from 0.5mm to 1.0mm. This trend was particularly clear on specimens actuated at Tr 60°C. Conversely, the total response time for all specimens at Tr of 65°C were almost similar, at approximately 4 seconds to actuate and 10 seconds to complete shape change despite the differences in thickness. The optimum Tr, 65°C was applied for the following experiments.

Table 6.7. Effect of Tr and structural thickness on the response rate and SCE.

Thickness (mm)	60°C			65°C		
	Ta (s)	T (s)	R	Ta (s)	T (s)	R
0.5	24	45	10	7	18	10
0.6	23	50	10	3	10	10
0.7	24	50	10	3	10	10
0.8	14	40	10	3	9	10
0.9	12	30	10	4	9	10
1.0	11	28	10	4	10	10

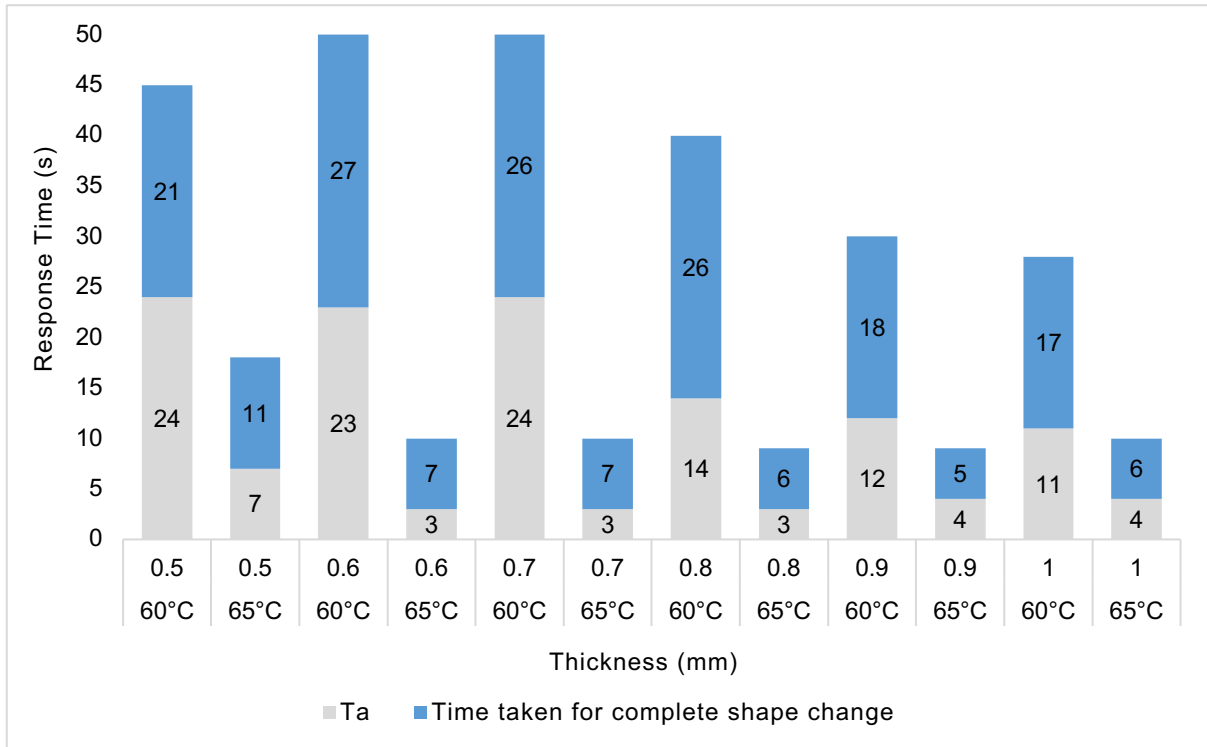
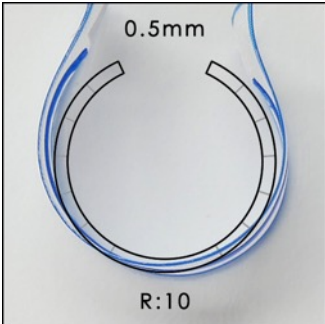
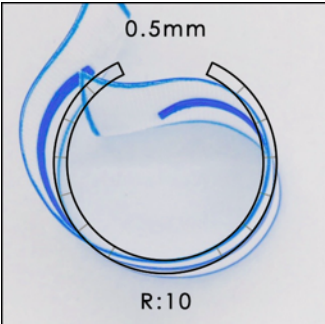
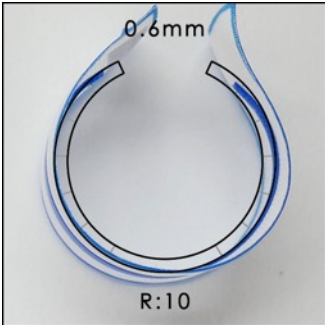
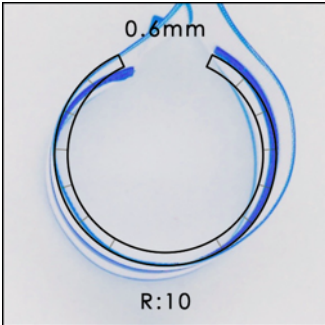
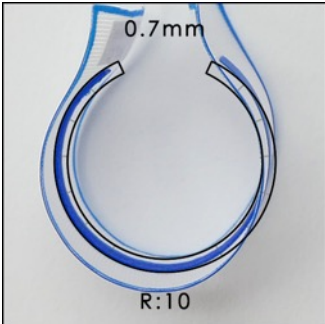
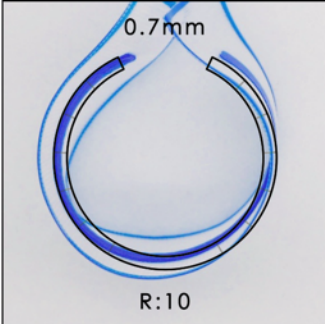
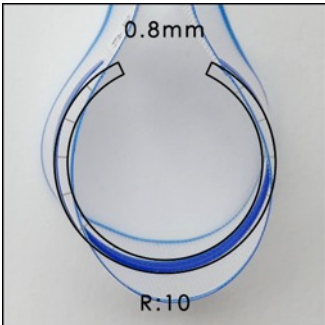
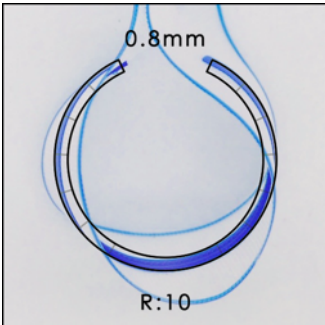
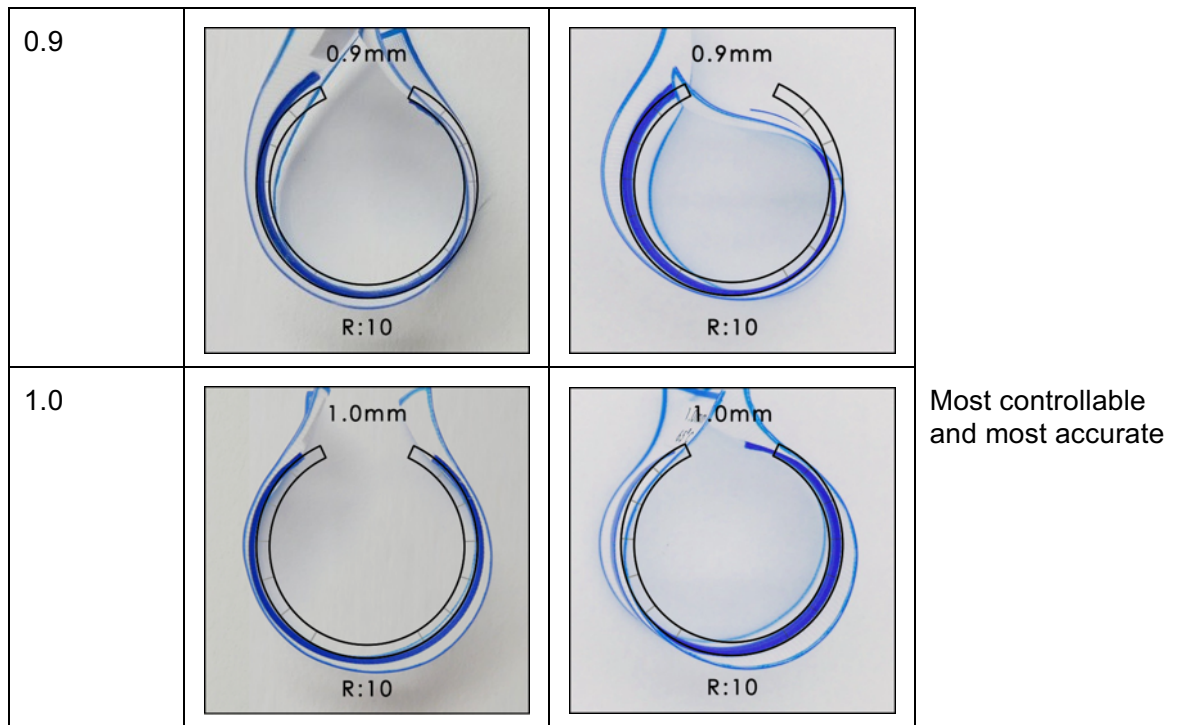


Figure 6.14. Effect of  $T_r$  and structural thickness on the response time.

Concerning the effect of structural thickness on the shape transformation behaviour, the controllability and accuracy of deformation increased when the structural thickness increased. In reference to Table 6.8, although all specimens in six different structural thicknesses can achieve the same degree of curvature at R:10, it was clear that the actuated shapes for specimens with a lower thickness of 0.5mm to 0.7mm were less controllable and less accurate. The printed structures were too thin and incapable of retaining their actuated shapes. Their actuated shapes were easily affected by the movement of the embedded textile in the water and by the pulling force while removing the specimen from the water bath (at  $T_r$ ) as the SMP was still in its rubbery and pliable state. There was greater control in deformation as the structural thickness increased from 0.8mm to 1.0mm. The structural thickness of 1.0mm provided the most controllable and accurate deformation, which therefore carried forward as a constant variable for the following experiments.

Table 6.8. Effect of structural thickness on the shape deformation.

Thickness (mm)	60°C	65°C	Deformation Classification
0.5			Least controllable and least accurate
0.6			
0.7			
0.8			



### 6.4.1.2. Experiment 2: Effect of Structural Width and Length

Experiment 2 examined the effect of structural width and length on the shape transformation behaviour. The results in Table 6.9 showed no indication of slower response time when the structural width and length increased. The total response time for the specimens was closely similar, at approximately 5 seconds to actuate and 12 seconds to complete shape change. The study discovered the diameter of bend deformation depends on the structural length. Two different bend patterns were produced, classified as semi-circle bend and circular bend. Semi-circle bend was produced from specimens with a structural length between 15mm to 35mm while circular bend was produced from the structural length between 45mm to 75mm. For the circular bends, there has been a steady increase in the bending diameter ( $\phi$ ) by 3mm when the structural length was increased by 10mm.

The structural width did not influence the diameter of the bend, but it controlled the accuracy of the actuated curvature. Based on the results shown in Table 6.10, it was obvious that the deformation became more controllable as the structural width increased. The actuated shapes for specimens with lower structural widths of 1.0mm and 1.5mm were distorted and least accurate. The specimens with a 3.5mm width provide the most predictable and most stable shape deformation. However, an interesting finding was that the specimens with the structural length of 15mm to 35mm demonstrated equally controllable deformation despite

the differences in structural widths. This may be due to the length-to-width ratio of the printed geometry.

The results from Experiment 1 and 2 revealed that the thickness and width of the printed SMP structure on the textile substrate played critical roles in controlling the deformation and the accuracy of the actuated shape. The structural thickness should be at least 0.8mm while the width should be at least 2.0mm to achieve controllable and accurate bend deformation. On the other hand, the structural length determined the bending diameter and the types of bend produced, either semi-circle bend or circular bend.

Table 6.9. Effect of structural width and length on the response rate and SCE.

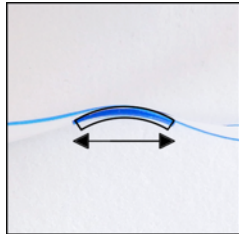
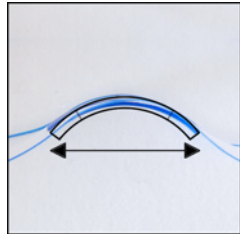
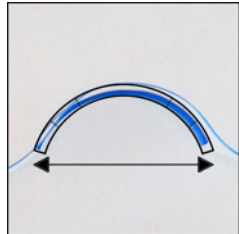
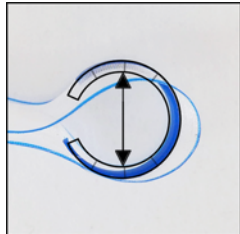
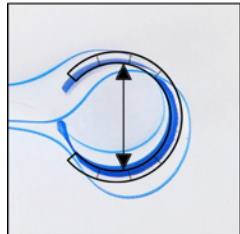
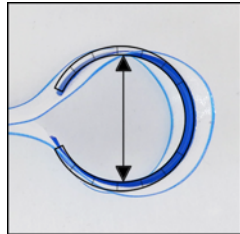
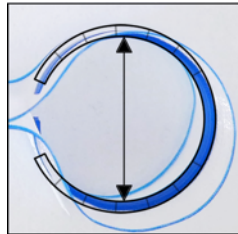
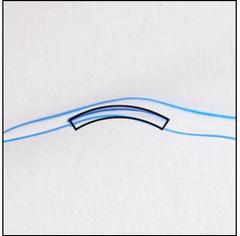
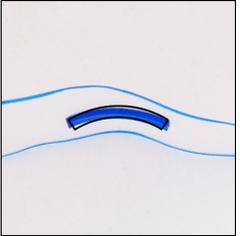
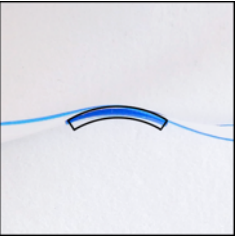
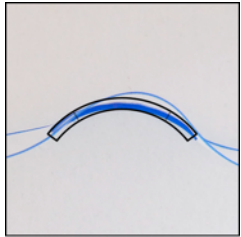
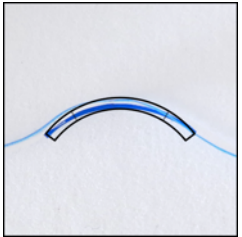
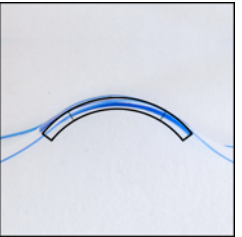
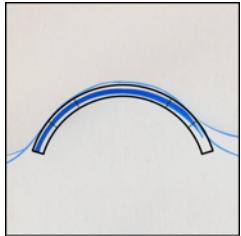
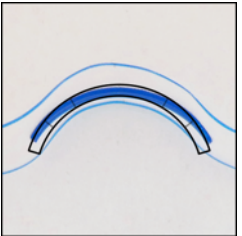
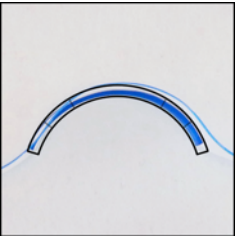
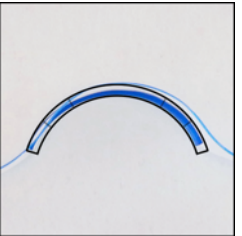
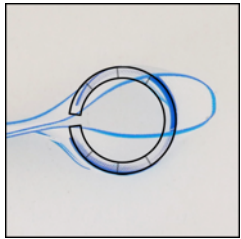
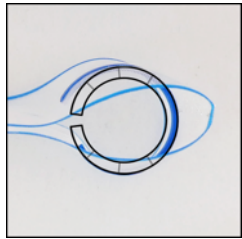
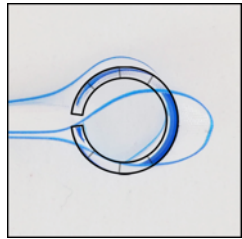
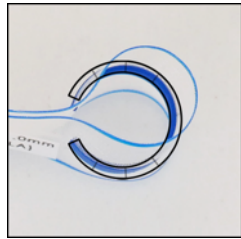
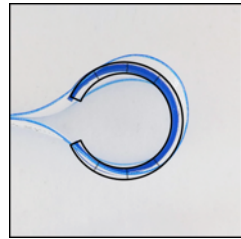
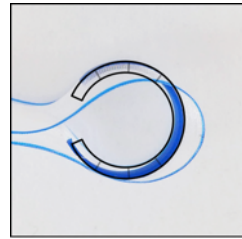
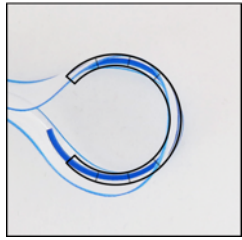
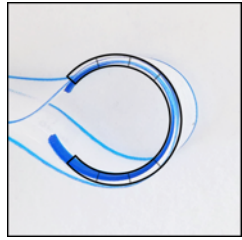
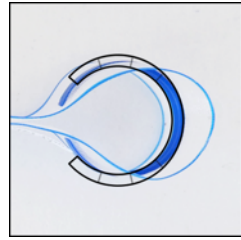
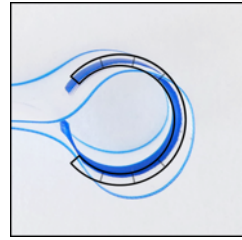
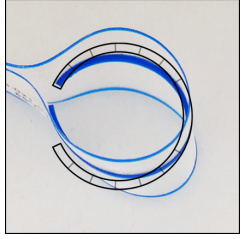
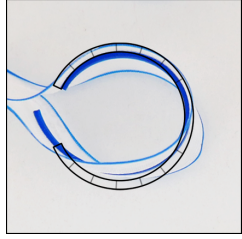
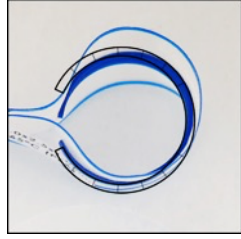
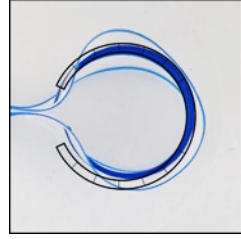
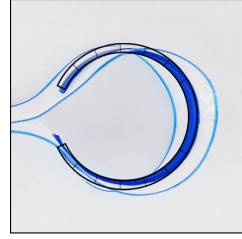
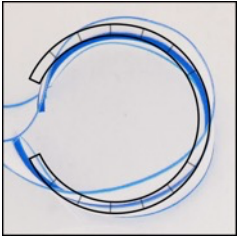
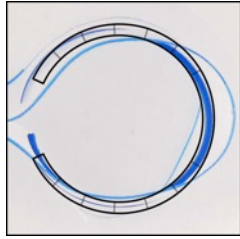
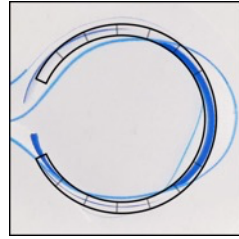
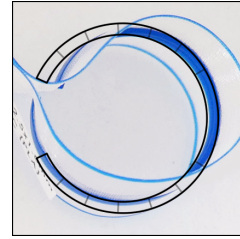
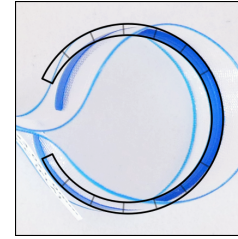
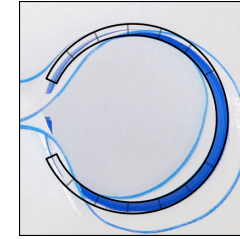
Width (mm)	Length (mm)																				
	15			25			35			45			55			65			75		
	Ta (s)	T (s)	R	Ta (s)	T (s)	R	Ta (s)	T (s)	R	Ta (s)	T (s)	R	Ta (s)	T (s)	R	Ta (s)	T (s)	R	Ta (s)	T (s)	R
1.0	5	15	10	4	13	10	4	15	10	4	18	13	4	13	13	5	13	10	5	10	10
1.5	5	11	10	3	9	10	4	17	10	4	12	13	5	15	13	4	13	10	5	10	10
2.0	4	9	10	3	8	10	3	16	10	5	12	13	5	10	13	4	13	10	5	10	10
2.5	5	9	10	3	9	10	3	15	10	5	14	12	5	10	12	5	12	10	6	10	10
3.0	5	9	10	3	10	10	3	13	10	5	14	12	5	10	12	5	13	10	6	11	10
3.5	4	9	10	4	11	10	5	18	10	5	15	12	5	11	12	5	12	10	6	11	10
∅ (mm)																					
	14mm			22mm			26mm			16mm			19mm			22mm			25mm		
Pattern	Semi-circle bend									Circular bend											

Table 6.10. Effect of structural width on the shape deformation.

Length (mm)	Width (mm)					
	1.0	1.5	2.0	2.5	3.0	3.5
15						
25						
35						
<b>Deformation Classification</b>	Equally controllable and accurate					

Length (mm)	Width (mm)					
	1.0	1.5	2.0	2.5	3.0	3.5
45						
55						
65						
<b>Deformation Classification</b>	Least controllable and least accurate		Average controllable and accurate		Most controllable and most accurate	

Length (mm)	Width (mm)					
	1.0	1.5	2.0	2.5	3.0	3.5
75						
<b>Deformation Classification</b>	Least controllable and least accurate		Average controllable and accurate		Most controllable and most accurate	

## **6.4.2. Structural Arrangements**

The following sections present the use of 4DP to create different types of projecting pleats, including, pinch pleats, cartridge pleats and pipe organ pleats, achieved by changing the arrangement of the printed SMP structure on the textile substrate. Pleat is a type of systematic folding method used to gather a wide piece of fabric to a smaller measurement. Projecting pleats are folds lifted from the surface of the fabric and arranged so that they can stand out from the fabric itself (Griffiths, 2021). Pleats are largely used in clothing and upholstery as a decorative feature or a functional feature to create fullness or texture to a shape (The Cutting Class, 2014; The Business of Fashion, 2021).

### **6.4.2.1. Experiment 3: Single Column and Multiple Rows**

Experiment 3 examined the correlation between the number of printed rows and structural width on the shape-shifting behaviour. The results in Table 6.11 showed a very slight increment in response time around 1 to 2 seconds as the structural width and the number of rows increased. The shape-shifting pattern was circular bending. The increment in the number of rows and structural widths do not influence the bending diameter. The bend rating remained unchanged at R:10 with a 25mm diameter.

Similar to the findings from Experiment 2, it can be seen from Table 6.12 that the actuated shape became more controllable and accurate as the structural width increased from 1.0mm to 3.0mm. The results also revealed that the deformation improved as the number of printed rows increased. Another striking finding was that multiple rows of narrow structures (i.e., five rows of 1.5mm) can achieve an equally controllable and accurate deformation as two rows of 3.0mm, as shown in Figure 6.15. This is a potential method to achieve the same deformation when the structural width cannot be modified.

Table 6.11. Effect of structural width and number of rows on the response rate and SCE.

Number or rows	Width (mm)														
	1.0			1.5			2.0			2.5			3.0		
	Ta (s)	T (s)	R	Ta (s)	T (s)	R	Ta (s)	T (s)	R	Ta (s)	T (s)	R	Ta (s)	T (s)	R
2	4	10	10	5	11	10	5	11	10	5	11	10	5	11	10
3	4	11	10	4	11	10	4	11	10	5	12	10	6	11	10
4	5	10	10	4	10	10	5	11	10	5	11	10	6	10	10
5	4	12	10	4	10	10	5	10	10	5	12	10	6	13	10

Equally controllable and accurate

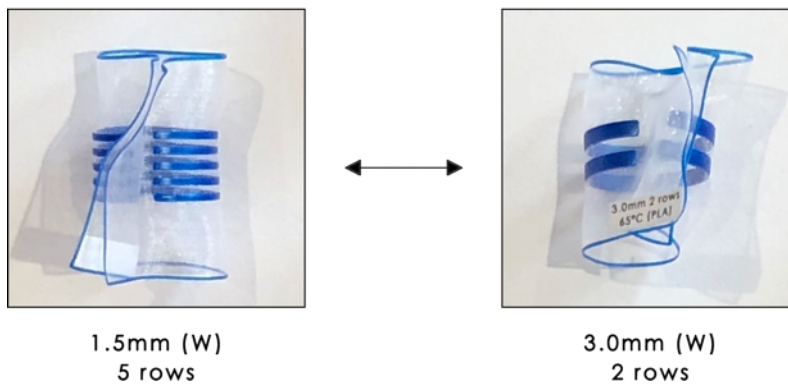
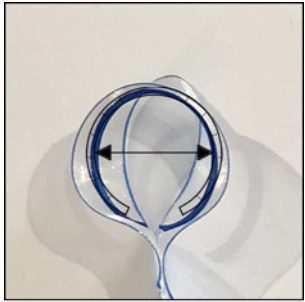
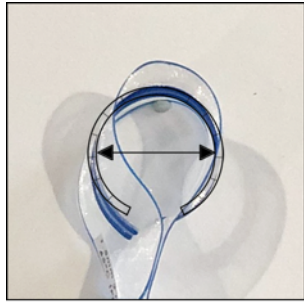
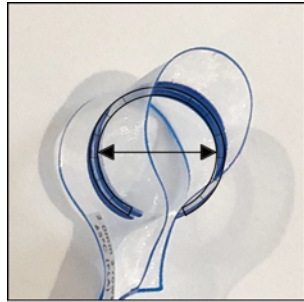
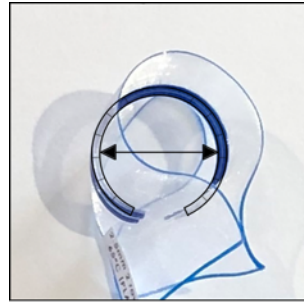
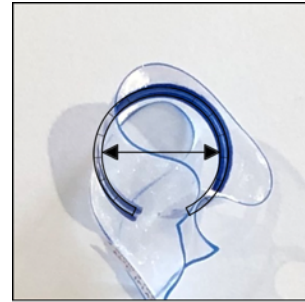


Figure 6.15. The controllability and accuracy of deformation can be improved by increasing the number of printed rows instead of modifying the structural width.

Table 6.12. Single column and multiple rows.

Number or rows	Width (mm)					Deformation Classification
	1.0	1.5	2.0	2.5	3.0	
2						Least controllable and least accurate
3						
4						

5						Most controllable and most accurate
Ø (mm)						
	25mm	25mm	25mm	25mm	25mm	
	Least controllable and least accurate		Average controllable and accurate		Most controllable and most accurate	

#### 6.4.2.2. Experiment 4: Multiple Columns and Single Row

The shape-shifting behaviours for the specimens printed in a single row and multiple columns can be seen in Table 6.13. This style of projecting pleats is known as continuous cartridge pleats, as shown in Figure 6.16. With a narrow column spacing of 0.5mm, sharp valleys were formed between the actuated curvatures on either side (Wolf, 2003). This resulted in a double pinch pleating effect on the other side of the specimen. The type of pleats displayed varies, depending on which side of the specimen was positioned to face the viewer.

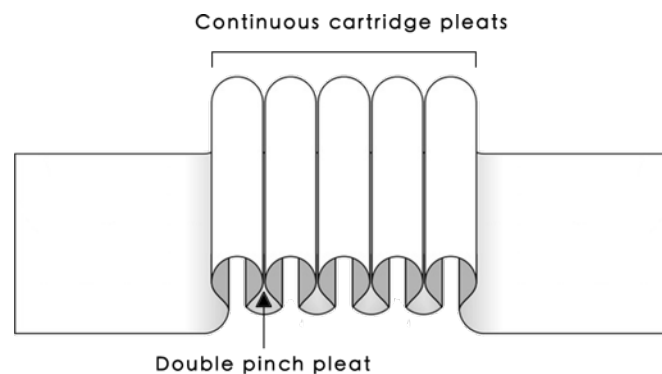


Figure 6.16. Continuous cartridge pleats with double pinch pleats on the other side.

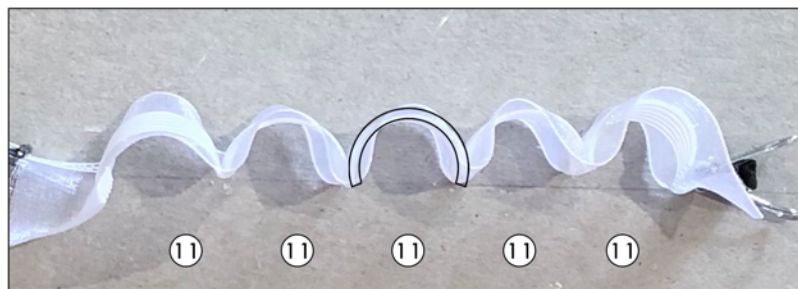
The response rate and SCE for the two sets of specimens with varied structural widths and lengths can be compared in Table 6.13. The response rate for both sets of specimens were identical despite a 10mm difference in structural length. The results indicated that the  $T_a$  was delayed by 1 second as the structural width increased by 1mm. However, there was no increase in the time taken for a complete shape change was detected.

In regard to the SCE, none of the specimens can achieve the most controllable and most accurate deformation. Structural width of 1mm showed the best shape-shifting behaviour among the three printed structural widths (Table 6.13). At least the continuous cartridge pleats were formed in a straight line. It can be seen that the deformation became harder to control and less precise as the structural width increased. The actuated SMP structures for specimens with structural width of 2mm and above curved in different directions, with some deformed upwards, downwards or slightly slanted. This can be seen particularly clearly on the two specimens, 35mm x 2mm and 45mm x 3mm (L x W).

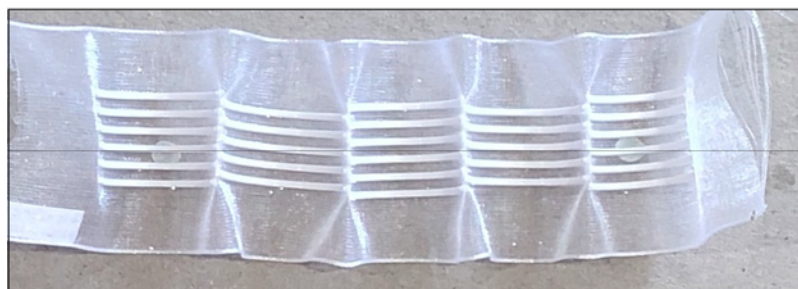
It was also observed that the actuated shapes and bending diameter were inconsistent. The bend ratings varied between R:10 and R:11 in most specimens. “X” was used to indicate the actuated shape that was distorted. Observations suggested that this may be linked to the narrow column spacing. The shape distortion was caused by the interference from the neighbouring structures during the shape transformation process. Other contributing factors would be the movement of the embedded textile in the water or by the pulling force while removing the specimen out from the water bath (at  $T_r$ ) as the SMP was still in its rubbery and pliable state. As a solution, the method (discovered in Experiment 3) was applied to increase the controllability and precision of the shape-shifting behaviour. As shown in Figure 6.17, the bends formed were more consistent in shape and size when multiple printed rows were introduced. The increment in the number of printed rows helped to reinforce the rolls of the pleats, which led to more visible continuous cartridge pleats and double pinch pleats.



Continuous cartridge pleats from the top



Pleat profile from the side

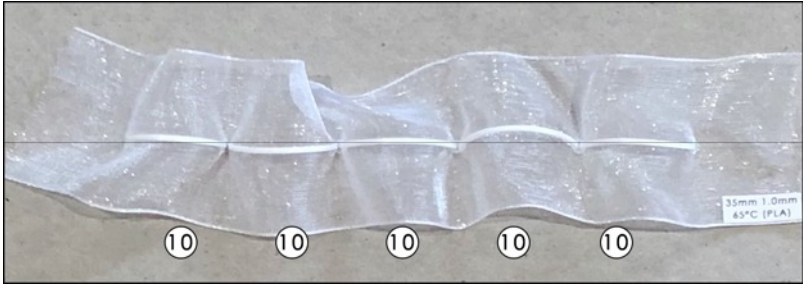
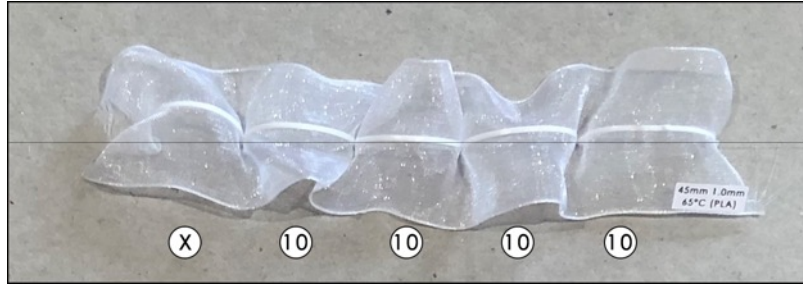
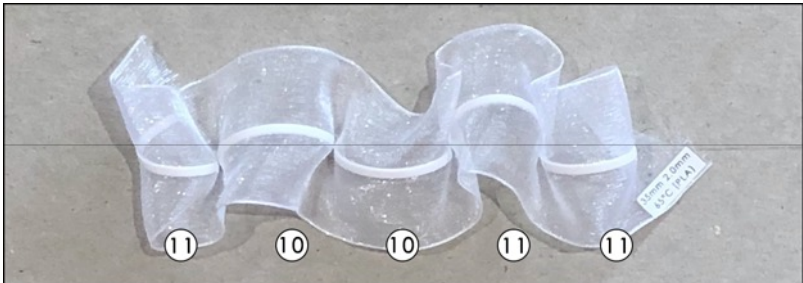
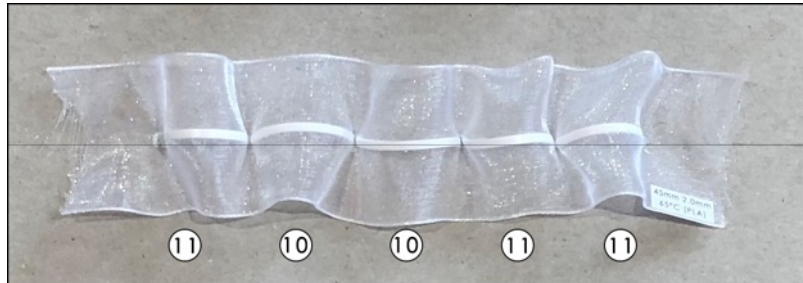


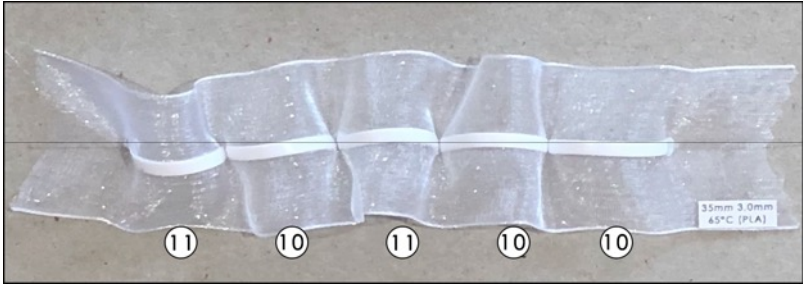
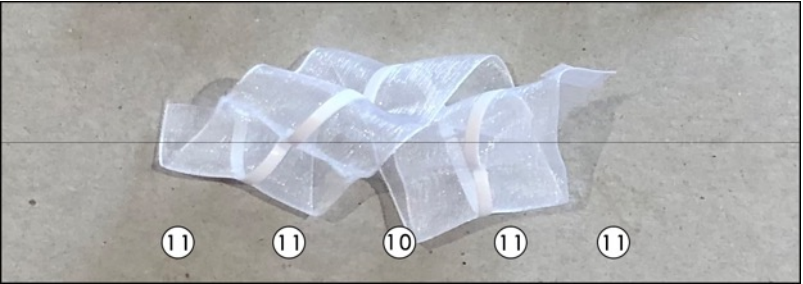
Double pinch pleats from the bottom

Figure 6.17. Increase the precision of the projecting pleats by introducing multiple printed rows.

Another additional finding was the actuated shapes (bend pattern) would vary according to their structural arrangements. The actuated shape for structural length 45mm was a circular bend when printed in a single column (Table 6.9) Whilst a semi-circle was formed when printed in multiple columns.

Table 6.13. The influence of structural width and length on the response rate and SCE of multiple columns and single row.

Width (mm)	Length (mm)					Deformation Classification
	35			45		
1						Average controllable and accurate
	Ta (s)	5	T(s)	20	R	
2						
	Ta (s)	5	T(s)	18	R	
2						
	Ta (s)	6	T(s)	18	R	
2						
	Ta (s)	6	T(s)	20	R	

3											Least controllable and least accurate
	<b>Ta (s)</b>	7	<b>T(s)</b>	18	<b>R</b>	10, 11	<b>Ta (s)</b>	7	<b>T(s)</b>	20	

### 6.4.2.3. Experiment 5: Multiple Columns and Rows

Figure 6.18 and Figure 6.19 illustrate another type of cartridge pleat (standard cartridge pleats) produced when the column spacing changed from 0.5mm to 35mm. This type of pleats also looked like pipe organ pleats (Wolf, 2003). This study revealed that different types of pleating effects can be created by varying the spacing between the printed columns.

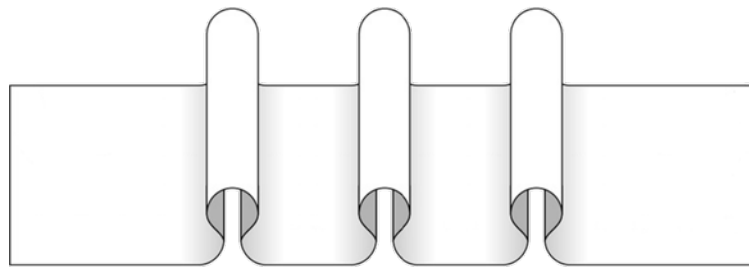
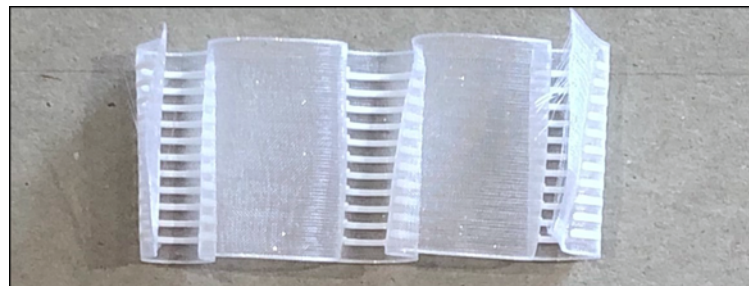
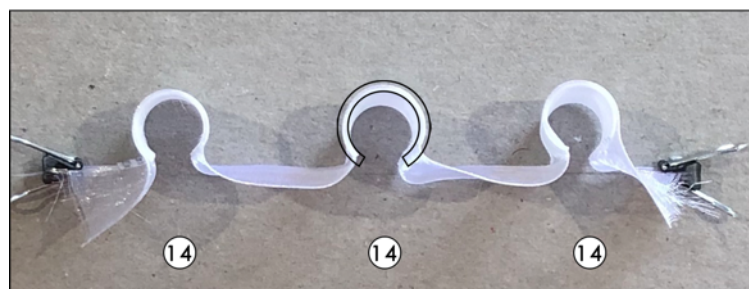


Figure 6.18. Pipe organ pleats.



Pipe organ pleat from the bottom



Pleat profile from the side

Figure 6.19. The shape-shifting behaviour when printed in multiple columns and rows with column spacing of 35mm.

In addition, the study revealed that the column spacing influenced the diameter and pattern of the bend. The bending diameter reduced as the column spacing increased. The bending

diameter reduced from 26mm to 11mm when the column spacing increased from 0.5mm to 35mm, which consequently changed the bend pattern from a semi-circle to a circular bend. (Table 6.14). One possible reason would be that with a narrow column spacing, the neighbouring structures act as a hinge that stops the transformation when they hit against each other. When the printed columns were more spaced out, there were sufficient space or tolerance for the printed structures to undergo full transformation without interference by the neighbouring structures.

Table 6.14. The influence of column spacing on the bending diameter and shape-shifting pattern.

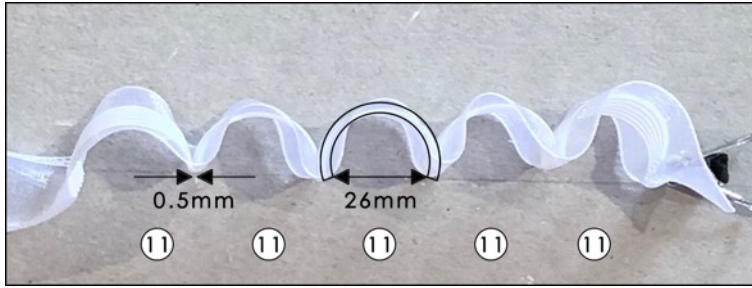
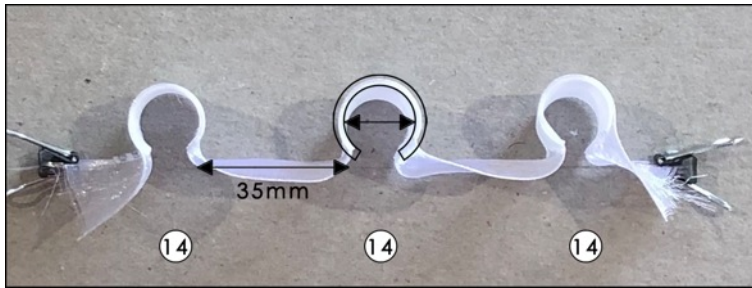
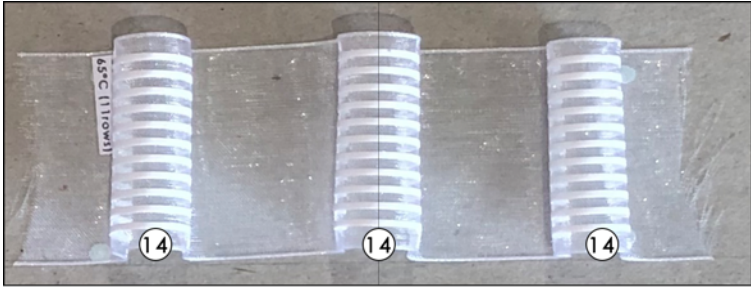
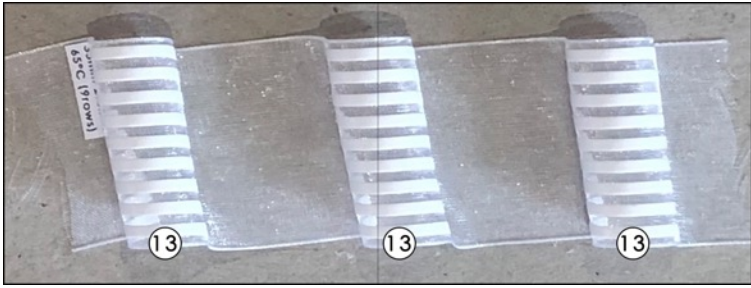
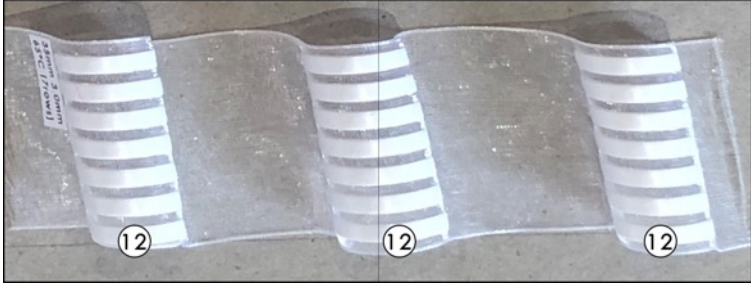
Width (mm)	Column Spacing (mm)	Length (mm)	Comments
		35	
1	0.5		The bending diameter reduced as the column spacing increased.
	35		

Table 6.15 presents the response rate and SCE of the specimens in three structural widths. Similar to the previous experiments, the specimen took approximately 5 seconds to actuate, with the  $T_a$  increased as the structural width increased. However, the time to complete shape change increased by nearly two times (from 18 seconds to 30 seconds) when multiple rows were introduced. Concerning the SCE, the bending diameter increased as the structural width increased. The structural width affected the angle of the pipe organ pleats produced. The printed column diverged from the vertical when the structural width was set at 2mm and 3mm, generating angled pipe organ pleats. The structural width needs to be at 1mm to obtain vertical pipe organ pleats.

Table 6.15. The influence of structural width on the response rate and SCE of multiple columns and rows.

Width (mm)	Length (mm)					Pattern	Deformation Classification
	35						
1						Vertical pipe organ pleats	Most controllable and most accurate
	Ta (s)	5	T(s)	30	R		
2						Angled pipe organ pleats	Average controllable and accurate
	Ta (s)	6	T(s)	32	R		
3						Angled pipe organ pleats	Least controllable and least accurate
	Ta (s)	7	T(s)	35	R		

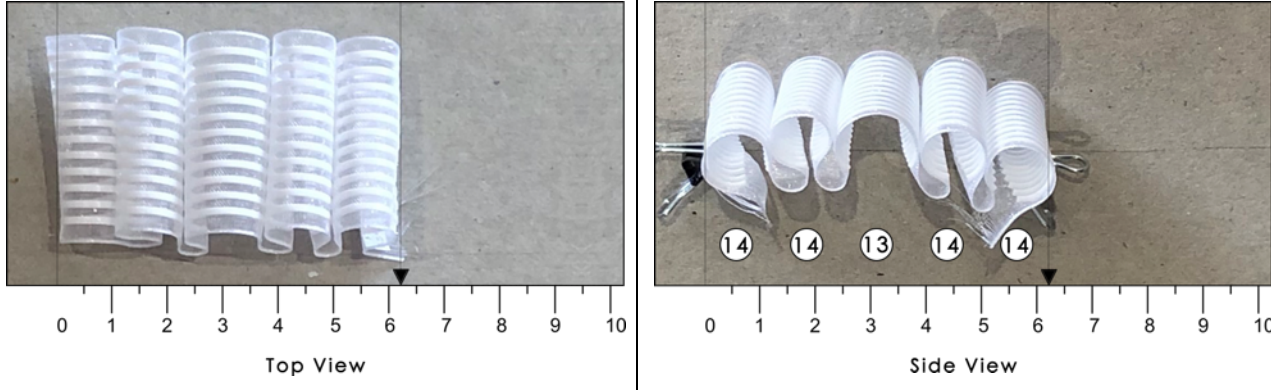
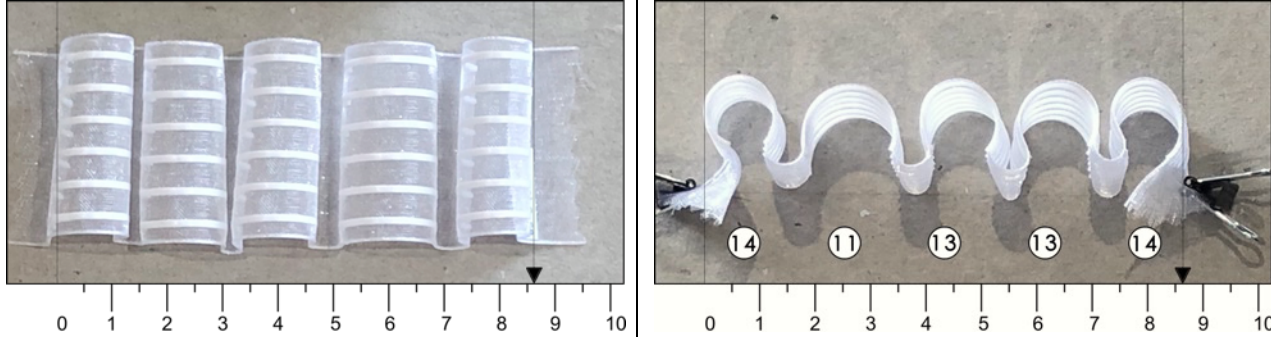
#### 6.4.2.4. Experiment 6: Varied Row arrangements

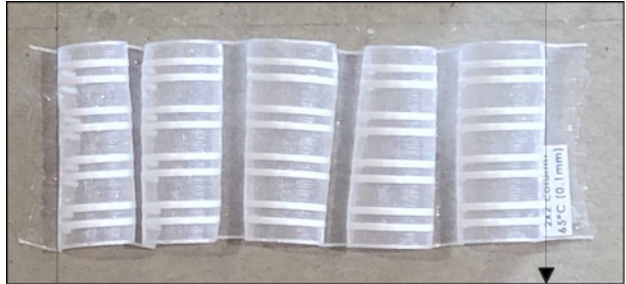
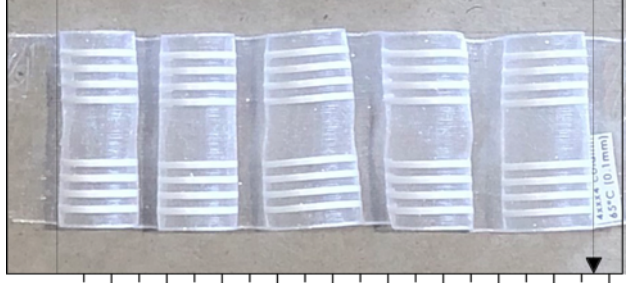
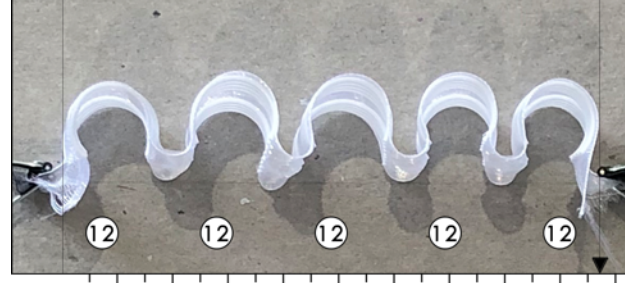
The results from Table 16 reported that the row arrangements of SMP structures have a significant impact on the gathering lengths and pleats interval. The cartridge pleats were more gathered when the rows were arranged closer to each other. On the contrary, the pleats were less gathered when the printed rows were further apart. This was due to the bending diameter was smaller when the rows were arranged closer to each other and were

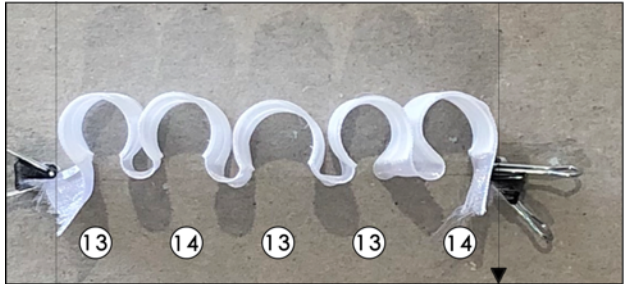
larger when the printed rows were further apart. Pattern No. 1 provided the most tightly gathered cartridge pleats, subsequently followed by patterns No. 4 and No. 6. These patterns would be most effective in gathering a large amount of fabric into a smaller circumference or shorter length. Whilst pattern No. 5 provided the least gathered pleats with the most spaced pleats interval.

The results also revealed that the deformation was more controllable when the printed rows were closer, with more consistent actuated shapes and bending diameter (i.e., patterns No. 4 and No. 5). However, this cannot prove that these patterns can always provide the exact results as there are other unforeseen factors during the heating activation and removal processes that may affect the shape-change result. The total response time for all specimens at Tr of 65°C were almost similar, at approximately 5 seconds to actuate and 33 seconds to complete shape change despite the differences in row arrangements.

Table 6.16. The influence of row arrangements on the response rate and SCE.

Pattern No.	Shape-shifting Behaviour	Ta (s)	T (s)	R	Deformation Classification
1	 <p>The top view shows five vertical columns of white corrugated material, each approximately 2 units wide, with a ruler below from 0 to 10. A black triangle points to the 6 mark. The side view shows the same material from a side perspective, held flat by clips, with a ruler below from 0 to 10. A black triangle points to the 6 mark. Circled numbers 14, 14, 13, 14, 14 are placed below the peaks of the columns.</p>	5	38	13, 14	Average controllable and accurate
2	 <p>The top view shows five vertical columns of white corrugated material, each approximately 2 units wide, with a ruler below from 0 to 10. A black triangle points to the 9 mark. The side view shows the same material from a side perspective, held flat by clips, with a ruler below from 0 to 10. A black triangle points to the 9 mark. Circled numbers 14, 11, 13, 13, 14 are placed below the peaks of the columns.</p>	4	35	11, 13, 14	Least controllable and least accurate

3	 <p>0 1 2 3 4 5 6 7 8 9 10</p>	 <p>0 1 2 3 4 5 6 7 8 9 10</p>	4	30	12, 13	Average controllable and accurate
4	 <p>0 1 2 3 4 5 6 7 8 9 10</p>	 <p>0 1 2 3 4 5 6 7 8 9 10</p>	5	35	14	Most controllable and most accurate
5	 <p>0 1 2 3 4 5 6 7 8 9 10</p>	 <p>0 1 2 3 4 5 6 7 8 9 10</p>	5	26	12	Most controllable and most accurate

6			5	30	13, 14	Average controllable and accurate
---	---	--	---	----	-----------	---

#### 6.4.2.5. Experiment 7: Print Configuration

Inspired by the sinusoidal strip demonstrated by Tibbits *et al.*, (2014) as shown in Figure 6.20, Experiment 7 recreated similar waving effects that can be produced by alternating the placement of the SMP structures on different sides of the textile substrate (Table 6.4).



Figure 6.20. Sinusoidal strip by Tibbits *et al.* (2014) operates under the principle of a bilayer actuator made up of expanding material (water-responsive hydrogel) and passive rigid material.

As explained in Figure 6.13, the bend direction was controlled by the position of the first SMP layer. Printing the SMP structures on different sides of the textile substrate interchanged the position of the first SMP layer, making the bends perform in opposite directions to create a waving effect (Figure 6.21). There was no need of using a bilayer mechanism or placement of another material to perform different interactions.

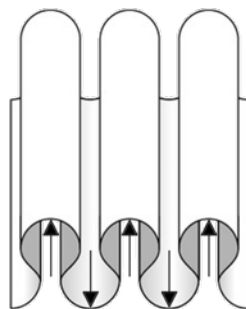


Figure 6.21. Cartridge pleats with waving effect.

The specimen with structural width of 1mm showed the best waving effect among the three printed structural widths (Table 6.17). Similar to the findings in Experiment 4, the actuated shapes and bending diameter were inconsistent when printed in a single row. The deformation also became harder to control and less accurate as the structural width increased. It was believed that increasing the number of rows (in Experiment 8) can lead to a higher deformation accuracy.

Regarding the response time, there was no difference in  $T_a$  compared to other sets of experiments. However, the overall time taken to complete this type of shape-shifting behaviour took approximately one minute. It was roughly three times longer compared to Experiment 4 which the set of specimens was also printed in a single row. The study revealed that more time was required to perform opposite movements.

Table 6.17. The influence of structural width on the response rate and shape-shifting behaviour.

Width (mm)	Length (mm)					Deformation Classification
	35					
1						Average controllable and accurate
	$T_a$ (s)	5	$T$ (s)	54	<b>R</b>	
2						Least controllable and least accurate
	$T_a$ (s)	5	$T$ (s)	52	<b>R</b>	
3						Least controllable and least accurate
	$T_a$ (s)	5	$T$ (s)	52	<b>R</b>	

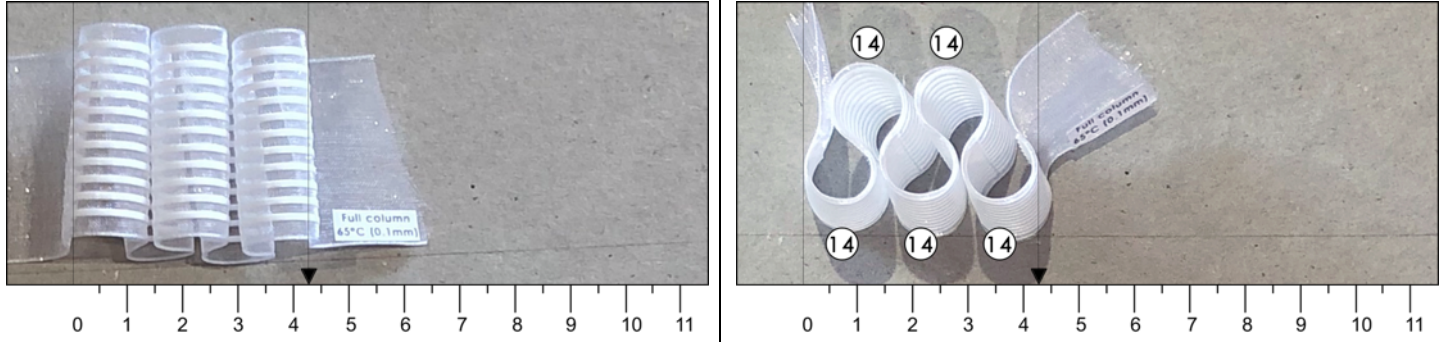
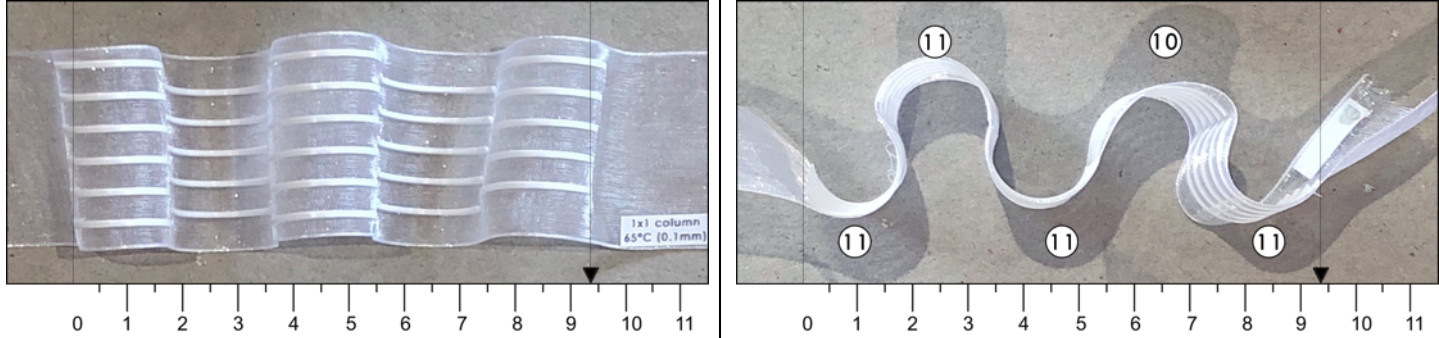
#### **6.4.2.6. Experiment 8: Print Configuration with Varied Row arrangements**

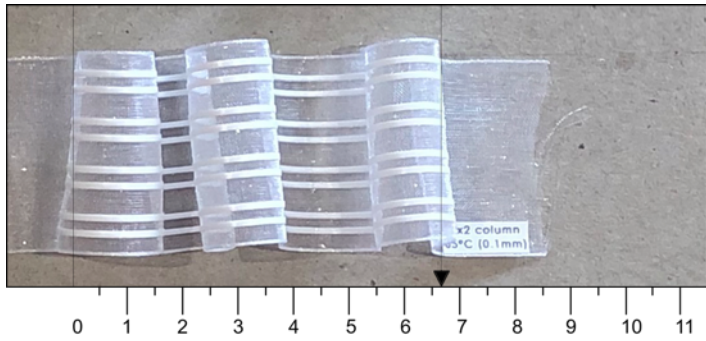
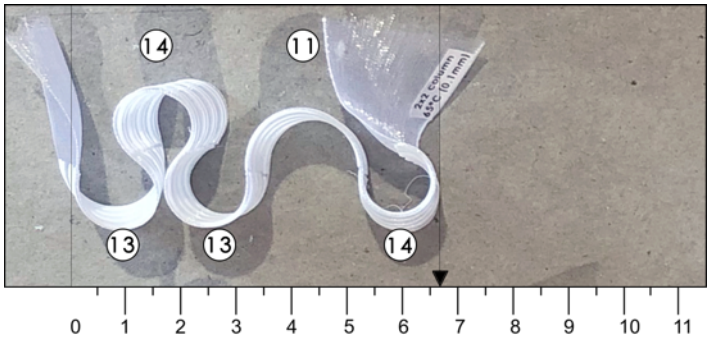
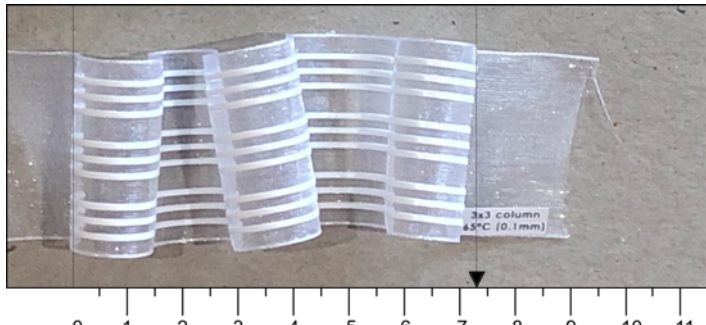
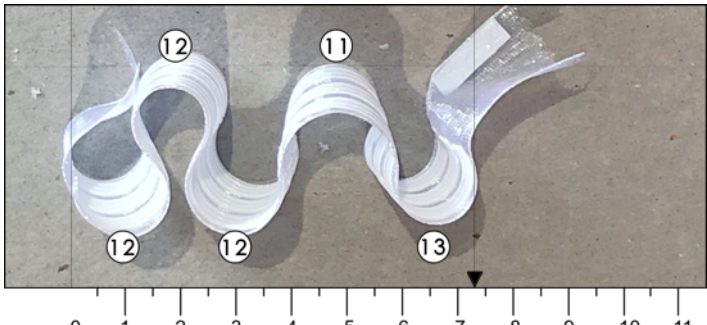
Table 6.18 compares the response time and shape-shifting behaviours for the specimens printed in multiple rows and different row arrangements. The response time for these specimens were almost the same, with approximately 5 seconds to actuate and slightly over one minute to complete shape change despite the differences in row arrangements.

The arrangement of the SMP structures on the textile substrate can be modified to achieve the pleats effect and silhouette required (i.e., designed to project a little or a lot). Similar to the findings for Experiment 6 (Table 6.16), the gathering lengths and pleats interval can be tailored by changing the row arrangements of SMP structures, without modifying the structural length and width. It can be seen that the waving effects became more visible when multiple rows were applied. Pattern No.1 transformed into the most gathered. This type of shape-shifting pattern is known as butted cartridge pleats, made up of a series of small rounded stand-away folds, creating a signature "figure 8" style structure (Wolf, 2003). Pattern No. 2 on the other hand, provided the least gathered pleats.

The results in Table 6.18 still showed inconsistencies in the bending diameters, particularly in specimens with patterns No. 2, 3 and 4. To avoid the actuated shape from being distorted by the pulling force while taken out from the water bath (at  $T_r$ ), it was suggested to remain the specimen in the water bath until the water temperature has cooled below the  $T_r$  or to room temperature before the removal process. This allows the SMP to reharden from its rubbery state so that the actuated shape can be preserved.

Table 6.18. The influence of row arrangements on the response rate and SCE.

Pattern No.	Shape-shifting Behaviour	Ta (s)	T (s)	R	Deformation Classification
1		5	61	14	Most controllable and most accurate
2		6	63	10, 11	Average controllable and accurate

3			5	65	11, 13, 14	Least controllable and least accurate
4			5	68	11, 12, 13	Average controllable and accurate

### 6.4.3. Potential Applications

Pleats construction is a labour-intensive and time-consuming process. They are commonly sewn by hand, which involved a lot of work, planning and highly trained skills in both design and construction stages. The skills required include but are not limited to the measurement, formation and arrangement of pleats, pressing technique, correct control of the iron settings and sewing the pleats onto base fabrics (Wolf, 2003; The Cutting Class, 2015). This research has demonstrated the use of 4DP as an alternative and novel technique for the 3D manipulation of textile fabrics, such as but not limited to pleats. In traditional textile-working techniques, some projecting pleats, such as pipe organ pleats, require stuffing (i.e., polyester fibrefill) as a support structure to hold the pleat. The rigidity and stiffness from the printed SMP on the 4DP thermo-responsive textiles can keep the pleats in place without the need for inserts. This is also a simplified method in fabricating curved structures or complex 3D shapes without the need for support structures to aid the printing process. This significantly reduces the printing time, material usage and waste (Rajkumar and Shanmugam, 2018; Sun et al., 2020).



Figure 6.22. 4DP as a novel technique for 3D manipulation of textile fabrics. (Top with 3D printed shoulder piece by Labeledby (2021)).

The potential applications envisioned from the findings of this research include shape-changing surface embellishments, textures and resizable garments. Surface embellishments can be printed as one-dimensional flat pieces directly onto a textile

substrate. The 4DP structures can be thermally actuated at  $T_r$  to transform into the targeted 3D shape when required. This method can offer a piece of wearable with two different aesthetic features, one style before and one after heat activation. It would also be an innovative technique for flat packaging garments that contain 3D surface embellishments. Designers and users do not need to worry that the 3D embellishments on the wearables will get compressed or damaged while being packaged. Wearables or accessories with shape-changing textures can also be produced.

4D printed thermo-responsive textiles creates an exciting new opportunity to create transformable clothing that can physically shape-change from one silhouette to another or even bend in specific ways to conform to irregularly shaped regions of the body. Another potential application is resizable garments that could shrink from a larger size to a smaller fitting. The different types of pleating effects demonstrated in this study can be incorporated into specific areas of a garment (i.e., waist or armscye) to gather the fabric into a smaller circumference, without the need for alteration. The garment would only be transformed from loose to tight-fitting when immersed in standing water at the appropriate temperature ( $T_r$ ). This concept would be particularly innovative for maternity clothing, allowing the clothing to be used even at the end of one's pregnancy. It is also common for clothing to fit loosely after losing weight. Resizable garments that can turn from initially loose fitting into smaller sizes that fit properly to the new body shape (i.e., from size 18 to size 14) would be practical, especially for users who are undergoing weight loss. This could help to reduce garment waste and the environmental impact in the textile and fashion industry.

#### **6.4.4. Limitations of the Study and Future Work**

Although several modifications and suggestions were made to improve the transformation accuracy of the 4D printed thermo-responsive textiles, which include actuating the specimen in a standing water environment (Figure 6.10), removing the specimen from the water bath after the SMP rehardens at below the  $T_r$  and increasing the number of printed rows (Chapter 6.4.2.1). There was still a high probability that the final shape will be distorted and have varying bending diameters. The specimen would not consistently actuate in an exact pattern as predicted (i.e., pleats not formed in a straight line). Future work should explore more methods to improve the accuracy and precision of the shape transformation.

4D printed shape-changing thermo-responsive textiles is currently in the exploration stage. Basic bending and different variation of projecting pleats were demonstrated in this study to

illustrate this novel concept of 4D printed shape-changing thermo-responsive textiles. However, this work is only the beginning of a larger exploration. The current findings are not readily applicable to the potential applications. Before moving on to create proof-of-concept level functional prototypes, further detailed shape transformation studies need to be conducted to fully understand the mechanism underpinning how the shape-shifting behaviour is influenced by, but not limited to, the geometrical dimensions and structural arrangements of the printed thermo-responsive SMP on the textile substrate.

The experiments for the shape transformation studies only tested horizontally printed structures. Future experiments can investigate the differences in shape transformation when the SMP structures are printed at a different angle (i.e., angled at 45° and vertically at 90°). The influences of process parameters such as the printing speed, fill pattern, angle and density, on the shape-shifting behaviour of 4DP thermo-responsive textiles can also be studied. Design tools that can inform the optimal geometrical dimensions, design and arrangement of the SMP structures for a specific shape change can be developed. Visual programming software and physics simulations software can be incorporated into the design process to simulate and inform the material system behaviour digitally as well as to optimise their compositions according to different parameters before fabrication. Further investigations are also required to study the performance, washability, durability and comfort of 4D printed thermo-responsive textiles, especially when realised into a product.

## **6.5. Chapter Summary**

The development and testing of self-actuated shape-changing thermo-responsive textile using direct ME of thermo-responsive SMP onto nylon mesh fabric were discussed. The shape transformation studies have demonstrated the ability to control the degree of deformation and shape-shifting patterns of 4D printed thermo-responsive textiles using the geometrical dimensions and structural arrangements of the printed thermo-responsive SMP on the textile substrate. The optimum geometric parameters to achieve the most predictable and accurate deformation were analysed and the structural arrangements to achieve particular shape-shifting patterns were reported. Table 6.19 specifies the key findings established from each experiment and the different types of projecting pleats produced.

Table 6.19. Summary of key findings.

Experiment Type	No.	Key Findings	Shape-shifting Patterns
Geometrical dimensions	1, 2	The thickness and width of the printed SMP structure on the textile substrate played critical roles in controlling the deformation and the accuracy of the actuated shape. The actuated bend was more accurate as the structural thickness and width increased. The structural thickness should be at least 0.8mm while the width should be at least 2.0mm to achieve controllable and accurate bend deformation. The structural length and width did not influence the diameter of the bend produced. On the other hand, the structural length influenced the bending diameter and the types of bend produced (semi-circle bend or circular bend).	Basic bend
Structural arrangements	3	The controllability and accuracy of deformation can be improved by increasing the number of printed rows instead of changing the structural width.	Basic bend
	4	The increment in the number of printed rows improves the shape-shifting behaviour by providing a more consistent bending diameter. It also helped to reinforce the rolls of the pleats, leading to additional visible pleats.	Continuous cartridge pleats and double pinch pleats
	5	The column spacing and print placement determine the style of pleats produced. Different pleating effects can be created by varying the spacing between the printed columns. The column spacing also influences the diameter and pattern of the actuated bend. The bending diameter increased when the column spacing increased.	Pipe organ pleats
	6	The row arrangements of SMP structures have a significant impact on the gathering lengths and pleats interval. The cartridge pleats were more gathered when the rows were arranged closer to each other. On the contrary, the pleats were less gathered when the rows were printed further apart.	Standard cartridge pleats
	7	Printing the SMP structures on different sides of the textile substrate interchanged the position of the first SMP layer, making the bends perform in opposite directions. The study revealed more time was required to perform opposite movements.	Waving effect
	8	The waving effects improved when multiple rows were introduced. The row arrangement of the SMP structures on the textile substrate influenced the pleats effect, particularly the gathering lengths and pleats interval.	Waving effect

This study enables further research to be taken in the novel area of 4D printed shape-changing thermo-responsive textiles. Researchers and designers can take advantage of the findings and results presented in this chapter to discover new shape transformations, apply them to demonstrate potential application in morphing structures for the fashion industry. The next chapter discusses the summary of the work and how the research objectives have been met. It also highlights the contributions that have been made, explains the limitations of the research and provides suggestions for future work.

## Chapter 7

### Conclusions and Suggestions for Future Work

Chapter seven concludes the thesis by presenting the summary of the work and how the research questions and objectives have been met. This chapter also describes the contribution to knowledge for each chapter and provides suggestions for future work.

#### 7.1. Summary of Work to Answer the Research Questions

This research has looked into four key subjects for the development of shape-changing thermo-responsive textiles. They are categorised as the following: (I) Functionally Graded Additive Manufacturing (FGAM) and 4D Printing (4DP), (II) commercial Additive Manufacturing (AM) materials for 4DP, (III) material extrusion (ME) polymer-textile composite and (IV) 4DP of thermo-responsive textile. This section outlines the summary of work carried out to achieve the research objectives as shown in Table 7.1

Table 7.1. Research questions and objectives defined for this research.

	<b>Research Question</b>	<b>Research Objective</b>	<b>Chapter</b>
1	What are the key differences between 4DP and FGAM?	To examine the state of the art of 4DP and FGAM through literature review and expert interviews.	2. FGAM 3. 4DP
2	How do we select suitable shape-memory polymers (SMPs) for ME to produce 4D printed parts?	To develop a material selection process to confirm the material characteristics that are suitable for 4DP.	4. Material Selection Framework for 4DP
3	Which ME build parameters and textile properties influence the adhesion of a polymer-textile composite?	To undertake literature reviews and experimental work to examine the build parameters and textile properties that influence the polymer and textile adhesion.	5. Development and Testing of ME Additive Manufactured Polymer-Textile Composite
4	How do the geometrical dimensions and structural arrangement influence the shape transformation of the thermo-responsive textile?	To undertake experimental work and analyse the results to highlight the factors that influence the shape transformation of thermo-responsive textiles.	6. 4D Printed Shape-Changing Thermo-Responsive Textiles

This research started by reviewing the state-of-the-art literature on FGAM and 4DP to define and distinguish their concept, capabilities, advancement and process flow. Some key terms and definitions were formulated. The present challenges and limitations in each AM strategy were also examined, and the gaps in knowledge related to the research scope were identified for investigation. Semi-structured expert interviews were conducted to validate the findings and confirm key terms and definitions regarding FGAM. The collected findings presented in chapters two and three resolved the research question (1) by identifying the key differences between FGAM and 4DP, which can be found in Chapter 3.7. The findings were analysed to identify the appropriate AM strategy and finalise a research direction to create shape-changing thermo-responsive textiles.

The second topic of investigation was the method and tools used to confirm the material characteristics that are suitable for 4DP to answer research question 2. The theoretical knowledge collected from chapter three was applied to develop a material selection framework to guide and support designers and researchers in exploiting commercially available thermoplastics as potential SMPs for use in ME 4DP. The material selection process comprised four experimental stages to progressively test and measure the shape fixity, response rate and cycle life of a material. The basic theoretical and practical knowledge to create a single-material thermo-responsive DSM active structure and the experimental procedure for programming-recovery characterisation was described. The developed framework was refined through workshop and semi-structured interviews to ensure its completeness, effectiveness and usability. The shape memory effect (SME) and repeatability of a list of commercial materials were investigated and reported.

Chapter five presented the development and adhesion testing of polymer-textile composites made up of PLA filaments on three different Polymer and Nylon mesh fabrics using direct ME. Details of the printing process to create polymer-textile composites and T-peel test methods were reported. The peel strength results and observed failure modes post-testing were used to identify the compatibility of materials. The appropriate combination of printing material, textile substrate and printer settings to achieve excellent polymer-textile adhesion was described, fulfilling research question 3.

The discovered top-performing material using the material selection framework and the polymer-textile orientation with the highest relative peel resistance is applied for 4DP of thermo-responsive textiles. Chapter six described the design, printing process, actuation and shape change characterisation methods for thermo-responsive textiles. Eight sets of experiments (Chapter 6.2) were carried out to systematically study the ability to control and produce various shape-shifting behaviours by changing the geometrical dimensions and

structural arrangement of the printed SMP structure on the textile substrate. The actuation results answered the research question 4 by specifying the effect of geometrical dimensions and structural arrangement on the deformation and shape-shifting behaviour of 4DP thermo-responsive textiles. The optimum settings to achieve the most predictable and accurate deformation were analysed and established into a design guideline to serve as the basis for producing relevant or more complex shape transformations. This research concluded by providing insight into the potential applications and the limitations in 4DP of thermo-responsive textiles.

## **7.2. Summary of Contribution to New Knowledge**

The outcomes of this thesis will be relevant to three groups of people, including but not limited to (I) academic researchers, (II) industrial, engineering, fashion and textile designers and (III) design and engineering students. Researchers and designers with the same area of interest can utilise the theoretical knowledge, tools, methods and results presented in this research to generate new research findings or develop new applications. The outcomes from this thesis can also be used as teaching material to train and educate designers and students about FGAM, 4DP and AM in fashion and textiles. The contributions derived from this research are as follows:

### **7.2.1. Theoretical Knowledge on FGAM and 4DP**

As FGAM and 4DP are two new emerging AM strategies introduced only in recent years, the existing theoretical contributions by other scholars are still limited and fragmented. New and existing researchers interested in these fields need to spend a great amount of time and effort in accessing and reviewing different sources using keyword-based searches to understand every aspect of the technology. This research helps to save time and provides access to information by compiling a comprehensive overview of FGAM and 4DP. The critical reviews presented in chapter two and chapter three provide an understand of fundamental concepts, key bases, process chain from design to manufacturing, advancements, capabilities and future perspectives.

Prior to this research, there was no general definition and clarification of key terms, especially for FGAM. There have been multiple different names proposed by different researchers in different publications. The most widely used terminologies and definitions are

clarified and validated through expert interviews and peer-reviews to provide a reliable source of information. The outcome from the literature reviews are published in an ISO/ASTM report (ISO/ASTM TR52912, 2020) and a journal paper (Pei, Loh and Nam, 2020) to encourage researchers to adopt a consistent approach and standardised set of vocabulary used for FGAM and 4DP, respectively.

This research also contributes to the theoretical knowledge by collecting lists of limitations and barriers that hinder the successful implementation of FGAM (Chapter 2.6) and 4DP (Chapter 3.6). By conducting a two days knowledge transfer workshop on FGAM for the INEX-ADAM (2021) project at the University of Zagreb in Croatia, it has provided the opportunity to further collect and analyse the limitations and research gaps of FGAM with AM experts (Figure 7.1), helped to establish the findings for Chapter 2.6. The findings throughout the course of this research are developed and produced into publications for wider knowledge dissemination (Refer to Page 282).

Other contributions to new knowledge include classifying the types of shape transformation actuation (self-shape change actuation and shape-memory actuation) and categorising the programmable behaviours in 4DP (Chapter 3.5), identifying the relationship of FGAM and 4DP in AM and establishing the key characteristics and aspects that separate and bridge FGAM and 4DP (Chapter 3.7). This benefits researchers and designers to recognise, select and implement the appropriate AM strategy and actions necessary for an intended design and application. In this research, the reviewed methodologies and guidelines on designing a 4D printed structure have aided the development of the material selection framework for commercially available thermoplastics as SMPs and the creation of shape-changing thermo-responsive textiles.

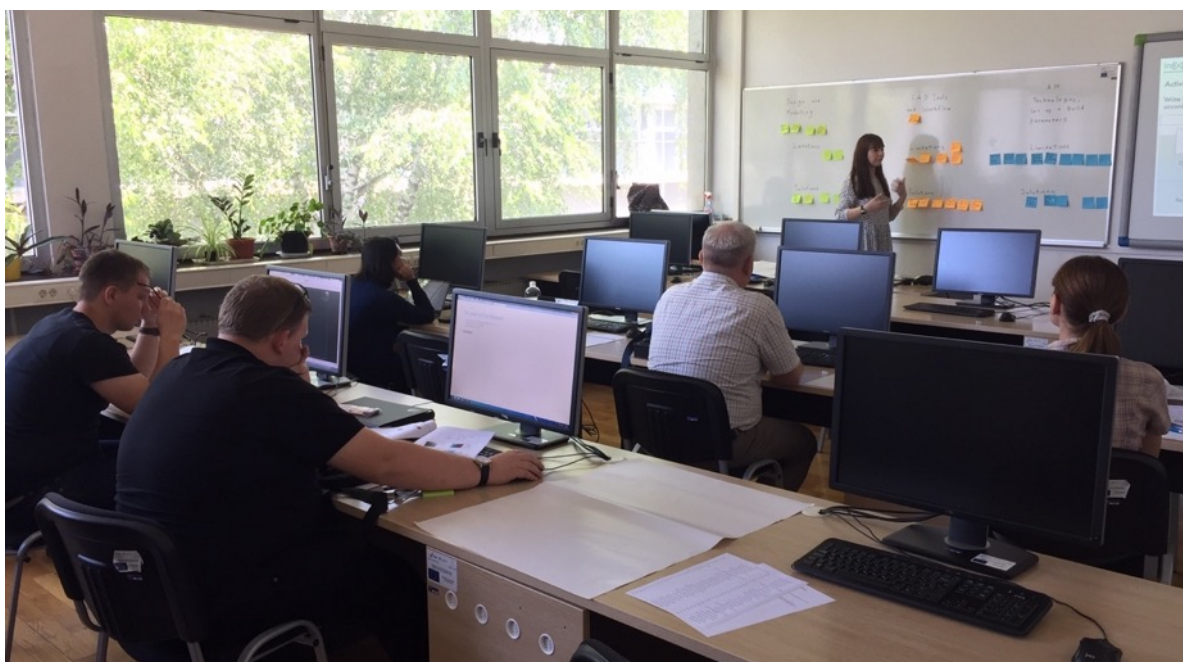


Figure 7.1. Brainstorming session with AM experts to specify and analyse the limitations and research gaps of FGAM.

### **7.2.2. Material Selection Framework for 4DP**

One of the collected constraints that hinder the successful implementation of 4DP is material availability. Sourcing and purchasing of commercial SMPs filaments are often expensive and subjected to high shipping costs. This framework can help to provide confidence towards selecting inexpensive and commercially available materials for 4DP. The material selection framework guides users in selecting the commercially available thermoplastics as potential SMPs for use in ME 4DP and detecting the strength and limitations of a material choice for an intended application, which was previously not available. It would be purposeful for the exploration and early development of 4DP, and help to accelerate new applications development and research outputs, such as thermo-responsive textiles

Most academic and research publications focused on advanced theory and characterisation methods for SMPs. This research is valuable as it discusses the shape memory properties and functionalities of SMPs, the design, analysis and experimental characterisation of a thermo-responsive DSM active structure at a feasible level for users with different backgrounds and knowledge levels in 4DP. Most characterisation methods present in the literature involve complex algorithms and the use of expensive specialist equipment. In this research, affordable and widely available tools and methods were used, and measuring charts were developed to test and measure the shape fixity and SME of a thermo-responsive

SMP to enable the widest uptake of this material selection framework (Chapter 4.3.4). Though, specialist measuring systems and scientific calculations for SMPs characterisation can always be introduced at the next stage of the investigation.

This research proved that commercial filaments for ME can be used for 4DP. The shape memory properties of different types of thermoplastic filaments including PLA, PCL, TPU, PU – PVA, and PP, were reported in Chapter 4.4. The experimental work performed in this research revealed that not all materials exhibit thermo-responsive SME despite belonging to the same material type. Some scholars claimed that TPU has good SME, but the results collected from the study have proven otherwise. Flexible materials like TPU have poor shape fixity and SME, which make them suitable as passive materials to create resistance to the shortening of the active layer in the multi-material 4DP structure. The SME of the materials in filament form and ME printed structure were examined and compared. The results showed that their response rate was closely similar, but the shape recovery results of the same material improved significantly and were more consistent when ME manufactured. The results also indicated that the shape recovery performance and repeatability of an SMP would vary according to the type of programming condition. This research confirmed that the potential commercially available thermoplastics could perform at least five consecutive shape memory cycles without any deterioration in response time and SME.

### **7.2.3. Development and Testing of ME Polymer-Textile Composite**

This research contributes to the current limited knowledge of developing a polymer-textile composite by using direct ME. A comprehensive list of the interconnected factors that affect the fabrication, polymer-textile adhesion and the overall quality of ME polymer-textile composites is presented in Chapter 5.2. The information is useful for designers and researchers in determining the appropriate combination of printing material, textile substrate, and printer settings to achieve excellent polymer-textile adhesion. This research also gave details on how to select the appropriate print layout, design and manufacturing process for the chosen textile substrate (Chapter 5.3.1). Literature review showed that different scholars apply or create different test methods to investigate the mechanical properties of the bonded ME polymer-textile composites. Besides, their studies usually do not clearly explain the design (i.e., the types of joint used, dimensions), the fabrication processes to create the adhesion test specimens, experimental setup, test procedures and analysis techniques. This research provides those details and encourages the use of appropriate and standardised adhesion test methods to determine the relative peel resistance of adhesive bonds between

thin flexible adherents in line with BS EN ISO 11339 (2010) (Chapter 5.3.2). This work serves as a reference for designers and researchers to develop new applications such as 3D surface patterning on textiles to facilitate future research in AM textiles development such as programmable or stimuli-responsive textiles.

This research quantified the adhesion strength of PLA – Nylon (net structure), PLA – Polyester (voile structure) and PLA – Nylon (voile structure) composites (Chapter 5.4). The T-peel test results revealed that the compatibility between the printing material and the textile substrate fibre type has a dominant effect on the peel resistance of ME polymer-textile composite. The average peel forces and strengths of PLA on Nylon textiles composites were nearly three times stronger than Polyester textile despite the differences in their mesh structures, pore properties and weave type.

#### **7.2.4. Development of 4D Printed Shape-Changing Thermo-Responsive Textiles**

This research established a fundamental understanding of fabricating and actuation techniques for 4D printed shape-changing thermo-responsive textiles. This research has demonstrated the use of 4DP as an alternative and novel technique for the 3D manipulation of textile fabrics. The shape transformation studies presented a proof-of-concept that the accuracy of deformation and shape-shifting behaviours can be controlled by the geometrical dimensions and structural arrangement of the printed SMP structure on the textile substrate. This research discloses the various types of shape-shifting patterns generated using particular structural arrangements. This includes basic bend, continuous cartridge pleats, double pinch pleats, pipe organ pleats, standard cartridge pleats and waving effect. The optimum parameters to achieve the most predictable and accurate deformation were reported. The study revealed that the thickness and width of the printed SMP structure on the textile substrate played critical roles in controlling the deformation and the accuracy of the actuated shape. Whilst the structural length controls the bending diameter and the types of bend produced (Chapter 6.4.1). The controllability and accuracy of deformation can be improved by increasing the number of printed rows instead of changing the structural width. The increment in the number of printed rows also improves the shape-shifting behaviour by providing a consistent bending diameter. This research also disclosed that the column spacing, print placement and row arrangement of SMP structures determine the shape-shifting patterns of the 4D printed shape-changing thermo-responsive textiles (Chapter 6.4.2).

Researchers and designers can take advantage of the findings and results presented in this chapter to recreate relevant shape transformations, discover new shape-shifting patterns, develop new applications or facilitate future research development in the novel area of 4D printed shape-changing thermo-responsive textiles, without having to spend great effort and time to test out each parameter.

### **7.3. Suggestions for Future Work**

The suggestions for further studies for the development of 4DP, materials for 4DP, and the fabrication opportunities of polymer-textile composite and thermo-responsive textile are as follows:

#### **7.3.1. Study on 4DP**

The state-of-art literature review of 4DP have identified a list of the current challenge and limitations concerning the materials, design, modelling and simulation, and AM processes that need to be addressed in order to exploit the true potential of these AM practices.

The future research opportunities for the development of 4DP include:

- (I) Extend the knowledge in the properties and characterisation process of SMPs for 4DP.
- (II) Comprehensive test methods to examine the cycle life and the mechanical degradation of materials.
- (III) Material selection tools that describe the material specification, energy-transforming functions, properties or behaviour change of SMPs for 4DP.
- (IV) Feasible design framework and standardised programming protocols to design and develop 4DP structures.
- (V) Design guidelines that inform a particular design solution, considering the material characterisation, material structure design, corresponding working mechanism, constitutive behaviour modelling and the fabrication process.
- (VI) A new approach of CAD and CAE analysis that can communicate the material properties, taking account of the material and fabrication constraints, predict and

control the shape transformation, and capture the actual behaviour of the modelled 4DP structure.

### **7.3.2. Material Selection Framework for 4DP**

The material selection framework can include an additional stage to investigate the moisture absorption properties of thermo-responsive SMPs and to study the effect of moisture trapping on the ME print quality, the SME and overall performance of the material. The framework can be further developed to test the shape memory properties of multi-material 4DP structure and other programming shapes besides folding and bending. The multi-material 4DP structure could be a combination of rigid and semi-rigid materials, two different active SMPs (i.e., PLA and PLA), or active SMP and passive material (i.e., PLA and TPU). Another future work includes publishing the framework online to increase accessibility and wider adoption by designers, practitioners, academics and students interested in 4DP.

Regarding the material characterisation and functional elements analysis, further investigation can be made on identifying why an inverse curvature only occurred on ME printed specimens when recovered from a fold deformation (See Figure 4.15). Different fold programming angles (i.e., 45°, 145°) can be tested to investigate whether the angle of deformation is the main influence on this effect. Additionally, the number of sequential shape memory cycle tests can be increased to investigate the maximum shape memory cycle life of the material.

### **7.3.3. Development and Testing of ME Polymer-Textile Composite**

The study in chapter five focused on printing regular PLA on perforated mesh textile substrate made from Polyester and Nylon to select the best polymer-textile combination for the development of thermo-responsive textiles. The peel test was based on the EN ISO 11339 (2010) standards requirement to check for print adhesion. Future work could focus on printing more complex geometrical structures on the textile substrate, explore different types of textile substrates of different fibre types and characteristics (i.e., weight and texture). The effect of pore properties such as the pore size, pore size distribution and pore shape of the textile substrate on polymer-textile adhesion can be examined. Printing material of different performances, mechanical properties and flexural characteristics can also be explored. The current work can be extended by carrying out an optical evaluation and

analysis on the interfacial bonding of how the printed polymer encloses the yarns or threads of the textile substrate using a confocal laser scanning microscope (CLSM) and digital microscope. This activity was meant to be conducted as part of this research but was not able to because of restricted access to the testing facilities due to COVID-19.

#### **7.3.4. Development of 4D Printed Shape-Changing Thermo-Responsive Textiles**

4D printed shape-changing thermo-responsive textiles is currently in the exploration stage. Further detailed shape transformation studies need to be conducted to fully understand the mechanism underpinning how the shape-shifting behaviour is influenced by, but not limited to, the geometrical dimensions and structural arrangements of the printed thermo-responsive SMP on the textile substrate. Future work should also explore additional methods to improve the accuracy and precision of the shape transformation. Future experiments can print the SMP structures at a different angle, such as angled at 45° or vertically at 90°. The influences of process parameters such as the printing speed, fill pattern, angle and density, on the shape-shifting behaviour of 4DP thermo-responsive textiles can also be studied. Design tools that can inform the optimal geometrical dimensions, design and arrangement of the SMP structures for a specific shape change can be developed. Visual programming software and physics simulations software can be incorporated into the design process to simulate and inform the material system behaviour digitally as well as to optimise their compositions according to different parameters before fabrication. Further investigations are also required to study the performance, washability, durability and comfort of 4D printed thermo-responsive textiles, especially when realised into a product. Nevertheless, FGAM can be incorporated with 4DP to create variable-property 4D printed thermo-responsive textiles with strategically tailored compositions or microstructure.

## List of Publications

### Published Journal Papers

Loh, G. H., Sotayo, A. and Pei, E. (2021) 'Development and testing of material extrusion additive manufactured polymer–textile composites', *Fashion and Textiles*. Springer Singapore, 8, 2. <https://doi.org/10.1186/s40691-020-00232-7>.

Loh, G.H., Pei, E., Gonzalez-Gutierrez, J. and Monzón, M. (2020) "An Overview of Material Extrusion Troubleshooting". *Applied Sciences*. July 2020, volume 10, 4776. <https://doi.org/10.3390/app10144776>.

Pei, E., Loh, G.H. and Nam, S (2020) "Concepts and Terminologies in 4D Printing". *Applied Sciences*. June 2020, volume 10, 4443. <https://doi.org/10.3390/app10134443>.

Pei, E. and Loh, G.H. (2018) "Technological considerations for 4D printing: An Overview". *Progress in Additive Manufacturing*. June 2018, volume 3, issue 1-2, pp 95-107. <https://doi.org/10.1007/s40964-018-0047-1>.

Loh, G.H., Pei, E., Harrison, D. and Monzón, M. (2018) "An Overview of Functionally Graded Additive Manufacturing". *Additive Manufacturing*. October 2018, volume 23, pp 34-44. <https://doi.org/10.1016/j.addma.2018.06.023>.

Pei, E., Loh, G.H., Harrison, D., Almeida, H.D.A., Monzon, M. and Paz, R. (2017) "A Study of 4D Printing and Functionally Graded Additive Manufacturing", *Assembly Automation*, volume 37 Issue: 2, pp147-153. <https://doi.org/10.1108/AA-01-2017-012>.

### Conference Papers

Kabir, I.R., Loh, G.H., Pei, E. (2020) "Functionally Graded Additive Manufacturing: A Teaching Case Study of INEX-ADAM". *Proceedings of the Design Society: DESIGN Conference*, June 2020, volume 1, pp 245-254. <https://doi.org/10.1017/dsd.2020.262>.

Pei, E, Loh, G.H., Nam, S, Azhar, F.E. (2019) Programming 4D Printed Parts Through Shape-Memory Polymers and Computer-Aided-Design. *Progress in Digital and Physical Manufacturing*. pp143-151. [https://doi.org/10.1007/978-3-030-29041-2\\_19](https://doi.org/10.1007/978-3-030-29041-2_19). International Conference of Progress in Digital and Physical Manufacturing (ProDPM 2019). 2 – 4th October 2019. Leiria, Portugal. [https://doi.org/10.1007/978-3-030-29041-2\\_19](https://doi.org/10.1007/978-3-030-29041-2_19).

Loh, G.H. and Pei, E. (2019) "Design for Material Extrusion on Mesh Fabrics". 16th Rapid Design, Prototyping and Manufacturing Conference (RDPM). Brunel University London. 4 – 5th April 2019. London, UK.

Loh, G.H. and Pei, E. (2017) "Building a conceptual understanding of Functionally Graded Additive Manufacturing". 15th Rapid Design, Prototyping and Manufacturing Conference (RDPM). Northumbria University. 27 – 28th April 2017. Newcastle, UK.

### **Book Chapter**

Pei, E. and Loh, G. H. (2018) 'Future challenges in functionally graded additive manufacturing', in Additive Manufacturing - Developments in Training and Education, pp. 219–226. [https://doi.org/10.1007/978-3-319-76084-1\\_15](https://doi.org/10.1007/978-3-319-76084-1_15).

### **Technical Report**

ISO Technical report TR52912 Design of Functionally Graded Additive Manufactured Parts. Document stage: (60) Publication.

## References

3D Printing Beta (2020) *Print Quality - Differences Between Moving Build Plate Vs. Extruder - 3D Printing Stack Exchange*. Available at:

<https://3dprinting.stackexchange.com/questions/1361/differences-between-moving-build-plate-vs-extruder> (Accessed: 28 July 2020).

3D Sourced (2021) *10 of the Best Dual Extruder 3D Printers 2021 | 3DSourced*. Available at: <https://www.3dsourced.com/3d-printers/dual-extruder-3d-printer/> (Accessed: 6 April 2021).

3D4Makers (2020) *PEI Ultem 1010 Filament | 3D4Makers | 3D printing*. Available at: <https://www.3d4makers.com/products/pei-filament> (Accessed: 6 May 2020).

3M (2020) *3D Printing with 3M™ Dyneon™ PTFE | 3M United Kingdom*. Available at: [https://www.3m.co.uk/3M/en\\_GB/design-and-specialty-materials-uk/3d-printing/](https://www.3m.co.uk/3M/en_GB/design-and-specialty-materials-uk/3d-printing/) (Accessed: 8 February 2021).

AbFab3D (2014) *SVX Format | AbFab3D*. Available at: <https://abfab3d.com/svx-format/> (Accessed: 6 May 2021).

Abuzied, H. *et al.* (2020) 'A Review of Advances in Design for Disassembly With Active Disassembly Applications', *Engineering Science and Technology, an International Journal*. Karabuk University, 23(3), pp. 618–624. doi: 10.1016/j.jestch.2019.07.003.

Ahrendt, D. and Karam, A. R. (2020) 'Development of a Computer-Aided Engineering–Supported Process for the Manufacturing of Customized Orthopaedic Devices By Three-Dimensional Printing Onto Textile Surfaces', *Journal of Engineered Fibers and Fabrics*, 15(June), pp. 1–11. doi: 10.1177/1558925020917627.

Alamy (2021) *Sensitive Plant, Shame Plant (Mimosa Pudica), Flower And Leaf, Leaves Stock Photo - Alamy*. Available at: <https://www.alamy.com/sensitive-plant-shame-plant-mimosa-pudica-flower-and-leaf-leaves-sensitiv-image8794074.html> (Accessed: 25 May 2021).

AM Platform (2014) *Strategic Research Agenda 2014*. Available at: <https://www.rm-platform.com/roadmapping-activities/strategic-research-agenda> (Accessed: 28 April 2021).

An, B. *et al.* (2018) 'Thermorph: Demonstrating Thermorph: Democratizing 4D Printing of Self-Folding Materials and Interfaces', in *Proceedings of the 2018 CHI Conference on Human Factors in Computing Systems*, pp. 1–12. doi: 10.1145/3173574.3173834.

Anstaett, C., Seidel, D.-I. C. and Reinhart, D.-I. G. (2017) 'Fabrication of 3D Multi-material Parts Using Laser-based Powder Bed Fusion', in *Proceedings of the 28th Annual International Solid Freeform Fabrication Symposium*. . Austin, Texas.

Aremu, A. O. *et al.* (2017) 'A Voxel-based Method of Constructing and Skinning Conformal and Functionally Graded Lattice Structures Suitable for Additive Manufacturing', *Additive Manufacturing*. Elsevier B.V., 13(November), pp. 1–13. doi: 10.1016/j.addma.2016.10.006.

Ashby, M. F. (2017) *Materials Selection in Mechanical Design: Fifth Edition*. Fifth. Edited by S. Merken. Butterworth-Heinemann. Available at:

[https://books.google.co.uk/books/about/Materials\\_Selection\\_in\\_Mechanical\\_Design.html?id=K4h4CgAAQBAJ&printsec=frontcover&source=kp\\_read\\_button&redir\\_esc=y#v=onepage&q&f=false](https://books.google.co.uk/books/about/Materials_Selection_in_Mechanical_Design.html?id=K4h4CgAAQBAJ&printsec=frontcover&source=kp_read_button&redir_esc=y#v=onepage&q&f=false) (Accessed: 5 November 2020).

Azhar, F. E. and Pei, E. (2019) *Investigating the Communication of 4D Printing among Product Designers and Manufacturing Engineers*. Available at:

<https://bura.brunel.ac.uk/bitstream/2438/18701/1/FullText.pdf> (Accessed: 14 April 2021).

Bader, C. *et al.* (2016) 'Data-Driven Material Modeling with Functional Advection for 3D Printing of Materially Heterogeneous Objects', *3D Printing and Additive Manufacturing*, 3(2), pp. 71–78. doi: 10.1089/3dp.2016.0026.

Bakarich, S. E. *et al.* (2015) '4D Printing with Mechanically Robust, Thermally Actuating Hydrogels', *Macromolecular Rapid Communications*, 36(12), pp. 1211–1217. doi: 10.1002/marc.201500079.

Banait, S. M. *et al.* (2020) 'Experimental Investigation on Laser Directed Energy Deposition of Functionally Graded Layers of Ni-Cr-B-Si and SS316L', *Optics and Laser Technology*. Elsevier Ltd, 121, p. 105787. doi: 10.1016/j.optlastec.2019.105787.

Bartlett, J. L. *et al.* (2018) 'In Situ Defect Detection in Selective Laser Melting via Full-Field Infrared Thermography', *Additive Manufacturing*. Elsevier B.V., 24, pp. 595–605. doi: 10.1016/j.addma.2018.10.045.

Bashir, M., Lee, C. F. and Rajendran, P. (2017) 'Shape Memory Materials and Their Applications in Aircraft Morphing: An introspective study', *ARPN Journal of Engineering and Applied Sciences*, 12(19), pp. 5434–5446.

Basit, A. (2016) *Development and Characterization of a Shape Memory Polymer Composite Actuator for Morphing Structures*. Université de Haute Alsace. Available at:

<https://tel.archives-ouvertes.fr/tel-01267578/document>.

Behl, M. *et al.* (2013) 'Reversible Bidirectional Shape-memory Polymers', *Advanced Materials*, 25(32), pp. 4466–4469. doi: 10.1002/adma.201300880.

Behl, M. and Lendlein, A. (2007) 'Shape-memory Polymers', *Materials Today*. Elsevier Ltd, 10(4), pp. 20–28. doi: 10.1016/S1369-7021(07)70047-0.

BioLogic (2015) *Tangible Media Group*. Available at:  
<https://tangible.media.mit.edu/project/biologic/> (Accessed: 26 July 2020).

Browne, A. L. and Johnson, N. L. (2009) 'Self-healing and Self-cleaning Tires Utilizing Active Material Actuation'. U.S. Provisional Patent Application. Available at:  
<https://patents.google.com/patent/US9211687B2/en#patentCitations> (Accessed: 12 January 2021).

Callister, W. D. J. and Rethwisch, D. G. (2018) *Fundamentals of Materials Science and Engineering an Integrated Approach*. Fifth, *Orbit An International Journal on Orbital Disorders And Facial Reconstructive Surgery*. Fifth. John Wiley & Sons.

Campbell, T. A., Tibbits, S. and Garrett, B. (2014) 'The Programmable World', *Scientific American*, 311(5), pp. 60–65. doi: 10.1038/scientificamerican1114-60.

Carroll, B. E. *et al.* (2016) 'Functionally Graded Material of 304L Stainless Steel and Inconel 625 Fabricated by Directed Energy Deposition: Characterization and thermodynamic modeling', *Acta Materialia*. Elsevier Ltd, 108, pp. 46–54. doi: 10.1016/j.actamat.2016.02.019.

Chatterjee, K. and Ghosh, T. K. (2020) '3D Printing of Textiles: Potential Roadmap to Printing with Fibers', *Advanced Materials*, 32(4), p. 1902086. doi: 10.1002/adma.201902086.

Chávez, F. A. *et al.* (2019) 'Characterisation of Phases and Deformation Temperature for Additively Manufactured Shape Memory Polymer Components Fabricated from Rubberised Acrylonitrile Butadiene Styrene', *Virtual and Physical Prototyping*, 14(2), pp. 188–202. doi: 10.1080/17452759.2018.1550694.

Chiodo, J. and Jones, N. (2012) 'Smart Materials Use in Active Disassembly', *Assembly Automation*, 32(1), pp. 8–24. doi: 10.1108/01445151211198683.

Choong, Y. Y. C. *et al.* (2017) '4D Printing of High Performance Shape Memory Polymer Using Stereolithography', *Materials and Design*. Elsevier, 126, pp. 219–225. doi: 10.1016/j.matdes.2017.04.049.

Chung, H. and Das, S. (2008) 'Functionally Graded Nylon-11/Silica Nanocomposites Produced by Selective Laser Sintering', *Materials Science and Engineering A*, 487(1–2), pp. 251–257. doi: 10.1016/j.msea.2007.10.082.

Chung, S., Song, S. E. and Cho, Y. T. (2017) 'Effective Software Solutions for 4D Printing: A Review and Proposal', *International Journal of Precision Engineering and Manufacturing - Green Technology*, 4(3), pp. 359–371. doi: 10.1007/s40684-017-0041-y.

Dalal, R. (2016) *Thermal Analysis of FGM Plates Using FEM Method*. Available at: <https://www.slideshare.net/RajaniDalal/thermal-analysis-of-fgm-plates-using-fem-method> (Accessed: 20 April 2021).

Díaz Lantada, A. *et al.* (2010) 'Intelligent Structures Based on the Improved Activation of Shape Memory Polymers Using Peltier Cells', *Smart Materials and Structures*, 19(5). doi: 10.1088/0964-1726/19/5/055022.

Ding, Z. *et al.* (2017) 'Direct 4D Printing via Active Composite Materials', *Science Advances*. American Association for the Advancement of Science, 3(4), p. e1602890. doi: 10.1126/sciadv.1602890.

El-Galy, I. M., Saleh, B. I. and Ahmed, M. H. (2019) 'Functionally Graded Materials Classifications and Development Trends from Industrial Point of View', *SN Applied Sciences*. Springer International Publishing, 1(11), pp. 1–23. doi: 10.1007/s42452-019-1413-4.

Elliot, A. F. (2015) *How to Care for Every Fabric in Your Wardrobe Revealed | Daily Mail Online, Daily Mail*. Available at: <https://www.dailymail.co.uk/femail/article-3043211/How-care-fabric-wardrobe-revealed.html> (Accessed: 14 July 2020).

EN ISO 10365 (1995) 'Adhesives — Designation of Main Failure Patterns'. British Standards Institution.

EN ISO 11339 (2010) 'Adhesives — T-peel Test for Flexible-to-flexible Bonded Assemblies'. British Standards Institution.

EN ISO 6133 (2015) 'Rubber and Plastics — Analysis of Multi-peak Traces Obtained in Determinations of Tear Strength and Adhesion Strength'. British Standards Institution.

Eos Project (2020) *Eos Project – Site for Computational Origami System Eos*. Available at: <https://www.i-eos.org/> (Accessed: 2 February 2021).

Eutionnat-Diffo, P. A. *et al.* (2019) 'Optimization of Adhesion of Poly Lactic Acid 3D Printed onto Polyethylene Terephthalate Woven Fabrics Through Modelling Using Textile Properties', *Rapid Prototyping Journal*, 26(2), pp. 390–401. doi: 10.1108/RPJ-05-2019-0138.

Fairclough, C. (2018) *Advancing Additive Manufacturing with Sequential Simulations* | *COMSOL Blog*. Available at: <https://www.comsol.com/blogs/advancing-additive-manufacturing-with-sequential-simulations/> (Accessed: 15 January 2021).

Federal Institute for Research on Building (2018) 'Graduated Building Components: Production Procedures and Areas of Use for Functionally Graduated Building Components in Construction.', in *Building the future: The magazine of the Zukunft Bau research initiative*. Berlin, Germany: Federal Ministry of Transport, Building and Urban Development, pp. 48–51. Available at: [https://inta-aiivn.org/images/cc/Habitat/backgrounddocuments/CCHabitat\\_Building\\_the\\_Future\\_Germany.pdf](https://inta-aiivn.org/images/cc/Habitat/backgrounddocuments/CCHabitat_Building_the_Future_Germany.pdf).

Flynt, J. (2019) *3D Printing Fashion: Advantages, Disadvantages, and Future - 3D Insider*. Available at: <https://3dinsider.com/3d-printing-fashion/> (Accessed: 27 July 2020).

Garces, I. T. *et al.* (2019) 'Effect of Moisture on Shape Memory Polyurethane Polymers for Extrusion-based Additive Manufacturing', *Materials*, 12(2), p. 244. doi: 10.3390/ma12020244.

Ge, Q. *et al.* (2016) 'Multimaterial 4D Printing with Tailorable Shape Memory Polymers', *Scientific Reports*. Nature Publishing Group, 6, p. 31110. doi: 10.1038/srep31110.

Ge, Q., Qi, H. J. and Dunn, M. L. (2013) 'Active Materials By Four-dimension Printing', *Applied Physics Letters*. American Institute of PhysicsAIP, 103(13), p. 131901. doi: 10.1063/1.4819837.

Gehrke, I. *et al.* (2019) *Smart Textiles Production: Overview of Materials, Sensor and Production Technologies for Industrial Smart Textiles*. First, *Smart Textiles Production*. First. Basel, Switzerland: MDPI: Basel, Switzerland. doi: 10.3390/books978-3-03897-498-7.

Ghosh, S. K. (2009) *Self-healing Materials: Fundamentals, Design Strategies, and Applications - Google Books*. Edited by S. K. Ghosh. John Wiley & Sons. Available at: [https://books.google.co.uk/books?id=4NH64BONX94C&source=gbs\\_navlinks\\_s](https://books.google.co.uk/books?id=4NH64BONX94C&source=gbs_navlinks_s) (Accessed: 17 November 2020).

Gibson, I., Rosen, D. W. and Stucker, B. (2010) *Additive Manufacturing Technologies: Rapid Prototyping to Direct Digital Manufacturing, Additive Manufacturing Technologies: Rapid*

*Prototyping to Direct Digital Manufacturing*. Springer US. doi: 10.1007/978-1-4419-1120-9.

Gilbert, C. *et al.* (2011) 'Digital Engineering of Bio-Adaptable Dental Implants', in Turkyilmaz, I. (ed.) *Implant Dentistry - A Rapidly Evolving Practice*. InTech. doi: 10.5772/17083.

Gonzalez, P. *et al.* (2019) 'Additive Manufacturing of Functionally Graded Ceramic Materials by Stereolithography', *Journal of Visualized Experiments*, (143). doi: 10.3791/57943.

Granta Design (2021) *Additive Manufacturing - the Senvol Database | Granta Design*. Available at: <https://www.grantadesign.com/industry/products/data/applications/additive-manufacturing/> (Accessed: 10 May 2021).

Gregurić, L. (2020) *PLA+/Plus Filament: What Is It & Is It Worth It?*, *All3DP*. Available at: <https://all3dp.com/2/pla-plus-filament-what-is-it/> (Accessed: 14 July 2020).

Griffin, M. (2019) *What's Soft PLA Filament & How Does It Compare to TPU?*, *All3DP*. Available at: <https://all3dp.com/2/what-s-soft-pla-filament-how-does-it-compare-to-tpu/> (Accessed: 14 July 2020).

Griffiths, A. (2021) *Pleats, Tucks and Gathers*. Available at: <http://www.pocketmouse.co.uk/cgs3pg.php> (Accessed: 10 August 2021).

Grigoriadis, K. (2018) *Computational and Conceptual Blends: The Epistemology of Designing with Functionally Graded Materials*. Royal College of Art.

Grigoriadis, K. (2019) 'Computational Blends: The Epistemology of Designing with Functionally Graded Materials', *Journal of Architecture*. Taylor & Francis, 24(2), pp. 160–192. doi: 10.1080/13602365.2019.1578074.

Grimmelsmann, N. *et al.* (2018) 'Adhesion of 3D Printed Material on Textile Substrates', *Rapid Prototyping Journal*. doi: 10.1108/RPJ-05-2016-0086.

Groeger, D., Chong Loo, E. and Steimle, J. (2016) 'HotFlex', in *Proceedings of the 2016 CHI Conference on Human Factors in Computing Systems*. San Jose, CA, pp. 420–432. doi: 10.1145/2858036.2858191.

Gupta, A. and Talha, M. (2015) 'Recent Development in Modeling and Analysis of Functionally Graded Materials and Structures', *Progress in Aerospace Sciences*. Elsevier Ltd, 79, pp. 1–14. doi: 10.1016/j.paerosci.2015.07.001.

Hadid, Z. (2015) *Zaha Hadid Architects Chair | 3D Printed Art & Design World*. Available at:

<https://3dprintedart.stratasys.com/zahahadidarchitectschair> (Accessed: 29 April 2021).

Ham, S. and Lee, Y.-G. (2016) 'A Study on the Automatic Design of 4D Printing to Follow the Target Shape', *Korean Journal of Computational Design and Engineering*. Society for Computational Design and Engineering, 21(3), pp. 306–312. doi: 10.7315/cde.2016.306.

Hascoet, J. Y., Muller, P. and Mognol, P. (2011) 'Manufacturing of Complex Parts with Continuous Functionally Graded Materials (FGM)', in *Proceedings of Solid Freeform Fabrication Symposium*. Austin, University of Texas, pp. 1–7.

Van Herpen, I. (2010) *Crystallization Runway*. Available at: <https://www.irisvanherpen.com/about>.

Hindman, D. (2013a) *Nonwoven Terms- Denier*. Available at: <http://www.nonwoventools.com/pdf/DefVol1No36Denier.pdf> (Accessed: 14 July 2020).

Hindman, D. (2013b) *Nonwoven Terms- Stitch Density*. Available at: <http://www.nonwoventools.com/pdf/DefVol1No26StitchDensity.pdf> (Accessed: 15 July 2020).

Hu, J. (2019) *Comparing UX Research Methods. Feeling Anxious About Moving Out of... | by John Hu | Facebook Research | Medium*. Available at: <https://medium.com/facebook-research/comparing-ux-research-methods-d315050b1698> (Accessed: 8 July 2021).

Hu, J. and Chen, S. (2010) 'A Review of Actively Moving Polymers in Textile Applications', *Journal of Materials Chemistry*, 20(17), pp. 3346–3355. doi: 10.1039/b922872a.

Huang, T. *et al.* (2009) 'Aqueous-based Freeze-form Extrusion Fabrication of Alumina Components', *Rapid Prototyping Journal*. Emerald Group Publishing Limited, 15(2), pp. 88–95. doi: 10.1108/13552540910943388.

Huang, W. M. *et al.* (2010) 'Shape Memory Materials', *Materials Today*, 13(7–8), pp. 54–61. doi: 10.1016/S1369-7021(10)70128-0.

Huang, W. M. (2012) *Shape Memory Polymers (SMPs) – Current Research and Future Applications*, *AZO Materials*. Available at: <https://www.azom.com/article.aspx?ArticleID=6038> (Accessed: 10 February 2021).

Huang, W. M. *et al.* (2012) 'Thermo/Chemo-responsive Shape Memory Effect in Polymers: A Sketch of Working Mechanisms, Fundamentals and Optimization', *Journal of Polymer Research*, 19, p. 9952. doi: 10.1007/s10965-012-9952-z.

INEX-ADAM (2021) *Increasing Excellence on Advanced Additive Manufacturing (INEX-ADAM)*. Available at: <http://inex-adam.eu/> (Accessed: 26 June 2021).

Invernizzi, M. *et al.* (2018) '4D Printed Thermally Activated Self-healing and Shape Memory Polycaprolactone-Based Polymers', *European Polymer Journal*. doi: 10.1016/j.eurpolymj.2018.02.023.

Ionov, L. (2013) '3D Microfabrication Using Stimuli-responsive Self-folding Polymer Films', *Polymer Reviews*, 53(1), pp. 92–107. doi: 10.1080/15583724.2012.751923.

ISO/ASTM 52900 (2017) *BS ISO/ASTM 52900:2015 Additive Manufacturing- General Principles- Terminology*, ISO/ ASTM. West Conshohocken, PA, USA: ISO/ ASTM: West Conshohocken, PA, USA.

ISO/ASTM TR52912 (2020) *Additive manufacturing — Design — Functionally Graded Additive Manufacturing*. Available at: <https://www.iso.org/obp/ui/#iso:std:iso-astm:tr:52912:ed-1:v1:en:ref:72> (Accessed: 28 April 2021).

ISO/ASTM52915 (2020) *ISO/ASTM52915 - 20 Specification for Additive Manufacturing File Format (AMF) Version 1.2*. Available at: <https://www.astm.org/Standards/ISOASTM52915.htm> (Accessed: 6 May 2021).

Jian, B. *et al.* (2018) 'Towards a Design Framework for Multifunctional Shape Memory Polymer Based Product in the Era of 4D Printing', in *Proceedings of the ASME 2018*. San Antonio, TX, USA: American Society of Mechanical Engineers, pp. 1–13. doi: 10.1115/smasis2018-7935.

Jose, S. *et al.* (2020) 'Introduction to Shape-memory Polymers, Polymer Blends and Composites: State of the Art, Opportunities, New Challenges and Future Outlook', in Parameswaranpillai, J. *et al.* (eds) *Shape Memory Polymers, Blends and Composites*. Springer, Singapore, pp. 1–19. doi: 10.1007/978-981-13-8574-2\_1.

Kačergis, L., Mitkus, R. and Sinapius, M. (2019) 'Influence of Fused Deposition Modeling Process Parameters on the Transformation of 4D Printed Morphing Structures', *Smart Materials and Structures*, 28(10), p. 105042. doi: 10.1088/1361-665X/ab3d18.

Keating, S. J. (2012) *Renaissance Robotics : Novel Applications of Multipurpose Robotic Arms Spanning Design Fabrication , Utility , and Art*, Massachusetts Institute of Technology. Massachusetts Institute of Technology.

- Kelly, B. E. *et al.* (2019) 'Volumetric Additive Manufacturing via Tomographic Reconstruction', *Science*, 363(6431), pp. 1075–1079. doi: 10.1126/science.aau7114.
- Khare, V. *et al.* (2017) 'From 3D to 4D Printing – Design, Material and Fabrication for Multi-functional Multi-materials', *International Journal of Precision Engineering and Manufacturing - Green Technology*, 4(3), pp. 291–299. doi: 10.1007/s40684-017-0035-9.
- Kim, J. *et al.* (2012) 'Thermally Responsive Rolling of Thin Gel Strips with Discrete Variations in Swelling', *Soft Matter*. The Royal Society of Chemistry, 8(8), pp. 2375–2381. doi: 10.1039/c2sm06681e.
- Kim, S. *et al.* (2019) 'A Study of the Development and Improvement of Fashion Products Using a FDM Type 3D Printer', *Fashion and Textiles*. Springer Singapore, 6(1). doi: 10.1186/s40691-018-0162-0.
- Knowledge Sourcing Intelligence (2020) *4D Printing Market Size & Share: Industry Report, 2020 - 2025*, Knowledge Sourcing Intelligence. Available at: <https://www.knowledgesourcing.com/report/4d-printing-market> (Accessed: 22 October 2020).
- Kočí, J. (2019) *3MF File Format and Why It's Great - Prusa Printers*. Available at: [https://blog.prusaprinters.org/3mf-file-format-and-why-its-great\\_30986/](https://blog.prusaprinters.org/3mf-file-format-and-why-its-great_30986/) (Accessed: 6 May 2021).
- Kolesov, I., Dolynchuk, O. and Radosch, H. J. (2015) 'Shape-memory Behavior of Cross-linked Semi-crystalline Polymers and Their Blends', *Express Polymer Letters*, 9(3), pp. 255–276. doi: 10.3144/expresspolymlett.2015.24.
- Kong, D. and Xiao, X. (2016) 'High Cycle-life Shape Memory Polymer at High Temperature', *Scientific Reports*. Nature Publishing Group, 6, p. 33610. doi: 10.1038/srep33610.
- Korger, M. *et al.* (2016) 'Possible Applications of 3D Printing Technology on Textile Substrates', *{IOP} Conference Series: Materials Science and Engineering*. {IOP} Publishing, 141, p. 12011. doi: 10.1088/1757-899x/141/1/012011.
- Kreikebaum, E. *et al.* (2017) '3D Printing of Braille on Textiles', *Melliand International* 23, June, pp. 114–116.
- Kuang, X., Chen, K., *et al.* (2018) '3D Printing of Highly Stretchable, Shape-memory, and Self-healing Elastomer toward Novel 4D Printing', *ACS Applied Materials and Interfaces*. American Chemical Society, 10(8), pp. 7381–7388. doi: 10.1021/acsami.7b18265.

Kuang, X., Roach, D. J., *et al.* (2018) 'Advances in 4D Printing: Materials and Applications', *Advanced Functional Materials*, p. 1805290. doi: 10.1002/adfm.201805290.

Kuang, X. *et al.* (2019) 'Grayscale Digital Light Processing 3D Printing for Highly Functionally Graded Materials', *Science Advances*, 5(5), p. eaav5790. doi: 10.1126/sciadv.aav5790.

Kuksenok, O. and Balazs, A. C. (2016) 'Stimuli-responsive Behavior of Composites Integrating Thermo-responsive Gels with Photo-responsive Fibers', *Materials Horizons*, 3, pp. 53–62. doi: 10.1039/c5mh00212e.

Kumar, K. S., Chen, P.-Y. and Ren, H. (2019) 'A Review of Printable Flexible and Stretchable Tactile Sensors', *Research*, 2019, p. 3018568. doi: 10.34133/2019/3018568.

Kumar, S. (2010) 'Development of Functionally Graded Materials by Ultrasonic Consolidation', *CIRP Journal of Manufacturing Science and Technology*, 3(1), pp. 85–87. doi: 10.1016/j.cirpj.2010.07.006.

Kumar, S. (2016) *Functionally Graded Material*. Available at: <https://www.slideshare.net/ErShambhuChauhan/functionally-graded-material> (Accessed: 22 April 2021).

Kumbhar, N. N. and Mulay, A. V. (2018) 'Post Processing Methods Used to Improve Surface Finish of Products which are Manufactured by Additive Manufacturing Technologies: A Review', *Journal of The Institution of Engineers (India): Series C*. Springer, 99(4), pp. 481–487. doi: 10.1007/s40032-016-0340-z.

Labeledby (2020) *LABELEDBY*. Available at: <https://www.labeledby.com/> (Accessed: 26 July 2020).

Labeledby (2021) *LABELEDBY. Top with 3D-Printed Shoulderpiece | LABELEDBY*. Available at: <https://www.labeledby.com/product-page/labeledby-top-with-3d-printed-shoulderpiece> (Accessed: 19 October 2021).

Lai, S. M. and Lan, Y. C. (2013) 'Shape Memory Properties of Melt-Blended Polylactic Acid (PLA)/Thermoplastic Polyurethane (TPU) Bio-based Blends', *Journal of Polymer Research*, 20, p. 140. doi: 10.1007/s10965-013-0140-6.

Laitinen, V. *et al.* (2020) 'Additive Manufacturing from the Point of View of Materials Research', in Collan, M. and Michelsen, K.-E. (eds) *Technical, Economic and Societal*

*Effects of Manufacturing 4.0: Automation, Adaption and Manufacturing in Finland and Beyond*. Cham: Springer International Publishing, pp. 43–83. doi: 10.1007/978-3-030-46103-4\_3.

Lang, R. J. (2015) *TreeMaker*. Available at: <https://langorigami.com/article/treemaker/> (Accessed: 12 February 2021).

Lee, A. Y., An, J. and Chua, C. K. (2017) 'Two-Way 4D Printing: A Review on the Reversibility of 3D-Printed Shape Memory Materials', *Engineering*. Elsevier LTD on behalf of Chinese Academy of Engineering and Higher Education Press Limited Company, 3(5), pp. 663–674. doi: 10.1016/J.ENG.2017.05.014.

Lefebvre, E. *et al.* (2014) 'Smart Materials: Development of New Sensory Experiences Through Stimuli Responsive Materials', in Coletta, C. *et al.* (eds) *5th STS Italia Conference A Matter of Design: Making Society through Science and Technology*. STS Italia Publishing, pp. 367–382.

Lefebvre, E. *et al.* (2015) 'Stimuli-responsive Materials : Definition, Classification and Descriptions', in *7th International Materials Education Symposium*. Cambridge.

Leist, S. K. *et al.* (2017) 'Investigating the Shape Memory Properties of 4D Printed Polylactic Acid (PLA) and the Concept of 4D Printing onto Nylon Fabrics for the Creation of Smart Textiles', *Virtual and Physical Prototyping*, 12(4), pp. 290–300. doi: 10.1080/17452759.2017.1341815.

Leu, M. C. *et al.* (2012) 'Freeze-form Extrusion Fabrication of Functionally Graded Materials', *CIRP Annals*, 61(1), pp. 223–226. doi: 10.1016/j.cirp.2012.03.050.

Li, L. *et al.* (2002) 'Composite Modeling and Analysis for Fabrication of FDM Prototypes With Locally Controlled Properties', *Journal of Manufacturing Processes*, 4(2), pp. 129–141. doi: 10.1016/S1526-6125(02)70139-4.

Li, W., Zhang, X. and Liou, F. (2018) 'Modeling Analysis of Argon Gas Flow Rate's Effect on Pre-Mixed Powder Separation in Laser Metal Deposition Process and Experimental Validation', *International Journal of Advanced Manufacturing Technology*. Springer London, 96(9–12), pp. 4321–4331. doi: 10.1007/s00170-018-1909-x.

Li, Y. *et al.* (2020) 'A Review on Functionally Graded Materials and Structures via Additive Manufacturing: From Multi-Scale Design to Versatile Functional Properties', *Advanced Materials Technologies*. Wiley-Blackwell, 5(6), p. 1900981. doi: 10.1002/admt.201900981.

Liu, C., Qin, H. and Mather, P. T. (2007) 'Review of Progress in Shape-memory Polymers', *Journal of Materials Chemistry*, 17, pp. 1543–1558. doi: 10.1039/b615954k.

Liu, Y. *et al.* (2020) 'Nonequilibrium Thermodynamic Calculation and Experimental Investigation of an Additively Manufactured Functionally Graded Material', *Journal of Alloys and Compounds*, 838, p. 155322. doi: 10.1016/j.jallcom.2020.155322.

Loh, G. H. *et al.* (2018) 'An Overview of Functionally Graded Additive Manufacturing', *Additive Manufacturing*, 23, pp. 34–44. doi: 10.1016/j.addma.2018.06.023.

Loh, G. H. *et al.* (2020) 'An Overview of Material Extrusion Troubleshooting', *Applied Sciences*, 10(14), p. 4776. doi: 10.3390/app10144776.

Loh, G. H. and Pei, E. (2019) *Design for Material Extrusion on Mesh Fabrics, 16th Rapid Design, Prototyping and Manufacturing Conference (RDPM2019)*. Available at: <http://bura.brunel.ac.uk/handle/2438/18700> (Accessed: 29 July 2020).

Loh, G. H., Sotayo, A. and Pei, E. (2021) 'Development and Testing of Material Extrusion Additive Manufactured Polymer–Textile Composites', *Fashion and Textiles*. Springer Singapore, 8, p. 2. doi: 10.1186/s40691-020-00232-7.

Lopez, C. (2020) *The Future of 3D Printing and Fashion Design Through the Eyes of LabeledBy*. Available at: <https://3dprint.com/236343/the-future-of-3d-printing-fashion-design-through-the-eyes-of-labeledby/> (Accessed: 26 July 2020).

Loughborough University (2021a) *Directed Energy Deposition | Additive Manufacturing Research Group | Loughborough University*. Available at: <https://www.lboro.ac.uk/research/amrg/about/the7categoriesofadditivemanufacturing/directenergydeposition/> (Accessed: 12 May 2021).

Loughborough University (2021b) *Material Extrusion | Additive Manufacturing Research Group | Loughborough University*. Available at: <https://www.lboro.ac.uk/research/amrg/about/the7categoriesofadditivemanufacturing/materialextrusion/> (Accessed: 12 May 2021).

Loughborough University (2021c) *Material Jetting | Additive Manufacturing Research Group | Loughborough University*. Available at: <https://www.lboro.ac.uk/research/amrg/about/the7categoriesofadditivemanufacturing/materialjetting/> (Accessed: 12 May 2021).

Loughborough University (2021d) *Powder Bed Fusion | Additive Manufacturing Research Group | Loughborough University*. Available at: <https://www.lboro.ac.uk/research/amrg/about/the7categoriesofadditivemanufacturing/powderbedfusion/> (Accessed: 10 May 2021).

Loughborough University (2021e) *Sheet Lamination | Additive Manufacturing Research Group | Loughborough University*. Available at: <https://www.lboro.ac.uk/research/amrg/about/the7categoriesofadditivemanufacturing/sheetlamination/> (Accessed: 12 May 2021).

Loughborough University (2021f) *Vat Photopolymerisation | Additive Manufacturing Research Group | Loughborough University*. Available at: <https://www.lboro.ac.uk/research/amrg/about/the7categoriesofadditivemanufacturing/vatphotopolymerisation/> (Accessed: 12 May 2021).

Luo, A. (2021) *Content Analysis | A Step-by-Step Guide with Examples*. Available at: <https://www.scribbr.com/methodology/content-analysis/> (Accessed: 7 July 2021).

Ma, C. *et al.* (2014) 'Supramolecular Lego Assembly Towards Three-Dimensional Multi-Responsive Hydrogels', *Advanced Materials*. Wiley-VCH Verlag, 26(32), pp. 5665–5669. doi: 10.1002/adma.201402026.

Ma, Q. *et al.* (2020) 'Recent 3D and 4D Intelligent Printing Technologies: A comparative Review and Future Perspective', *Procedia Computer Science*, 167, pp. 1210–1219. doi: 10.1016/j.procs.2020.03.434.

Mageean, L. (2018) *The Rise of 3D Printing in Fashion - WhichPLM*. Available at: <https://www.whichplm.com/rise-3d-printing-fashion/> (Accessed: 28 July 2020).

Mahamood, R. M. *et al.* (2012) 'Functionally Graded Material: An Overview', *Lecture Notes in Engineering and Computer Science*, 3, pp. 1593–1597.

Mahamood, R. M. and Akinlabi, E. T. (2017a) *Functionally Graded Materials*. 1st edn. Springer International Publishing (Topics in Mining, Metallurgy and Materials Engineering). doi: 10.1007/978-3-319-53756-6.

Mahamood, R. M. and Akinlabi, E. T. (2017b) 'Processing Methods of Functionally Graded Materials', in *Topics in Mining, Metallurgy and Materials Engineering*. Springer Science and Business Media Deutschland GmbH, pp. 23–45. doi: 10.1007/978-3-319-53756-6\_3.

Malengier, B. *et al.* (2017) '3D Printing on Textiles: Testing of Adhesion', in *ITMC2017 – International Conference on Intelligent Textiles and Mass Customisation*. Ghent, pp. 1–17.

Mao, Y. *et al.* (2015) 'Sequential Self-Folding Structures by 3D Printed Digital Shape Memory Polymers', *Scientific Reports*. Nature Publishing Group, 5, p. 1361. doi: 10.1038/srep13616.

Mao, Y. *et al.* (2016) '3D Printed Reversible Shape Changing Components with Stimuli Responsive Materials', *Scientific Reports*, 6, p. 24761. doi: 10.1038/srep24761.

Maskery, I. *et al.* (2016) 'A Mechanical Property Evaluation of Graded Density Al-Si10-Mg Lattice Structures Manufactured By Selective Laser Melting', *Materials Science and Engineering: A*, 670, pp. 264–274. doi: 10.1016/j.msea.2016.06.013.

McCombes, S. (2019) *How to Write Methodology | A Step-by-Step Guide*. Available at: <https://www.scribbr.co.uk/thesis-dissertation/methodology/> (Accessed: 3 July 2021).

Melnikova, R., Ehrmann, A. and Finsterbusch, K. (2014) '3D Printing of Textile-based Structures by Fused Deposition Modelling (FDM) with Different Polymer Materials', *IOP Conference Series: Materials Science and Engineering*, 62, p. 012018. doi: 10.1088/1757-899X/62/1/012018.

Memarian, F., Fereidoon, A. and Ghorbanzadeh Ahangari, M. (2018) 'Effect of Acrylonitrile Butadiene Styrene on the Shape Memory, Mechanical, and Thermal Properties of Thermoplastic Polyurethane', *Journal of Vinyl and Additive Technology*. John Wiley and Sons Ltd, 24(S1), pp. 96–104. doi: 10.1002/vnl.21601.

Meyer, P., Döpke, C. and Ehrmann, A. (2019) 'Improving Adhesion of Three-Dimensional Printed Objects on Textile Fabrics by Polymer Coating', *Journal of Engineered Fibers and Fabrics*, 14, pp. 1–7. doi: 10.1177/1558925019895257.

Michalatos, P. and Payne, A. (2016) *Monolith: The Biomedical Paradigm and the Inner Complexity of Hierarchical Material Design*. Available at: [http://papers.cumincad.org/data/works/att/ecaade2016\\_203.pdf](http://papers.cumincad.org/data/works/att/ecaade2016_203.pdf) (Accessed: 5 May 2021).

Momeni, F. *et al.* (2017) 'A Review of 4D Printing', *Materials and Design*, 122, pp. 42–79. doi: 10.1016/j.matdes.2017.02.068.

Momeni, F. and Ni, J. (2020) 'Laws of 4D Printing', *Engineering*. Chinese Academy of Engineering, 6(9), pp. 1035–1055. doi: 10.1016/j.eng.2020.01.015.

- Monzón, M. D. *et al.* (2017) '4D Printing: Processability and Measurement of Recovery Force in Shape Memory Polymers', *International Journal of Advanced Manufacturing Technology*, 89, pp. 1827–1836. doi: 10.1007/s00170-016-9233-9.
- Mpofu, N. S. *et al.* (2019) 'Use of Regression to Study the Effect of Fabric Parameters on the Adhesion of 3D Printed PLA Polymer onto Woven Fabrics', *Fashion and Textiles*, 6, p. 24. doi: 10.1186/s40691-019-0180-6.
- Mpofu, N. S. *et al.* (2020) 'The Use of Statistical Techniques to Study the Machine Parameters Affecting the Properties of 3D Printed Cotton/Polylactic Acid Fabrics', *Journal of Engineered Fibers and Fabrics*, 15, pp. 1–10. doi: 10.1177/1558925020928531.
- Muller, P., Hascoet, J. Y. and Mognol, P. (2014) 'Toolpaths for Additive Manufacturing of Functionally Graded Materials (FGM) Parts', *Rapid Prototyping Journal*. Emerald Group Publishing Ltd., 20(6), pp. 511–522. doi: 10.1108/RPJ-01-2013-0011.
- Muller, P., Mognol, P. and Hascoet, J. Y. (2012) 'Functionally Graded Material (FGM) Parts: From Design to the Manufacturing Simulation', in *ASME 2012 11th Biennial Conference on Engineering Systems Design and Analysis, ESDA 2012*. Nantes, France: American Society of Mechanical Engineers Digital Collection, pp. 123–131. doi: 10.1115/ESDA2012-82586.
- Naebe, M. and Shirvanimoghaddam, K. (2016) 'Functionally Graded Materials: A Review of Fabrication and Properties', *Applied Materials Today*. Elsevier Ltd, 5, pp. 223–245. doi: 10.1016/j.apmt.2016.10.001.
- Nam, S. and Pei, E. (2019) 'A Taxonomy of Shape-changing Behavior for 4D Printed Parts Using Shape-memory Polymers', *Progress in Additive Manufacturing*. Springer International Publishing, 4(2), pp. 167–184. doi: 10.1007/s40964-019-00079-5.
- Nam, S. and Pei, E. (2020) 'The Influence of Shape Changing Behaviors From 4D Printing Through Material Extrusion Print Patterns and Infill Densities', *Materials*, 13, p. 3754. doi: 10.3390/MA13173754.
- Narula, A. *et al.* (2018) 'Effect of Knit and Print Parameters on Peel Strength of Hybrid 3-D Printed Textiles', *Journal of Textiles and Fibrous Materials*, 1, pp. 1–10. doi: 10.1177/2515221117749251.
- Neffe, A. T. *et al.* (2009) 'Polymer Networks Combining Controlled Drug Release, Biodegradation, and Shape Memory Capability', *Advanced Materials*. John Wiley & Sons, Ltd, 21(32–33), pp. 3394–3398. doi: 10.1002/adma.200802333.

Niendorf, T. *et al.* (2014) 'Functionally Graded Alloys Obtained by Additive Manufacturing', *Advanced Engineering Materials*, 16(7), pp. 857–861. doi: 10.1002/adem.201300579.

Oxman, N. (2011) 'Variable Property Rapid Prototyping', *Virtual and Physical Prototyping*, 6(1), pp. 3–31. doi: 10.1080/17452759.2011.558588.

Oxman, N. (2021) *Projects*. Available at: <https://web.media.mit.edu/~neri/site/projects/projects.html> (Accessed: 28 April 2021).

Oxman, N., Keating, S. and Tsai, E. (2012) 'Functionally Graded Rapid Prototyping', in *Innovative Developments in Virtual and Physical Prototyping - Proceedings of the 5th International Conference on Advanced Research and Rapid Prototyping*. Taylor & Francis, pp. 483–489. doi: 10.1201/b11341-78.

Papakonstantinou, N. (2015) *Fabricflation by Nina Papakonstantinou - Issuu*. Available at: <https://issuu.com/ninapapakonstantinou/docs/fabricflation> (Accessed: 26 July 2020).

Parameswaranpillai, J. *et al.* (2020) *Shape Memory Polymers, Blends and Composites: Advances and Applications*. Springer Singapore. doi: 10.1007/978-981-13-8574-2.

Parihar, R. S., Setti, S. G. and Sahu, R. K. (2018) 'Recent Advances in the Manufacturing Processes of Functionally Graded Materials: A Review', *IEEE Journal of Selected Topics in Quantum Electronics*, 25(2), pp. 309–336. doi: 10.1515/secm-2015-0395.

Patil, D. and Song, G. (2017) 'A Review of Shape Memory Material's Applications in the Offshore Oil and Gas Industry', *Smart Materials and Structures*. Institute of Physics Publishing, 26(9), p. 093002. doi: 10.1088/1361-665X/aa7706.

Pei, E. *et al.* (2017) 'A Study of 4D Printing and Functionally Graded Additive Manufacturing', *Assembly Automation*, 37(2). doi: 10.1108/AA-01-2017-012.

Pei, E. *et al.* (2020) *Programming 4D Printed Parts Through Shape-Memory Polymers and Computer-Aided-Design, Lecture Notes in Mechanical Engineering*. doi: 10.1007/978-3-030-29041-2\_19.

Pei, E. *et al.* (2021) 'Functionally Graded Additive Manufacturing', in Singh, S. and Hussain, C. (eds) *Additive Manufacturing with Functionalized Nanomaterials*. Elsevier, pp. 35–54. doi: 10.1016/B978-0-12-823152-4.00006-5.

Pei, E. and Loh, G. H. (2018a) 'Future Challenges in Functionally Graded Additive Manufacturing', in *Additive Manufacturing - Developments in Training and Education*, pp.

219–226. doi: 10.1007/978-3-319-76084-1\_15.

Pei, E. and Loh, G. H. (2018b) 'Technological Considerations for 4D printing: An Overview', *Progress in Additive Manufacturing*, 3, pp. 95–107. doi: 10.1007/s40964-018-0047-1.

Pei, E., Loh, G. H. and Nam, S. (2020) 'Concepts and Terminologies in 4D Printing', *Applied Sciences (Switzerland)*, 10(13). doi: 10.3390/app10134443.

Pei, E., Shen, J. and Watling, J. (2015) 'Direct 3D Printing of Polymers onto Textiles: Experimental Studies and Applications', *Rapid Prototyping Journal*. Edited by Dr. Eujin Pei, 21(5), pp. 556–571. doi: 10.1108/RPJ-09-2014-0126.

Peraza-Hernandez, E. A. *et al.* (2013) 'Towards Building Smart Self-folding Structures', *Computers and Graphics*, 37(6), pp. 730–742. doi: 10.1016/j.cag.2013.05.022.

Peraza-Hernandez, E. A. *et al.* (2014) 'Origami-inspired Active Structures: A Synthesis and Review', *Smart Materials and Structures*. Institute of Physics Publishing, 23(9), p. 094001. doi: 10.1088/0964-1726/23/9/094001.

Pérez, M. *et al.* (2020) 'Current Advances in Additive Manufacturing', in *Procedia CIRP*, pp. 439–444. doi: 10.1016/j.procir.2020.05.07.

Pretsch, T. (2010) 'Review on the Functional Determinants and Durability of Shape Memory Polymers', *Polymers*, 2(3), pp. 120–158. doi: 10.3390/polym2030120.

Prusa Research (2021) *Original Prusa i3 Multi Material 2.0 - Prusa3D - 3D Printers from Josef Průša*. Available at: <https://www.prusa3d.com/original-prusa-i3-multi-material-2-0/> (Accessed: 15 January 2021).

Prusa3D (2018) *3D Printing Handbook. User Manual for 3D Printers: Original Prusa i3 MK3 Kit, Original Prusa i3 MK3*. Available at: [www.prusa3d.de/treiber/](http://www.prusa3d.de/treiber/) (Accessed: 6 May 2020).

Qian, T. *et al.* (2014) 'Microstructure of TA2/TA15 Graded Structural Material by Laser Additive Manufacturing Process', *Transactions of Nonferrous Metals Society of China*, 24(9), pp. 2729–2736. doi: 10.1016/S1003-6326(14)63404-X.

Ragab, A. *et al.* (2017) 'Determination of Pore Size, Porosity and Pore Size Distribution of Woven Structures by Image Analysis Techniques', *Journal of Textile Science & Engineering*, 7, p. 314. doi: 10.4172/2165-8064.1000314.

Rajkumar, A. R. and Shanmugam, K. (2018) 'Additive Manufacturing-enabled Shape

Transformations via FFF 4D printing', *Journal of Materials Research*, 33(24), pp. 4362–4376. doi: 10.1557/jmr.2018.397.

Raviv, D. *et al.* (2014) 'Active Printed Materials for Complex Self-evolving Deformations', *Scientific Reports*, 4, p. 7422. doi: 10.1038/srep07422.

Redwood, B., Schöffner, F. and Garret, B. (2017) *The 3D Printing Handbook*. First Edit, 3D Hubs. First Edit. Amsterdam, The Netherlands: 3D Hubs B.V.

Richards, D. and Amos, M. (2014) 'Designing with Gradients: Bio-Inspired Computation for Digital Fabrication', in *ACADIA 2014 Design Agency. Proceedings of the 34th Annual Conference of the Association for Computer-Aided Design in Architecture*. Los Angeles, California, pp. 101–110. Available at: [https://e-space.mmu.ac.uk/608356/1/Designing with Gradients\\_ACCEPTED.pdf](https://e-space.mmu.ac.uk/608356/1/Designing%20with%20Gradients_ACCEPTED.pdf) (Accessed: 28 April 2021).

Rigid.Ink (2019) *Complete 3D Printing Filament Comparison Guide 2019 [All 17 Compared]*. Available at: <https://rigid.ink/pages/filament-comparison-guide> (Accessed: 13 July 2020).

Robson, C. and McCartan, K. (2015) *Real World Research : A Resource for Users of Social Research Methods in Applied Settings*. Fourth. Edited by C. Robson and K. McCartan. Hoboken, New Jersey: Wiley.

Rosales, C. A. G. *et al.* (2019) 'Characterization of Shape Memory Polymer Parts Fabricated Using Material Extrusion 3D Printing Technique', *Rapid Prototyping Journal*, 25(2), pp. 322–331. doi: 10.1108/RPJ-08-2017-0157.

Roudbarian, N. *et al.* (2019) 'An Experimental Investigation on Structural Design of Shape Memory Polymers', *Smart Materials and Structures*, 28, p. 095017. doi: 10.1088/1361-665X/ab3246.

Ryu, J. *et al.* (2014) 'Photo-origami — Bending and Folding Polymers with Light', 100, p. 161908. doi: 10.1063/1.3700719.

Sabantina, L. *et al.* (2015) 'Combining 3D printed Forms with Textile Structures - Mechanical and Geometrical Properties of Multi-material Systems', in *IOP Conference Series: Materials Science and Engineering*. Beijing, China. doi: 10.1088/1757-899X/87/1/012005.

Salcedo, E. *et al.* (2018) 'Simulation and Validation of Three Dimension Functionally Graded Materials by Material Jetting', *Additive Manufacturing*, 22, pp. 351–359. doi: 10.1016/j.addma.2018.05.027.

- Saleh, B. *et al.* (2020) '30 Years of Functionally Graded Materials: An overview of Manufacturing Methods, Applications and Future Challenges', *Composites Part B: Engineering*, 201, p. 108376. doi: 10.1016/j.compositesb.2020.108376.
- Sanatgar, R. H., Campagne, C. and Nierstrasz, V. (2017) 'Investigation of the Adhesion Properties of Direct 3D Printing of Polymers and Nanocomposites on Textiles: Effect of FDM Printing Process Parameters', *Applied Surface Science*, 403, pp. 551–563. doi: 10.1016/j.apsusc.2017.01.112.
- Sarathchandra, D. T., Subbu, S. K. and Venkaiah, N. (2018) 'Functionally Graded Materials and Processing Techniques: An Art of Review', *Materials Today: Proceedings*. Elsevier Ltd, 5(10), pp. 21328–21334. doi: 10.1016/j.matpr.2018.06.536.
- Scalet, G. (2020) 'Two-way and Multiple-way Shape Memory Polymers for Soft Robotics: An Overview', *Actuators*, 9, p. 10. doi: 10.3390/act9010010.
- Sew Guide (2020) *Fabric texture : An Overview - Sew Guide*. Available at: <https://sewguide.com/fabric-texture/> (Accessed: 21 July 2020).
- Shen, B. *et al.* (2019) 'Programming the Time into 3D Printing: Current Advances and Future Directions in 4D Printing', *Multifunctional Materials*. IOP Publishing, 3, p. 012001. doi: 10.1088/2399-7532/ab54ea.
- Shevchik, S. A. *et al.* (2018) 'Acoustic Emission for In Situ Quality Monitoring in Additive Manufacturing Using Spectral Convolutional Neural Networks', *Additive Manufacturing*. Elsevier B.V., 21, pp. 598–604. doi: 10.1016/j.addma.2017.11.012.
- Shinohara, Y. (2013) 'Functionally Graded Materials', in Somiya, S. (ed.) *Handbook of Advanced Ceramics: Materials, Applications, Processing, and Properties: Second Edition*. Second Edi. Elsevier, pp. 1179–1187. doi: 10.1016/B978-0-12-385469-8.00061-7.
- Singh, S., Prakash, C. and Ramakrishna, S. (2020) 'Three-dimensional Printing in the Fight Against Novel Virus COVID-19: Technology Helping Society During an Infectious Disease Pandemic', *Technology in Society*, 62, p. 101305. doi: 10.1016/j.techsoc.2020.101305.
- Sobota, M. *et al.* (2017) 'Crystallinity as a Tunable Switch of Poly(L-lactide) Shape Memory Effects', *Journal of the Mechanical Behavior of Biomedical Materials*, 66, pp. 144–151. doi: 10.1016/j.jmbbm.2016.11.009.
- Soldini, S. *et al.* (2020) *Manufacturing of 3D-printed Morphing Origami Solar Sails for the*

*Next Generation of CubeSats*. Available at:

<https://connectedeverythingmedia.files.wordpress.com/2020/04/3dprinted-morphing-origami-solar-sails.pdf> (Accessed: 20 January 2021).

Sossou, G. *et al.* (2018) 'Design for 4D Printing: Rapidly Exploring the Design Space Around Smart Materials', in *Procedia CIRP*. Belfort Cedex, France: Elsevier, pp. 120–125. doi: 10.1016/j.procir.2018.02.032.

Sossou, G. *et al.* (2019) 'Design for 4D Printing: Modeling and Computation of Smart Materials Distributions', *Materials and Design*, 181, p. 108074. doi: 10.1016/j.matdes.2019.108074.

Spahiu, T. *et al.* (2017) 'Effect of 3D Printing on Textile Fabrics', in *1st International Conference "Engineering and Entrepreneurship" Proceedings*. Tirana, Albania.

Standard Fiber (2020) *About Denier - Standard Fiber*. Available at:

<https://standardfiber.com/about-denier> (Accessed: 20 July 2020).

Steuben, J. C., Iliopoulos, A. P. and Michopoulos, J. G. (2016) 'Implicit Slicing for Functionally Tailored Additive Manufacturing', *Computer-Aided Design*. Elsevier Ltd, 77, pp. 107–119. doi: 10.1016/j.cad.2016.04.003.

Stevenson, K. (2018) *3D Design Futures: An Interview with Dr. Daniel Richards, Part 2* « *Fabbaloo*. Available at: <https://www.fabbaloo.com/blog/2018/1/17/3d-design-futures-an-interview-with-dr-daniel-richards-part-2> (Accessed: 27 April 2021).

Stratasys (2021a) *Find Materials and Filaments for 3D Printing | Stratasys*. Available at: <https://www.stratasys.com/en/materials/search?technologies=731e07a1a51b42419acd1cb75142df6&sortIndex=0> (Accessed: 12 May 2021).

Stratasys (2021b) *Tango: A Soft Flexible 3D Printing Material | Stratasys*. Available at: <https://www.stratasys.com/materials/search/tango> (Accessed: 15 January 2021).

Stratasys (2021c) *Vero: A Realistic Multi-color 3D Printing Material | Stratasys*. Available at: <https://www.stratasys.com/materials/search/vero> (Accessed: 15 January 2021).

Streefkerk, R. (2019) *Inductive vs. Deductive Research Approach (with Examples)*. Available at: <https://www.scribbr.com/methodology/inductive-deductive-reasoning/> (Accessed: 7 July 2021).

Strzelec, K., Sienkiewicz, N. and Szmechtyk, T. (2020) 'Classification of Shape-memory

Polymers, Polymer Blends, and Composites', in Parameswaranpillai, J. et al. (eds) *Shape Memory Polymers, Blends and Composites*. Springer, Singapore, pp. 21–52. doi: 10.1007/978-981-13-8574-2\_2.

Sun, J. et al. (2016) 'Morphing Aircraft Based on Smart Materials and Structures: A state-of-the-art Review', *Journal of Intelligent Material Systems and Structures*. SAGE Publications Ltd, 27(17), pp. 2289–2312. doi: 10.1177/1045389X16629569.

Sun, L. et al. (2012) 'Stimulus-responsive Shape Memory Materials: A Review', *Materials and Design*, 33(1), pp. 577–640. doi: 10.1016/j.matdes.2011.04.065.

Sun, L. et al. (2019) 'A Brief Review of the Shape Memory Phenomena in Polymers and Their Typical Sensor Applications', *Polymers*. MDPI AG, p. 1049. doi: 10.3390/polym11061049.

Sun, L. et al. (2020) '4DTexture : A Shape-changing Fabrication Method for 3D Surfaces with Texture', in *CHI EA '20: Extended Abstracts of the 2020 CHI Conference on Human Factors in Computing Systems*. Honolulu, HI, pp. 1–7. doi: 10.1145/3334480.3383053.

Takahashi, T. et al. (2016) *FAV File Format Specification*. Available at: [https://www.fujifilm.com/fbglobal/eng/company/technology/communication/3d/pdf/fav\\_format\\_specification\\_ver1\\_en.pdf](https://www.fujifilm.com/fbglobal/eng/company/technology/communication/3d/pdf/fav_format_specification_ver1_en.pdf) (Accessed: 6 May 2021).

Tamicare (2020) *Technology | Tamicare*. Available at: <https://www.tamicare.com/manufacture> (Accessed: 26 July 2020).

Tammam-Williams, S. and Todd, I. (2017) 'Design for Additive Manufacturing with Site-Specific Properties in Metals and Alloys', *Scripta Materialia*. Elsevier Ltd, 135, pp. 105–110. doi: 10.1016/j.scriptamat.2016.10.030.

Taylor, D. L. and Panhuis, M. in het (2016) 'Self-Healing Hydrogels', *Advanced Materials*, 28(41), pp. 9060–9093. doi: 10.1002/adma.201601613.

Tech Target (2007) *What is Voxel? - Definition from WhatIs.com*. Available at: <https://whatis.techtarget.com/definition/voxel> (Accessed: 22 April 2021).

Teoh, J. E. M. (2018) *4D Printing of Polymer-based Smart Structures by Thermal Activation*. Nanyang Technological University Singapore. doi: 10.32657/10356/74351.

Thakur, S. and Hu, J. (2017) 'Polyurethane: A Shape Memory Polymer (SMP)', *Aspects of Polyurethanes*, pp. 53–71. doi: 10.5772/intechopen.69992.

The Business of Fashion (2021) *Pleats | Fashion A-Z | BoF Education | The Business of Fashion | #BoFEducation*. Available at:

<https://www.businessoffashion.com/education/fashion-az/pleats> (Accessed: 10 August 2021).

The Cutting Class (2014) *Creating Cartridge Pleats - The Cutting Class*. Available at:

<https://www.thecuttingclass.com/creating-cartridge-pleats/> (Accessed: 10 August 2021).

The Cutting Class (2015) *Ribboned Pleats at Dior Haute Couture - The Cutting Class*.

Available at: <https://www.thecuttingclass.com/ribboned-pleats-at-dior-haute-couture/> (Accessed: 16 August 2021).

Thérien-Aubin, H. *et al.* (2013) 'Multiple Shape Transformations of Composite Hydrogel Sheets', *Journal of the American Chemical Society*. *J Am Chem Soc*, 135(12), pp. 4834–4839. doi: 10.1021/ja400518c.

Thérien-Aubin, H. *et al.* (2015) 'Shape Transformations of Soft Matter Governed by Bi-axial Stresses', *Soft Matter*, 11, pp. 4600–4605. doi: 10.1039/c5sm00561b.

Tibbits, S. (2013) *The Emergence of 4D Printing*, *TED 2013*. Available at:

[https://www.ted.com/talks/skylar\\_tibbits\\_the\\_emergence\\_of\\_4d\\_printing?language=en](https://www.ted.com/talks/skylar_tibbits_the_emergence_of_4d_printing?language=en) (Accessed: 5 October 2020).

Tibbits, S. (2014) '4D Printing: Multi-material Shape Change', *Architectural Design*. John Wiley & Sons, Ltd, 84(1), pp. 116–121. doi: 10.1002/ad.1710.

Tibbits, S. *et al.* (2014) '4D Printing and Universal Transformation', in *ACADIA 2014 - Design Agency: Proceedings of the 34th Annual Conference of the Association for Computer Aided Design in Architecture*, pp. 539–548.

Tibbits, S. (2017) *Self-assembly Lab: Experiments in Programming Matter*. First Edit. Routledge Taylor and Francis Group. doi: 10.4324/9781315693613.

Tyson, E. (2020a) *3D Printing Nylon Filament - Step-by-step Settings & Problems Solved*.

Available at: <https://rigid.ink/blogs/news/3d-printing-nylon-filament-heres-why-and-how-you-should-use-it> (Accessed: 13 July 2020).

Tyson, E. (2020b) *How To Print PETG Filament 2020*. Available at:

<https://rigid.ink/blogs/news/175700615-petg-filament-heres-what-you-need-to-know> (Accessed: 13 July 2020).

Tyson, E. (2020c) *PLA 3D Printing Filament 2020 Guide*. Available at: <https://rigid.ink/blogs/news/3d-printing-basics-how-to-get-the-best-results-with-pla-filament> (Accessed: 13 July 2020).

Tyson, E. (2020d) *TPE & TPU Flexible Filament Compared & Step-by-Step Guide to Print*. Available at: <https://rigid.ink/blogs/news/172062855-what-is-the-difference-between-tpe-and-tpu-flexible-filament> (Accessed: 13 July 2020).

Tyson, E. (2020e) *Want to Use ABS in Hot Sun? We Compare ABS vs ASA Filaments*. Available at: <https://rigid.ink/blogs/news/175845063-the-difference-between-abs-and-asa> (Accessed: 13 July 2020).

Unger, L. *et al.* (2018) 'Increasing Adhesion of 3D Printing on Textile Fabrics by Polymer Coating', *Tekstilec*, 61(4), pp. 265–271. doi: 10.14502/Tekstilec2018.61.265-271.

Uysal, R. and Stubbs, J. B. (2019) 'A New Method of Printing Multi-material Textiles by Fused Deposition Modelling (FDM)', *Tekstilec*. University of Ljubljana, 62(4), pp. 248–257. doi: 10.14502/Tekstilec2019.62.248-257.

Vaezi, M. *et al.* (2013) 'Multiple Material Additive Manufacturing - Part 1: A Review: This Review Paper Covers a Decade of Research on Multiple Material Additive Manufacturing Technologies Which Can Produce Complex Geometry Parts with Different Materials', *Virtual and Physical Prototyping*, 8(1), pp. 19–50. doi: 10.1080/17452759.2013.778175.

Van der Velden, N. M., Kuusk, K. and Köhler, A. R. (2015) 'Life Cycle Assessment and Eco-design of Smart Textiles: The Importance of Material Selection Demonstrated Through E-Textile Product Redesign', *Materials and Design*. Elsevier Ltd, 84, pp. 313–324. doi: 10.1016/j.matdes.2015.06.129.

VoxCad (2021) *VoxCad*. Available at: <https://sites.google.com/site/voxcadproject/> (Accessed: 5 May 2021).

Wagermaier, W. *et al.* (2009) 'Characterization Methods for Shape-Memory Polymers', in Lendlein, A. (ed.) *Shape-Memory Polymers. Advances in Polymer Science*. Springer, Berlin, Heidelberg, pp. 97–145. doi: 10.1007/12\_2009\_25.

Wan, X. *et al.* (2019) '3D Printing of Shape Memory Poly(d,l-lactide-co-trimethylene carbonate) by Direct Ink Writing for Shape-changing Structures', *Journal of Applied Polymer Science*, 136(44), pp. 1–12. doi: 10.1002/app.48177.

- Wang, J. *et al.* (2018) 'Characterization of Wire Arc Additively Manufactured Titanium Aluminide Functionally Graded Material: Microstructure, Mechanical Properties and Oxidation Behaviour', *Materials Science and Engineering: A*, 734, pp. 110–119. doi: 10.1016/j.msea.2018.07.097.
- Wang, Q. *et al.* (2018) 'Programmable Morphing Composites with Embedded Continuous Fibers by 4D Printing', *Materials and Design*, 155, pp. 404–413. doi: 10.1016/j.matdes.2018.06.027.
- Wang, W., Liu, Y. and Leng, J. (2016) 'Recent Developments in Shape Memory Polymer Nanocomposites: Actuation Methods and Mechanisms', *Coordination Chemistry Reviews*, 320–321, pp. 38–52. doi: 10.1016/j.ccr.2016.03.007.
- Wei, H. *et al.* (2017) 'Direct-write Fabrication of 4D Active Shape-changing Structures Based on a Shape Memory Polymer and Its Nanocomposite', *ACS Applied Materials and Interfaces*. American Chemical Society, 9(1), pp. 876–883. doi: 10.1021/acsami.6b12824.
- Wischke, C. and Lendlein, A. (2010) 'Shape-memory Polymers As Drug Carriers- A Multifunctional System', *Pharmaceutical Research*. Springer, pp. 527–529. doi: 10.1007/s11095-010-0062-5.
- Wohlers Associates (2021) 'Wohlers Annual Report: Additive Manufacturing and 3D Printing State of the Industry'. Available at: <https://wohlersassociates.com/2021report.htm> (Accessed: 21 July 2021).
- Wolf, C. (2003) *The Art of Manipulating Fabric*. Second Edi. Edited by R. Fanning and R. Cooke. Krause Publications.
- Wu, J. *et al.* (2016) 'Multi-shape Active Composites by 3D Printing of Digital Shape Memory Polymers', *Scientific Reports*. doi: 10.1038/srep24224.
- Wu, J. *et al.* (2018) 'Reversible Shape Change Structures by Grayscale Pattern 4D Printing', *Multifunctional Materials*, 1(1), pp. 1–4. doi: 10.1088/2399-7532/aac322.
- Wu, J. J. *et al.* (2018) '4D Printing: History and Recent Progress', *Chinese Journal of Polymer Science (English Edition)*, 36(5), pp. 563–575. doi: 10.1007/s10118-018-2089-8.
- Wu, X. *et al.* (2013) 'Mechanisms of the Shape Memory Effect in Polymeric Materials', *Polymers*, 5(4), pp. 1169–1202. doi: 10.3390/polym5041169.
- Wu, X., Liu, W. and Wang, M. Y. (2008) 'A CAD Modeling System for Heterogeneous

- Object', *Advances in Engineering Software*. Elsevier Ltd, 39(5), pp. 444–453. doi: 10.1016/j.advenzsoft.2007.03.002.
- Wu, Z. L. *et al.* (2013) 'Three-dimensional Shape Transformations of Hydrogel Sheets Induced by Small-scale Modulation of Internal Stresses', *Nature Communications*. Nature Publishing Group, 4, p. 1586. doi: 10.1038/ncomms2549.
- Wykrzykowska, J. J., Onuma, Y. and Serruys, P. W. (2009) 'Advances in Stent Drug Delivery: The Future Is In Bioabsorbable Stents', *Expert Opinion on Drug Delivery*. Expert Opin Drug Deliv, pp. 113–126. doi: 10.1517/17425240802668495.
- Xometry Europe (2020) *3D Printing File Formats Compared: OBJ, STL, AMF, 3MF | Xometry*. Available at: <https://xometry.eu/en/3d-printing-file-formats-compared-obj-stl-amf-and-3mf/> (Accessed: 6 May 2021).
- Xu, J. and Song, J. (2011) 'Thermal Responsive Shape Memory Polymers for Biomedical Applications', in *Biomedical Engineering - Frontiers and Challenges*. doi: 10.5772/19256.
- Yang, W. G. *et al.* (2014) 'Advanced Shape Memory Technology to Reshape Product Design, Manufacturing and Recycling', *Polymers*. doi: 10.3390/polym6082287.
- Yap, Y. L., Sing, S. L. and Yeong, W. Y. (2020) 'A Review of 3D Printing Processes and Materials for Soft Robotics', *Rapid Prototyping Journal*, 26(8), pp. 1345–1361. doi: 10.1108/RPJ-11-2019-0302.
- Yu, K. *et al.* (2015) 'Controlled Sequential Shape Changing Components by 3D Printing of Shape Memory Polymer Multimaterials', *Procedia IUTAM*. Elsevier B.V., 12, pp. 193–203. doi: 10.1016/j.piutam.2014.12.021.
- Yüce, İ. (2017) 'Shape Memory Polymers and Shape Memory Alloys: Use in Smart Textiles', *International Journal of Development Research*, 07(11), pp. 16730–16736. Available at: <http://www.journalijdr.com>.
- Zafar, M. Q. and Zhao, H. (2019) '4D Printing: Future Insight in Additive Manufacturing', *Metals and Materials International*, 26, pp. 564–585. doi: 10.1007/s12540-019-00441-w.
- Zapfl, D. (2019) *How 3D Printing in the Textile Industry is Leading into a New Era*. Available at: <https://www.lead-innovation.com/english-blog/3d-printing-in-the-textile-industry> (Accessed: 29 July 2020).
- Zare, M. *et al.* (2019) 'Thermally-induced Two-way Shape Memory Polymers: Mechanisms,

Structures, and Applications', *Chemical Engineering Journal*. Elsevier, 374(February), pp. 706–720. doi: 10.1016/j.cej.2019.05.167.

Zarek, M. *et al.* (2016) '3D Printing of Shape Memory Polymers for Flexible Electronic Devices', *Advanced Materials Special Issue: Flexible and Stretchable Devices*, 28(22), pp. 4449–4454. doi: 10.1002/adma.201503132.

Zarek, M. *et al.* (2017) '4D Printing of Shape Memory-based Personalized Endoluminal Medical Devices', *Macromolecular Rapid Communications*. Wiley-VCH Verlag, 38, p. 1600628. doi: 10.1002/marc.201600628.

Zhang, B. *et al.* (2016) 'Additive Manufacturing of Functionally Graded Objects: A review', in *Proceedings of the ASME Design Engineering Technical Conference*. American Society of Mechanical Engineers (ASME). doi: 10.1115/DETC2016-60320.

Zhang, Q. *et al.* (2015) 'Pattern Transformation of Heat-shrinkable Polymer by Three-Dimensional (3D) Printing Technique', *Scientific Reports*. doi: 10.1038/srep08936.

Zhang, X. X. and Tao, X. (2001) 'Smart Textiles (2): Active Smart', *Textile Asia*, 32(7), pp. 49–52. Available at: <https://research.polyu.edu.hk/en/publications/smart-textiles-2-active-smart> (Accessed: 22 July 2021).

Zhang, Z., Demir, K. G. and Gu, G. X. (2019) 'Developments in 4D-Printing: A Review on Current Smart Materials, Technologies, and Applications', *International Journal of Smart and Nano Materials*. Taylor and Francis Ltd., 10(3), pp. 205–224. doi: 10.1080/19475411.2019.1591541.

Zhao, Q. *et al.* (2009) 'Synthesis of Macroporous Thermosensitive Hydrogels: A Novel Method of Controlling Pore Size', *Langmuir*, 25(5), pp. 3249–3254. doi: 10.1021/la8038939.

Zhou, C. *et al.* (2013) 'Digital Material Fabrication Using Mask-image-projection-based Stereolithography', *Rapid Prototyping Journal*. doi: 10.1108/13552541311312148.

Zhou, Nanjia *et al.* (2017) 'Gigahertz Electromagnetic Structures via Direct Ink Writing for Radio-Frequency Oscillator and Transmitter Applications', *Advanced Materials*, 29, p. 1605198. doi: 10.1002/adma.201605198.

Zhou, Y. *et al.* (2015) 'From 3D to 4D Printing: Approaches and Typical Applications', *Journal of Mechanical Science and Technology*, 29, pp. 4281–4288. doi: 10.1007/s12206-015-0925-0.

Zhu, Y. *et al.* (2006) 'Development of Shape Memory Polyurethane Fiber with Complete Shape Recoverability', *Smart Materials and Structures*. IOP Publishing, 15(5), p. 1385. doi: 10.1088/0964-1726/15/5/027.



## Appendix II. Semi-structured Expert Interview Questions

### INTERVIEW SCRIPT

#### Confirming the Terms, Definition and Findings of FGAM

(This interview is carried out as part of ISO/TC 261/ JG67 study)

Thank you for agreeing to participate in our interview. We are contacting you as an expert in AM to provide us with information and valuable feedback to refine and validate the terms, definitions and current findings on FGAM, helping us to state out the areas that requires further clarification.

This interview should last no longer than 30 minutes.

**Question 1.** We have defined FGAM as “a single additive manufacturing by gradationally mixing materials to fabricate freeform geometries with variable-property within one component”. Do you agree with the given definition of FGAM?

- Agree
- Disagree, please clarify the definition of FGAM in your own words.
- Somehow Agree, please clarify the definition of FGAM in your own words.

**Question 2.** If to tackle the limitation, which factor(s) would you think is the greatest limitation in realising the current state of FGAM.

- Additive Manufacturing technologies
- Materials (i.e., Material characterisation, Bi compatibility)
- CAD
- Application
- Manufacturing processes (i.e., Toolpath planning)

**Question 3.** Please specify other limitation(s) not identified above.

- Please provide your answer.

**Question 4.** Do you agree with the key manufacturing process of FGAM as stated below?

Step 1: Description of the Part Geometry and Material Distribution	Description of the geometry and the material distribution followed by classifying the material distribution (the dimension of the gradient). Three criteria are required: the dimension of the gradient, the shape of composition surfaces and the distribution of composition surfaces.
---	--

- Agree
- Disagree, please comment.

Step 2: Determination of manufacturing strategies	Material data that concerns the chemical composition and characteristics of the two (or more) materials used is gathered. The material distribution and orientation of slices are defined. The toolpaths are evaluated and calculated. The mathematical data is used to find the most appropriate manufacturing strategy.
--	---

- Agree

Disagree, please comment.

Step 3: Numerical Control (NC) programming	Numerical Control (NC) programming, involving paths and process parameters is generated with the G programming language (ISO 6983) from the toolpath route. A 3D grid with machine data and the material distribution is generated to the defined paths.
---	--

Agree

Disagree, please comment.

Step 4: Manufacturing	The NC program is used by a CNC controller. The operation involves fabricating slices in order to build three-dimensional cross-section profiles to construct the component layer by layer with pre-determined specific material deposition. The file is sent to the AM machine for the production sequence to commence.
--------------------------	--

Agree

Disagree, please comment.

**Question 5.** What is/are the file format(s) or data transfer format(s) that you are aware of that can support FGAM?

AMF

3MF

FAV

Other, please specify.

**Question 6.** Please provide any other general feedback.

Please provide your feedback.

### Contact for further information and complaints

Thank you for taking part in this study. Please contact us for further information or any issues regarding participating in this study.

Researcher Name: Hsiang Hsiang Loh

Email: [Hsiang.Loh@brunel.ac.uk](mailto:Hsiang.Loh@brunel.ac.uk)

Supervisor Name: Dr Eujin Pei

Email: [Eujin.Pe@brunel.ac.uk](mailto:Eujin.Pe@brunel.ac.uk)

### Appendix III. Summary of FGAM Findings

In conjunction with the study for ISO/ ASTM JG67, six respective field experts were interviewed to verify the definition and some aspects of FGAM. The descriptions of each participants were listed in Table 1.

Table 1. The general background of participants.

<b>Participants</b>	<b>Professions</b>	<b>Disciplines</b>
A	Academic professional	Mechanical engineering
B	Industry professional	Mechanical engineering
C	Industry professional	System architecture
D	Industry professional	Mechanical engineering
E	Academic and industry professional	Additive manufacturing
F	Academic professional	Additive manufacturing

According to Figure 1, only one out of six participants agreed with the initially proposed FGAM definition, which is defined as “a single additive manufacturing by gradationally mixing materials to fabricate freeform geometries with variable-property within one component”. The remaining five participants have somehow agreed and provided their suggestions to improve the definition. Participants A, B, C and D have suggested that the word “intentionally” should be included. The notion of intention is important. Participant B has also recommended removing the word “single” and “freeform”. Participant C explained that mixing of material is one way of FGAM, but it is not the only way. This is not a process of just modifying material composition but also modifying the mechanical properties. Participant D suggested that the phrase AM “process” should be replaced with AM “technique”. Whilst Participant E did not provide any elaboration on his selection. The improved versions of the FGAM definition were followed up with the participants for validation until all agreed (Table 2).

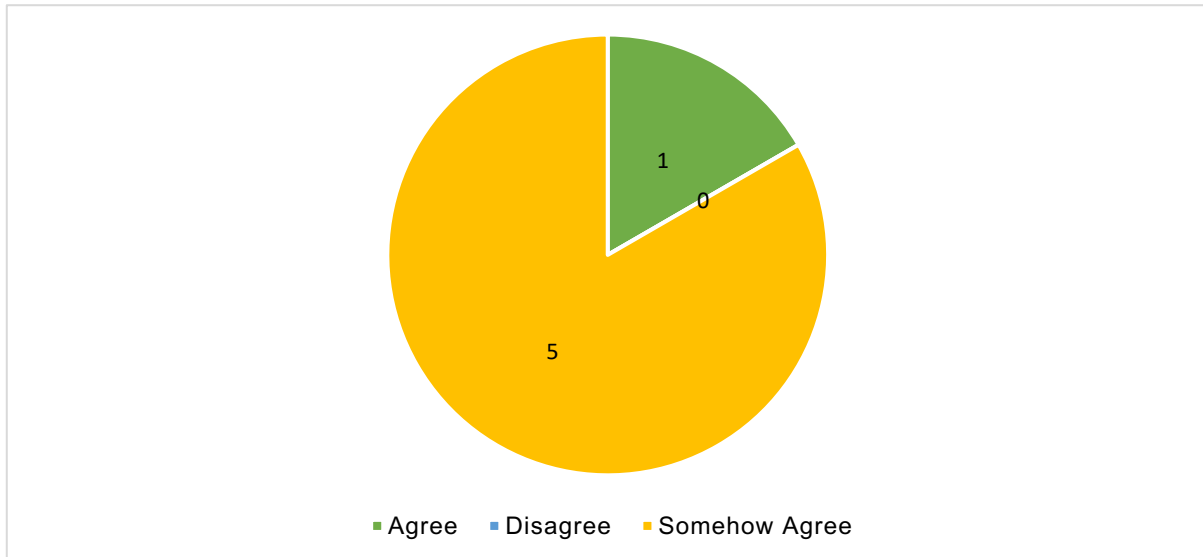


Figure 1. The definition of FGAM.

Table 2. The development of FGAM definition.

Version	Definition
1	FGAM is a single additive manufacturing by gradationally mixing materials to fabricate freeform geometries with variable-property within one component.
2	FGAM is a layer-by-layer fabrication technique that involves gradationally varying the ratio of the material organization within a component to meet an intended function
3	FGAM is a layer-by-layer fabrication technique that involves gradationally varying the material organization within a component to meet an intended function.
4	FGAM is a layer-by-layer fabrication technique that intentionally modifies process parameters and gradationally varies the spatial of the material(s) organisation within one component to meet the intended function

Figure 2 shows the ranking of limitations in realising the current state of FGAM. The majority of participants felt that the manufacturing technology and CAD, which include the data exchange formats, are the two limitations that require the most extensive research and investment for advancement. Special printers need to be developed for the FGAM strategy. One participant mentioned that the melting temperature and time for solidification are quite demanding for multi-material FGAM printing, no matter pre-mixed or in-printing mixing. This is followed by the materials, applications and manufacturing processes. Participant F commented that all factors are critically important. They are all interlinked limitations that need to overcome to make FGAM competent for practical applications on an industrial scale.

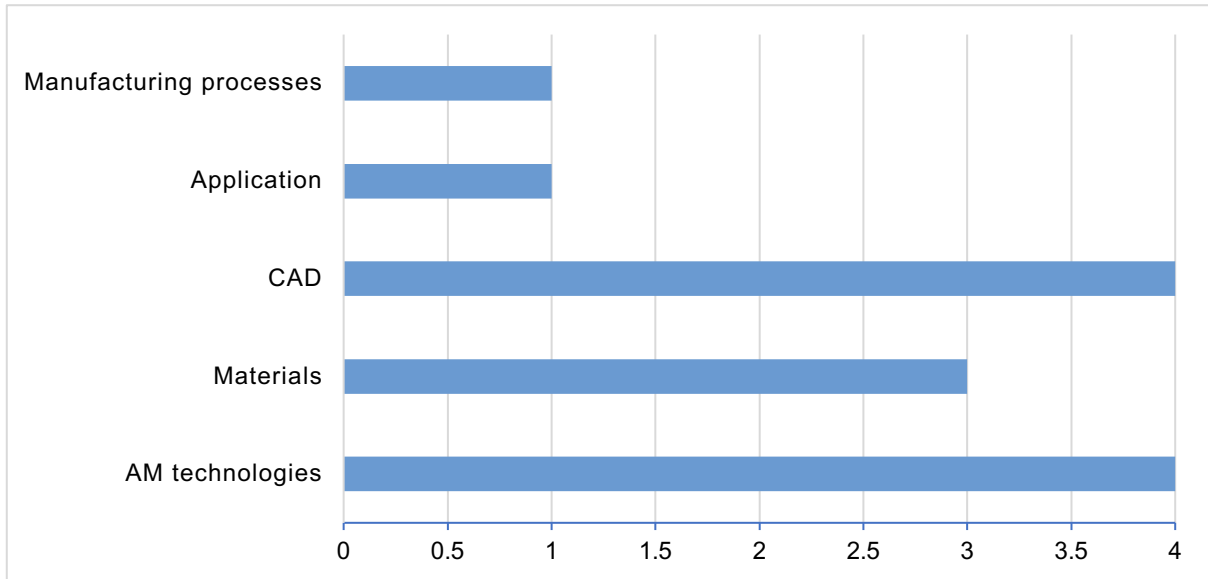


Figure 2. The limitations in realising the current state of FGAM.

Table 3 presents the comments received regarding the four stages of the modelling process for FGAM.

Table 3. Feedback on the proposed modelling process for FGAM.

Stage	Description	Agree	Disagree	Comments
Stage 1: Description of the Part Geometry and Material Distribution	Description of the geometry and the material distribution followed by classifying the material distribution (the dimension of the gradient). Three criteria are required: the dimension of the gradient, the shape of composition surfaces and the distribution of composition surfaces.	3	3	Participant C commented that function could be a valid description regarding to ASME descriptions and discussion. Participant D highlighted that function needs to be defined. Participant E said that it should be expressed by voxel.
Step 2: Determination of manufacturing strategies	Material data that concerns the chemical composition and characteristics of the two (or more) materials used is gathered. The material distribution and orientation of slices are defined. The toolpaths are evaluated and calculated. The mathematical data is used to find the most	4	2	Participant D explained that it can be one material. Participant F was unsure that this description has to do with determining the manufacturing strategy.

	appropriate manufacturing strategy.			
Step 3: Numerical Control (NC) programming	Numerical Control (NC) programming, involving paths and process parameters is generated with the G programming language (ISO 6983) from the toolpath route. A 3D grid with machine data and the material distribution is generated to the defined paths.	5	1	Participant F commented that it has nothing on FGM.
Step 4: Manufacturing	The NC program is used by a CNC controller. The operation involves fabricating slices in order to build three-dimensional cross-section profiles to construct the component layer by layer with pre-determined specific material deposition. The file is sent to the AM machine for the production sequence to commence.	5	1	Participant F commented that it has nothing on FGM.

Four out of six participants recognised that AMF would be the most suitable data exchange format to support FGAM (Figure 3). Another potential data exchange format is FAV. None of them knows much about 3MF. Participant C commented that 3MF was presenting intent in 2015. Standard would be available in 2017. Their report can reflect the actual standard implementation. When discussed about FAV would be the first 3D data exchange format capable of retaining information on the surface of a 3D model, Participant C described that “as presented during the FAV presentation and roadmap in Stockholm, this is not exact as the representation of the surfaces is planned in FAV and not functional yet. While voxels have implicit boundaries, defining the surface of a part through the boundaries of a voxel presents significant issues, first of which an aliasing effect that can interfere not only with surface properties and continuity but also with the gradients and/or structures inside the manufactured pieces, especially with respects to the orientation of the structure vs the voxel set referential. This element is significant enough that it should be considered in the context of FGAM”.

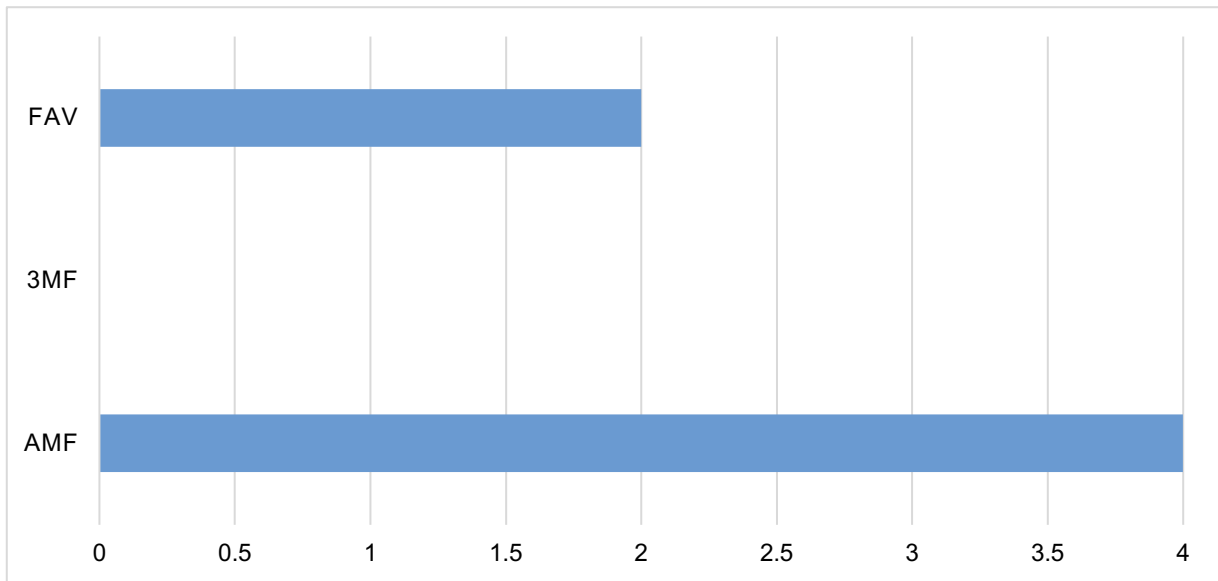


Figure 3. Data exchange formats for FGAM.

Regarding additional feedback, Participants A and D suggested that there should be an additional stage (Stage 5) to the modelling process of FGAM that address verification and conformance—“How do we capture the function that is being designed? How is this verified?”. Stage 5 should provide information on verification, validation and/or inspection methods to ensure the part produced is the intended design.

## Appendix IV. BREO Acceptance Letter



College of Engineering, Design and Physical Sciences Research Ethics Committee  
Brunel University London  
Kingston Lane  
Uxbridge  
UB8 3PH  
United Kingdom  
[www.brunel.ac.uk](http://www.brunel.ac.uk)

2 September 2020

### LETTER OF APPROVAL

APPROVAL HAS BEEN GRANTED FOR THIS STUDY TO BE CARRIED OUT BETWEEN 3/09/2020 AND 31/12/2020

Applicant (s): Ms Hsiang Loh

Project Title: A Framework Validation for Selecting 4D Printed Thermo-Responsive Materials

Reference: 25238-LR-Sep/2020- 27784-1

Dear Ms Hsiang Loh

The Research Ethics Committee has considered the above application recently submitted by you.

The Chair, acting under delegated authority has agreed that there is no objection on ethical grounds to the proposed study. Approval is given on the understanding that the conditions of approval set out below are followed:

- Approval is given for remote (online/telephone) research activity only. Face-to-face activity and/or travel will require approval by way of an amendment.
- The agreed protocol must be followed. Any changes to the protocol will require prior approval from the Committee by way of an application for an amendment.
- In addition to the above, please ensure that you monitor and adhere to all up-to-date Government health advice for the duration of your project.

#### Please note that:

- Research Participant Information Sheets and (where relevant) flyers, posters, and consent forms should include a clear statement that research ethics approval has been obtained from the relevant Research Ethics Committee.
- The Research Participant Information Sheets should include a clear statement that queries should be directed, in the first instance, to the Supervisor (where relevant), or the researcher. Complaints, on the other hand, should be directed, in the first instance, to the Chair of the relevant Research Ethics Committee.
- Approval to proceed with the study is granted subject to receipt by the Committee of satisfactory responses to any conditions that may appear above, in addition to any subsequent changes to the protocol.
- The Research Ethics Committee reserves the right to sample and review documentation, including raw data, relevant to the study.
- You may not undertake any research activity if you are not a registered student of Brunel University or if you cease to become registered, including abeyance or temporary withdrawal. As a deregistered student you would not be insured to undertake research activity. Research activity includes the recruitment of participants, undertaking consent procedures and collection of data. Breach of this requirement constitutes research misconduct and is a disciplinary offence.

A handwritten signature in black ink, appearing to read 'Hua Zhao'.

Professor Hua Zhao

Chair of the College of Engineering, Design and Physical Sciences Research Ethics Committee

Brunel University London

## **Appendix V. Participation Information Sheet**

### **PARTICIPANT INFORMATION SHEET**

#### **A Framework Validation for Selecting Thermo-Responsive Shape Memory Polymers for 4D Printing**

##### **Study title**

A validation of material selection framework for designers to select commercially available thermoplastics as potential Shape Memory Polymers (SMPs) for use in Material Extrusion (ME) 4D Printing.

Invitation Paragraph

You are invited to take part in an online interview to review and provide valuable feedback on a proposed material selection framework for 4D Printing. Before you decide, it is important for you to understand why the research is being done and what it will involve. Please take time to read the following information carefully and discuss it with us if there is anything that is not clear or if you would like more information. Please take time to decide whether or not you wish to take part.

##### **What is the purpose of the study?**

A designer needs to be equipped with adequate theoretical and practical knowledge about the shape memory properties of SMPs as a system and have wider access to materials to exploit the full potential of 4DP. A material selection framework for designers to discover, define and select commercially available thermoplastics as potential SMPs for use in material extrusion (ME) thermo-responsive 4DP is developed. The aim of the interview is to review and collect feedback from experts in the field to refine and validate the proposed framework.

##### **Why have I been invited to participate?**

You have been recognised as an expert in 4D Printing and we are inviting you to help us providing necessary data for the study.

##### **Do I have to take part?**

As participation is entirely voluntary, it is up to you to decide whether or not to take part. If you do decide to take part, you will be given this information sheet to keep and be asked to sign a consent form. If you decide to take part, you are still free to withdraw at any time and without giving a reason.

##### **What will happen to me if I take part?**

You will be engaged in an online semi-structured interview. You will be asked with some questions and provide feedback about the proposed framework. The online interview should last no more than one hour.

##### **What do I have to do?**

You will be replying six closed-ended questions, four sets of Likert scale questions, three open-ended questions and engage in discussion about the proposed framework.

##### **What are the possible disadvantages and risks of taking part?**

The possible disadvantages and risks of taking part is minimal, with the exception of issues pertaining to confidentiality.

##### **What if something goes wrong?**

The principal investigator will get in direct contact with the participants to resolve issues and if necessary, also inform the Research Ethics Office.

**Will my taking part in this study be kept confidential?**

All the personal data of the participants will be anonymised and collected data regarding institutes, research and projects will be kept secure using data encryption methods and all research data will be kept confidential.

**What will happen to the results of the research study?**

The results of the study will help us develop an effective material selection framework for designers to select potential commercially available thermoplastics as Shape Memory Polymers (SMPs) for use in ME 4D Printing.

**Who is organising and funding the research?**

The researcher.

**Who has reviewed the study?**

The study has been reviewed by the Research Ethics Committee of the College of Engineering, Design and Physical Sciences at Brunel University London. Brunel University is committed to comply with the Universities UK Research Integrity Concordat. We are committed to the highest level of integrity from our researchers during the course of the research.

**Contact for further information and complaints**

Thank you for taking part in this study. Please contact us for further information or any issues regarding participating in this study.

Researcher Name: Hsiang Hsiang Loh

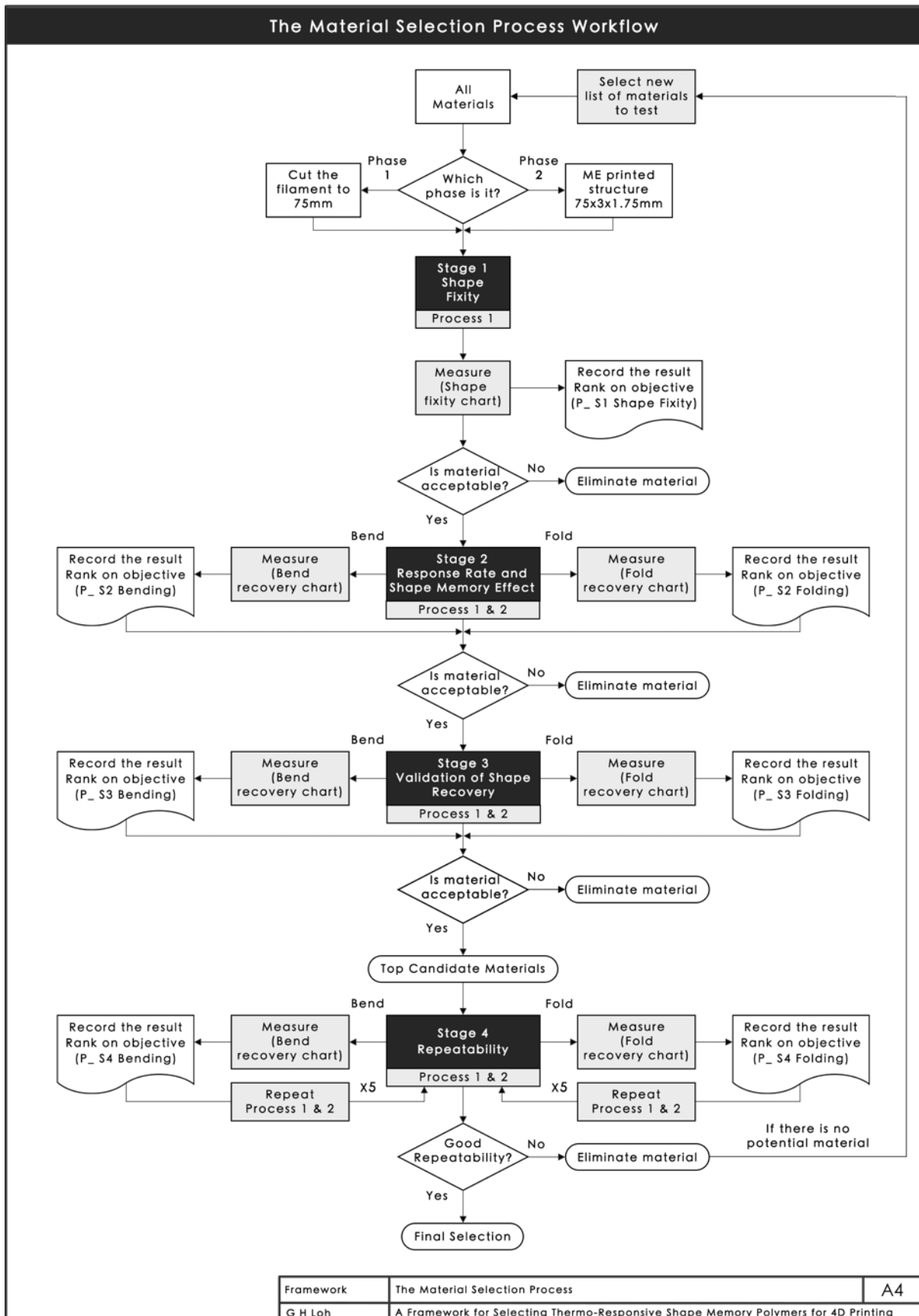
Email: [Hsiang.Loh@brunel.ac.uk](mailto:Hsiang.Loh@brunel.ac.uk)

Supervisor Name: Dr Eujin Pei

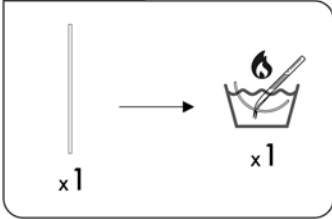
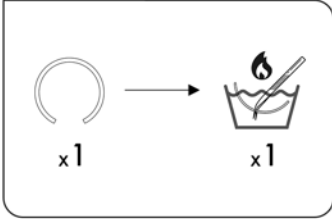
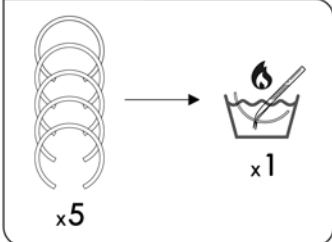
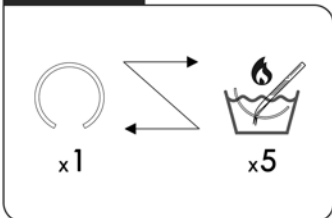
Email: [Eujin.Pe@brunel.ac.uk](mailto:Eujin.Pe@brunel.ac.uk)

## Appendix VI. Material Framework Selection User Guide

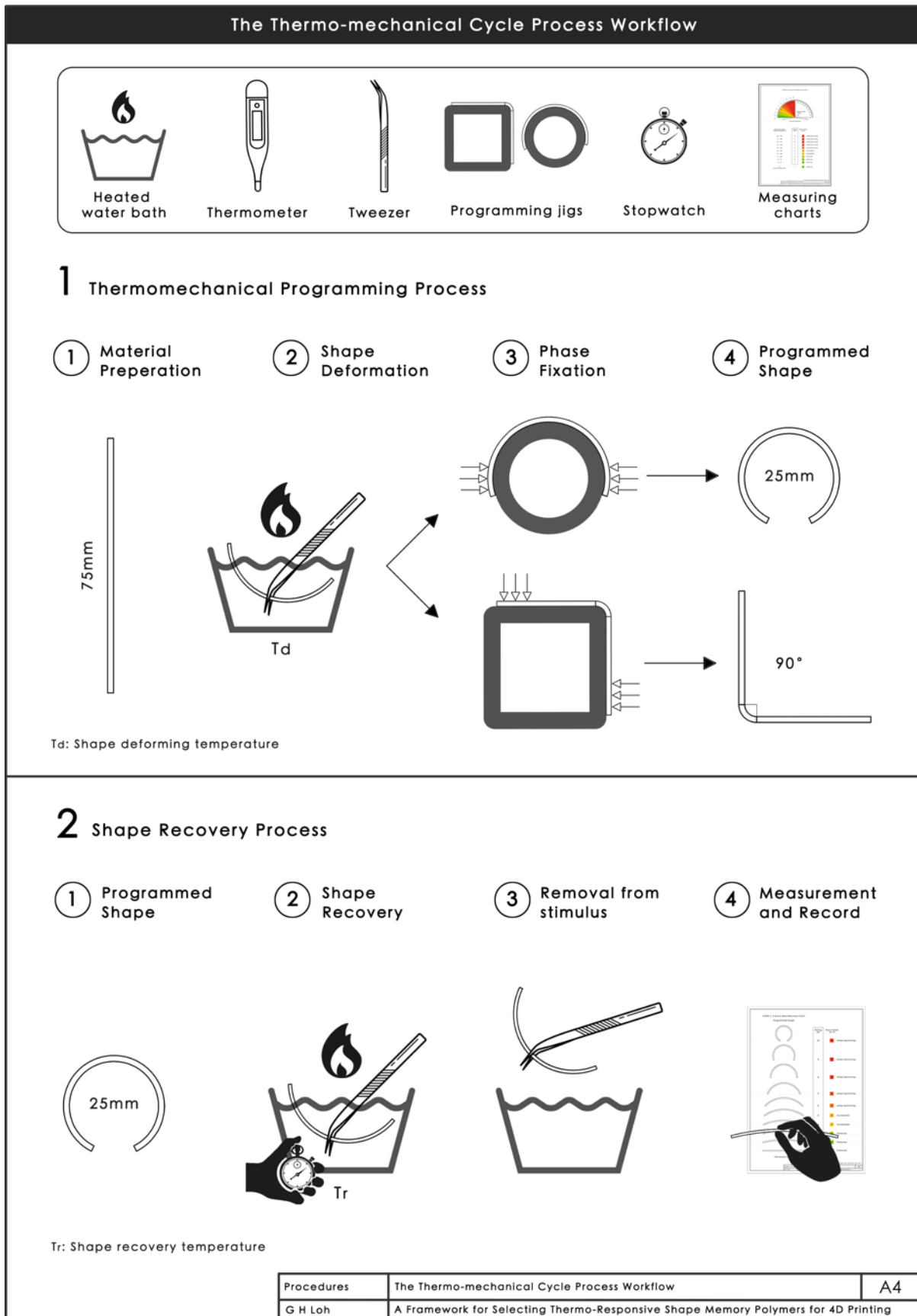
### (1) The Material Framework Selection Process Workflow



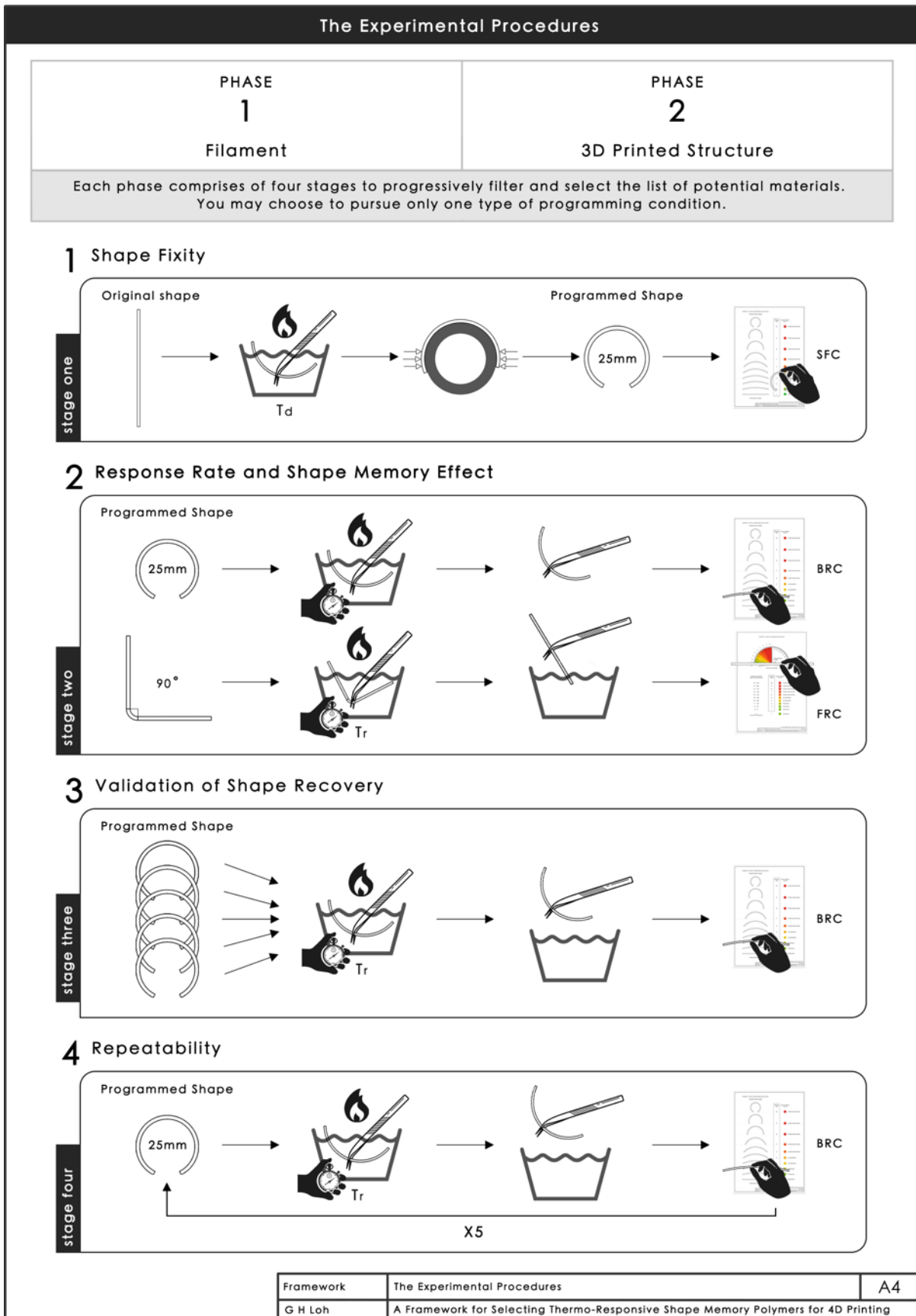
(2) The Objective and Description of The Experimental Stages

The Objective and Description of The Experimental Stages								
<p>PHASE <b>1</b></p> <p>Filament 75mm</p>  <p>From the material list</p>	<p>PHASE <b>2</b></p> <p>3D Printed Structure 75mm x 3mm x 1.75mm</p>  <p>Materials from Phase 1 Stage 3</p>							
<p><b>Experimental Stages</b></p>								
<p><b>1</b> Shape Fixity</p> <p>Stage 1 examines the ability of the material to be successfully fixed or retained at its programmed shape.</p>	<p>Number of test specimens and number of tests required</p> <p><b>stage one</b></p> 							
<p><b>2</b> Response Rate and Shape Memory Effect</p> <p>Stage 2 observes the differences in the response rate, which include the rate of shape morphing activation (<math>T_a</math>) and the time taken for complete shape recovery, as well as the SME of the material when activated at different shape recovery temperatures (<math>T_r</math>).</p>	<p><b>stage two</b></p> 							
<p><b>3</b> Validation of Shape Recovery</p> <p>Stage 3 analyses <i>five</i> specimens per material to observe the consistency and calculate the average value of shape memory properties. Five specimens are a recommended average, although more (or less) samples could be tested by users which determines the accuracy of the results.</p>	<p><b>stage three</b></p> 							
<p><b>4</b> Repeatability</p> <p>Stage 4 investigates the changes in shape memory properties of the material after going through multiple shape memory cycles. Five memory cycles are a recommended average, although more (or less) cycles could be tested by users which determines the accuracy of the results.</p>	<p><b>stage four</b></p> 							
<table border="1"> <tr> <td>Framework</td> <td>The Objective and Description of The Experimental Stages</td> <td>A4</td> </tr> <tr> <td>G H Loh</td> <td>A Framework for Selecting Thermo-Responsive Shape Memory Polymers for 4D Printing</td> <td></td> </tr> </table>	Framework	The Objective and Description of The Experimental Stages	A4	G H Loh	A Framework for Selecting Thermo-Responsive Shape Memory Polymers for 4D Printing			
Framework	The Objective and Description of The Experimental Stages	A4						
G H Loh	A Framework for Selecting Thermo-Responsive Shape Memory Polymers for 4D Printing							

### (3) The Thermo-mechanical Cycle Process Workflow



(4) The Experimental Procedures



## Appendix VII. Expert Interview Questions

### INTERVIEW SCRIPT

#### A Framework Validation for Selecting Thermo-Responsive Shape Memory Polymers for 4D Printing

Thank you for agreeing to participate in our interview. We are contacting you as an expert in 4D Printing to provide us with information and valuable feedback to refine and validate the proposed material selection framework for selecting 4D Printed thermo-responsive materials.

This interview should last no longer than one hour.

The information you provide will be kept confidential and the ethical consent for this project has been sought by the Research Ethics Committee of the College of Engineering, Design and Physical Sciences at Brunel University London. The participation in this interview is anonymous and voluntary. By participating, you are consenting that the interviewer can process the data collected.

**Question 1.** Please identify which category of discipline do you belong to?

- Designer
- Engineer
- Material Scientist
- Other, please specify.

**Question 2.** Which level best describe your knowledge and background on 4D Printing?

- Beginner
- Intermediate
- Advanced

**Question 3.** Are you aware of any framework for selecting thermo-responsive materials for 4D Printing currently available?

- No
- Yes, please specify.

**Question 4.** Do you agree with the tools and equipment use?

- Yes
- No, please specify.

**Question 5.** Do you agree with the procedure in Process 1 and 2 to complete the shape memory cycle of a dual state mechanism (DSM) heat-induced component?

- Yes
- No, please specify.

**Question 6.** Based on the four experimental stages discussed, do you agree the structure of this framework?

Yes

No, please specify.

**Question 7.** Are there any stages to add, reduce or require improvement?

Please provide your feedback.

**Question 8.** Based on your opinion, what are the advantages and the drawbacks of this material selection framework?

Please provide your feedback.

**Question 9.** Please provide any other general feedback.

Please provide your feedback.

**Question 10.** Please kindly recommend an expert in 4D Printing to expand this research study.

Please provide their email address.

**Likert Scale Question 1.** The Material Selection Process

Please rate the following aspects on scale 1 to 5, with 1 being poor and 5 being excellent.

	1 Very Poor	2 Poor	3 Neutral	4 Good	5 Excellent
Concept	<input type="checkbox"/>				
Easy to understand	<input type="checkbox"/>				
Easy to use	<input type="checkbox"/>				
Accuracy	<input type="checkbox"/>				
Usefulness	<input type="checkbox"/>				

**Likert Scale Question 2.** The Shape Fixity Chart

Please rate the following aspects on scale 1 to 5, with 1 being poor and 5 being excellent.

	1 Very Poor	2 Poor	3 Neutral	4 Good	5 Excellent
Easy to understand	<input type="checkbox"/>				
Easy to use	<input type="checkbox"/>				
Accuracy	<input type="checkbox"/>				

**Likert Scale Question 3.** The Bend Recovery Chart

Please rate the following aspects on scale 1 to 5, with 1 being poor and 5 being excellent.

	1 Very Poor	2 Poor	3 Neutral	4 Good	5 Excellent
Easy to understand	<input type="checkbox"/>				
Easy to use	<input type="checkbox"/>				
Accuracy	<input type="checkbox"/>				

**Likert Scale Question 4.** The Fold Recovery Chart

Please rate the following aspects on scale 1 to 5, with 1 being poor and 5 being excellent.

	1 Very Poor	2 Poor	3 Neutral	4 Good	5 Excellent
	<input type="checkbox"/>				

Easy to understand	<input type="checkbox"/>				
Easy to use	<input type="checkbox"/>				
Accuracy	<input type="checkbox"/>				

**Contact for further information and complaints**

Thank you for taking part in this study. Please contact us for further information or any issues regarding participating in this study.

Researcher Name: Hsiang Hsiang Loh

Email: [Hsiang.Loh@brunel.ac.uk](mailto:Hsiang.Loh@brunel.ac.uk)

Supervisor Name: Dr Eujin Pei

Email: [Eujin.Pei@brunel.ac.uk](mailto:Eujin.Pei@brunel.ac.uk)